2014

Design and synthesis of novel heterocycles for organic semiconducting materials

Achala Bhuwalka
Iowa State University

Design and synthesis of novel heterocycles for organic semiconducting materials

by

Achala Bhuwalka

A dissertation submitted to the graduate faculty

in partial fulfillment of the requirements for the degree of

DOCTOR OF PHILOSOPHY

Major: Organic Chemistry

Program of Study Committee:

Malika Jeffries-EL, Major Professor
William Jenks
Art Winter
Javier Vela
Sumit Chaudhary

Iowa State University

Ames, Iowa

2014

TABLE OF CONTENTS

CHAPTER 1

INTRODUCTION

1.1 Outline of the Dissertation

This dissertation summarizes the work performed by the author in the Jeffries-EL research group from 2008 - 2014. The research goals involve the design, synthesis, characterization, and understanding of structure – property relationships of organic semiconducting polymers as well as the evaluation of these materials in organic photovoltaic cells (OPV)s.

Chapter 1 provides a general introduction to organic semiconductors and the effect of structural modifications on their physical and electronic properties. This is followed by an overview of organic solar cells and the background and significance of the materials studied in this dissertation. The chapter is closed by a summary of the key points affecting the performance of organic semiconductors.

Chapter 2 is an article that is under review for publication in RSC Advances. It describes an efficient synthesis of various bithiophene – based carboxaldehydes from a common intermediate. The bulk of the synthetic work was done by the author of this dissertation along with writing the experimental section of the article and significant contributions to the main manuscript. Dr. Malika Jeffries-EL wrote the remainder of the article. Dr. Jeremy Intemann synthesized the dithienosilole intermediate. Dr. Ellern Arkady carried out the crystallographic analysis for several key intermediates. Dr. Jared

Mike synthesized the 2,6-dimethyl benzo[1,2-*d*;4,5-*d´*]bisoxazolediethylphosphonate and 2,6-dimethyl benzo[1,2-*d*;5,4-*d´*]bisoxazole-diethylphosphonate.

Chapter 3 is a manuscript that was published in *Macromolecules* (**2011**, *44* (24), pp 9611–9617) that describes the effect of heteroatom placement and on the optical and electronic properties of Quaterthiophene – Benzobisazole Copolymers for Photovoltaic Cells. The bulk of the synthetic work and polymer characterization was done by the author of this dissertation along with writing the supporting information. Dr. Jared Mike synthesized the 2,6-bis(4-octylthiophen-2-yl)benzo[1,2-*d*; 5,4-*d*']bisoxazole, 2,6-bis(4-octylthiophen-2-yl)benzo[1,2-*d*; 4,5-*d*']bisoxazole, and 2,6-bis(4-octylthiophen-2-yl)benzo[1,2-*d*; 4,5-*d*']bisthiazole. Dr. Jeremy Intemann synthesized an intermediate for the 2,6-bis(4-octylthiophen-2-yl)benzo[1,2-*d*; 4,5-*d*']bisthiazole. OPV fabrication and characterization was performed by Dr. Meng He under the supervision of Dr. Zhiqui Lin formerly of Iowa State University (Materials Science and Engineering). Transistor fabrication and mobility measurements were performed by Dr. Toby Nelson at Carnegie Mellon University (Pittsburgh, PA). X-ray data of the polymer films was collected by Dr. Robert Roggers. Atomic force microscopy images were obtained by Monique D. Ewan. The manuscript was compiled by Dr. Malika Jeffries-EL.

Chapter 4 is a paper that is submitted for review in *Polymer Chemistry* at the time of writing this dissertation. It involves improving the organic photovoltaic cell performance of benzobisazole terpolymers through the use of a two-dimensional comonomer. The bulk of the synthetic work and polymer characterization was done by the author of this dissertation along with writing the supporting information and contributing to the main manuscript. Dr. Jared Mike synthesized the 2,6-bis(4-

octylthiophen-2-yl)benzo[1,2-*d*; 5,4-*d*']bisoxazole , 2,6-bis(4-octylthiophen-2-yl)benzo[1,2-*d*; 4,5-*d*']bisoxazole, and 2,6-bis(4-octylthiophen-2-yl)benzo[1,2-*d*; 4,5-*d*']bisthiazole. OPV fabrication and characterization and mobility and external quantum efficiency measurements were performed by Monique D. Ewan under the supervision of Dr. Sumit Chaudhary. Atomic force microscopy images were obtained by Moneim Elshobaki under the supervision of Dr. Sumit Chaudhary. Thermal studies were performed by Michael Zenner. The manuscript was compiled by Dr. Malika Jeffries-EL.

Chapter 5 is an article that is submitted for review in *Journal of Polymer Science* at the time of writing the dissertation. It describes the synthesis, characterization and photovoltaic properties of dithienylbenzobisazole-dithienylsilole copolymers. The bulk of the synthetic work and polymer characterization was done by the author of this dissertation along with writing the supporting information and contributing to the body of the manuscript. Dr. Jared Mike synthesized the 2,6-bis(4-octylthiophen-2-yl)benzo[1,2-*d*; 5,4-*d*']bisoxazole , 2,6-bis(4-octylthiophen-2-yl)benzo[1,2-*d*; 4,5-*d*']bisoxazole, and 2,6-bis(4-octylthiophen-2-yl)benzo[1,2-*d*; 4,5-*d*']bisthiazole. OPV fabrication, characterization and mobility measurements, as well as external quantum efficiency measurements were performed by Monique D. Ewan under the supervision of Dr. Sumit Chaudhary. Atomic force microscopy images were obtained by Moneim Elshobaki under the supervision of Dr. Sumit Chaudhary. The manuscript was compiled by Dr. Malika Jeffries-EL.

Chapter 6 outlines research based on a new pyridine based ‘small molecule’ for organic solar cells. This study features the synthesis, characterization, and optical properties of several new small molecule chromophores prepared from thiazolopyridine

based acceptor monomers. All of the synthetic work and analytical characterization of the small molecules was performed by the author of this dissertation. Theoretical calculations were performed by Dr. Aimée Tomlinson at North Georgia State University.

Chapter 7 describes the use of furan based donors in organic semiconducting polymers. This study explored the synthesis and characterization of benzodifuran and naphthodifuran based donors and their incorporation into donor-acceptor copolymers with furanyl-diketopyrrolopyrrole acceptor for organic solar cells. A new synthetic route for benzodifurans was established by the author of this dissertation. The majority of the synthetic work was done by the author. Benjamin J. Hale synthesized 3,6-bis(5-bromofuran-2-yl)-2,5-bis(2-butyloctyl)pyrrolo[3,4-*c*]pyrrole-1,4(2*H*,-5*H*)-dione.

Finally, Chapter 8 draws some general conclusions of the work performed and discusses its possible future directions. The author's acknowledgments conclude this chapter.

1.2 Introduction to organic semiconducting polymers

Significant progress has been made in understanding the fundamental principles that govern the properties of organic semiconducting polymers over the past three decades. Although reports of conductivity from organic materials originated in the 1950s,[1,2] these materials only garnered significant scientific attention after the discovery of electrical conductivity from doped polyacetylene in the 1970s.[3,4] Since then, conjugated polymers have been thoroughly explored for applications in organic photovoltaic cells (OPV)s,[5-10] organic light emitting diodes (OLED)s,[11-15] and organic field effect transistors (OFET)s.[16-20] Current commercial photovoltaic technology

incorporates semiconductors derived from inorganic materials such as silicon, cadmium, indium and other metalloids.[21] However, these materials suffer from fundamental drawbacks, such as high costs associated with achieving ultra-pure crystalline silicon; severe toxicity of cadmium, and the limited supply of indium.[22] Furthermore, inorganic semiconductors commonly employ expensive fabrication techniques which further increase their manufacturing costs. In order to circumvent these high costs, the use of lower-cost amorphous silicon has been investigated for solar cell applications.[23] However, such cells tend to suffer from lower efficiencies and can degrade relatively quickly in comparison to crystalline silicon – based semiconductors.[24]

Organic semiconductors offer potential solutions to the aforementioned concerns. They are lightweight, flexible, and solution-processable.[25,26] This allows for these devices to be manufactured and processed on a large area by relatively inexpensive techniques such as inkjet printing, spin-coating and screen printing.[27-29] Moreover, their optical and electrochemical properties can be tuned by chemical synthesis.[30,31] As a result, organic semiconductors can be specifically tailored for the applications they are being investigated for. Although they are not yet as efficient as silicon based solar cells, due to their promising properties, research in the field of organic conjugated polymers for organic electronics has grown tremendously in the last two decades.

For organic polymers to be electrically conducting, they need to possess a conjugated backbone (i.e., a backbone comprising alternating single and double bonds).[32] Let us consider the case of a simple polyene such as polyacetylene (PA) (Figure 1). Each carbon atom is sp^2 hybridized. It forms three σ bonds: one with the hydrogen it is directly bonded to, and one each with the two neighboring carbon atoms. The electrons in these σ

bonds are immobile and hold the polymer backbone together. Each sp^2 hybridized carbon atom also contains one unpaired electron (π electron) in its p_z orbital (π orbital), which is orthogonal to the main chain. The electrons in the π orbital are mobile and are free to move around along the polymer backbone imparting on the polymer its semiconducting properties.[33]

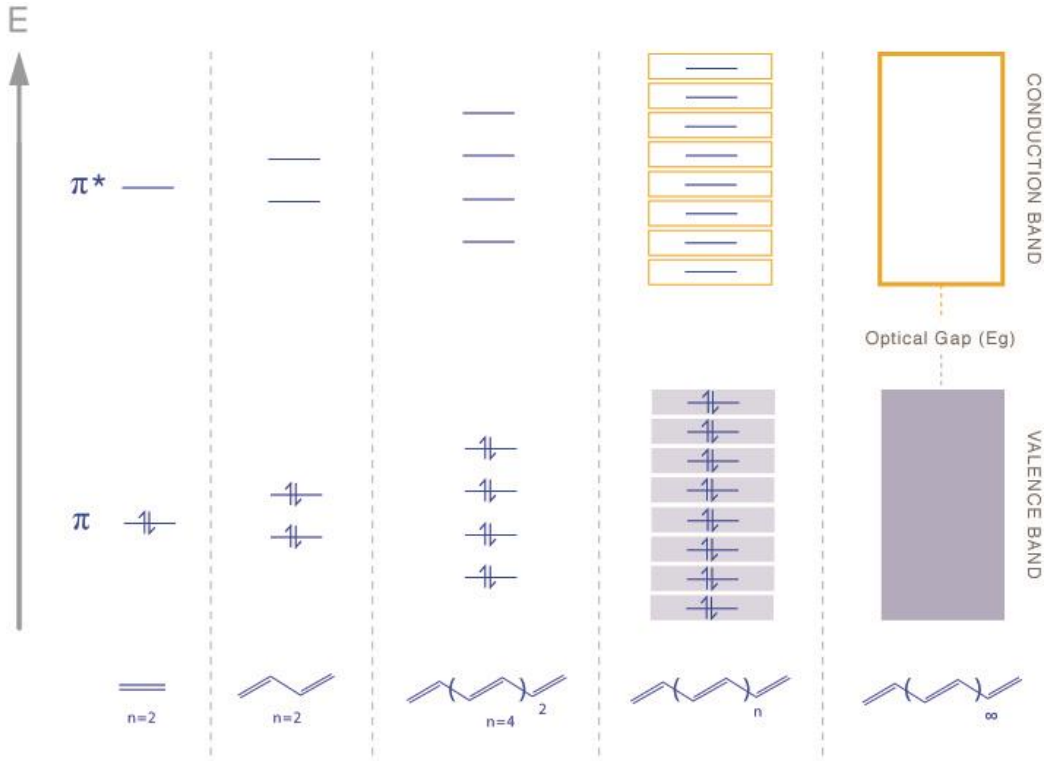

Figure 1.1 Effect of increasing conjugation on the energy levels of the conjugated polymer.

As demonstrated in figure 1.1, when two atomic π orbitals in ethylene combine, it results in the formation of two molecular orbitals, the π bonding orbital and the π* anti-bonding orbital. Both the electrons occupy the lower energy π bonding orbital. As the degree of conjugation increases, a greater number of atomic orbitals overlap to form the

corresponding number of molecular orbitals with filled π orbitals and empty π* orbitals, until they start to resemble the band structure observed in inorganic semiconductors, with a filled valence band and the empty conduction band.[32] As a result of increase in conjugation, the energy of the highest occupied molecular orbital (HOMO) increases whereas the energy of the lowest unoccupied molecular orbital (LUMO) decreases.[33] The energy gap between the HOMO and the LUMO is denoted by the band gap (E_g). The band gap is a critical factor in determining the application of the organic semiconductor and can be engineered for a specific application via chemical synthesis. It is expected that as the energy level of the HOMO increases and the energy level of the LUMO decreases, the two energy levels should converge resulting in the absence of a band gap as is the case in metal conductors, allowing for electrons to readily occupy the conduction band.

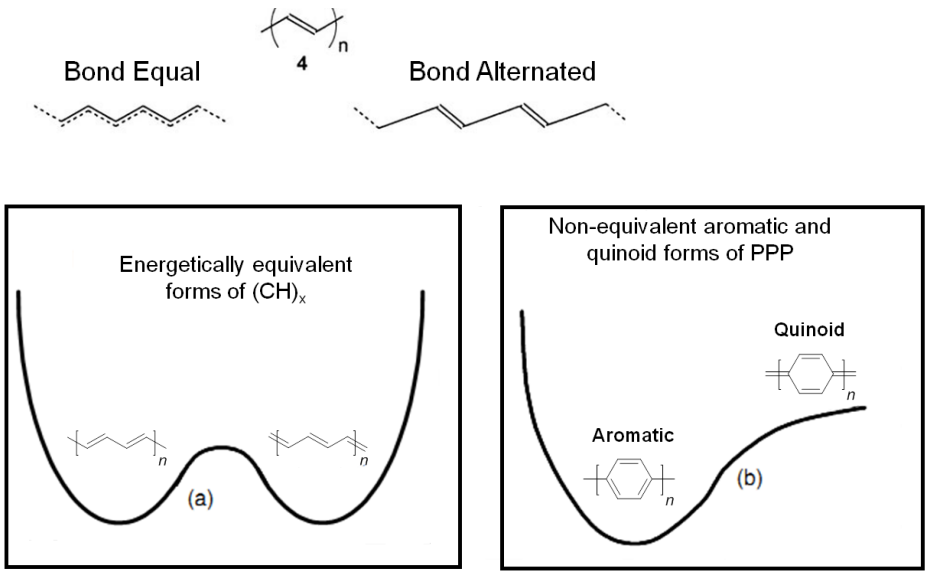

Figure 1.2 Bond length alteration and energy level diagrams of conjugated polymers. (Adapted from ref. 33)

For this to occur, the single and double bonds in the PA backbone should be of equal lengths. NMR and X–ray studies have showed that this is indeed not the case; in fact, the actual bond lengths are 1.35 Å and 1.45 Å respectively (Figure 1.2).[34] This alteration in bond length causes a geometric distortion (Peirel's distortion) in the polymer backbone and is responsible for the splitting of the energy levels, ultimately resulting in the formation of the band gap.[35]

An increase in conjugation also affects the optical and electrochemical properties of the polymer. As illustrated in figure 1.3, as the number of repeat units in the oligomer/polymer backbone increase, the absorption onset of the oligomer/polymer is bathochromically shifted.[36] In this case, the absorption onset of oligofurans (OF) gradually red-shifts to lower energy (higher wavelength) as the number of repeat units increase. When the polymer reaches approximately seven (OF 7) to eight (OF 8) repeat units, increase in the number of repeat units no longer alters the optical properties of the polymer.[36] The polymer is said to have reached its effective conjugation length.

The effective conjugation length of a polymer is basically the length to which a polymer grows before it twists, either due to inherent defects in the polymer backbone or due to steric hindrance. As a result of the twisting, the π electrons are not delocalized over the entire polymer backbone but instead are delocalized only over certain chain lengths. The effective conjugation length differs for each polymer and can vary from eight to twenty repeat units.[37] Any increase in the chain length beyond the effective conjugation length does not affect the energy gap or optical properties of the polymer.[38,39]

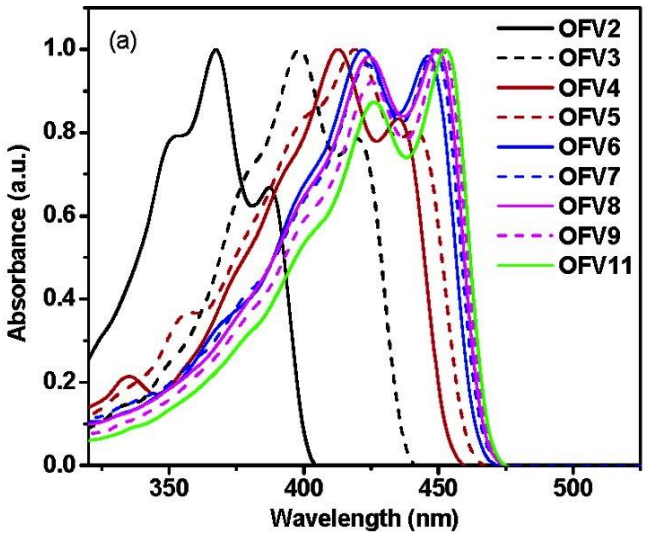

Figure 1.3 Effect of increase in conjugation on polymer absorption. (Adapted from ref. 36)

As mentioned earlier, the effective conjugation length of a polymer is dependent on the amount of twisting in the polymer backbone: greater steric-induced twisting in the backbone leads to a shorter effective conjugation length whereas a smaller steric induced twisting in the backbone leads to a longer effective conjugation length. Typically, utilization of fused ring structures and π-spacers between units in the polymer backbone reduces the steric interactions between neighboring units, thereby leading to materials with higher effective conjugation length and narrower band gaps.[40]

Narrow band gaps can also be achieved by utilizing systems that favor the quinoid configuration.[41,42] Conjugated polymers have two possible non-degenerate ground states – the aromatic (benzenoid) and the quinoid states. In the benzenoid form, the π electrons are essentially localized in the ring system.

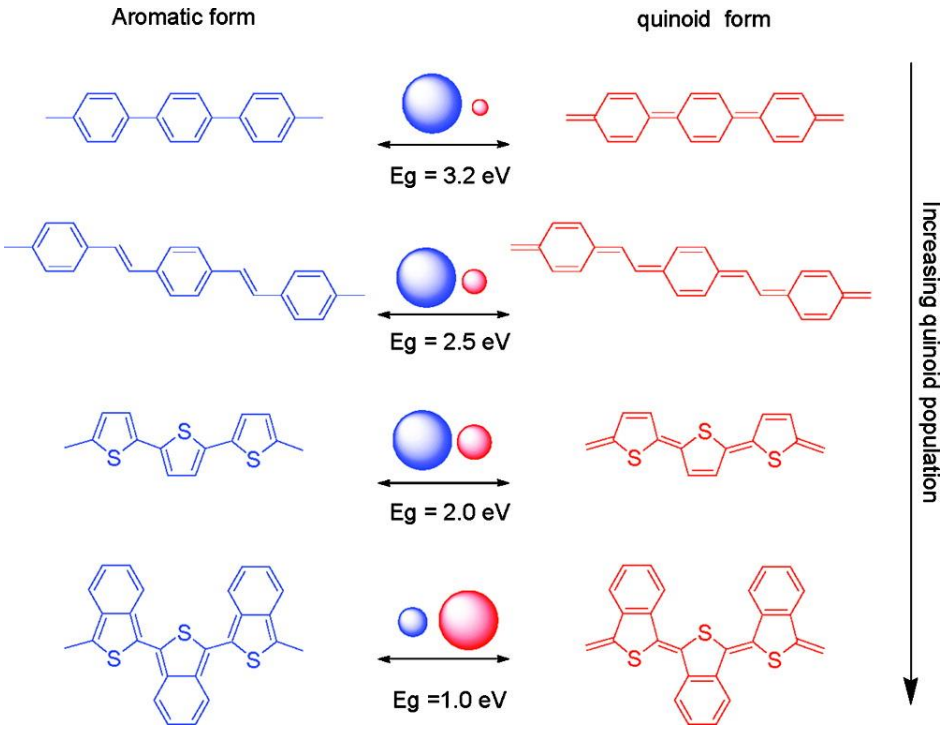

Figure 1.4 Narrowing of band gap by incorporating units that favor the quinoid state. (Adapted from ref.5)

The benzenoid form is more stable and lower in energy. Its resonance form, the quinoid form, is less stable and higher in energy.[5] As shown in figure 1.4, in the quinoid resonance form the positions of the single and double bonds are switched. As a result, the π electrons are delocalized between the ring systems, and neighboring units are held together by double bonds. This results in a more rigid and planar structure, with a longer effective conjugation length, and narrower band gaps than the benzenoid form. The ratio of the aromatoid to quinoid forms is denoted by the value of bond length alternation (BLA), which is the average of the difference in length between adjacent carbon-carbon bonds in a polyene chain.[5] A larger BLA value is indicative of a greater degree of aromatic character, whereas a smaller BLA suggests a greater prevalence of quinoid character in the polymer's ground state: the band gap of the polymer decreases as the

quinoid character increases.[43] Since the BLA and the band gap are highly dependent on the aromatic stabilization resonance energy of the aromatic unit, any decrease in aromaticity of the carbocycle/heterocycle should result in a greater degree of its quinoid character. Therefore, by utilizing "less aromatic" systems such as thiophene and furan, polymers with a narrow band gap can be obtained. Additionally, stabilization of the quinoid state can be achieved by employing systems that stay aromatic in the quinoid state. As illustrated in figure 1.4, a polymer with repeating phenylene units in the backbone favors the aromatic form over the quinoid form due to its greater stabilization energy. Introducing vinylene linkers between repeating phenylene units encourages π electron delocalization as well as reduces the steric twisting of the polymer backbone. This results in a longer effective conjugation length and narrower band gap material. In the third case, since a) thiophene is less aromatic than benzene and b) polythiophene adopts the quinoid form more readily than polyphenylene, still narrower band gap materials are obtained. Lastly, in the case of polyisothianapthene, still narrower band gaps have been obtained. Such effect is observed because in the quinoid form, the benzene ring with greater aromatic stabilization energy, gains aromaticity which results in a more stable structure; as a result the quinoid form is favored over the aromatoid form.[41] The strong preference for adopting the quinoid form leads to extremely small band gaps, making polyisothianapthene one of the narrowest band gap materials reported to date.

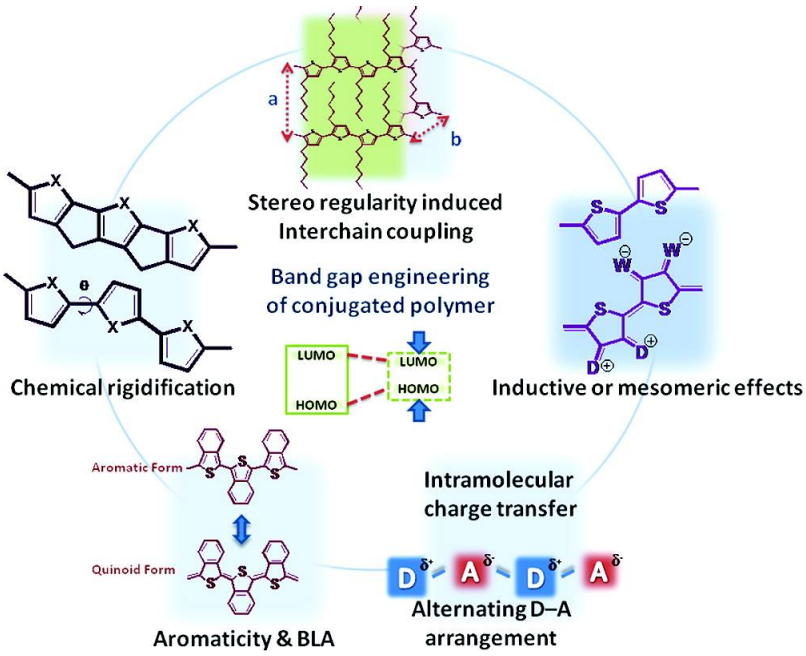

Figure 1.5. Different strategies to tune the polymer energy levels and band gap. (Adapted from ref. 5)

From a synthetic standpoint, polymer properties can be further tweaked by incorporating different substituents in the polymer backbone as well as utilizing fused ring systems to reduce undesired steric twisting (chemical rigidification).[5] Typically, introducing electron withdrawing substituents leads to a decrease in the polymer LUMO levels, whereas introducing electron rich substituents raises the HOMO energy levels.[44] One of the most effective strategies to fine-tune the molecular orbitals involves the use of donor-acceptor copolymers. In such a system, when the frontier molecular orbitals of the donor and acceptor undergo orbital mixing, they give rise to a new set of energy levels (Figure 1.6). The HOMO of the resulting donor-acceptor (D-A) system is higher in energy than the HOMO for either the donor or the acceptor whereas the LUMO level for the D-A system is lower in energy than that of either the donor or acceptor.[45] This leads to narrowing of the band gap. Moreover, the HOMO of the D-A system is influenced to a greater degree by the HOMO of the donor material whereas the LUMO of the D-A

system is influenced to a greater degree by the LUMO of the acceptor. Thus by judiciously selecting the donor and acceptor materials, the polymer energy levels and band gap can be better tailored for a specific application.

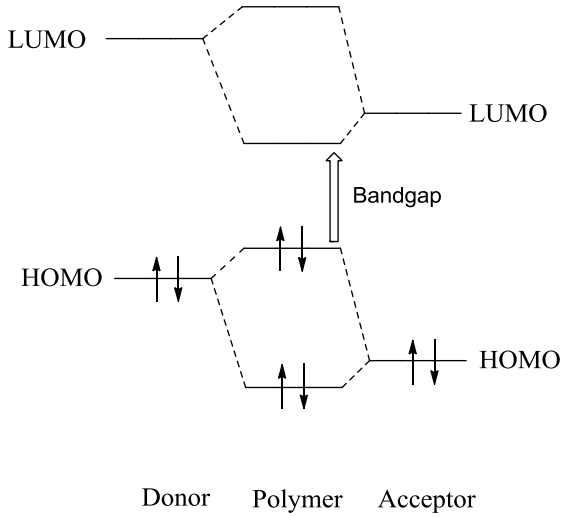

Figure 1.6. Orbital mixing gives rise to a higher HOMO and lower LUMO.

Some of the commonly used donors and acceptors are shown in figure 1.7. The donors are chosen such that they have a deep HOMO level. This is important because in polymers with high HOMO levels, oxygen can easily remove an electron from the HOMO of the polymer leading to oxidative instability as observed in the case of poly(3-alkylthiophene)s. Nonetheless, donor-acceptor copolymers typically have deeper HOMO levels than homopolymers, leading to greater oxidative stability.[7]

One common feature in all the donors and acceptors seen in figure 1.7 is the presence of –R (alkyl) groups. These are essential for good solubility of the resulting polymers. However, it is very important to pick the right alkyl chain for a polymer series since the alkyl chains not only have a significant impact on the solubility of the polymer,

but also on the polymer's morphology.[46] Alkyl chains are insulators by nature and can disrupt crystallinity in the solid state.

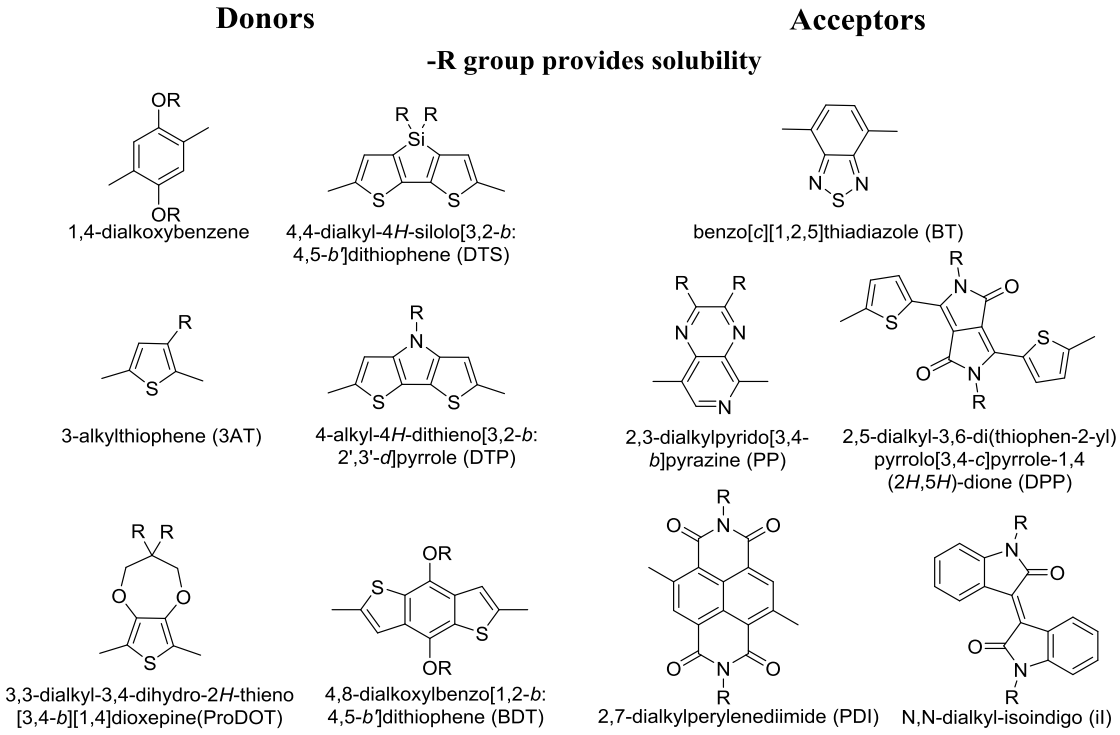

Figure 1.7 Commonly used donors and acceptors

Studies on influence of alkyl chains have revealed that while shorter alkyl chains favor order and crystallinity in the solid state, they are detrimental to the solubility of the polymer in common organic solvents.[47,48] Conversely, longer alkyl chains improve the solubility of the polymers but they disrupt the π-stacking.[46] Use of short branched alkyl chains typically result in a good balance between the "short" and "long" alkyl chains. They impart better solubility than the short linear chains and at the same time allow for better π-stacking than the long linear alkyl chains.[47] Good solubility of conjugated polymers is key to their performance in organic electronic devices. Soluble polymers with high molecular weights allow for easy processing as well as improved film forming

abilities. This, in turn, leads to better charge transport and overall higher efficiencies in organic solar cells.

Charge transport in conjugated polymers occurs via hopping; the electrons and holes hop from one polymer chain to the next.[49] Imbalance in charge carrier mobility, kinks in the polymer backbone, grain and phase segregation boundaries, charge traps formed by polymer defects, functional end-groups, and impurities (such as residual metal catalysts) can reduce charge carrier mobility leading to lower power conversion efficiencies in solar cells.[50,51] Charge carrier mobility is also dependent on how the polymer self assembles in the solid state. This is in turn dependent on the processing conditions such as the processing solvent and time, molecular weight of the polymer, the interchain interactions of the units that make up the polymer backbone, nature of alkyl chains as well as the regioregularity of the polymer.[50,52,53] Overall it can be noted that careful design of the polymer backbone e.g. of its repeat units as well as the solubilizing chain, is crucial to the overall performance of the polymer.

1.3 Development of Materials for Organic Photovoltaic Cells.

1.3.1 Benzobisazoles: Benzobisoxazole and Benzobisthiazole

Benzobisazoles are electron-deficient units that were first developed in the 1970s by Osman et al. for use as dyes.[54-56] Later, these compounds were investigated by Wolfe et al. for use as high performance materials for the Air Force.[57,58]

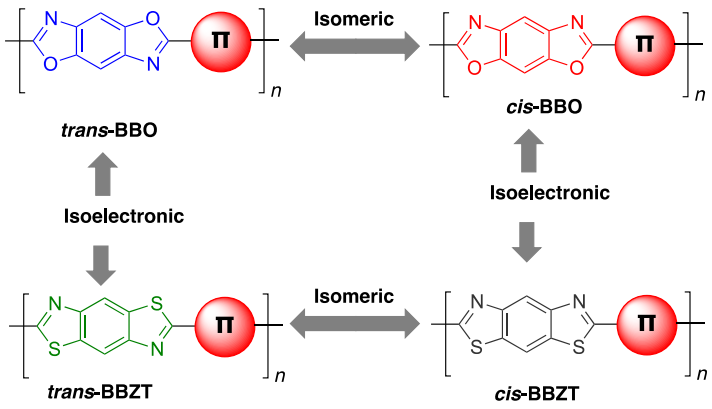

Figure 1.8 The different isomers of benzobisoxazoles and isoelectronic benzobisthiazoles

These rigid rod-like materials exhibit excellent mechanical strength, high thermal, and oxidative stability.[59] Additionally, they display enhanced electron transport,[20,60] photoluminescence,[61,62] and promising third-order nonlinear optical properties.[20,63] Inspite of these promising properties, the use of polybenzobisazoles (PBA)s for organic electronic devices was not investigated due to the harsh reaction conditions required for their synthesis and processing.

Traditionally, PBAs were synthesized by the acid-catalyzed condensation of 2,5-diamino-1,4-benzenedithiol, or 2,4-diaminoresorcinol with 1,4-benzenedicarboxylic acid (Figure 1.9).[54,55] These condensations require high reaction temperatures and strongly acidic conditions.[64,65] Not only was the removal of residual acid from the resulting polymers challenging, the reaction conditions do not allow for most functional groups to be retained on the molecules.

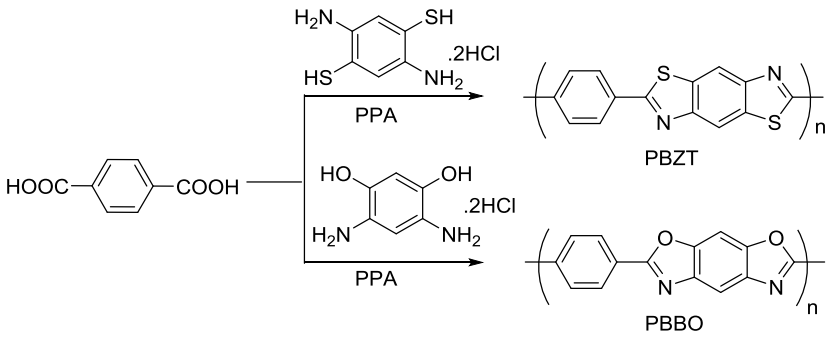

Figure 1.9 Traditional synthesis of PBAs

Moreover, only polymers incorporating the benzo[1,2-*d*;5,4-*d*']bisoxazole (*cis*-BBO) and benzo[1,2-*d*;4,5-*d*']bisthiazole (*trans*-BBZT) could be studied because the starting material (2,5-diaminohydroquinone) required for the synthesis of benzo[1,2-*d*;4,5-*d*']bisoxazole (*trans*-BBO) is not stable under the aforementioned reaction conditions.[66]

One of the early goals of the Jeffries-EL group was to find a route to more accessible benzobiazoles. To this effect, Dr. Jared Mike pioneered the mild synthesis of benzobisazoles via the Jeffries-EL – Mike orthoester method under mild reaction conditions (Figure 1.10).[67,68] Benzobisazoles for single bond as well as vinylene-linked polymers could be accessed using the developed synthetic route.[7,69-72] Solution-processable benzobisazole polymers were then synthesized and investigated for organic electronics by the author of this dissertation.[7,73] However, polymers based on benzo[1,2-*d*;5,4-*d*']bisthiazole could not be studied due to the synthetic inaccesability of preparing 4,6-diaminobenzene-1,3-dithiol.

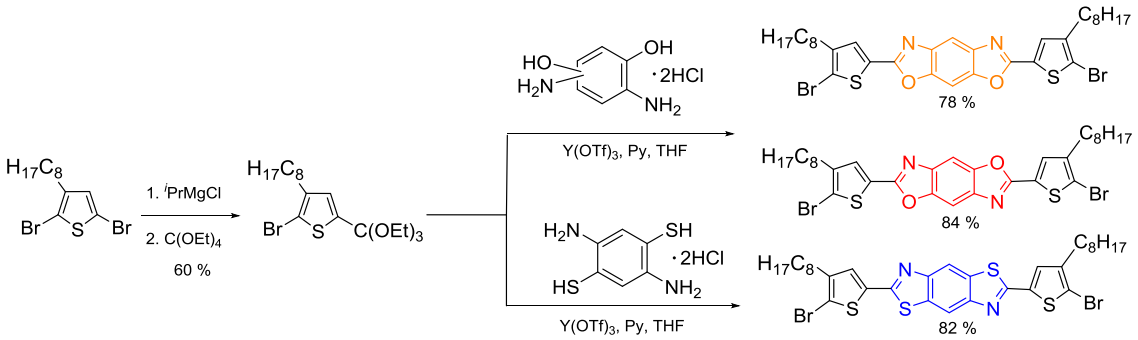

Figure 1.10: Mike – Jeffries EL orthoester reaction for the synthesis of benzobisazoles

1.2.2 New donor and acceptor materials for OPVs

Thiazolopyridines. The higher electronegativity of nitrogen (3.04 on Pauling scale) as compared to carbon (2.55 on Pauling scale) results in the pyridine ring being more electron-deficient than benzene.[74] Furthermore, the lone pair of electrons on the nitrogen atom is easily protonated, making the ring less reactive towards electrophilic aromatic substitution. Due to their electron-deficient nature and high electron affinity, polymers utilizing pyridine and its derivatives as acceptors in donor-acceptor copolymers have shown tremendous promise as electron-transport materials for OLEDs.[75,76] Mobilities as high as 0.6 cm^2 V^{-1} s^{-1} have been achieved in OPVs with polymers incorporating pyridine in their backbone.[77] However, the biggest drawback for materials incorporating CPs is the lack of batch-to-batch reproducibility. This leads to differing processing conditions as well as inconsistent device performance.[78] In order to circumvent this, monodisperse small molecules are being actively studied for their use in OPVs and OLEDs.[79-83] Pyridalthiadiazoles have emerged as a particularly promising class of acceptors for small molecule OPVs. Efficiencies nearing 7 % have been achieved in small molecule organic solar cells incorporating these systems.[84] Conversely, the use

of thiazolopyridines for organic solar cells is yet to be investigated. Thiazolopyridines have primarily been investigated for their pharmaceutical properties,[85-87] with few examples of their application in disperse dyes also being reported.[88]

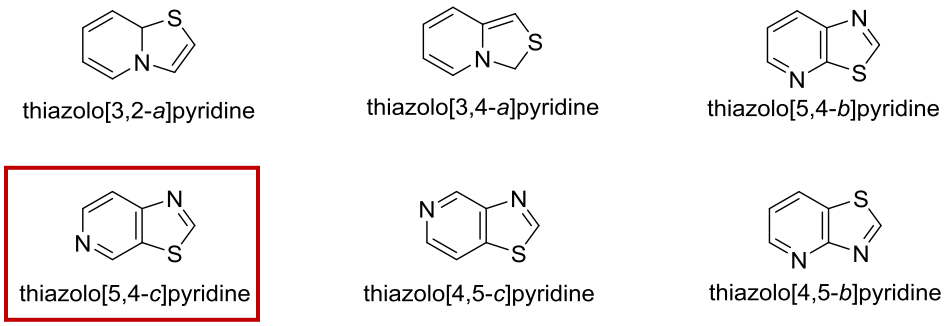

Figure 1.11 Isomers of thiazolopyridines

Thiazolopyridine is expected to have a higher electron affinity than pyridine since thiazole ring contains an imine nitrogen atom which pulls the electron density from the ring making an electron deficient pyridine ring even more electron-deficient. Although there are six possible isomers of thiazolopyridines (Fig 1.11), only thiazolo[5,4-*c*]pyridine and its derivatives were studied by the author of this dissertation. Much of the inspiration for this work was derived from previous studies on benzobisazoles as well as reports of efficient small molecule solar cells fabricated from systems incorporating pyridalthiadiazole as the acceptor.[77,84] New 'acceptor-donor-acceptor' and 'acceptor-π-donor-π-acceptor' type small molecules were synthesized and studied by the author of this dissertation and will be discussed in greater detail in chapter 6 (Figure 1.12).

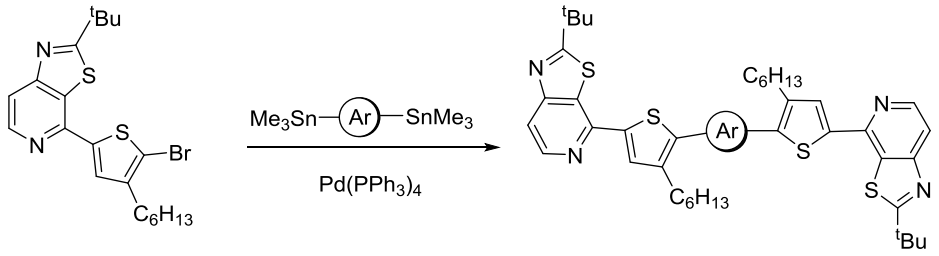

Figure 1.12 Thiazolopyridines based small molecules

Benzodifurans and napthodifurans. Narrow band gap donor – acceptor copolymers incorporating substituted benzodithiophene (BDT) units as the donor have displayed improved power conversion efficiencies (PCE)s in organic solar cells.[89,90] Scientists are continuously tweaking structural and device parameters in order to further improve PCEs. Structural parameters involve modifications of the side chains on the polymer backbone as well as studying the effects of heteroatom substitution on the polymer properties. In the case of BDT, replacement of alkoxy side chains with alkylthienyl side chains was found to lower the HOMO levels of the polymer which in turn increases the open circuit voltage and thus the overall efficiency of the device.[91,92] In order to study the effects of the heteroatom, scientists have substituted the thiophenes in BDT for other heterocycles such as furan (BDF) or selenophenes (BDSe).[9,93] Recently, polymers incorporating benzodifuran have generated a lot of interest with PCEs of 5 % being reported.[94,95] Since furan has a smaller atomic radius than thiophene, there is less steric interaction and therefore less twisting in the polymer backbones employing BDF as compared to BDT.[96,97] Furthermore, since furan is less aromatic than thiophene, theoretically, it can better stabilize the quinoid state leading to smaller band gaps.[9,96] A

new synthetic route to substituted benzodifurans has been developed by the author of this dissertation and is discussed in chapter 7.

Another effective strategy to improve PCEs involves promotion of π-stacking interactions through the use of larger π-conjugated systems,[98] which leads to higher hole mobilities. NDT-based systems have shown hole mobilites of 3.3 x 10^{-3} cm^2 V^{-1} s^{-1} as compared to mobility values of 2.0 x 10^{-5} cm^2 V^{-1} s^{-1} exhibited by BDT-based systems.[99,100] Even higher hole mobility have been reported in FETs derived from NDF as compared with NDT based systems.[98] However, only limited examples of NDFs in donor-acceptor polymers for OPVs have been reported.

1.4 Organic Photovoltaic Cells

A large part of world's current electricity supply is generated from fossil fuels such as coal, oil, and natural gas. However, these traditional sources of energy are non-renewable and are depleting at a rapid rate. Furthermore, the high costs associated with importing oil and the environmental hazards associated with burning fossil fuels have led to an increase in research based on renewable energy. Renewable energy resources include solar, wind, geothermal, hydropower energy among others. Most of the renewable energy resources are derived either directly or indirectly from the sun.[101] The global energy requirement by 2050 is projected to be ~ 30 TW. The sun provides approximately 120,000 TW of energy annually i.e. more sunlight energy strikes the earth in 1 hour than all the energy consumed worldwide in an entire year.[102] It has been reported that 150 km^2 of Nevada covered with 15% efficient solar cells could provide the

entire United States of America with electricity.[103] Therefore, efficient harvesting of solar energy could potentially address some of the rising global energy concerns.

Although promising, the current photovoltaic technology is very expensive to be commercially feasible. This is because it employs the use of silicon-based inorganic solar cells which requires extremely high purity silicon, elaborate processing conditions and has high fabrication costs associated with its manufacture.[104] Conversely, organic solar cells are solution-processable and require less elaborate processing conditions. Moreover, they are lightweight and can be cast over flexible substrates.[105] It is suggested that the cost of manufacturing a 10% efficient solution-processable OPV via roll to roll processing is expected to be around $\$50/m^2$ as opposed to $\$350/m^2$ for inorganic solar cells.[106] Due to these advantages, OPVs are being investigated as cheaper alternatives to silicon-based solar cells. In fact, in the last decade tremendous progress has been made in the field of OPV research.

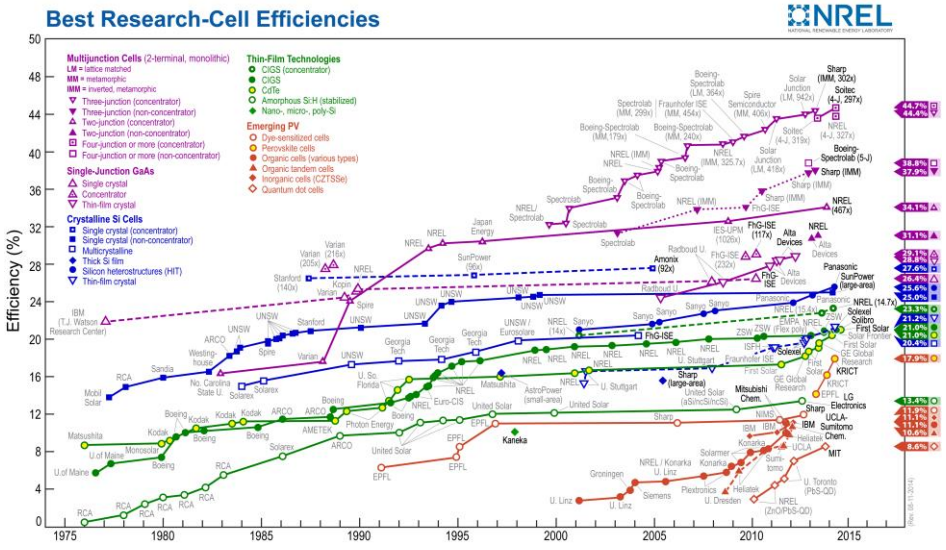

Figure 1.13 Progress in photovoltaic research from 1975 to 2014[107]

Multiple accounts of power conversion efficiencies around 7–9% in organic photovoltaics employing the bulk heterojunction concept have been reported (Figure 1.13).[108-111] Isolated examples of even higher performing OPVs have also been reported.[112,113] Despite these gains in PCE, improvements in device engineering and the development of new materials remains a fundamental and important criterion for the development of commercial organic photovoltaics.[108,114,115]

Organic solar cells convert light energy into electrical energy via the following processes (Figure 1.14).[5]

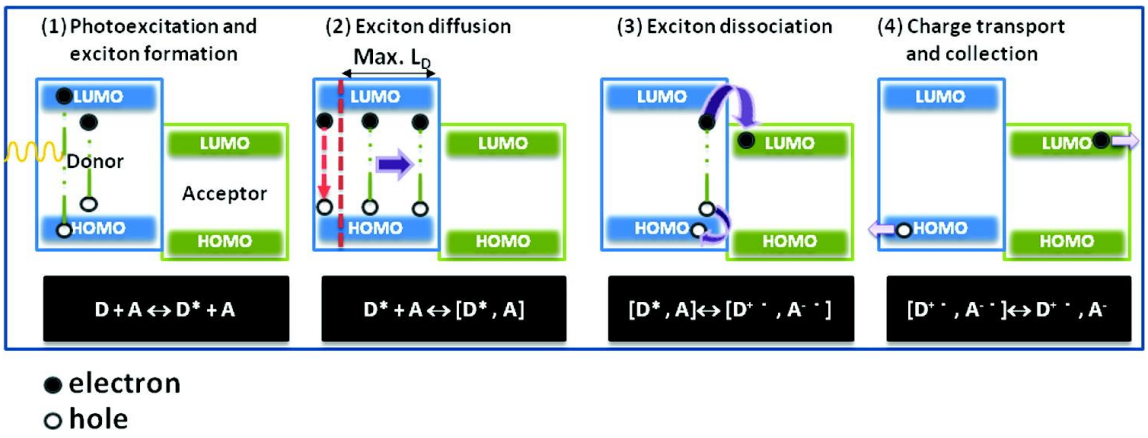

Figure 1.14: Charge processes taking place in a bulk heterojunction solar cell (adapted from ref. 5)

Initially, a photon is absorbed by the donor material (1). This leads to photoexcitation of an electron from the HOMO of the donor to the LUMO of the donor resulting in the formation of a coulombically-bound electron – hole pair also known as an exciton. An exciton in an organic solar cell has a typical binding energy of 0.1 – 0.3 eV, as opposed to a much smaller binding energy in an inorganic device. This is one of the

major differences between organic and inorganic solar cells. Nonetheless, organic materials typically exhibit high absorption coefficients (~10^5 cm^{-1}). Therefore, only a very thin layer (~100 nm) of the absorbing material is required to harvest most of the photons and avoid loss of efficiency through recombination.[116] Once formed, the exciton diffuses to the donor acceptor interface (2). Typically excitons are short lived species with a maximum diffusion length of 10 nm before they recombine or decay to the ground state.[30] As a result, excitons generated farther than 10 nm from the acceptor are almost completely lost leading to a significant loss in PCE. Once at the donor–acceptor interface, the excitons dissociate via an electron transfer process to form a charge pair also known as a geminate pair(3).[117] The geminate pairs are still coloumbically bound and have to be separated by an internal field. For efficient dissociation of excitons, the LUMO energy offset must be greater than the exciton binding energy.[118] Once dissociated, the electrons and holes must be transported and collected at their respective electrodes within their lifetimes (4). The overall efficiency of the above steps is denoted by the external quantum efficiency (EQE) which represents the percentage of total photons that are converted into charge carriers which are collected at the electrodes. Limited absorption of the solar spectrum by the active layer and/ or recombination of excitons lead to low EQEs.

The performance of a solar cell is measured in terms of its power conversion efficiency (PCE). The PCE (η) is dependent on three important factors, namely the short circuit current density (J_{sc}), open circuit voltage (V_{oc}) and the fill factor (FF). PCE can be calculated using the following equation

$$\eta = \frac{P_{out}}{P_{in}} = \frac{J_{sc} V_{oc} FF}{P_{in}}$$

The short – circuit current density (J_{sc}), is the current flowing through the cell in the absence of an externally applied voltage. It is defined as the short-circuit current (I_{sc}/Area of the solar cell) and is dictated by the number of charge carriers generated and collected at the electrodes. It is the largest current that may be drawn from the cell. J_{sc} is dependent on the morphology and carrier mobility in the active layer and the external quantum efficiency of the solar cell.[30]

The open–circuit voltage (V_{oc}) is the maximum voltage that can be derived from the solar cell. It is measured when there is no current flowing through the device. The V_{oc} is dependent on energy levels of the donor and acceptor. It is also affected by the morphology of the active layer in bulk heterojunction solar cells.[119]

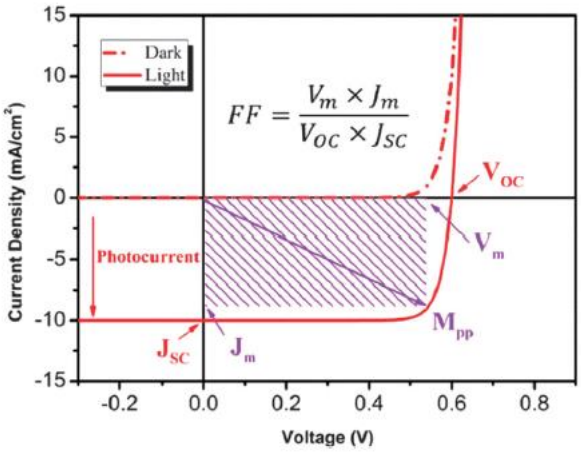

Figure 1.15: Typical current–voltage characteristics for dark and light current in a solar Cell (adapted from ref.120)

Fill factor (*FF*) is defined as the ratio of the maximum power from the solar cell to the product of V_{oc} and $J_{sc.}$ Graphically, it defines the overall squareness of the *J-V* curve. It is a measure of the charge carriers reaching the electrodes and is affected by the series and shunt resistance.[120] It can be calculated by the following equation

$$FF = \frac{V_m \cdot J_m}{V_{oc} \cdot J_{sc}}$$

In order to achieve a high *FF* value, the shunt resistance should be very high to prevent leakage currents and the series resistance should be very small to get a sharp rise in the forward current.[30] The series resistance adds up from bulk transport, interface transfer and transport through the contacts.[121]

Early solar cell studies were based on single layered photovoltaic devices. These devices contained an organic semiconducting layer sandwiched between two metal electrodes. Indium tin oxide (ITO) was commonly employed as the anode due to its high work function and transparent nature whereas low work function metals (such as aluminum, calcium and magnesium) were used as the cathode.[122] Difference in work functions of the two electrodes causes band bending and creates an electric field in the polymer layer. Absorption of light by the polymer results in the formation of excitons. These excitons are columbically bound, and under electric field separate into holes and electrons. Once separated, the holes travel to the anode and the electrons travel to the cathode, resulting in a photocurrent.[49,122] However, because the external field generated from the difference in work function of the electrodes is not strong enough to efficiently overcome the columbic forces holding the exciton together, most of the excitons recombine resulting in a loss of efficiency.[122] Further loss of efficiency is suffered through the disordered nature of organic semiconductors as well as imbalanced charge carrier transport.[123]

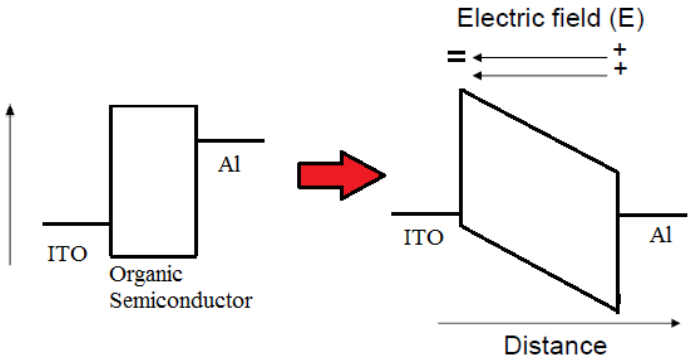

Figure 1.16 Single-layered organic photovoltaic cells.

In order to address this problem, bilayer solar cell architecture was developed by Tang et al.[124] A bilayer device consists of two different semiconducting polymers (Figure1.17); an electron-rich donor layer and an electron-poor acceptor layer stacked on top of each other.[30,125-127] These two layers are placed between electrodes that are chosen such that they align closely with the HOMO of the donor and the LUMO of the acceptor. Light is absorbed by the donor material and an electron is photoexcited from the HOMO to the LUMO of the donor material. Charge separation takes place at the interface of the donor and the acceptor material.[13,30] The driving force for charge separation is the large potential difference at the donor–acceptor interface.[121,128]

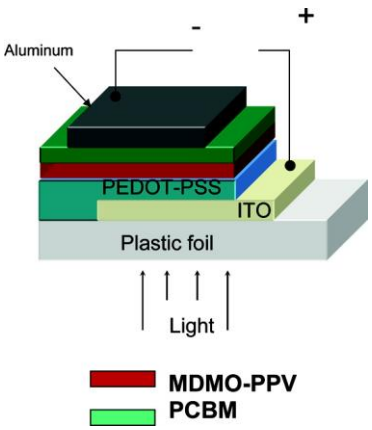

Figure 1.17: Bilayer solar cell (adapted from ref 30)

However, as mentioned earlier, the energy offset between the LUMO levels of the donor and acceptor needs to be greater than the exciton dissociation energy (~0.2 eV). Once separated, electrons travel through the acceptor material while holes 'travel' through the donor material to their respective electrodes, generating a photocurrent. Since the charge carriers travel through different materials, efficiency loss through recombination is greatly reduced as compared with a single layer OPV.[121] For efficient harvesting of the solar spectrum, the active layers are typically ~100 nm in thickness. However, since excitons have a limited diffusion length, only those electrons generated within 10 nm of the acceptor are transferred to the LUMO of the acceptor material, resulting in a significant loss of charge carriers and overall low efficiencies.[129]

This drawback could perhaps be best addressed through the realization of an ordered heterojunction architecture in which 10-20 nm thick layers of the donor and acceptor alternate each other side by side. As a result, all the excitons generated through photoexcitation should be within 10 nm of a donor-acceptor interface allowing for their extraction and collection at the electrodes within their diffusion length lifetimes. Although promising, this type of ordered heterojunction has currently not yet been achieved, most likely due to elaborate fabrication techniques that are required. Nonetheless, groundbreaking work done by the groups of Heeger and Halls, led to the development of the bulk heterojunction (BHJ) device architecture.[130,131] In a BHJ, the donor and acceptor materials are blended together in solution and are drop-cast to make up a single active layer. This layer encompasses an interpenetrating donor-acceptor network with a large surface area which serves two purposes. Firstly, due to the close proximity of the donor and acceptor, most of the excitons formed at the interface would

be within their diffusion length. This should reduce loss in efficiency from undesired recombination. Secondly, the interpenetrating donor–acceptor network acts as a charge transport channel for the holes and electrons once they are completely dissociated. This further reduces the probability for recombination as the charge carriers are transported through different materials. Further improvements in efficiency have been made through manipulation of molecular structure and fabrication techniques.[114] The BHJ is currently the most promising and widely studied device architecture for OPVs.

Early studies on the BHJ employed two conjugated polymers with offset energy levels as materials for the active layer. An electron-rich polymer acted as the donor material whereas an electron poor polymer acted as the acceptor material. Through careful optimization of materials, efficiencies of nearly 2% were realized.[132] Remarkable progress in the field was further achieved when Sariciftci, et al. observed efficient photoinduced electron transfer in fullerene-polymer blends.[133] Ever since this discovery, fullerenes and their derivatives have been thoroughly investigated as acceptors in donor-acceptor BHJ solar cells. Since simple fullerenes exhibited limited solubility in organic solvents, functionalized fullerenes, such as [6,6]-Phenyl C_{61} butyric acid methyl ester ($PC_{61}BM$) and [6,6]-Phenyl C_{71} butyric acid methyl ester ($PC_{71}BM$), are commonly used. Fullerenes have a low-lying LUMO which thermodynamically favors electron transport from the donor to the fullerene.[134] Also, this system is triply degenerate and can accept up to six electrons and effectively stabilize negative charge.[5] Additionally, electron transfer from a polymer to a fullerene occurs on a much faster time scale than photoluminescence, thereby enhancing charge separation and minimizing carrier loss.[135] Lastly, fullerenes also exhibit high electron mobility as observed in FETs.[136] Through careful optimization

of molecular structure and device fabrication techniques in donor – acceptor BJH solar cells, several examples of systems with PCEs exceeding 7% have been achieved.[111-113]

One of the current challenges in systems employing polymer-fullerene donor-acceptor BHJs is controlling the phase segregation between the fullerene and polymer within the film.[137,138] This is a crucial factor because if the domain sizes of the polymer or fullerene are very large, then excitons are not be able to reach the donor–acceptor interface within their lifetime, resulting in a loss of charge carriers.[139] Moreover, during co-crystallization portions of the polymer and fullerene may become isolated (as seen in vertical phase segregation) from the electrode.[140] As a result, any holes and electrons formed in these regions would be trapped due to the lack of a transport pathway, leading to reduction of efficiency through loss of carrier species. In order to address this, tremendous efforts are being directed at understanding the factors influencing the morphology and mobility of the active layer.[141] The V_{oc}, J_{sc}, *FF*, carrier transport (and therefore the PCE) are directly or indirectly influenced by the morphology of the active layer.[142,143] Structural modifications are being incorporated to encourage self-assembly within the active layer.[144-146] Influence of casting solvent and solvent additives, [35,143,147-149] concentration of the solution,[143,150] post production treatment and annealing temperature on the morphology are all being continually investigated.[151-153]

Structure and solubility of the polymer and fullerene also play an important role in determining the morphology of the active layer.[143,154] Incorporation of side chains into the polymer backbone has been found to significantly improve its solubility.[143] The optimal position and size of the side chain varies with polymer structure. It has been found that the side chain should be positioned such that it causes the least amount of

backbone twisting possible.[154] Orientation of the alkyl chains also influences solubility and morphology.[48,155] Studies have revealed that the length and shape of the alkyl chains have a significant effect on the *FF* and J_{sc}.[47,48,156,157] While the most commonly employed side chains are nonaromatic alkyl chains, the influence of aromatic and end-group functionalized substituents has also been investigated.[92,158]

Other polymer properties that heavily influence OPV performance include the absorption profile, energy level alignment, and band gap of the polymer. For maximum capture of the photon flux, low band gap polymers (E_g = 1.6 - 1.7 eV) with good overlap between the polymer absorption and solar spectrum (peak intensity ~ 700 nm at sea level) must be utilized (Figure 1.18)[159].

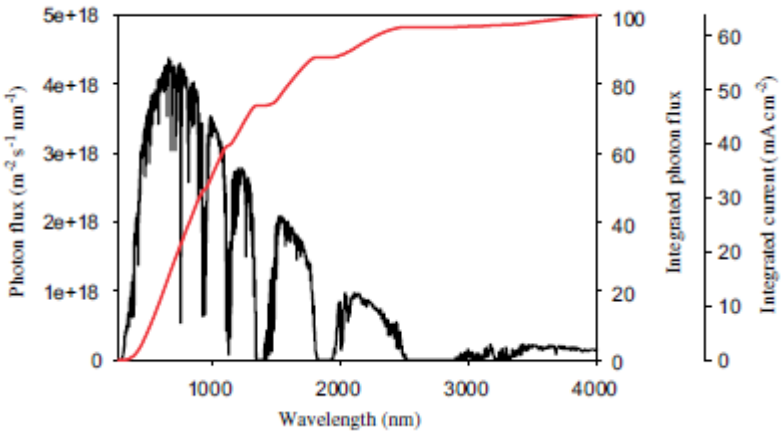

Figure 1.18 Photon flux from the sun (adapted from ref 159)

Several approaches towards narrowing the band gap have been investigated with the most successful ones include engineering the polymer energy levels, such that a low-lying HOMO is obtained to ensure high V_{oc}, while at the same time maintaining the offset required for efficient exciton dissociation between the LUMO of the polymer and

fullerene. Finding the right balance between the efficient absorption of solar radiation, deep energy levels and high V_{oc} and J_{sc} is of vital importance. For systems integrating PCBM as the acceptor, LUMO levels around -3.7 to -4.0 eV and HOMO levels ranging from -5.2 to -5.7 eV were shown to be ideal.[160,161]

In conclusion, the following factors must be considered when developing a material for organic solar cells:

1. Physical characteristics of the polymer: The polymer should have a high molecular weight (encouraged through the use of short-branched alkyl chains) and narrow PDI. High molecular weights are beneficial for film forming ability of the polymer and therefore lead to improved morphology of the materials. Additionally, the materials must display high thermal (compromised by incorporation of alkyl chains) and oxidative stability (enhanced by utilizing donors which lower the HOMO levels of the resulting polymers).
2. Well aligned energy levels: Offset between the LUMO levels of the donor and acceptor should be greater than the exciton dissociation energy (~0.2 eV); the HOMO of the polymer should be low-lying to ensure air stability as well as high V_{oc}
3. Narrow band gaps: low band gap polymers (E_g = 1.6–1.7 eV) with good overlap between the polymer absorption and solar spectrum should be employed for maximum harvesting of solar photon flux; can be achieved by a) utilizing polymers that favor the quinoid form; b) reducing steric interactions in polymer backbone; c) through use of large fused aromatic systems

Wide absorption profile, factors affecting charge transport and mobility of charge carriers as well as π-stacking of polymer in solid state must also be considered. Since any slight modification in polymer structure may cause significant impact on polymer properties, systematic study of polymer structure – property relationships and development of new materials, both electron-rich and electron-poor, remains crucial to the development and enhancement of the field of organic semiconductors.

1.5 References

(1) McNeill, R.; Weiss, D.; Willis, D. *Australian Journal of Chemistry* **1965**, *18*, 477.
(2) Bolto, B.; Weiss, D.; Willis, D. *Australian Journal of Chemistry* **1965**, *18*, 487.
(3) Shirakawa, H.; Louis, E. J.; MacDiarmid, A. G.; Chiang, C. K.; Heeger, A. J. *Journal of the Chemical Society, Chemical Communications* **1977**, 578.
(4) Chiang, C. K.; Druy, M. A.; Gau, S. C.; Heeger, A. J.; Louis, E. J.; MacDiarmid, A. G.; Park, Y. W.; Shirakawa, H. *Journal of the American Chemical Society* **1978**, *100*, 1013.
(5) Cheng, Y.-J.; Yang, S.-H.; Hsu, C.-S. *Chemical Reviews* **2009**, *109*, 5868.
(6) Lu, L.; Yu, L. *Advanced Materials* **2014**, *26*, 4413.
(7) Bhuwalka, A.; Mike, J. F.; He, M.; Intemann, J. J.; Nelson, T.; Ewan, M. D.; Roggers, R. A.; Lin, Z.; Jeffries-El, M. *Macromolecules* **2011**, *44*, 9611.
(8) Beaujuge, P. M.; Fréchet, J. M. J. *Journal of the American Chemical Society* **2011**, *133*, 20009.
(9) Kobilka, B. M.; Hale, B. J.; Ewan, M. D.; Dubrovskiy, A. V.; Nelson, T. L.; Duzhko, V.; Jeffries-El, M. *Polymer Chemistry* **2013**, *4*, 5329.
(10) Huang, H.; Zhou, N.; Ortiz, R. P.; Chen, Z.; Loser, S.; Zhang, S.; Guo, X.; Casado, J.; López Navarrete, J. T.; Yu, X.; Facchetti, A.; Marks, T. J. *Advanced Functional Materials* **2014**, *24*, 2782.
(11) Friend, R. H.; Gymer, R. W.; Holmes, A. B.; Burroughes, J. H.; Marks, R. N.; Taliani, C.; Bradley, D. D. C.; Santos, D. A. D.; Bredas, J. L.; Logdlund, M.; Salaneck, W. R. *Nature* **1999**, *397*, 121.
(12) Intemann, J. J.; Hellerich, E. S.; Tlach, B. C.; Ewan, M. D.; Barnes, C. A.; Bhuwalka, A.; Cai, M.; Shinar, J.; Shinar, R.; Jeffries-El, M. *Macromolecules* **2012**, *45*, 6888.
(13) Tang, C. W. *Applied Physics Letters* **1986**, *48*, 183.
(14) Zhang, L.; Hu, S.; Chen, J.; Chen, Z.; Wu, H.; Peng, J.; Cao, Y. *Advanced Functional Materials* **2011**, *21*, 3760.
(15) Forrest, S. R. *Organic Electronics* **2003**, *4*, 45.
(16) Bronstein, H.; Chen, Z.; Ashraf, R. S.; Zhang, W.; Du, J.; Durrant, J. R.; Shakya Tuladhar, P.; Song, K.; Watkins, S. E.; Geerts, Y.; Wienk, M. M.; Janssen, R. A.

J.; Anthopoulos, T.; Sirringhaus, H.; Heeney, M.; McCulloch, I. *Journal of the American Chemical Society* **2011**, *133*, 3272.
(17) Lee, W.-Y.; Giri, G.; Diao, Y.; Tassone, C. J.; Matthews, J. R.; Sorensen, M. L.; Mannsfeld, S. C. B.; Chen, W.-C.; Fong, H. H.; Tok, J. B. H.; Toney, M. F.; He, M.; Bao, Z. *Advanced Functional Materials* **2014**, *24*, 3524.
(18) Jones, B. A.; Ahrens, M. J.; Yoon, M.-H.; Facchetti, A.; Marks, T. J.; Wasielewski, M. R. *Angewandte Chemie* **2004**, *116*, 6523.
(19) Zhan, X.; Tan, Z. a.; Domercq, B.; An, Z.; Zhang, X.; Barlow, S.; Li, Y.; Zhu, D.; Kippelen, B.; Marder, S. R. *Journal of the American Chemical Society* **2007**, *129*, 7246.
(20) Babel, A.; Jenekhe, S. A. *The Journal of Physical Chemistry B* **2002**, *106*, 6129.
(21) Gaudiana, R.; Brabec, C. *Nat Photon* **2008**, *2*, 287.
(22) Peter, L. M. *Philosophical Transactions of the Royal Society A: Mathematical, Physical and Engineering Sciences* **2011**, *369*, 1840.
(23) Jørgensen, M.; Norrman, K.; Krebs, F. C. *Solar Energy Materials and Solar Cells* **2008**, *92*, 686.
(24) Klaver, A.; van Swaaij, R. A. C. M. M. *Solar Energy Materials and Solar Cells* **2008**, *92*, 50.
(25) Allard, S.; Forster, M.; Souharce, B.; Thiem, H.; Scherf, U. *Angewandte Chemie International Edition* **2008**, *47*, 4070.
(26) Shaheen, S. E.; Ginley, D. S.; Jabbour, G. E. *MRS Bulletin* **2005**, *30*, 10.
(27) Hoth, C. N.; Schilinsky, P.; Choulis, S. A.; Brabec, C. J. *Nano Letters* **2008**, *8*, 2806.
(28) Hebner, T. R.; Wu, C. C.; Marcy, D.; Lu, M. H.; Sturm, J. C. *Applied Physics Letters* **1998**, *72*, 519.
(29) Yang, Y.; Wudl, F. *Advanced Materials* **2009**, *21*, 1401.
(30) Günes, S.; Neugebauer, H.; Sariciftci, N. S. *Chemical Reviews* **2007**, *107*, 1324.
(31) Roncali, J. *Chemical Reviews* **1997**, *97*, 173.
(32) van Mullekom, H. A. M.; Vekemans, J. A. J. M.; Havinga, E. E.; Meijer, E. W. *Materials Science and Engineering: R: Reports* **2001**, *32*, 1.
(33) Moliton, A.; Hiorns, R. C. *Polymer International* **2004**, *53*, 1397.
(34) Yannoni, C. S.; Clarke, T. C. *Physical Review Letters* **1983**, *51*, 1191.
(35) Peierls, R. E. *Quantum Theory of Solids*; Oxford University Press: London, 1956.
(36) Liu, Q.; Liu, W.; Yao, B.; Tian, H.; Xie, Z.; Geng, Y.; Wang, F. *Macromolecules* **2007**, *40*, 1851.
(37) Havinga, E. E.; Rotte, I.; Meijer, E. W.; Hoeve, W. T.; Wynberg, H. *Synthetic Metals* **1991**, *41*, 473.
(38) Bredas, J. L.; Silbey, R.; Boudreaux, D. S.; Chance, R. R. *Journal of the American Chemical Society* **1983**, *105*, 6555.
(39) Rissler, J. *Chemical Physics Letters* **2004**, *395*, 92.
(40) Mei, J.; Heston, N. C.; Vasilyeva, S. V.; Reynolds, J. R. *Macromolecules* **2009**, *42*, 1482.
(41) Wudl, F.; Kobayashi, M.; Heeger, A. J. *The Journal of Organic Chemistry* **1984**, *49*, 3382.
(42) Pomerantz, M.; Gu, X. *Synthetic Metals* **1997**, *84*, 243.
(43) Brédas, J. L. *The Journal of Chemical Physics* **1985**, *82*, 3808.

(44) Mahmood, K.; Lu, H.; Liu, Z.-P.; Li, C.; Lu, Z.; Liu, X.; Fang, T.; Peng, Q.; Li, G.; Li, L.; Bo, Z. *Polymer Chemistry* **2014**, *5*, 5037.
(45) Brocks, G.; Tol, A. *The Journal of Physical Chemistry* **1996**, *100*, 1838.
(46) Kanimozhi, C.; Yaacobi-Gross, N.; Burnett, E. K.; Briseno, A. L.; Anthopoulos, T. D.; Salzner, U.; Patil, S. *Physical Chemistry Chemical Physics* **2014**, *16*, 17253.
(47) Yang, L.; Zhou, H.; You, W. *The Journal of Physical Chemistry C* **2010**, *114*, 16793.
(48) Szarko, J. M.; Guo, J.; Liang, Y.; Lee, B.; Rolczynski, B. S.; Strzalka, J.; Xu, T.; Loser, S.; Marks, T. J.; Yu, L.; Chen, L. X. *Advanced Materials* **2010**, *22*, 5468.
(49) Nelson, J. *Current Opinion in Solid State and Materials Science* **2002**, *6*, 87.
(50) Kline, R. J.; McGehee, M. D.; Kadnikova, E. N.; Liu, J.; Fréchet, J. M. J. *Advanced Materials* **2003**, *15*, 1519.
(51) Lin, J. D. A.; Liu, J.; Kim, C.; Tamayo, A. B.; Proctor, C. M.; Nguyen, T.-Q. T. *RSC Advances* **2014**.
(52) Shirota, Y.; Kageyama, H. *Chemical Reviews* **2007**, *107*, 953.
(53) Arias, A. C.; MacKenzie, J. D.; Stevenson, R.; Halls, J. J. M.; Inbasekaran, M.; Woo, E. P.; Richards, D.; Friend, R. H. *Macromolecules* **2001**, *34*, 6005.
(54) Osman, A. M. M., S. A *Indian Journal of Chemistry* **1973**, *11*, 868.
(55) Osman, A. M. M., S. A. *United Arab Republic Journal of Chemistry* **1971**, *15* 475.
(56) Osman, A.-M.; Khalil, Z. H. *Journal of Applied Chemistry and Biotechnology* **1975**, *25*, 683.
(57) Wolfe, J. F.; Arnold, F. E. *Macromolecules* **1981**, *14*, 909.
(58) Choe, E. W.; Kim, S. N. *Macromolecules* **1981**, *14*, 920.
(59) Allen, S. R.; Filippov, A. G.; Farris, R. J.; Thomas, E. L.; Wong, C. P.; Berry, G. C.; Chenevey, E. C. *Macromolecules* **1981**, *14*, 1135.
(60) Alam, M. M.; Jenekhe, S. A. *Chemistry of Materials* **2002**, *14*, 4775.
(61) Jenekhe, S. A.; Osaheni, J. A. *Chemistry of Materials* **1994**, *6*, 1906.
(62) Osaheni, J. A.; Jenekhe, S. A. *Macromolecules* **1993**, *26*, 4726.
(63) Reinhardt, B. A.; Unroe, M. R.; Evers, R. C.; Zhao, M.; Samoc, M.; Prasad, P. N.; Sinsky, M. *Chemistry of Materials* **1991**, *3*, 864.
(64) Imai, Y.; Itoya, K.; Kakimoto, M.-a. *Macromolecular Chemistry and Physics* **2000**, *201*, 2251.
(65) Imai, Y.; Taoka, I.; Uno, K.; Iwakura, Y. *Die Makromolekulare Chemie* **1965**, *83*, 167.
(66) Kricheldorf, H. R.; Domschke, A. *Polymer* **1994**, *35*, 198.
(67) Mike, J. F.; Makowski, A. J.; Jeffries-El, M. *Organic Letters* **2008**, *10*, 4915.
(68) Mike, J. F.; Inteman, J. J.; Ellern, A.; Jeffries-El, M. *The Journal of Organic Chemistry* **2009**, *75*, 495.
(69) Mike, J. F.; Intemann, J. J.; Cai, M.; Xiao, T.; Shinar, R.; Shinar, J.; Jeffries-El, M. *Polymer Chemistry* **2011**, *2*, 2299.
(70) Mike, J. F.; Nalwa, K.; Makowski, A. J.; Putnam, D.; Tomlinson, A. L.; Chaudhary, S.; Jeffries-El, M. *Physical Chemistry Chemical Physics* **2011**, *13*, 1338.

(71) Intemann, J. J.; Mike, J. F.; Cai, M.; Bose, S.; Xiao, T.; Mauldin, T. C.; Roggers, R. A.; Shinar, J.; Shinar, R.; Jeffries-El, M. *Macromolecules* **2010**, *44*, 248.
(72) Mike, J. F.; Makowski, A. J.; Mauldin, T. C.; Jeffries-El, M. *Journal of Polymer Science Part A: Polymer Chemistry* **2010**, *48*, 1456.
(73) Tlach, B. C.; Tomlinson, A. L.; Bhuwalka, A.; Jeffries-El, M. *The Journal of Organic Chemistry* **2011**, *76*, 8670.
(74) Pauling, L. *Journal of the American Chemical Society* **1932**, *54*, 3570.
(75) Lin, H.-W.; Lu, C.-W.; Lin, L.-Y.; Chen, Y.-H.; Lin, W.-C.; Wong, K.-T.; Lin, F. *Journal of Materials Chemistry A* **2013**, *1*, 1770.
(76) Su, S.-J.; Chiba, T.; Takeda, T.; Kido, J. *Advanced Materials* **2008**, *20*, 2125.
(77) Ying, L.; Hsu, B. B. Y.; Zhan, H.; Welch, G. C.; Zalar, P.; Perez, L. A.; Kramer, E. J.; Nguyen, T.-Q.; Heeger, A. J.; Wong, W.-Y.; Bazan, G. C. *Journal of the American Chemical Society* **2011**, *133*, 18538.
(78) Thompson, B. C.; Fréchet, J. M. J. *Angewandte Chemie International Edition* **2008**, *47*, 58.
(79) Yook, K. S.; Lee, J. Y. *Advanced Materials* **2014**, *26*, 4218.
(80) Duan, L.; Hou, L.; Lee, T.-W.; Qiao, J.; Zhang, D.; Dong, G.; Wang, L.; Qiu, Y. *Journal of Materials Chemistry* **2010**, *20*, 6392.
(81) Lin, Y.; Li, Y.; Zhan, X. *Chemical Society Reviews* **2012**, *41*, 4245.
(82) Lee, O. P.; Yiu, A. T.; Beaujuge, P. M.; Woo, C. H.; Holcombe, T. W.; Millstone, J. E.; Douglas, J. D.; Chen, M. S.; Fréchet, J. M. J. *Advanced Materials* **2011**, *23*, 5359.
(83) Sharenko, A.; Proctor, C. M.; van der Poll, T. S.; Henson, Z. B.; Nguyen, T.-Q.; Bazan, G. C. *Advanced Materials* **2013**, *25*, 4403.
(84) van der Poll, T. S.; Love, J. A.; Nguyen, T.-Q.; Bazan, G. C. *Advanced Materials* **2012**, *24*, 3646.
(85) Park, H. R.; Kim, J.; Kim, T.; Jo, S.; Yeom, M.; Moon, B.; Choo, I. H.; Lee, J.; Lim, E. J.; Park, K. D.; Min, S.-J.; Nam, G.; Keum, G.; Lee, C. J.; Choo, H. *Bioorganic & Medicinal Chemistry* **2013**, *21*, 5480.
(86) G. A. M. El-Hag Ali; A. Khalil; A. H. A. Ahmed; El-Gaby, M. S. A. *Acta Chim. Slov* **2002**, 365
(87) Shen, T. Y.; Clark, R. L.; Pessolano, A. A.; Witzel, B. E.; Lanza, T. J.; Google Patents: 1978.
(88) Chen, J. J.; Ing Jing, W. *Dyes and Pigments* **1996**, *30*, 173.
(89) Liang, Y.; Xu, Z.; Xia, J.; Tsai, S.-T.; Wu, Y.; Li, G.; Ray, C.; Yu, L. *Advanced Materials* **2010**, *22*, E135.
(90) Zhou, H.; Yang, L.; Stuart, A. C.; Price, S. C.; Liu, S.; You, W. *Angewandte Chemie International Edition* **2011**, *50*, 2995.
(91) Ye, L.; Zhang, S.; Huo, L.; Zhang, M.; Hou, J. *Accounts of Chemical Research* **2014**, *47*, 1595.
(92) Huo, L.; Hou, J.; Zhang, S.; Chen, H.-Y.; Yang, Y. *Angewandte Chemie International Edition* **2010**, *49*, 1500.
(93) Nakano, M.; Niimi, K.; Miyazaki, E.; Osaka, I.; Takimiya, K. *The Journal of Organic Chemistry* **2012**, *77*, 8099.
(94) Huo, L.; Huang, Y.; Fan, B.; Guo, X.; Jing, Y.; Zhang, M.; Li, Y.; Hou, J. *Chemical Communications* **2012**, *48*, 3318.

(95) Huo, L.; Li, Z.; Guo, X.; Wu, Y.; Zhang, M.; Ye, L.; Zhang, S.; Hou, J. *Polymer Chemistry* **2013**, *4*, 3047.
(96) Zhang, Y.; Gao, L.; He, C.; Sun, Q.; Li, Y. *Polymer Chemistry* **2013**, *4*, 1474.
(97) Liu, B.; Chen, X.; Zou, Y.; He, Y.; Xiao, L.; Xu, X.; Li, L.; Li, Y. *Polymer Chemistry* **2013**, *4*, 470.
(98) Mitsui, C.; Soeda, J.; Miwa, K.; Tsuji, H.; Takeya, J.; Nakamura, E. *Journal of the American Chemical Society* **2012**, *134*, 5448.
(99) Ding, P.; Zhong, C.; Zou, Y.; Pan, C.; Wu, H.; Cao, Y. *The Journal of Physical Chemistry C* **2011**, *115*, 16211.
(100) Shi, S.; Xie, X.; Jiang, P.; Chen, S.; Wang, L.; Wang, M.; Wang, H.; Li, X.; Yu, G.; Li, Y. *Macromolecules* **2013**, *46*, 3358.
(101) http://www.renewableenergyworld.com/rea/tech/home.
(102) Lewis, N. S.; Nocera, D. G. *Proceedings of the National Academy of Sciences* **2006**, *103*, 15729.
(103) Turner, J. A. *Science* **1999**, *285*, 687.
(104) Powell, D. M.; Winkler, M. T.; Choi, H. J.; Simmons, C. B.; Needleman, D. B.; Buonassisi, T. *Energy & Environmental Science* **2012**, *5*, 5874.
(105) Brabec, C. J.; Sariciftci, N. S.; Hummelen, J. C. *Advanced Functional Materials* **2001**, *11*, 15.
(106) Fairley, P. In *IEEE Spectrum* 2004.
(107) http://www.nrel.gov/ncpv/images/efficiency_chart.jpg.
(108) Son, H. J.; Carsten, B.; Jung, I. H.; Yu, L. *Energy & Environmental Science* **2012**, *5*, 8158.
(109) He, Z.; Zhong, C.; Huang, X.; Wong, W.-Y.; Wu, H.; Chen, L.; Su, S.; Cao, Y. *Advanced Materials* **2011**, *23*, 4636.
(110) Chu, T.-Y.; Lu, J.; Beaupré, S.; Zhang, Y.; Pouliot, J.-R.; Zhou, J.; Najari, A.; Leclerc, M.; Tao, Y. *Advanced Functional Materials* **2012**, *22*, 2345.
(111) Chu, T.-Y.; Lu, J.; Beaupré, S.; Zhang, Y.; Pouliot, J.-R.; Wakim, S.; Zhou, J.; Leclerc, M.; Li, Z.; Ding, J.; Tao, Y. *Journal of the American Chemical Society* **2011**, *133*, 4250.
(112) He, Z.; Zhong, C.; Su, S.; Xu, M.; Wu, H.; Cao, Y. *Nat Photon* **2012**, *6*, 591.
(113) http://www.heliatek.com/wp-content/uploads/2013/01/130116_PR_Heliatek_achieves_record_cell_effiency_for_OPV.pdf 2013.
(114) Dennler, G.; Scharber, M. C.; Brabec, C. J. *Advanced Materials* **2009**, *21*, 1323.
(115) Kalowekamo, J.; Baker, E. *Solar Energy* **2009**, *83*, 1224.
(116) Min Nam, Y.; Huh, J.; Ho Jo, W. *Solar Energy Materials and Solar Cells* **2010**, *94*, 1118.
(117) Groves, C. *Energy & Environmental Science* **2013**, *6*, 1546.
(118) Dou, L.; You, J.; Hong, Z.; Xu, Z.; Li, G.; Street, R. A.; Yang, Y. *Advanced Materials* **2013**, *25*, 6642.
(119) Liu, J.; Shi, Y.; Yang, Y. *Advanced Functional Materials* **2001**, *11*, 420.
(120) Qi, B.; Wang, J. *Physical Chemistry Chemical Physics* **2013**, *15*, 8972.
(121) Hoppe, H.; Sariciftci, N. S. *Journal of Materials Research* **2004**, *19*, 1924.
(122) Marks, R. N.; Halls, J. J. M.; Bradley, D. D. C.; Friend, R. H.; Holmes, A. B. *Journal of Physics: Condensed Matter* **1994**, *6*, 1379.

(123) Wöhrle, D.; Meissner, D. *Advanced Materials* **1991**, *3*, 129.
(124) Tang, C. W. *Applied Physics Letters* **1986**, *48*, 183.
(125) Uchida, S.; Xue, J.; Rand, B. P.; Forrest, S. R. *Applied Physics Letters* **2004**, *84*, 4218.
(126) Jenekhe, S. A.; Yi, S. *Applied Physics Letters* **2000**, *77*, 2635.
(127) Breeze, A. J.; Salomon, A.; Ginley, D. S.; Gregg, B. A.; Tillmann, H.; Hörhold, H.-H. *Applied Physics Letters* **2002**, *81*, 3085.
(128) Peumans, P.; Yakimov, A.; Forrest, S. R. *Journal of Applied Physics* **2003**, *93*, 3693.
(129) Winder, C.; Sariciftci, N. S. *Journal of Materials Chemistry* **2004**, *14*, 1077.
(130) Yu, G.; Heeger, A. J. *Journal of Applied Physics* **1995**, *78*, 4510.
(131) J. J. M. Halls; C. A. Walsh; N. C. Greenham; E. A. Marseglia; R. H. Friend; &, S. C. M.; Holmes, A. B. *Nature* **1995**, *376*.
(132) M. Granström; K. Petritsch; A. C. Arias; A. Lux; &, M. R. A.; Friend, R. H. *Nature* **1998**, 257.
(133) N. S. Sariciftci; L. Smilowitz; A. J. Heeger; Wudl, a. F. *Science* **1992**, 1474.
(134) Allemand, P. M.; Koch, A.; Wudl, F.; Rubin, Y.; Diederich, F.; Alvarez, M. M.; Anz, S. J.; Whetten, R. L. *Journal of the American Chemical Society* **1991**, *113*, 1050.
(135) Brabec, C. J.; Zerza, G.; Cerullo, G.; De Silvestri, S.; Luzzati, S.; Hummelen, J. C.; Sariciftci, S. *Chemical Physics Letters* **2001**, *340*, 232.
(136) Singh, T. B.; Marjanović, N.; Matt, G. J.; Günes, S.; Sariciftci, N. S.; Montaigne Ramil, A.; Andreev, A.; Sitter, H.; Schwödiauer, R.; Bauer, S. *Organic Electronics* **2005**, *6*, 105.
(137) Treat, N. D.; Chabinyc, M. L. *Annual Review of Physical Chemistry* **2014**, *65*, 59.
(138) Campoy-Quiles, M.; Ferenczi, T.; Agostinelli, T.; Etchegoin, P. G.; Kim, Y.; Anthopoulos, T. D.; Stavrinou, P. N.; Bradley, D. D. C.; Nelson, J. *Nat Mater* **2008**, *7*, 158.
(139) Chen, L.-M.; Hong, Z.; Li, G.; Yang, Y. *Advanced Materials* **2009**, *21*, 1434.
(140) Lin, R.; Wright, M.; Gong, B.; Chan, K. H.; Tayebjee, M. J. Y.; Uddin, A. *physica status solidi (RRL) – Rapid Research Letters* **2014**, *9999*, n/a.
(141) van Duren, J. K. J.; Yang, X.; Loos, J.; Bulle-Lieuwma, C. W. T.; Sieval, A. B.; Hummelen, J. C.; Janssen, R. A. J. *Advanced Functional Materials* **2004**, *14*, 425.
(142) Shaheen, S. E.; Brabec, C. J.; Sariciftci, N. S.; Padinger, F.; Fromherz, T.; Hummelen, J. C. *Applied Physics Letters* **2001**, *78*, 841.
(143) Hoppe, H.; Sariciftci, N. S. *Journal of Materials Chemistry* **2006**, *16*, 45.
(144) Hammer, B. A. G.; Bokel, F. A.; Hayward, R. C.; Emrick, T. *Chemistry of Materials* **2011**, *23*, 4250.
(145) Lindner, S. M.; Hüttner, S.; Chiche, A.; Thelakkat, M.; Krausch, G. *Angewandte Chemie International Edition* **2006**, *45*, 3364.
(146) Chochos, C. L.; Choulis, S. A. *Progress in Polymer Science* **2011**, *36*, 1326.
(147) Yu, G.; Gao, J.; Hummelen, J. C.; Wudl, F.; Heeger, A. J. *Science* **1995**, *270*, 1789.
(148) Yao, E.-P.; Chen, C.-C.; Gao, J.; Liu, Y.; Chen, Q.; Cai, M.; Hsu, W.-C.; Hong, Z.; Li, G.; Yang, Y. *Solar Energy Materials and Solar Cells* **2014**, *130*, 20.

(149) Rispens, M. T.; Meetsma, A.; Rittberger, R.; Brabec, C. J.; Sariciftci, N. S.; Hummelen, J. C. *Chemical Communications* **2003**, 2116.
(150) Hoppe, H.; Niggemann, M.; Winder, C.; Kraut, J.; Hiesgen, R.; Hinsch, A.; Meissner, D.; Sariciftci, N. S. *Advanced Functional Materials* **2004**, *14*, 1005.
(151) Padinger, F.; Rittberger, R. S.; Sariciftci, N. S. *Advanced Functional Materials* **2003**, *13*, 85.
(152) Camaioni, N.; Ridolfi, G.; Casalbore-Miceli, G.; Possamai, G.; Maggini, M. *Advanced Materials* **2002**, *14*, 1735.
(153) Berggren, M.; Gustafsson, G.; Inganäs, O.; Andersson, M. R.; Wennerström, O.; Hjertberg, T. *Applied Physics Letters* **1994**, *65*, 1489.
(154) Uy, R. L.; Price, S. C.; You, W. *Macromolecular Rapid Communications* **2012**, *33*, 1162.
(155) Balakrishnan, K.; Datar, A.; Naddo, T.; Huang, J.; Oitker, R.; Yen, M.; Zhao, J.; Zang, L. *Journal of the American Chemical Society* **2006**, *128*, 7390.
(156) Yiu, A. T.; Beaujuge, P. M.; Lee, O. P.; Woo, C. H.; Toney, M. F.; Fréchet, J. M. J. *Journal of the American Chemical Society* **2011**, *134*, 2180.
(157) Li, Z.; Zhang, Y.; Tsang, S.-W.; Du, X.; Zhou, J.; Tao, Y.; Ding, J. *The Journal of Physical Chemistry C* **2011**, *115*, 18002.
(158) Kim, J. S.; Lee, Y.; Lee, J. H.; Park, J. H.; Kim, J. K.; Cho, K. *Advanced Materials* **2010**, *22*, 1355.
(159) Bundgaard, E.; Krebs, F. C. *Solar Energy Materials and Solar Cells* **2007**, *91*, 954.
(160) Scharber, M. C.; Mühlbacher, D.; Koppe, M.; Denk, P.; Waldauf, C.; Heeger, A. J.; Brabec, C. J. *Advanced Materials* **2006**, *18*, 789.
(161) Blouin, N.; Michaud, A.; Gendron, D.; Wakim, S.; Blair, E.; Neagu-Plesu, R.; Belletête, M.; Durocher, G.; Tao, Y.; Leclerc, M. *Journal of the American Chemical Society* **2007**, *130*, 732.

CHAPTER 2

A VERSATILE AND EFFICIENT SYNTHESIS OF BITHIOPHENE-BASED DICARBOXALDEHYDES

Submitted for review in RSC Advances

Achala Bhuwalka, Jared F. Mike, Jeremy J. Intemann, Arkady Ellern and Malika Jeffries-EL*

Department of Chemistry, Iowa State University, Ames IA 50011.

2.1 Abstract

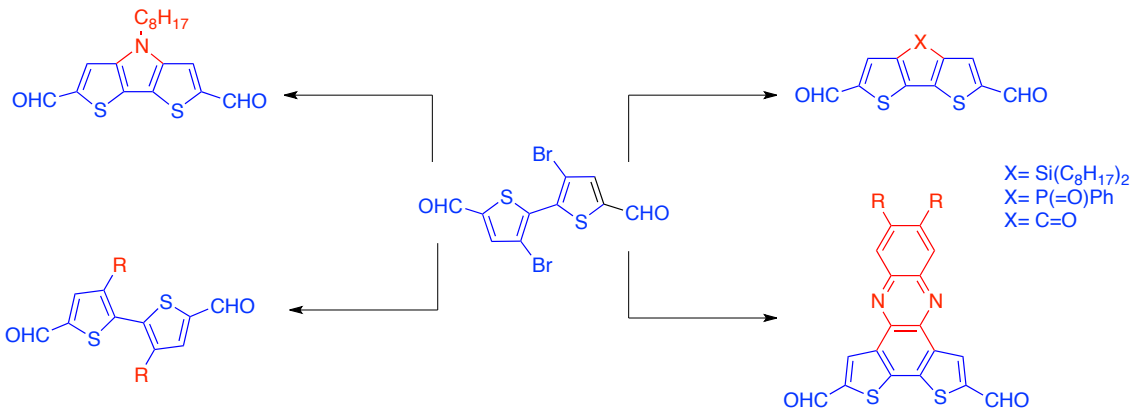

We report the synthesis of 2,2'-(3,3'-dibromo-[2,2'-bithiophene]-5,5'-diyl)bis(5,5-dimethyl-1,3-dioxane) in two high yielding steps from 3,3',5,5'-tetrabromo-2,2'-bithiophene. Subsequent reactions can be used to transform this

synthon into a variety of bithiophene-based dicarboxaldehydes, also in high yields. These functional molecules are promising building blocks for the development of arylene vinylene-based conjugated polymers.

2.2 Introduction

Conjugated polymers are continuingly being developed for use in organic semiconducting applications, such as field effect transistors (OFET)s,[1,2] light-emitting diodes (OLED)s,[3-5] and organic photovoltaic cells (OPV)s.[6,7] Of late, the synthesis of materials with alternating electron-donating and electron-accepting moieties has emerged as a useful approach for tailoring the properties of conjugated polymers.[8,9] Among building blocks, bridged bithiophenes such as 4*H*-cyclopenta[2,1-*b*:3,4- *b*']dithiophen-4-ones,[10,11] 4,4-dialkyl-4*H*- cyclopenta[2,1-*b*;3,4-*b'*]dithiophenes,[12,13] N-alkyl dithieno-[2,3-*b*:2',3'-*d*]pyrroles,[14-16] dialkyl-dithieno-[2,3-*b*:2', 3'-*d*]siloles,[12,17] and aryl-dithieno-[2,3-*b*:2',3'-*d*]phospholes[18,19] are promising for the development of polymers for use in bulk heterojunction photovoltaic cells. Materials comprising bridged bithiophenes possess broad optical absorption bands and high charge-carrier mobilities resulting in high photocurrent efficiencies.[10-12,17]

The properties of conjugated polymers can be further modified by the insertion of double bonds between the donor and acceptor units.[20-22] Vinylene spacers can reduce torsional interactions between the aromatic rings, thus increasing planarity and effective conjugation length while potentially decreasing the band-gap.[20-22] The Horner-Wadsworth-Emmons coupling reaction is an

excellent way to prepare vinylene-linked donor–acceptor (D-A) copolymers, provided that the acceptor is stable under the basic reaction conditions.[23,24] The benefits of this approach are that it produces exclusively *trans*-double bonds, does not require the use of expensive metal catalysts and is free of metal residue. Typically, the bridged 2,2'- bithiophene-5,5'- dicarboxaldehyde monomers required for this approach are synthesized by a ring closing reaction of 3,3'-dibromo-2,2'-bithiophene followed by formylation at the 5 and 5' positions via a Vilsmeier-Haack reaction using a large excess of both $POCl_3$ and DMF.[25,26] Alternatively, lithiation followed by quenching with DMF can be used. However, from our experience this approach often results in a mixture of the monoformylated and diformylated species, which can be difficult to separate. Herein, we report an efficient synthesis of a variety of bithiophene dialdehydes. The benefits of this approach include the use of a readily available starting materials, high yields, and access to a diverse assortment of functionalized arenes.

2.3 Results and Discussion

The synthesis for the 2,2'-(3,3'-dibromo-2,2'-bithiophene-5,5'-diyl)bis(5,5-dimethyl-1,3-dioxane) is shown in Scheme 2.1. 3,3',5,5'-tetrabromo-2,2'-bithiophene **(1)** was prepared in 79% yield over two steps: the nickel-catalyzed Kumada coupling reaction of commercially available 2-bromothiophene, followed by bromination of the resulting 2,2'-bithiophene in a mixture of $CHCl_3$ and AcOH.[27] Initially, **1** was first treated with ^{n}BuLi and then quenched the reaction with cold, dilute acid to obtain 3,3'-2,2'-dibromobithiophene in 75% yield. This

intermediate was then reacted with freshly prepared LDA to form a dianion, which upon reaction with anhydrous DMF afforded the 3,3'-dibromo-2,2'-bithiophene-5,5'-dicarbaldehyde **(2)** in 62% yield. This was an overall yield of 49%. A one pot synthesis of **2** was then attempted by first treating **1** with 2 equivalents of ^{n}BuLi followed by quenching with DMF (Scheme 2.1).[28] Using this approach the dialdehyde was obtained in 84% overall yield. In both cases, the product was easily isolated by precipitation, followed by filtration and recrystallization.

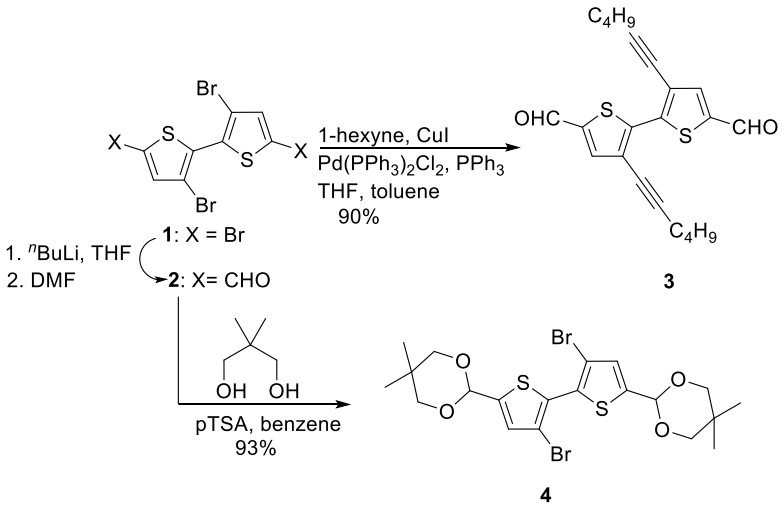

Scheme 2.1. Synthesis of 2,2'-(3,3'-dibromo-[2,2'-bithiophene]-5,5'-diyl)bis(5,5-dimethyl-1,3-dioxane) **4** and 3,3'-di(hex-1-yn-1-yl)-[2,2'-bithiophene]-5,5'-dicarbaldehyde **3**

2 is a useful intermediate for the synthesis a variety of different alkynyl substituted bithiophene-dicarboxaldehydes since the aldehyde groups are stable to the reaction conditions, eliminating the need for protecting groups. The Sonogashira cross-coupling reaction of **2** and 1-hexyne produced 3,3'-di(hex-1-ynyl)-2,2'-bithiophene-5,5'-dicarbaldehyde **(3)** in 90% yield. Furthermore, the

alkynes can be hydrogenated to yield the respective dialkyl compounds if desired. The dialdehyde **2** is also readily protected by reacting with neopentyl alcohol in the presence of catalytic amounts of *p*-toluenesulfonic acid in benzene to yield 2,2'-(3,3'-dibromo-[2,2'-bithiophene]-5,5'-diyl)bis(5,5-dimethyl-1,3-dioxane) **(4)** in 95% yield. Alternatively, ethylene glycol could be used to protect the aldehyde, however, we found that the diacetal made from neopentyl alcohol was more stable and allowed for easier purification. Furthermore, **4** is a solid that can be purified by recrystallization, facilitating large-scale synthesis.

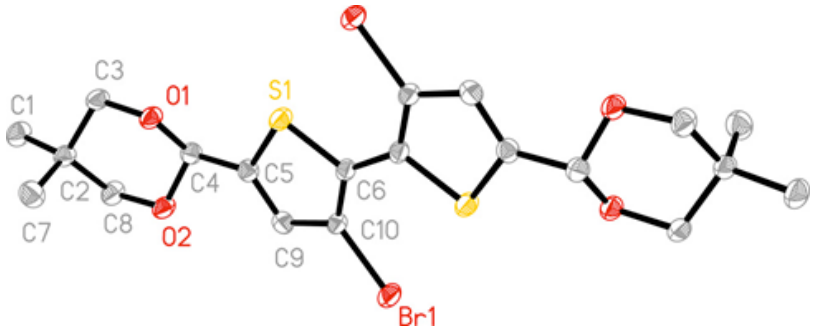

Figure 2.1 ORTEP of 4 drawn at 50% probability

We were able to obtain X-Ray quality crystals of **4** suitable for analyses via recrystallization. Detailed crystallographic data can be found in the Supporting Information, and the structure is shown in Figure 2.1. In addition to confirming the identity of this new compound, the X-Ray analyses indicate that the molecule is completely planar with the thiophene rings being orientated coplanar to each other. Despite the orientation of the rings, the cyclization reactions to form compounds **6** - **9** proceed readily.

As shown in Scheme 2.2, diacetal **4** can be used for the synthesis of various heterocyclic compounds from one common intermediate. The Hartwig-Buchwald reaction of **4** with octyl amine produced 2-(5,5'-dimethyl-1,3-dioxan-2-yl)-6-(2,2-dimethyl-1,3-dioxan-5-yl)-4-octyl-4*H*-dithieno[3,2-*b*:2',3'-*d*]pyrrole, which upon reaction with TFA affords the dialdehyde **(5)** in 52% yield after purification via column chromatography. The reaction of diacetal **4** with ^{n}BuLi in a 1:2 mixture of dry THF and ether produced a dianion, which can react with a number of electrophiles. The mixture of THF/ether was found to be advantageous as the lithium-bromine exchange was slow in neat THF and led to the formation of side-products. However, **4** is insoluble in neat diethyl ether; thus a mixture of ethyl ether and THF must be used. Quenching the anion of **4** with n-octyldichlorosilane, afforded the 2,6-bis(5,5'- dimethyl-1,3-dioxan-2-yl)-4,4-dioctyl-4*H*-silolo[3,2-*b*:4,5-*b'*]dithiophene **(6)** in 65% yield after recrystallization. The diacetal **6** was readily deprotected by refluxing with TFA in dichloromethane overnight to afford 4,4 -dioctyl-4*H*- silolo[3,2-*b*:4,5-*b'*]dithiophene-2,6-dicarboxaldehyde **(10)** in 67% yield as a low melting solid that was purified by cold crystallization.

The use of dichlorophenylphosphine as the electrophile produced 2,6-bis(5,5-dimethyl-1,3-dioxan-2- yl)-4-phenyl-4*H*-phospholo[3,2-*b*:4,5-*b'*]dithiophene 4-oxide (7) instead of the expected phosphole. The structure of 7 was confirmed by the ^{31}P-NMR, Figure 2.7.25 as well as X-ray crystallography (Figure 2.2).

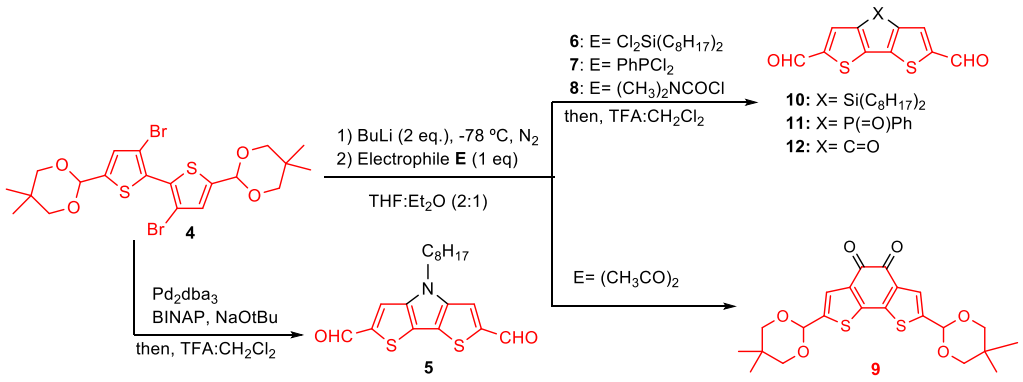

Scheme 2.2 Elaboration of ,2'-(3,3'-dibromo-[2,2'-bithiophene]-5,5'-diyl)bis(5,5-dimethyl-1,3-dioxane) **(4)**

Compound 7 was deprotected to produce 4-phenyl-4*H*-phospholo[3,2*b*:4,5-*b'*]dithiophene-2,6-dicarbaldehyde 4-oxide (11) in 75% yield after recrystallization. The use of N,N- dimethylcarbamoyl chloride as the electrophile yields 2,6- bis(5,5'-dimethyl-1,3-dioxan-2-yl)- 4*H*-cyclopenta[1,2-*b*:5,4-*b'*]dithiophen-4-one **(8)** as a bright red solid in 83% after purification via column chromatography. 4-oxo-4*H*-cyclopenta[1,2-*b*:5,4-*b'*]dithiophene-2,6-dicarbaldehyde **(12)** is obtained in 67% after recrystallization yield upon treating diacetal 8 with TFA. The structure of **12** was confirmed by X-Ray crystallography, (Figure 2.2).

The reaction of the dianion of 4 with dimethyloxalate produces 2,7-bis(5,5'-dimethyl-1,3-dioxan-2-yl)benzo[1,2-*b*:6,5-*b'*]dithiophene-4,5-dione (9), in 50% yield. Compound 9 is a versatile compound that can be further elaborated using condensation reactions to afford other new fused bithiophene dicarbaldehydes such

as dithienobenzofurazans, dithienobenzothiadiazoles or dithienobenzotriazoles as recently demonstrated.[29]

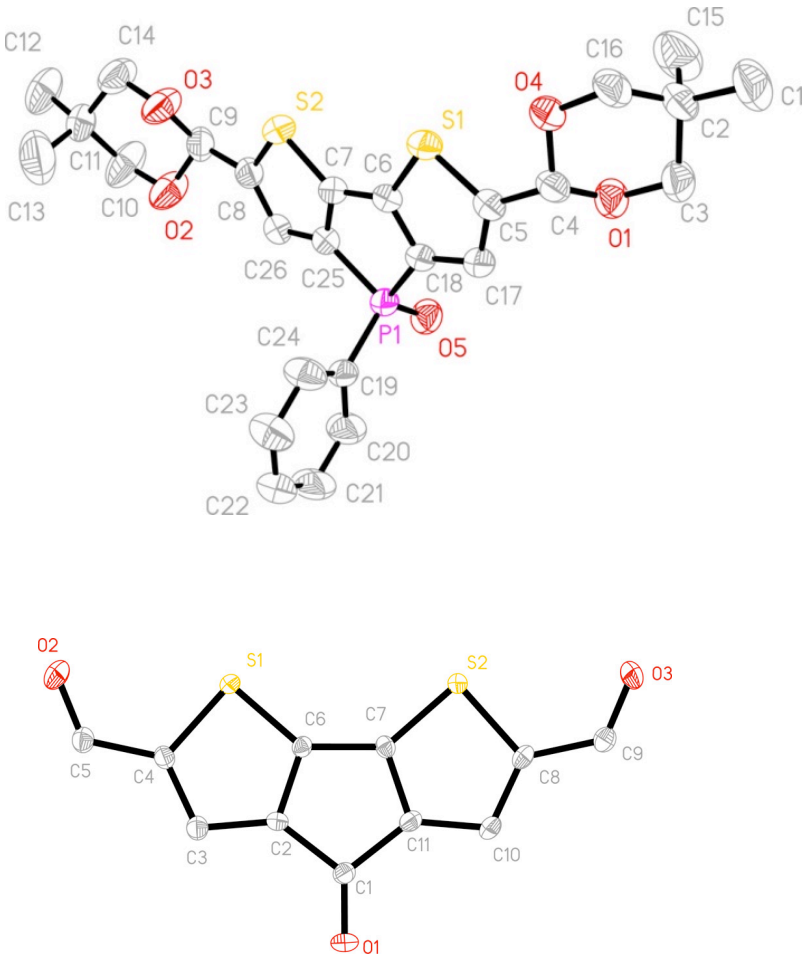

Figure 2.2 ORTEP of 7 (top) and 11 (bottom); ellipsoids are plotted at 50% probability, and the hydrogen atoms and a solvent molecule are not shown

For example, the condensation of **9** with 4,5-dibromobenzene-1,2-diamine afforded 9,10-dibromo-2,5-bis(5,5'-dimethyl-1,3-dioxan-2-yl)dithieno[3,2-*a*:2',3'-*b*]phenazine (**13)** in 80% yield, Scheme 2.3. The bromine atoms on **13** are reactive handles for further substitution to improve solubility or tune optical properties.

Thieno[3,4-*b*]pyrazines[30-32] and dithieno[3,2-*f*:2’ ,3’ -*h*]quinoxalines[33] have both been used as monomers for the synthesis of low band-gap conjugated polymers. As such, the related dithienophenazines are promising building blocks although they have not been as widely studied.[13,34]

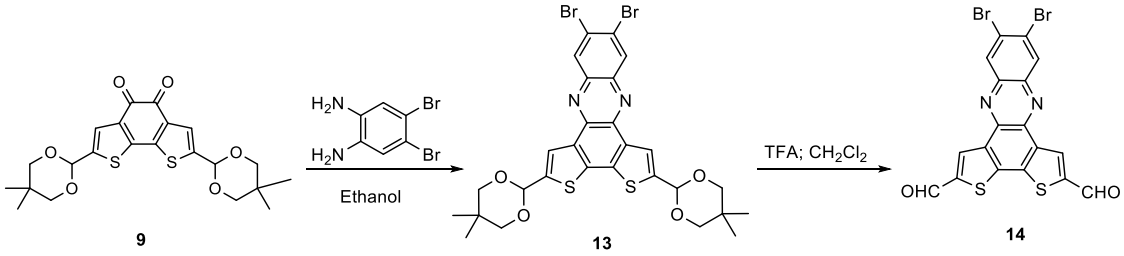

Scheme 2.3 Synthesis of dithieno[3,2-*a*:2',3'-*c*]phenazines

2.4 Conclusions

In conclusion, we report the efficient synthesis of a variety of bridged bithiophene dicarbaldehydes. The highlights of this work are the overall high yields of the reactions, the easy purification and the ability to synthesize a variety of compounds from one synthetic intermediate. We are currently developing new conjugated materials based on these compounds for use in OPVs, OLEDs and OFETs.

2.5 Experimental

2.5.1 Materials and General Experimental Details.

Tetrahydrofuran was dried using an Innovative Technologies solvent purification system. 2,2'-bithiophene, 3,3',5,5'-tetrabromo-2,2'-bithiophene **(1)** and 4,5-dibromobenzene-1,2-diamine were prepared according to literature procedures. All other compounds were purchased from commercial sources and used without further purification unless noted otherwise. All reactions were run under argon at ambient temperature unless otherwise noted.

Chromatographic separation was performed using 35 – 70 μm silica gel, using the eluents indicated. High-resolution mass spectra were recorded on a double-focusing magnetic sector mass spectrometer using EI at 70 eV. Uncorrected melting points were obtained using a melting point apparatus, upper temperature limit 260 °C.

2.5.2Instrumentation

Nuclear magnetic resonance spectra were obtained on a 400 MHz spectrometer (^{1}H at 400 MHz and ^{13}C at 100 MHz). ^{1}H NMR samples were referenced internally to residual protonated solvent ^{13}C NMR are referenced to the middle carbon peak of $CDCl_3$. In both instances chemical shifts are given in δ ppm relative to tetramethylsilane.

3,3'-dibromo-2,2'-bithiophene-5,5'-dicarbaldehyde (2)[28] 3,3',5,5'-tetrabromo-2,2'-bithiophene (20.0 g, 41.5 mmol) was dissolved in 200 mL of anhydrous THF

in a flame-dried round bottom flask. The solution was cooled to -78 °C in an acetone/dry ice bath. *n*-butyllithium (37.4 mL, 2.5 M in hexanes) was added drop wise. The resulting dianion was stirred at -78 °C for 2 hours, after which anhydrous DMF (8.0 mL, 103.7 mmol) was added. The solution was allowed to warm to room temperature overnight. The reaction was quenched by addition of 6 M HCl. The resulting solid was then filtered and washed with water. It was recrystallized from DMSO to give 13.2 g product as yellow needles in 84% yield, mp 247 – 248 ˚C.^{1}H NMR (400 MHz, DMSO-d_6) δ 9.93 (s, 2H), 8.23 (s, 2H); ^{13}C NMR (100 MHz, DMSO-d_6): δ 114.37, 135.80, 139.95, 144.30, 184.12.

3,3'-di(hex-1-ynyl)-2,2'-bithiophene-5,5'-dicarbaldehyde (3)[35]

3,3'-dibromo-2,2'-bithiophene-5,5'-dicarbaldehyde (2.0 g, 5.26 mmol), 1-hexyne (1.9 mL,15.8 mmol), triethylamine (6 mL), copper(I) iodide (6 mol%), triphenylphosphine (3 mol%) and THF (6mL) were added to a 2-neck round bottom flask equipped with a stir bar, condenser and an argon inlet. The solution was deoxygenated for 1 hour followed by the addition of bis(triphenylphosphine)palladium(II) dichloride (3 mol%). The resulting solution was refluxed for 6 hrs. Deoxygenated toluene (10 mL) was added and the reaction was refluxed overnight. The reaction was poured into water and the two layers were separated. The organic layer was rinsed with saturated NH_4Cl, brine and then dried over $MgSO_4$. After removal of the solvent, the crude product was purified via column chromatography (hexanes/EtOAc = 90:10) to give 1.8 g of a yellow solid in 90% yield, mp 78 - 80 ˚C. ^{1}H NMR (400 MHz, $CDCl_3$) δ 0.98 (t, J = 10 Hz,

6H), 1.69 (t, *J* = 10 Hz, 8H), 2.57 (t, *J* = 8 Hz, 4H), 7.71 (s, 2H), 9.91 (s, 2H); ^{13}C NMR (400 MHz, $CDCl_3$): 13.59, 19.75, 22.17, 29.96, 75.64, 101.56, 122.74, 139.27, 140.83, 143.67, 182.82. *m/z*: $[M + H]^+$ (EI) calcd for $C_{22}H_{23}O_2S_2$ = 383.1134, found 383.1127, deviation 1.83 ppm.

2,2'-(3,3'-dibromo-2,2'-bithiophene-5,5'-diyl)bis(5,5-dimethyl-1,3-dioxane) (4)[36]

In a round bottom flask equipped with a stir bar, dean stark apparatus, reflux condenser and an argon inlet, 3,3'-dibromo-2,2'-bithiophene-5,5'-dicarbaldehyde (8.0 g, 21. mmol), pTSA (0.36 g ,1.6 mmol) and neopentyl glycol (21.9 g, 210.5 mmol) were refluxed in benzene (200 mL) for 18 hours. Water was added to the reaction and the layers separated. The organic layer was washed thoroughly with water to remove excess neopentyl glycol (8 X 100 mL), followed by brine and then dried over $MgSO_4$. The solvent was removed *in vacuo*. The solid obtained was recrystallized from a mixture of hexanes and ethyl acetate to give 11.03 g of a light pink solid in 95% yield, mp 136 – 138 °C. ^{1}H NMR (400 MHz, $CDCl_3$) δ 0.80 (s, 6H), 1.26 (s, 6H), 3.63 (d, *J* = 4 Hz, 4H), 3.76 (d, *J* = 4 Hz, 4H), 5.58 (s, 2H), 7.10 (s, 2H); ^{13}C NMR: δ (100 MHz, $CDCl_3$) δ 21.79, 22.95, 30.23, 77.46, 97.38, 111.76, 128.50, 129.03, 142.98.. *m/z*: $[M + H]^+$ (EI) calcd for $C_{20}H_{24}Br_2O_4S_2$ = 550.9556, found 550.9549, deviation 1.19 ppm

2-(5,5-dimethyl-1,3-dioxan-2-yl)-6-(2,2-dimethyl-1,3-dioxan-5-yl)-4-octyl-4*H*-dithieno[3,2-*b*:2',3'-*d*]pyrrole (S2.1)[37]

(4) (1.5g, 2.7 mmol), BINAP (169 mg, 271.5 µmols) and NaO^{t}Bu (0.63 g, 6.5 mmol) were dissolved in dry toluene (8 mL). The solution was purged with argon for 20 minutes. An argon purged solution of tris(dibenzylideneacetone)-dipalladium(0) (74.6 mg, 81.47 µmol) dissolved in dry toluene (2 mL) was added to the flask and the resulting solution was further purged with argon for 15 minutes. *n*-Octylamine (386 mg, 2.99 mmol) was then added and the reaction was allowed to stir at 110 °C for 48 hours. The reaction was cooled to room temperature and water (15 mL) was then added. The product was extracted with diethyl ether, washed with water, and dried over Na_2SO_4. The solvent was removed under reduced pressure. Recrystallization from a mixture of hexanes/Et_2O gave 0.75g product as a yellow solid in 53% yield, mp 200 – 201 ˚C. NMR (400 MHz, $CDCl_3$) δ 0.81 (s, 6H), 0.870 (t, J = 6 Hz, 3H), 1.23- 1.28 (m, 10H), 1.30 (s, 6H), 1.81 (t, 6 Hz, 2H), 3.66 (d, J = 4 Hz, 4H), 3.78 (d, J = 4 Hz, 4H), 4.1 (t, 8 Hz, 2H), 5.67(s, 2H), 7.08 (s, 2H); ^{13}C NMR (100 MHz, $CDCl_3$: δ 14.07, 21.86, 22.60, 23.00, 26.96, 29.13, 29.20, 30.26, 30.36, 31.78, 47.27, 77.53, 98.77, 109.21, 114.68, 138.50, 143.22. *m/z*: $[M + H]^+$ (EI) calcd for $C_{28}H_{42}NO_4S_2$=520.255, found 519.2477, deviation 0.73 ppm.

4-octyl-4*H*-dithieno[3,2-*b*:2',3'-*d*]pyrrole-2,6-dicarbaldehyde (5)[36]

(S1) (0.4g, 0.76 mmol) was dissolved in TFA (28 mL) and water (3 mL). The solution was heated to boiling and then allowed to cool to room temperature. It

was then poured into water. The product was extracted with dichloromethane and carefully washed with 6M NaOH, followed by water. The crude product was purified by column chromatography using dichloromethane as the eluent to give 0.14 g as a yellow solid in 52% yield, mp 118-120 °C. ^{1}H NMR (400 MHz, $CDCl_3$) δ 0.86 (t, 3H, J = 8 Hz), 1.25 (s, 10H, broad), 1.30 (s, 3H, broad), 1.92 (t, J = 6 Hz, 2H), 4.27 (t, J = 6 Hz, 2H), 7.69(s, 2H), 9.95(s, 2H); ^{13}C NMR (100 MHz, $CDCl_3$): δ 14.04, 22.56, 27.00, 29.06, 29.11, 29.69, 30.25, 31.70, 47.68, 118.71, 121.94, 144.12, 147.25, 183.22. *m/z*: $[M + H]^+$ (EI) calcd for $C_{18}H_{21}NO_2S_2$ = 348.1086, found 348.1092, deviation -1.59ppm.

2,6-bis(5,5-dimethyl-1,3-dioxan-2-yl)-4,4-dioctyl-4*H*-silolo[3,2-*b*:4,5-*b*′]dithiophene (6)[38]

(4) (5.52 g, 10 mmol) was dissolved in THF (50 mL) and anhydrous ethyl ether (100 mL) in a flame-dried round bottom flask. The solution was cooled to -78 °C. *n*-butyllithium (8 mL, 2.5 M in hexanes) was added drop wise. The mixture was allowed to stir for 2 hours at -78 °C followed by the addition of dichlorodioctylsilane (3.25 g, 10 mmol). The reaction was kept at -78 °C for 2 more hours and then allowed to warm up to room temperature overnight. Saturated ammonium chloride solution (100 mL) was added to the reaction flask and the mixture was extracted with ether (3x100 mL). The organic extracts were combined and washed with brine and then dried over $MgSO_4$ followed by evaporation of the solvent. The residue was then recrystallized from 95% ethanol to give 4.2 g of a yellow solid in 65% yield, mp 96-97 °C. ^{1}H NMR (400 MHz,

$CDCl_3$) δ 0.80-0.85 (br, 10H), 0.86 (t, J = 6 Hz, 6H), 1.20 – 1.30 (br, 30H), 3.64 (d, J = 4 Hz, 4H), 3.76 (d, J = 6 Hz, 4H), 5.63 (s, 2H), 7.06 (s, 2H); ^{13}C NMR (100 MHz, $CDCl_3$): δ 9.214, 11.531, 19.246, 19.265, 20.068, 20.429, 21.528, 26.568, 26.649, 27.623, 29.284, 30.738, 75.033, 95.868, 125.083, 138.437, 138.930, 146.937. *m/z*: $[M + H]^+$ (EI) calcd for $C_{36}H_{58}O_4S_2Si$ = 647.3619 found 647.3601, deviation 2.71 ppm.

2,6-bis(5,5-dimethyl-1,3-dioxan-2-yl)-4-phenyl-4*H*-phospholo[3,2-*b*:4,5-*b'*]dithiophene 4-oxide (7)[39]

(4) (1.5 g, 2.7 mmol) was dissolved in anhydrous ethyl ether (40 mL), and anhydrous THF (15 mL). TMEDA (3 eq) was then added. The solution was cooled to -78 ˚C. *n*-butyllithium (2.2 mL, 2.5 M in hexanes) was added drop wise. The solution was stirred at this temperature for 1 hr before it was raised to approximately -20 ˚C. Dichlorophenylphosphine (0.38 mL, 2.7 mmol) was then slowly added to the reaction mixture which was allowed to warm quickly to room temperature. The solvent was removed under reduced pressure; the residue was taken up in pentanes, and filtered through neutral alumina. The solvent was removed under reduced pressure to obtain product. The compound was recrystallized from a mixture of hexanes and chloroform to give 1.1 g product as a yellow solid in 79% yield. ^{1}H NMR (400 MHz, $CDCl_3$) δ 0.78 (s, 6H), 1.25 (s, 6H), 3.61 (d, J = 11.5 Hz, 4H), 3.78 – 3.69 (m, 4H), 5.57 (s, 2H), 7.12 (d, 2H), 7.37 (td, J = 7.6, 3.2 Hz, 2H), 7.49 (td, J = 7.3, 1.5 Hz, 1H), 7.64–7.73 (m, 2H). ^{31}P NMR (162 MHz, $CDCl_3$) δ 18.87; ^{13}C NMR (100 MHz, $CDCl_3$) δ 21.75, 22.91,

30.18, 77.47 (d, J = 2.2 Hz), 97.54 (d, J = 1.4 Hz), 123.72 (d, J = 14.5 Hz), 128.83 (d, J = 13.1 Hz), 129.24 (d, J = 108 Hz), 130.90 (d, J = 11.5 Hz), 132.38 (d, J = 3.1 Hz), 137.80 (d, J = 112.3 Hz), 145.34 (d, J = 13.9 Hz), 145.74 (d, J = 23.5 Hz) *m/z*: $[M + H]^+$ (EI) calcd for $C_{26}H_{29}PS_2O_5$ = 517.1267, found 517.1261, deviation 1.12 ppm.

2,6-bis(5,5-dimethyl-1,3-dioxan-2-yl)-4-oxo-4*H*-Cyclopenta[2,1-*b*:3,4-*b*′]dithiophene (8)[40]

(4) (0.6 g, 1.09 mmol) was dissolved in anhydrous ethyl ether (24 mL) and anhydrous THF (10 mL). The flask was cooled to -78˚C and *n*-butyllithium (0.9 mL, 2.5 M in hexanes) was added drop wise. The resulting solution was stirred for 1 hr at-78 °C before addition of N,N-dimethylcarbamoyl chloride (0.1 mL, 1.09 mmol) in THF (1 mL). The reaction was warmed to 0˚C and stirred for 8 hrs. The reaction was quenched by addition of sat NH_4Cl, extracted with ether, dried over $MgSO_4$, filtered and the solvent was removed *in vacuo*. The product was purified by column chromatography (hexanes: ethyl acetate = 3:1) to give 0.46 g of deep red solid in 83% yield, mp 226 – 228 ˚C. NMR (400 MHz, $CDCl_3$) δ 0.79 (s, 6H), 1.26 (s, 6H), 3.615 (d, J = 6 Hz, 4H), 3.735 (d, J = 6 Hz, 4H), 5.530 (s, 2H), 6.980 (s, 2H). ^{13}C NMR (100 MHz, $CDCl_3$): 21.76, 22.87, 30.14, 7.41, 97.50, 119.50, 140.82, 144.29, 149.23, 182.85. *m/z*: $[M + H]^+$ (EI) calcd for $C_{21}H_{24}O_5S_2$ = 421.1138, found 421.1145 deviation -1.69 ppm.

2,7-bis(5,5-dimethyl-1,3-dioxan-2-yl)benzo[1,2-*b*:6,5-*b'*]dithiophene-4,5-dione (9)[40]

(4) (1.2 g, 2.18 mmol) was dissolved in anhydrous ethyl ether (30 mL) and anhydrous THF (15 mL). The solution was cooled to -78 ˚C and *n*-butyllithium (2.0 mL, 2.5 M in hexanes) was added drop wise. The solution was stirred for 1 h at -78 °C before addition of dimethyloxalate (0.26 g, 2.18 mmol). The solution was allowed to warm to room temperature overnight. The reaction was quenched with satd. NH_4Cl followed by extraction with ethyl ether. The organic layer was dried over $MgSO_4$, filtered, and the solvent was removed under reduced pressure. The compound was purified by column chromatography (Hexanes: EtOAc = 70:30) to give a 0.7 g of a deep red solid in 70% yield, mp 208 – 210 ˚C.

^{1}H NMR (400 MHz, $CDCl_3$) δ 7.47 (s, 2H), 5.58(s, 2H), 3.75 (d, *J* = 6 Hz, 4H), 3.63 (d, *J* = 6 Hz, 4H), 1.27(s, 6H), 0.81(s, 6H). ^{13}C NMR (100 MHz, $CDCl_3$): δ 21.73, 22.87, 30.18, 77.41, 96.98, 125.04, 134.75, 142.42, 143.78,174.28. *m/z*: $[M + H]^+$ (EI) calculated for $C_{22}H_{24}O_6S_2$ = 449.1087, found 448.1014, deviation 0.46 ppm.

4*H*-silolo[3,2-b:4,5-b']dithiophene-2,6-dicarboxaldehyde, 4,4-dioctyl- (10)[36]

(6) (0.35 g, 0.5 mmol) was dissolved in dichloromethane (10 mL) and water (1 mL). TFA (4 mL) was added and the resulting solution was refluxed overnight. The reaction was cooled to room temperature, quenched by the careful addition of satd. sodium bicarbonate and extracted with dichloromethane. The organic layer was dried over $MgSO_4$, filtered and the solvent was removed under reduced

pressure. Recrystallization from cold pentanes gave a 0.17 g of product as a yellow solid in 67% yield, mp 27 – 28 ˚C.

^{1}H NMR (400 MHz, $CDCl_3$) δ 0.860 (t, *J* =6.8 Hz, 6H), 0.970 (t, *J* = 8.0 Hz, 4H), 1.215 - 1.271 (m, 24H), 7.756 (s, 2H), 9.934 (s, 2H); ^{13}C NMR (100 MHz, $CDCl_3$): δ 11.449, 14.081, 22.609, 24.041, 29.049, 29.109, 31.790, 33.055, 138.844, 146.194, 147.040, 156.292, 182.876. *m/z*: $[M + H]^+$ (EI) calcd for $C_{26}H_{39}O_2S_2Si$ =475.2155 found 474.2082, deviation 0.26ppm

4-phenyl-4*H*-phospholo[3,2-*b*:4,5-*b'*]dithiophene-2,6-dicarbaldehyde 4-oxide (11)[36]

(7) (0.8 g, 1.5 mmol) was dissolved in dichloromethane (10 mL) and water (2 mL). TFA (7 mL) was added and the solution was refluxed overnight. The reaction was cooled to ambient temperature, poured into water and carefully neutralized with sodium bicarbonate. The organic layer was separated, washed with water and dried over $MgSO_4$. The solvent was removed under reduced pressure and the product was purified via recrystallization from mixture of hexanes and chloroform to give 1.1 g of a yellow solid in 75% yield, mp 220-222 ˚C

^{31}P NMR (162 MHz, $CDCl_3$) δ 16.45. ^{1}H NMR (400 MHz, $CDCl_3$) δ 7.49 (s, 2H), 7.62 (t, 1H, *J* = 8.0 Hz), 7.72 (dd, 2H), 7.83 (s, 2H), 9.90 (s, 2H); ^{13}C NMR (100 MHz, $CDCl_3$) δ 127.21 (d, *J* = 111.2 Hz), 129.39 (d, *J* = 13.5 Hz), 130.77 (d, *J* = 11.6 Hz), 133.48 (d, *J* = 3.1 Hz), 134.01 (d, *J* = 13.3 Hz), 142.15 (d, *J* = 109.4 Hz), 149.10 (d, *J* = 12.2 Hz), 151.35 (d, *J* = 21.8 Hz), 182.23. *m/z*: $[M + H]^+$ (EI) calcd for $C_{16}H_9PS_2O_3$ = 344.9803, found 344.9813, deviation -2.77 ppm.

4-oxo-4*H*-cyclopenta[1,2-*b*:5,4-*b*']dithiophene-2,6-dicarbaldehyde (12)[36]

(8) (0.25 g, 0.6 mmol) was dissolved in dichloromethane (50 mL), TFA (7 mL), and water (1 mL). The solution was refluxed overnight. The reaction was cooled to room temperature, poured into water and carefully neutralized with sodium bicarbonate. The organic layer was separated, washed with water and dried over $MgSO_4$. The solvent was removed under reduced pressure and the product was purified via recrystallization from DMSO to give 0.1 g of a red solid in 67% yield. NMR (400 MHz, $CDCl_3$): δ 8.04 (s, 2H), 9.86 (s, 2H).

9,10-dibromo-2,5-bis(5,5-dimethyl-1,3-dioxan-2-yl)dithieno[3,2-*a*:2',3'-*c*]phenazine (13)[34]

(15) (1.0 g, 2.2 mmol) and 4,5-dibromobenzene-1,2-diamine (0.59 g, 2.2 mmol) were dissolved in 95% ethanol (50 mL). The resulting solution was refluxed overnight. The reaction was cooled in an ice bath for 2 hours and then filtered. 1.2 g of the product was obtained in 80% yield) as a yellow solid and used without further purification.

^{1}H NMR (400 MHz, $CDCl_3$) δ 8.58 (s, 2H), 8.36 (s, 2H), 5.84 (s, 2H), 3.85 (d, J = 6 Hz, 4H), 3.75 (d, J = 6 Hz, 4H), 1.34 (s, 6H), 0.86 (s, 6H) ^{13}C NMR (100 MHz, $CDCl_3$) δ 21.86, 23.02, 30.32, 77.59, 97.98, 122.83, 126.13, 133.14, 134.07, 136.74, 140.33, 140.57, 141.31. The compound did not melt below 260 ˚C. *m/z*: $[M + H]^+$ (EI) calcd for $C_{28}H_{26}Br_2N_2O_4S_2$ = 676.9774, found 676.9701, deviation 1.41 ppm.

9,10-dibromodithieno[3,2-*a*:2',3'-*c*]phenazine-2,5-dicarbaldehyde (14)[36]

(13) (0.15 g, 0.2 mmol) was dissolved in TFA (7 mL) and water (1 mL). The solution was heated to boiling directly on hot plate. The reaction was cooled to room temperature, poured into water and carefully neutralized. The solid obtained was filtered and washed with water. 0.08 g of product was obtained in 72% yield. Due to poor solubility in any of the solvents, only ^{1}H-NMR was obtained.

^{1}H NMR (400 MHz, $CDCl_3$): δ 8.68 (s, 2H), 9.05 (s, 2H), 10.24(s, 2H). The compound did not melt below 260 ˚C

2.6 Acknowledgements

We are grateful to the National Science Foundation (DMR-0846607) for their generous support of this work. We thank Dr. Kamel Harrata and the Mass Spectroscopy Laboratory Iowa State University (ISU) and the ISU Crystallographic facility for analysis of our compounds. We thank Professor Aaron Sadow for help with processing the crystallographic data and Sarah Cady for assistance with phosphorus NMR.

2.7 Supplementary Information

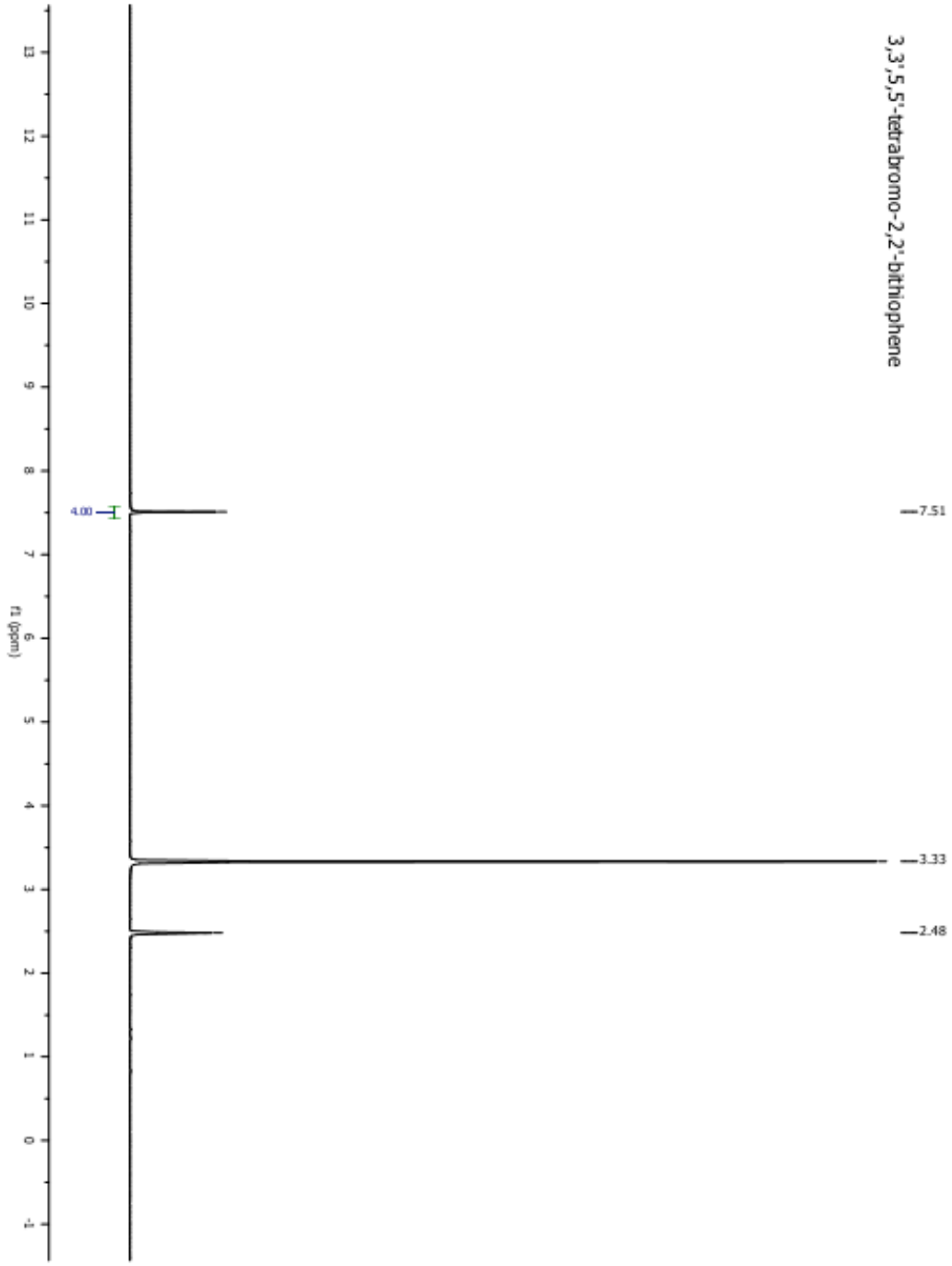

Figure 2.7.1: ^{1}H NMR spectra of compound 1

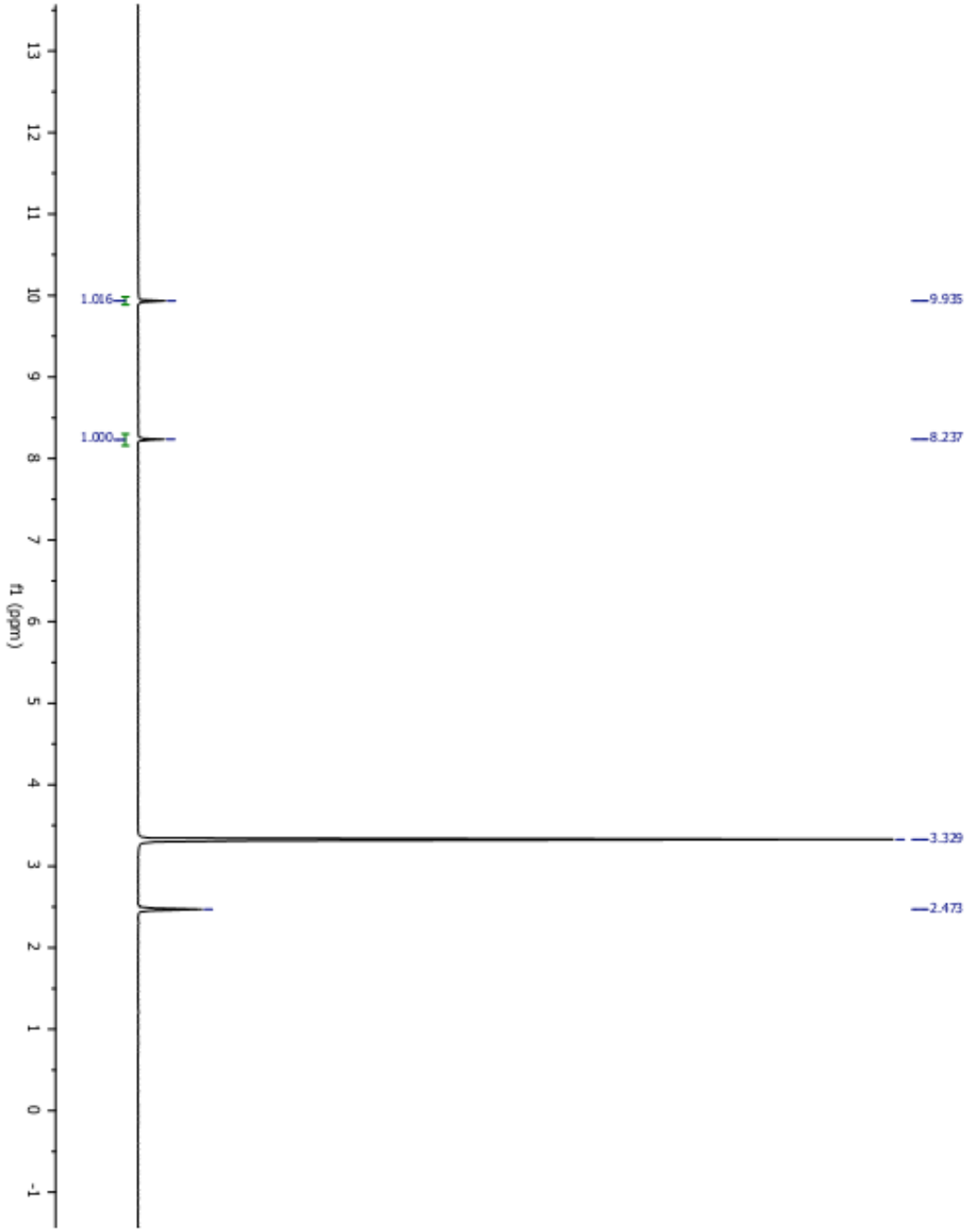

Figure 2.7.2: ^{1}H NMR spectra of compound 2

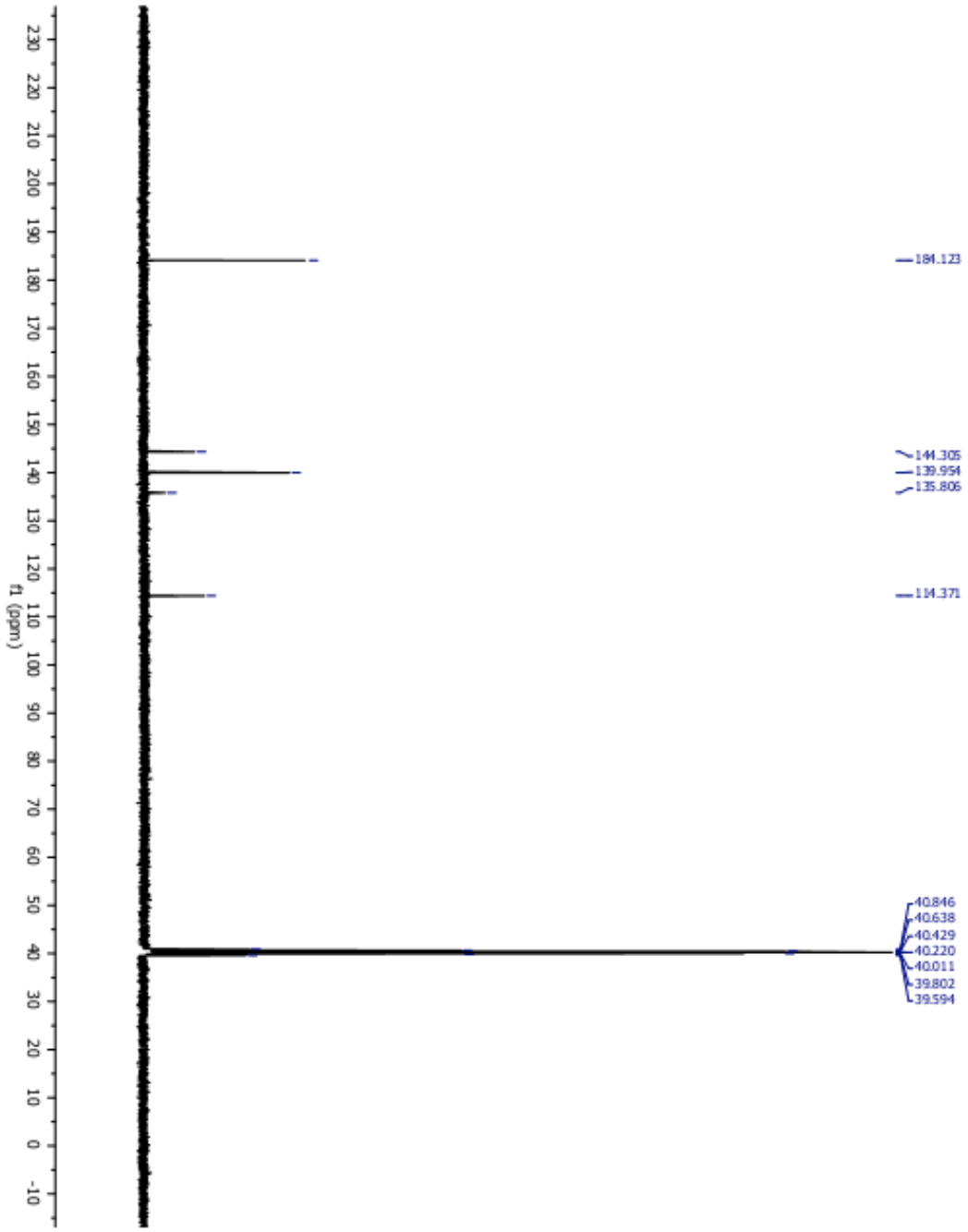

Figure 2.7.3: ^{13}C NMR spectra of compound 2

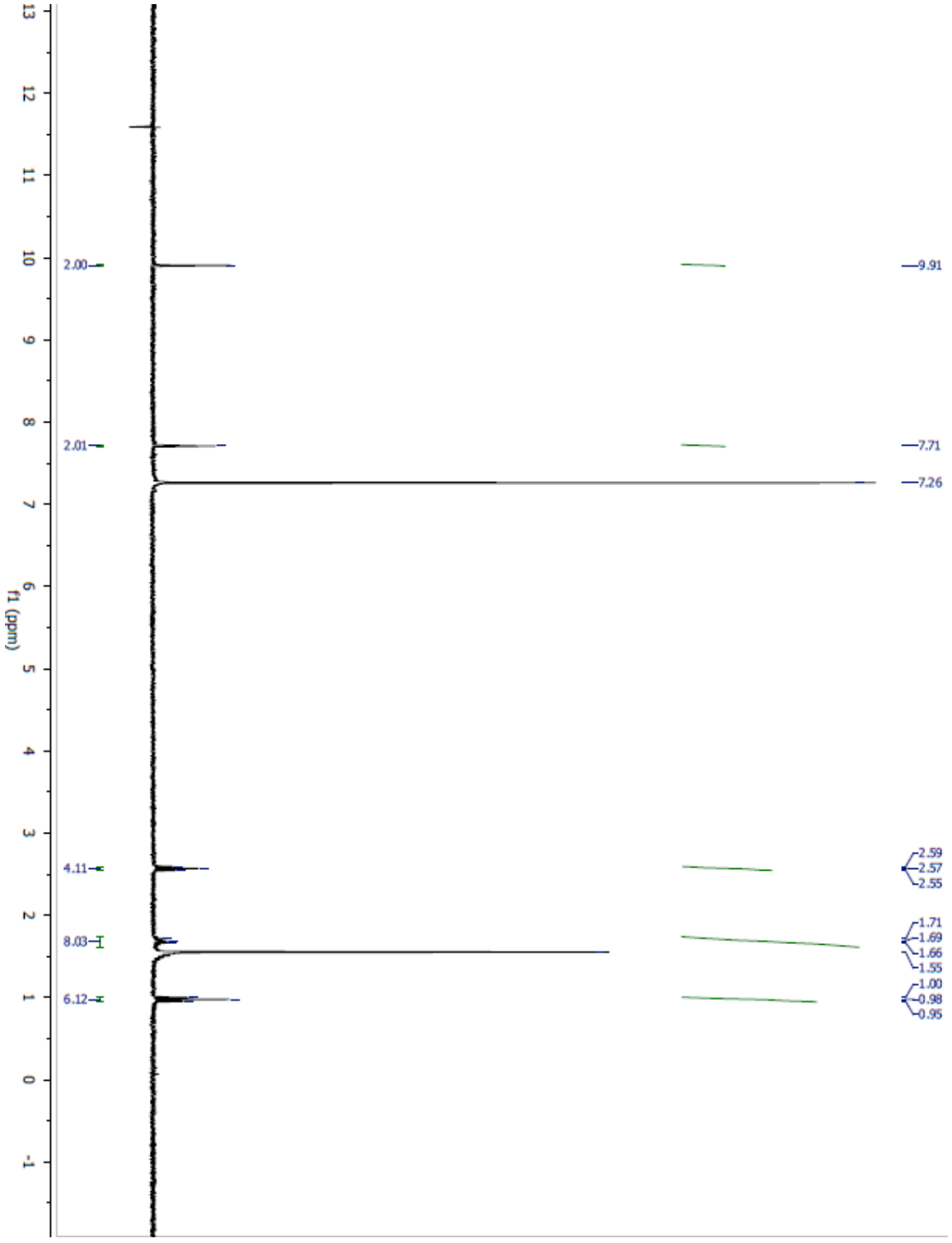

Figure 2.7.4: ^{1}H NMR spectra of compound 3

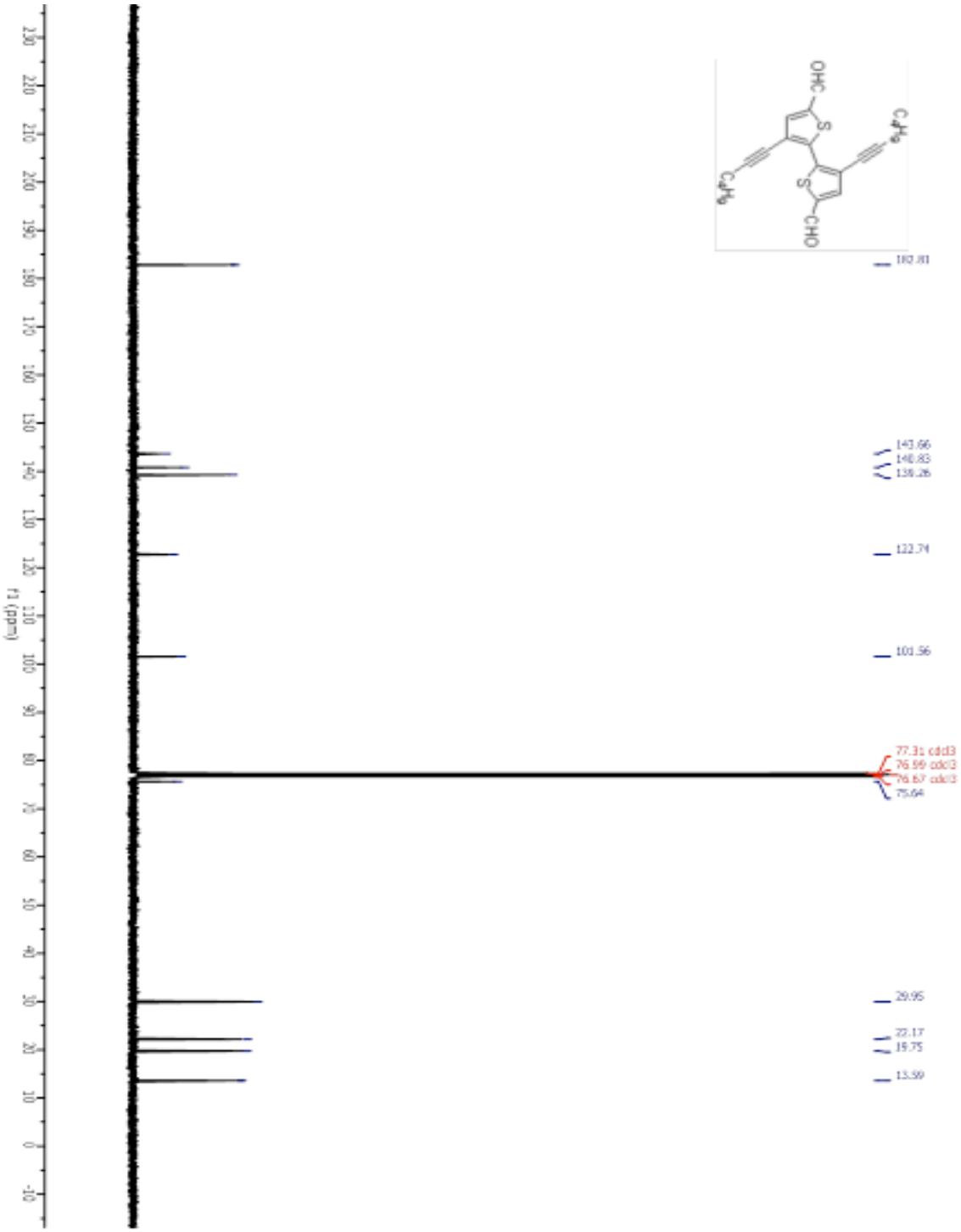

Figure 2.7.5: ^{13}C NMR spectra of compound 3

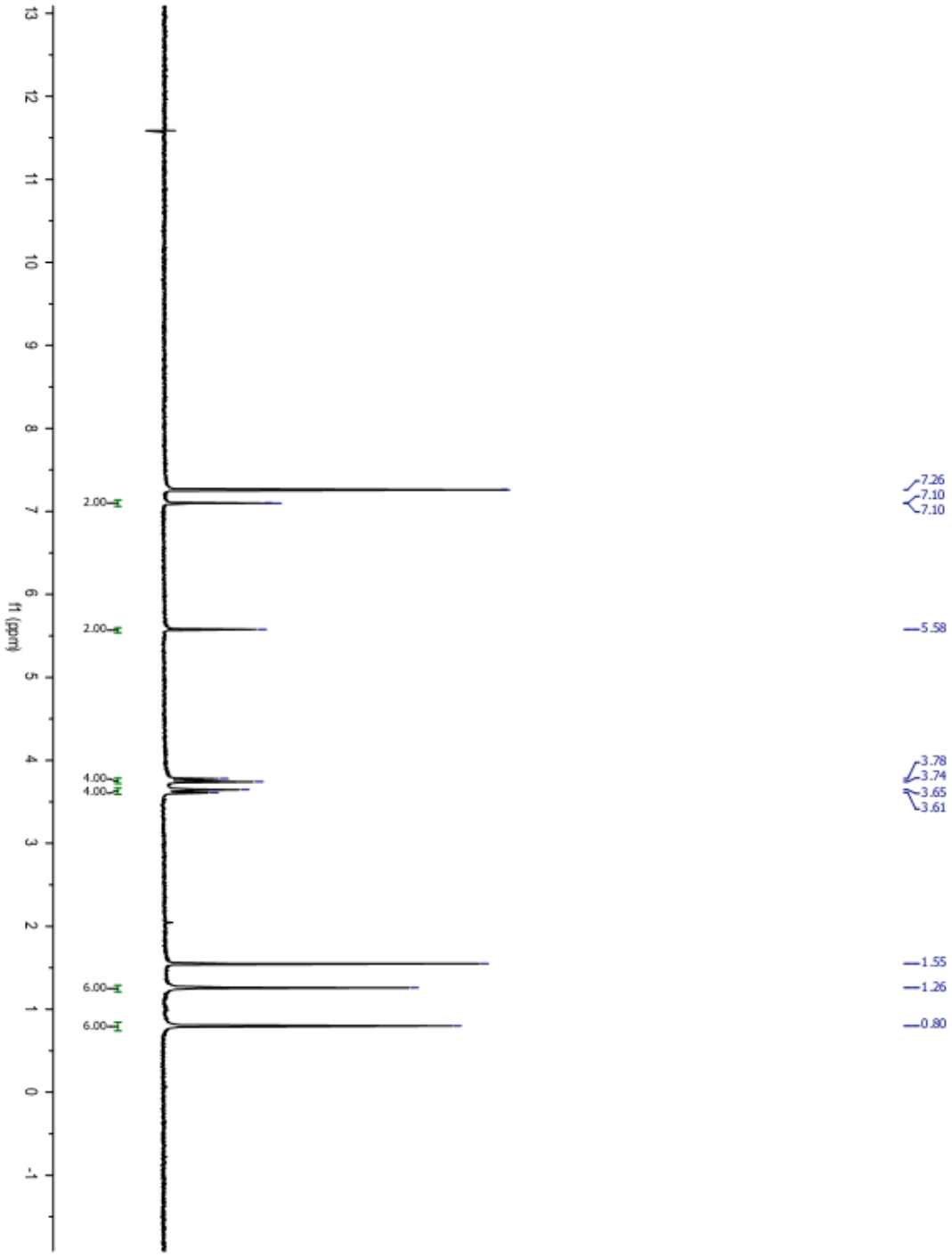

Figure 2.7.6: ^{1}H NMR spectra of compound 4

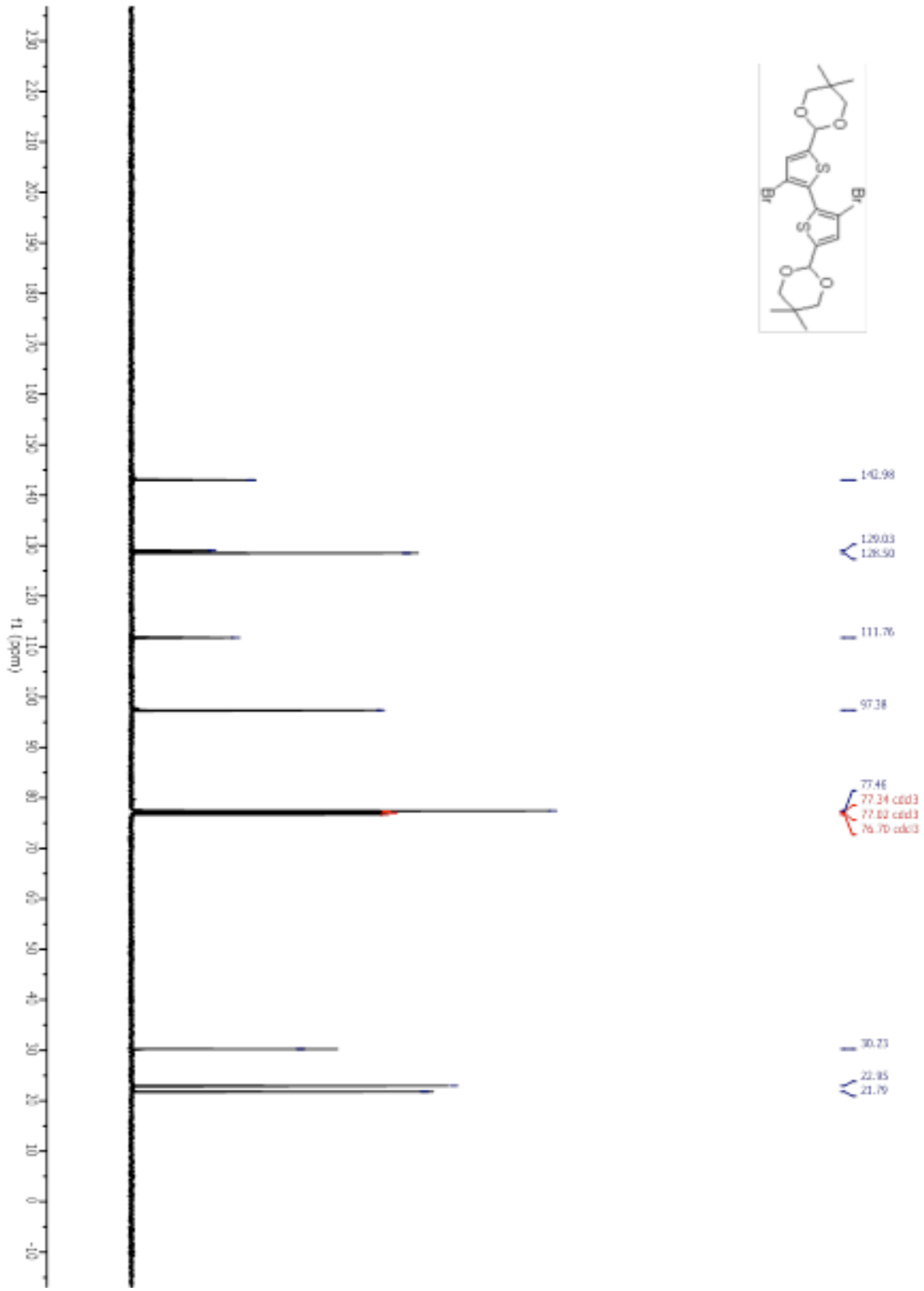

Figure 2.7.7: ^{13}C NMR spectra of compound 4

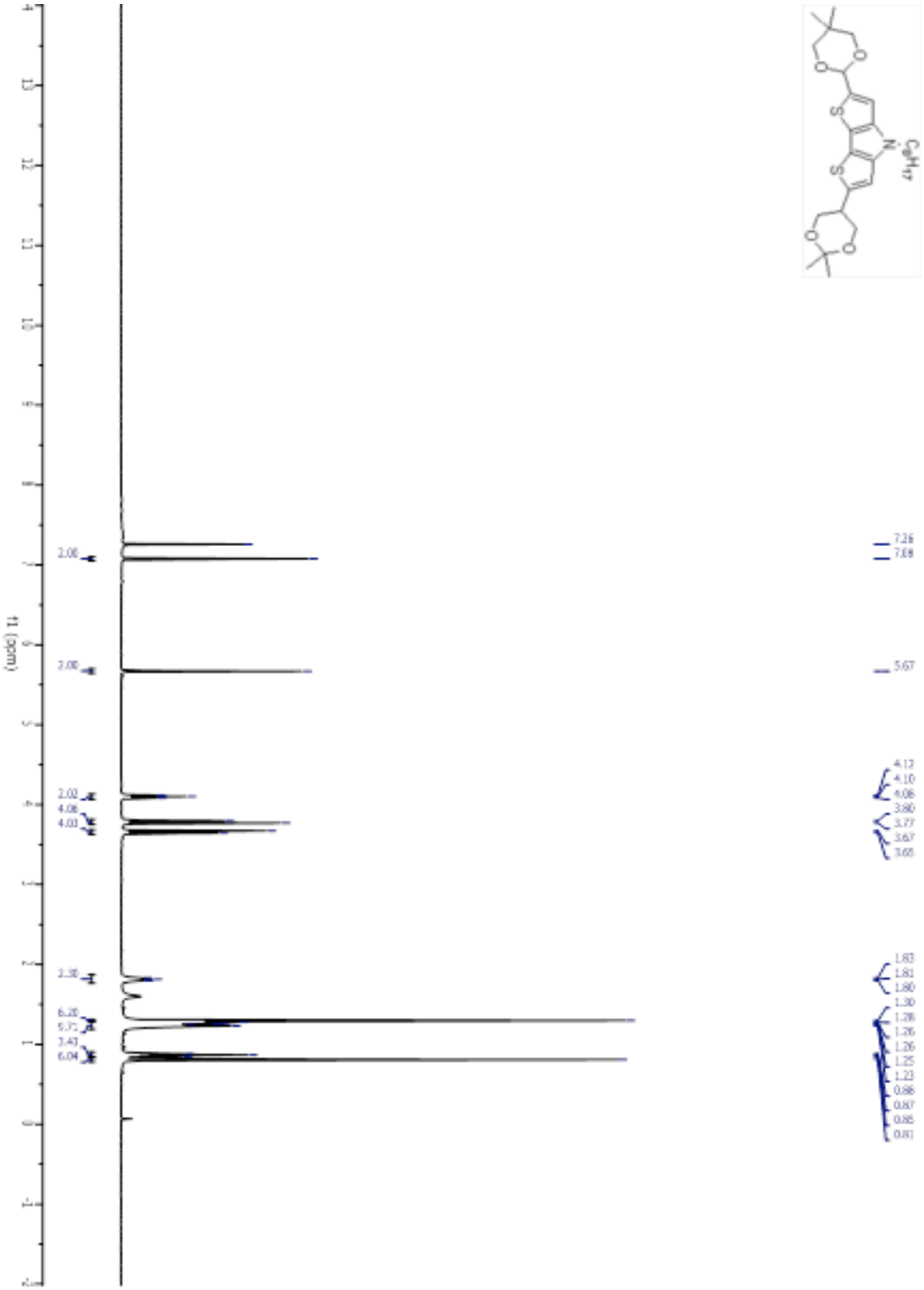

Figure 2.7.8: ^{1}H NMR spectra of compound S2

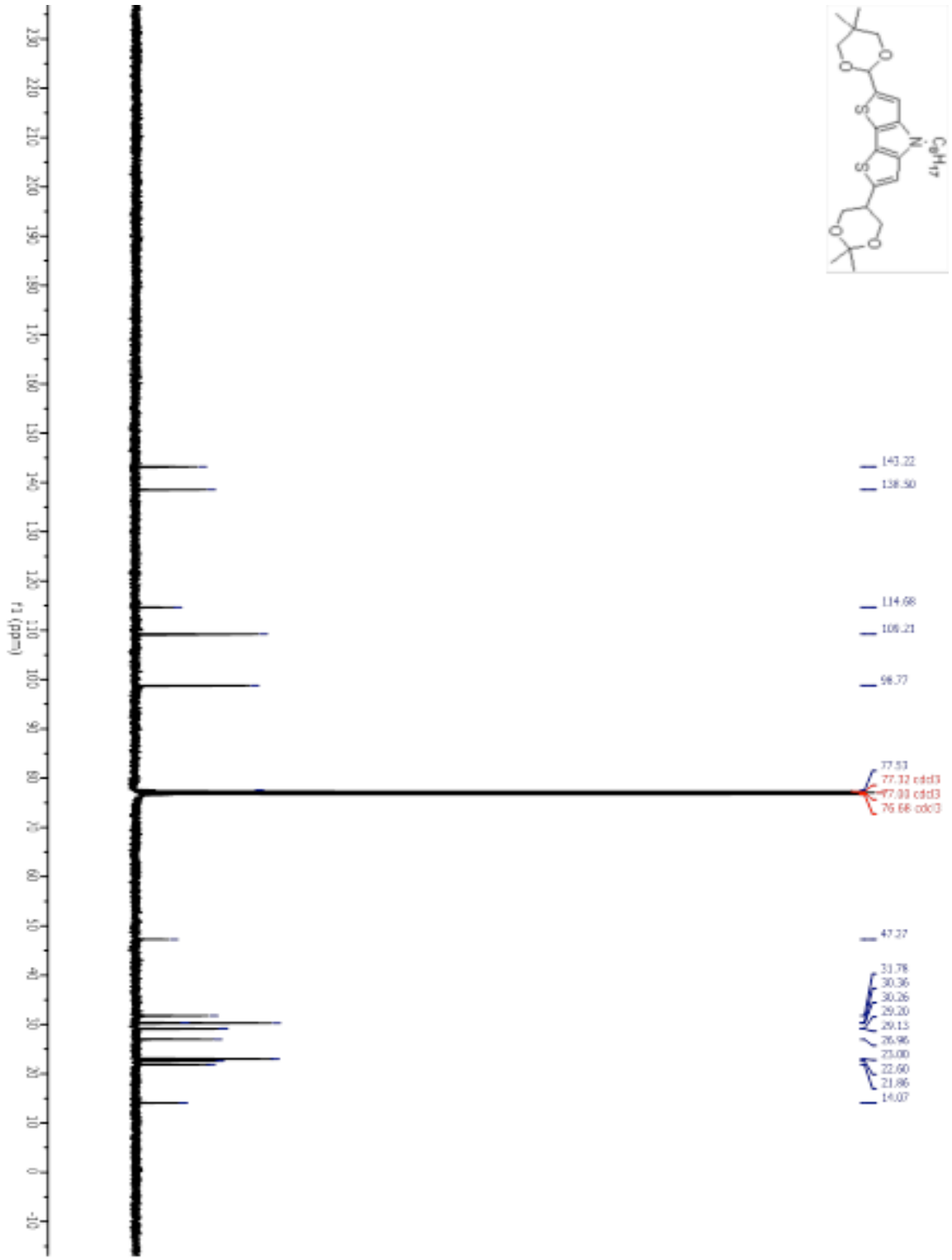

Figure 2.7.9: ^{13}C NMR spectra of compound S2

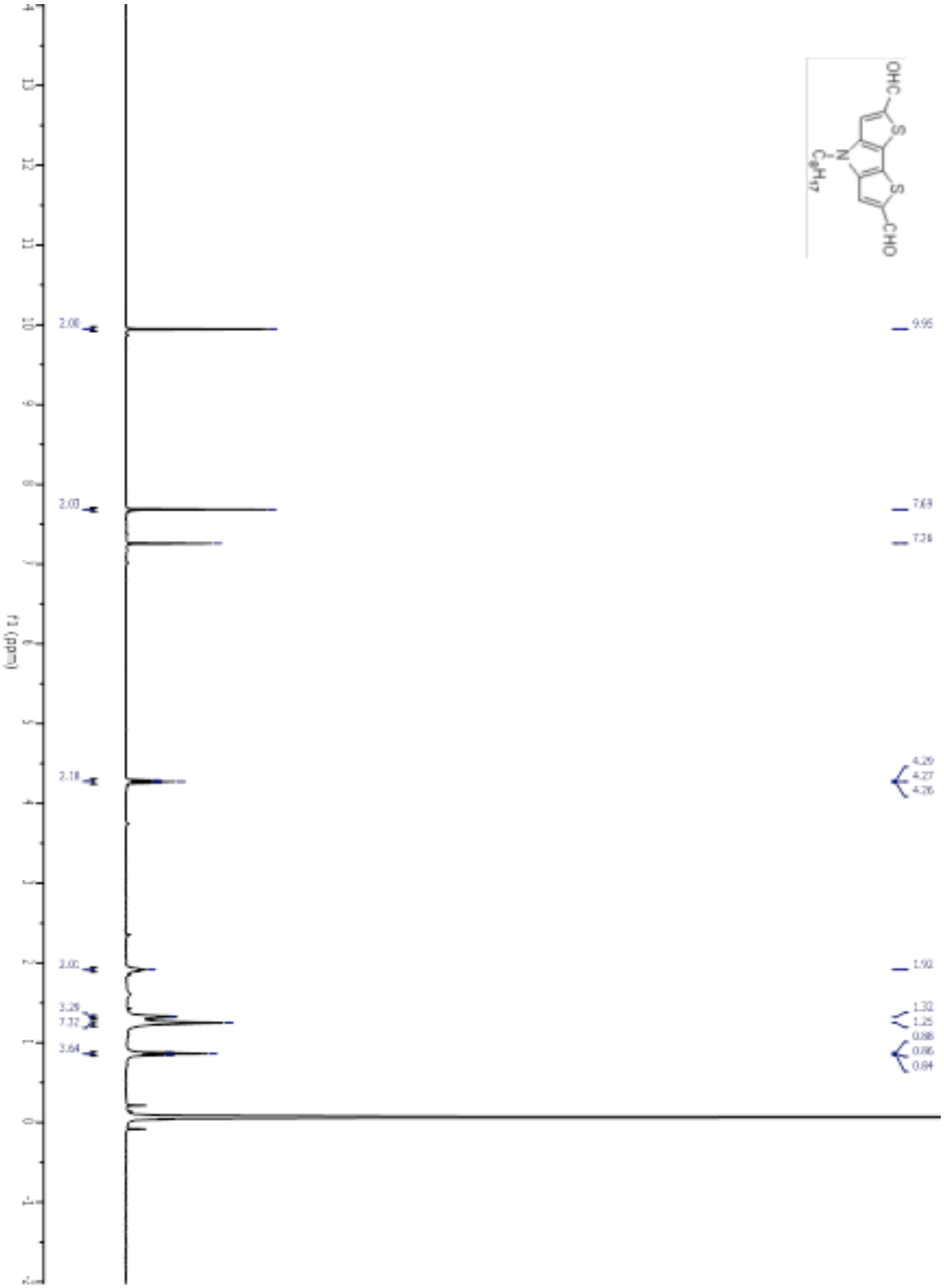

Figure 2.7.10: ^{1}H NMR spectra of compound 5

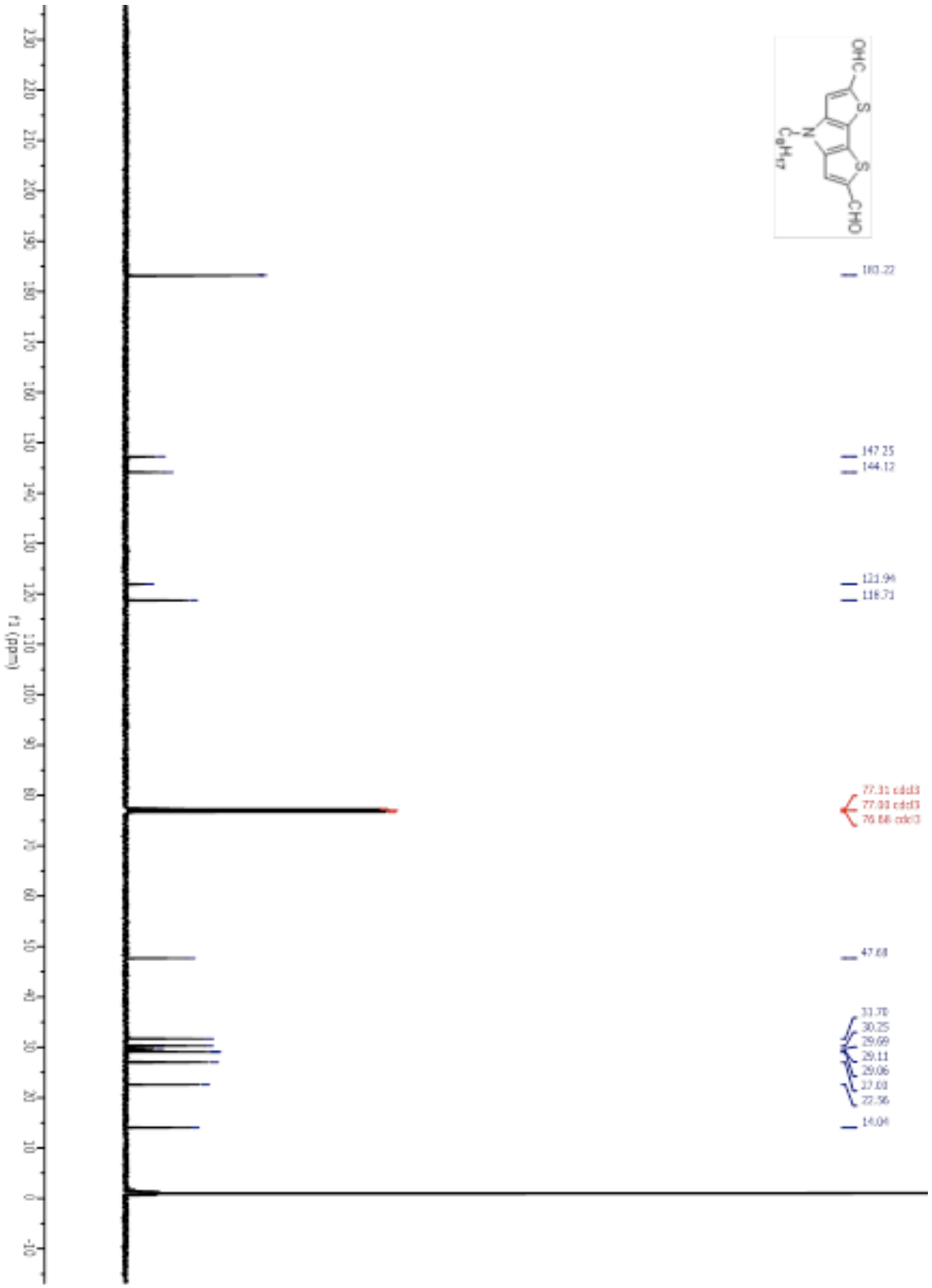

Figure 2.7.11: ^{13}C NMR spectra of compound 5

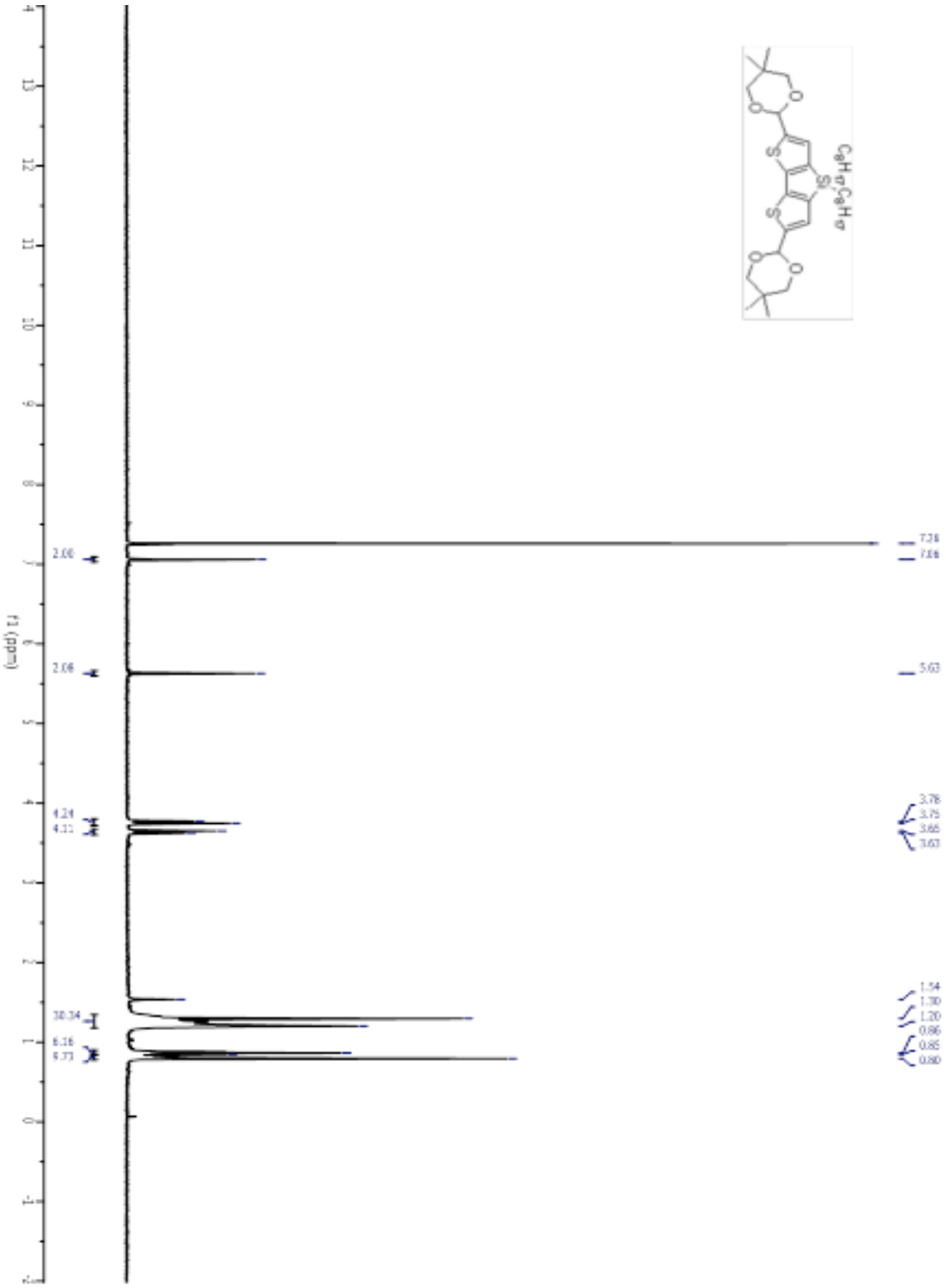

Figure 2.7.12: ^{1}H NMR spectra of compound 6

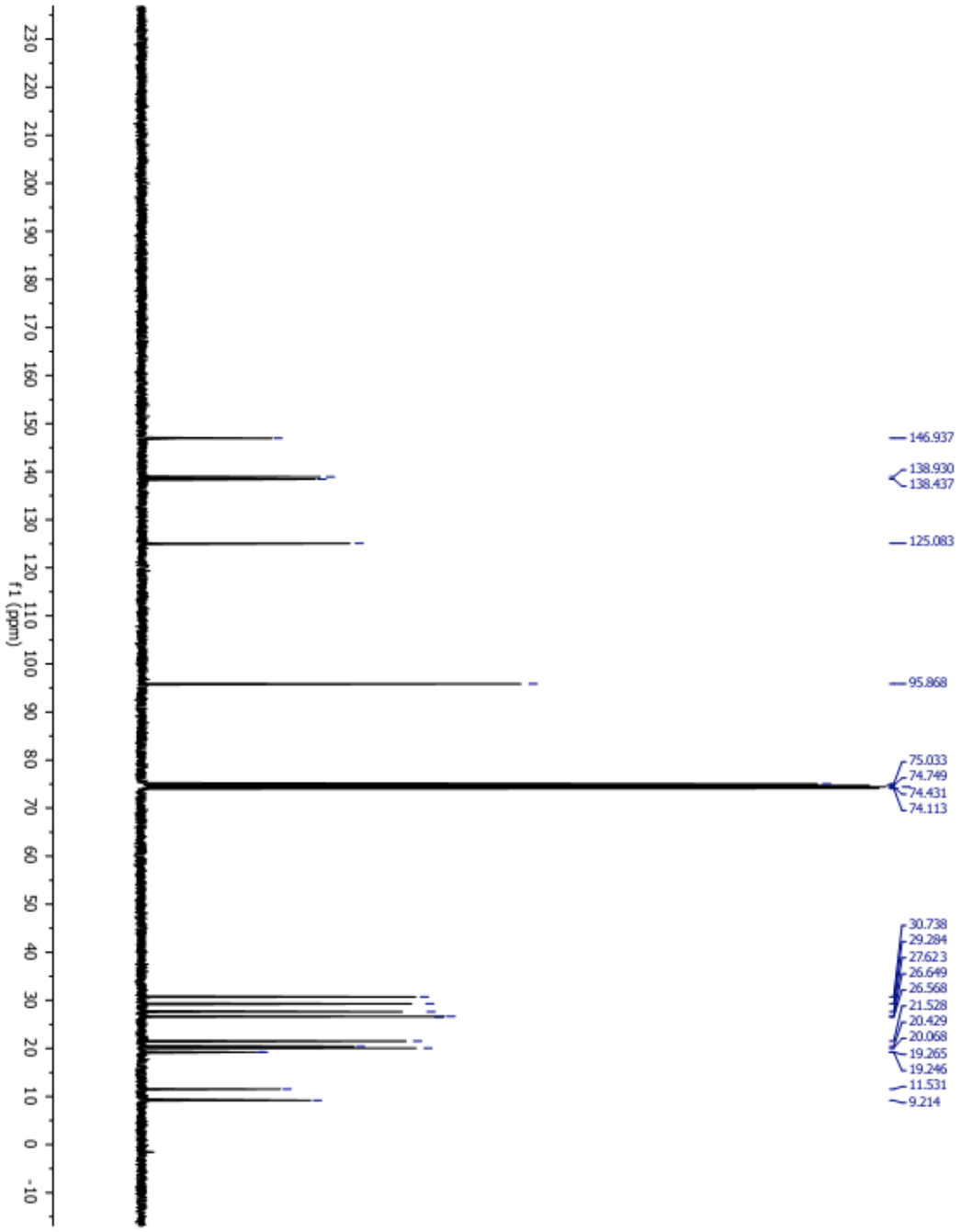

Figure 2.7.13: ^{13}C NMR spectra of compound 6

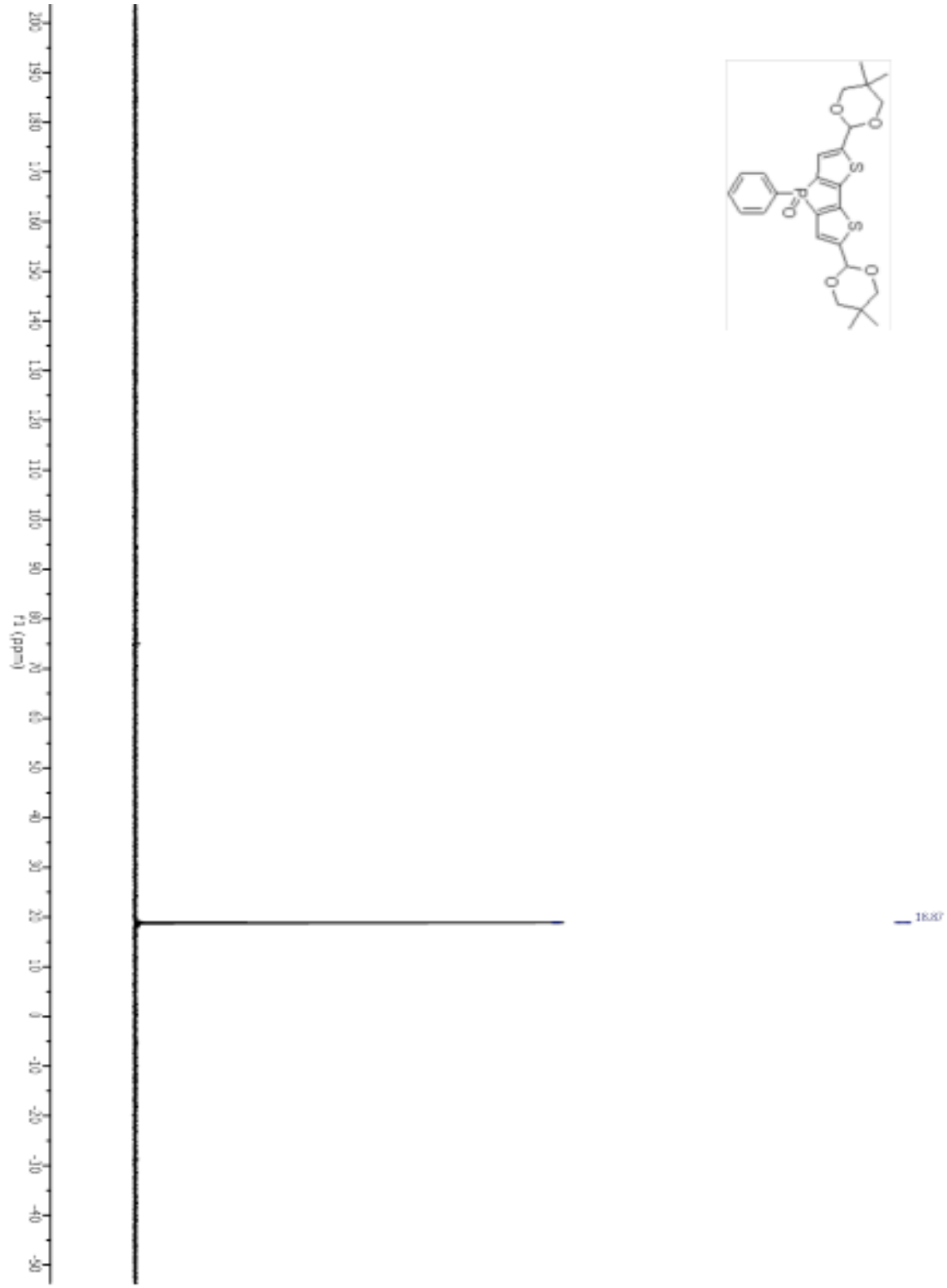

Figure 2.7.14: ^{31}P NMR spectra of compound 7

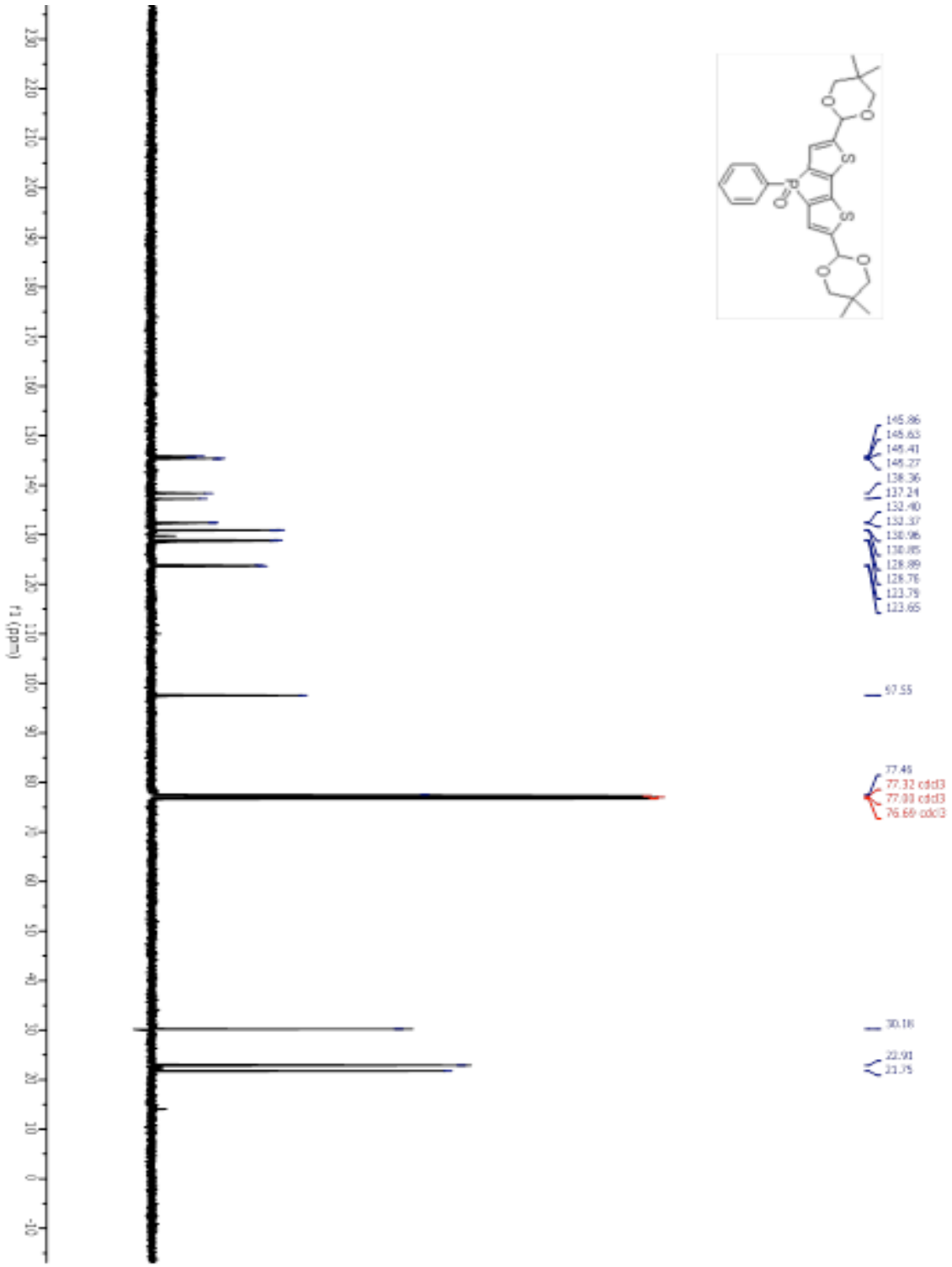

Figure 2.7.15: ^{13}C NMR spectra of compound 7

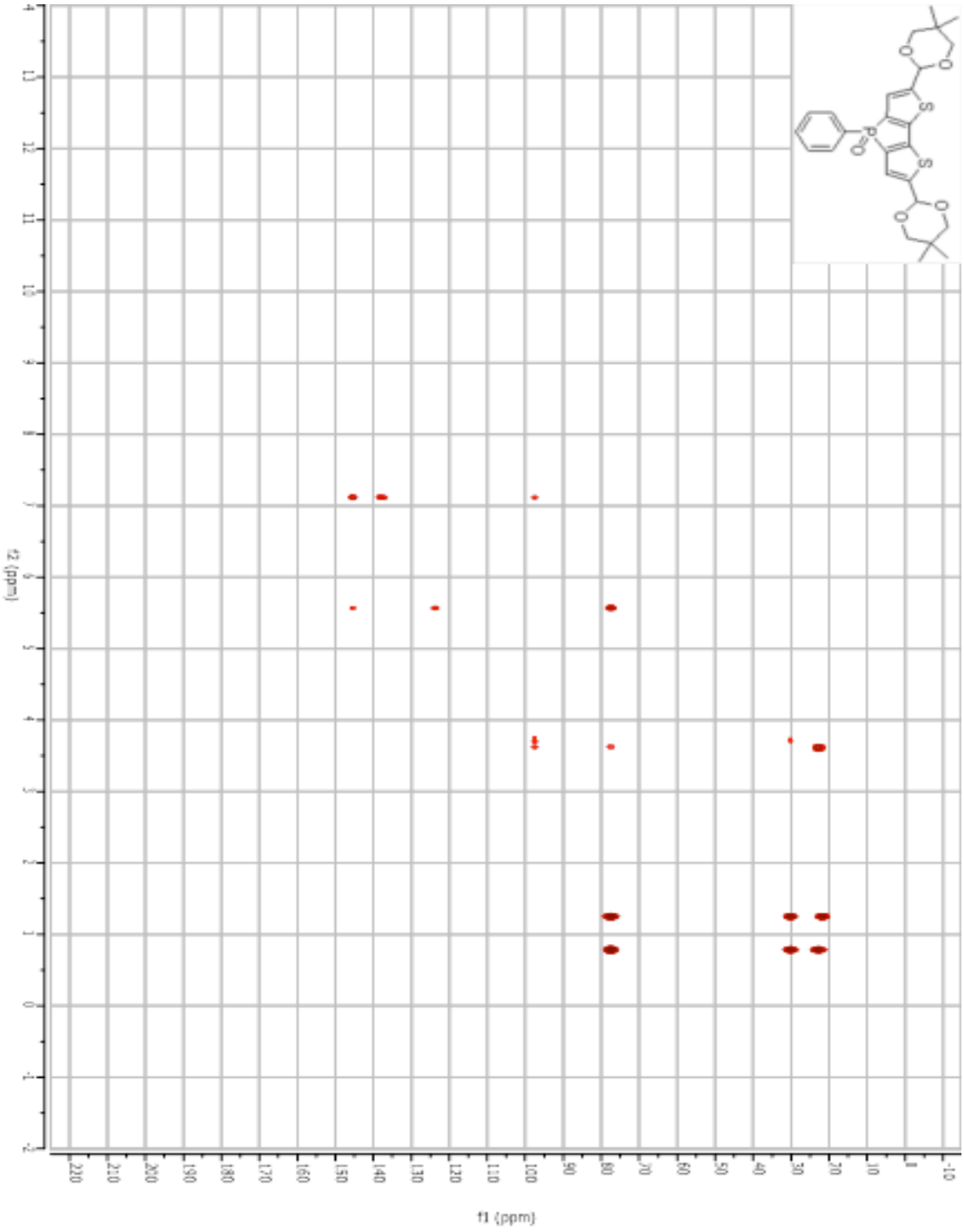

Figure 2.7.16: CIGARAD spectra of compound 7

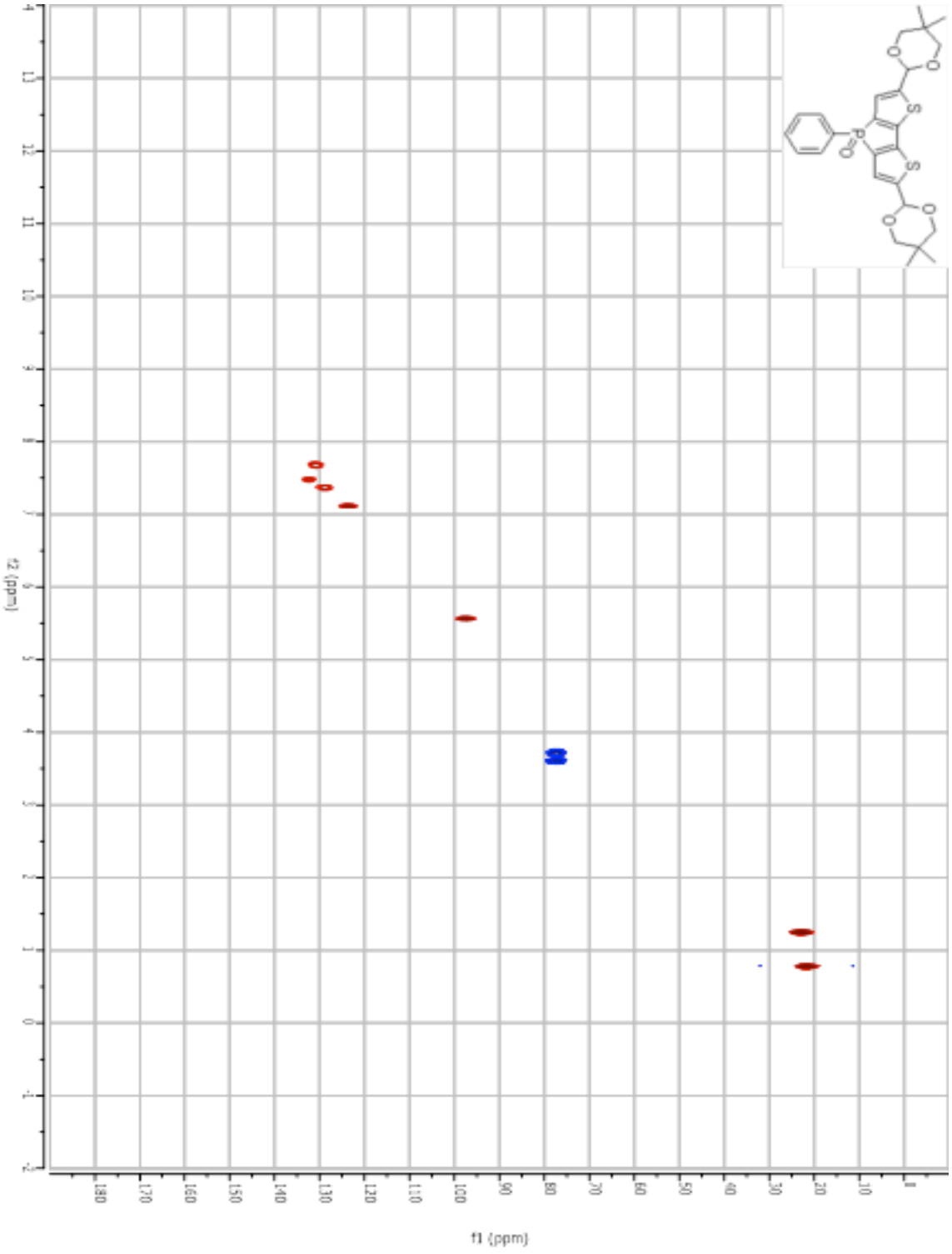

Figure 2.7.17: HSQC spectra of compound 7

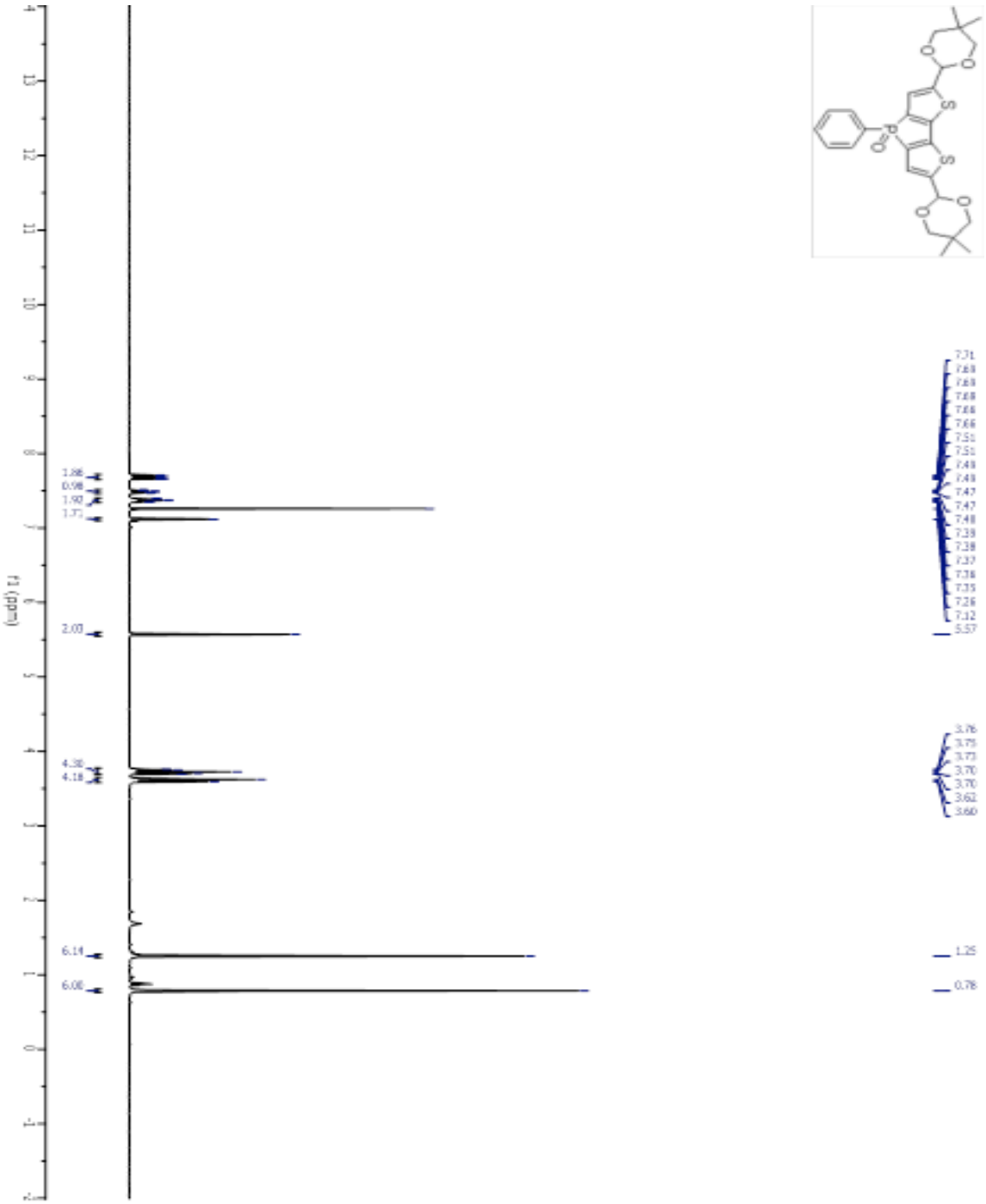

Figure 2.7.18: ^{1}H spectra of compound 7

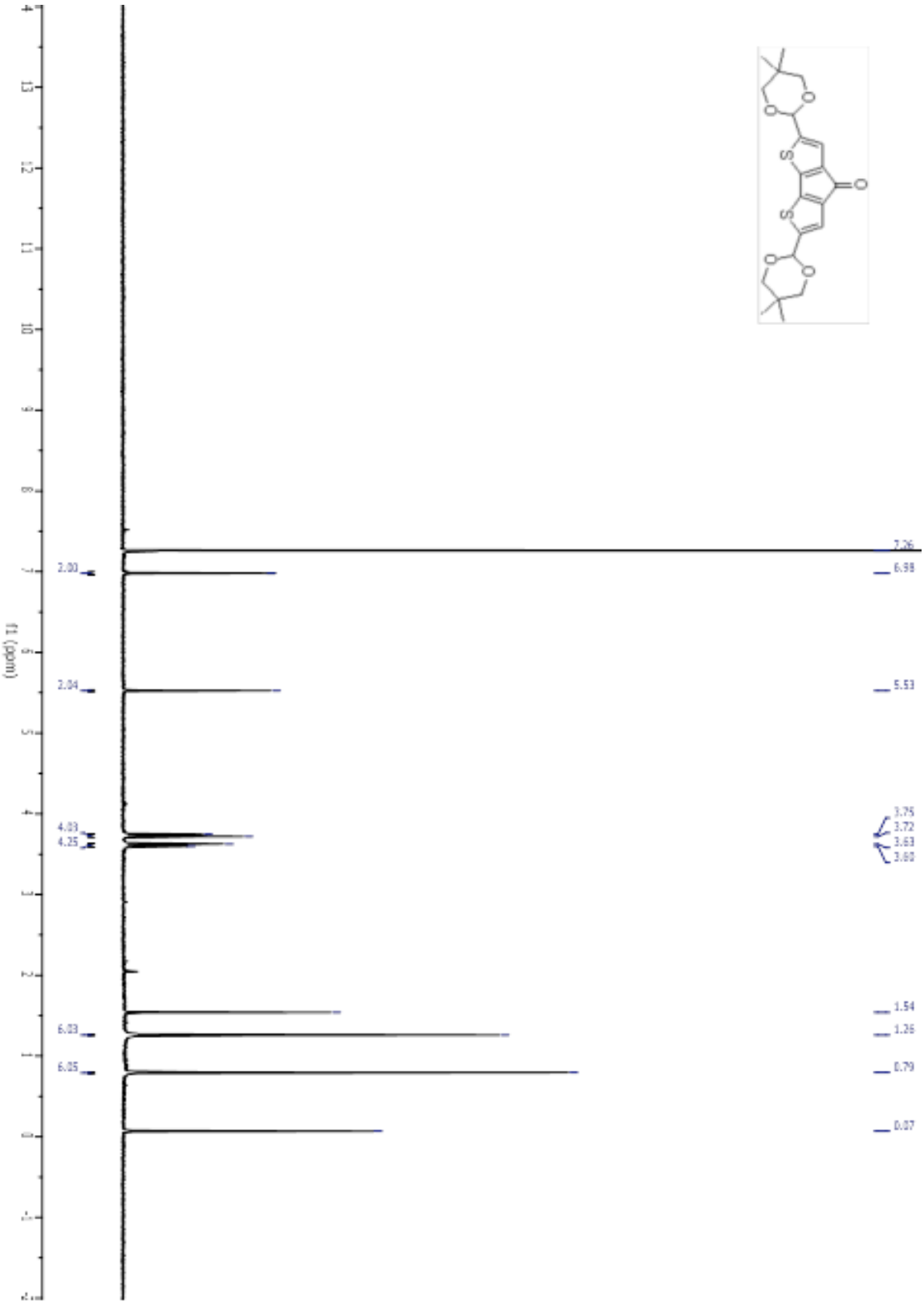

Figure 2.7.19: ^{1}H NMR spectra of compound 8

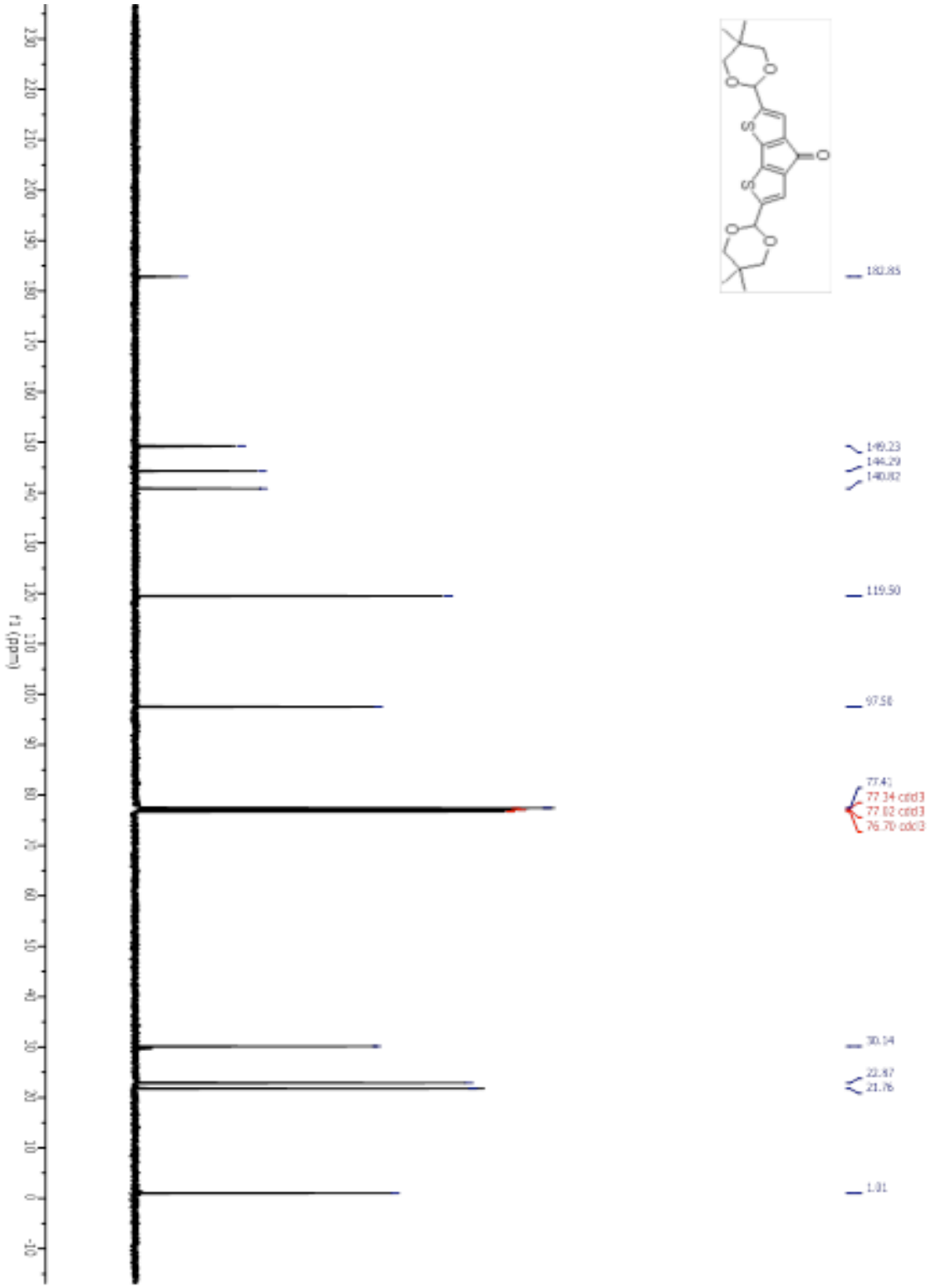

Figure 2.7.20: ^{13}C NMR spectra of compound 8

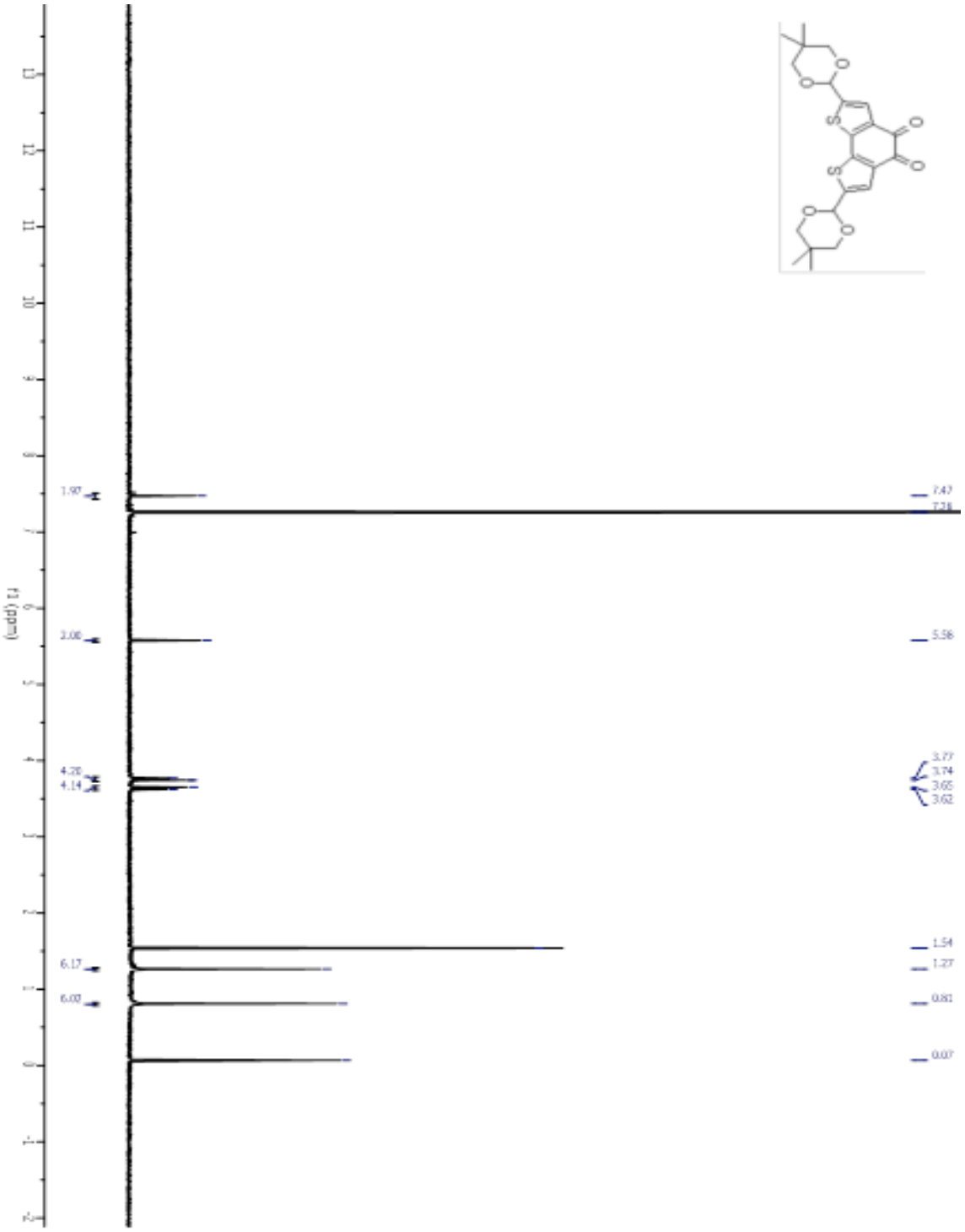

Figure 2.7.21: ^{1}H NMR spectra of compound 9

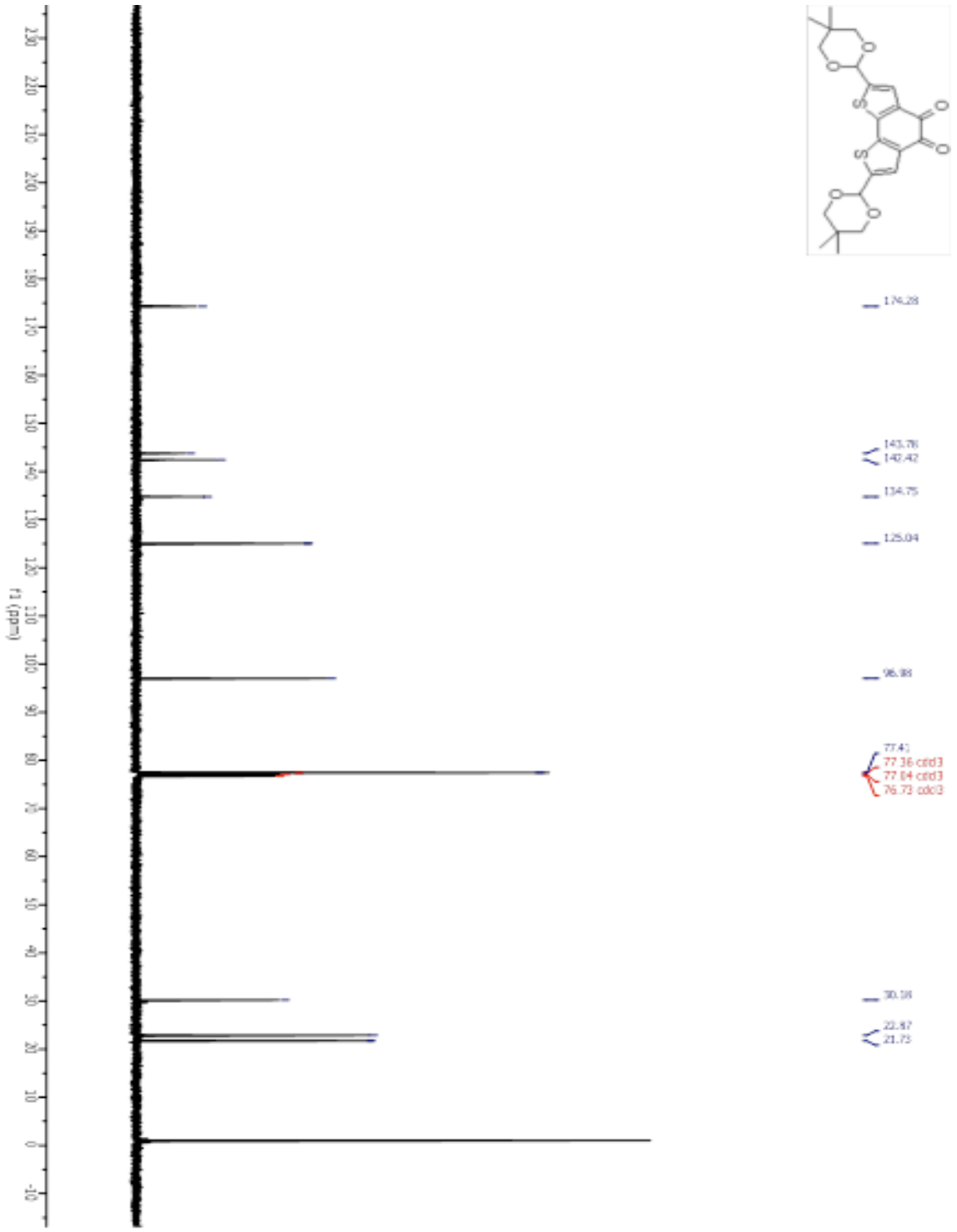

Figure 2.7.22: ^{13}C NMR spectra of compound 9

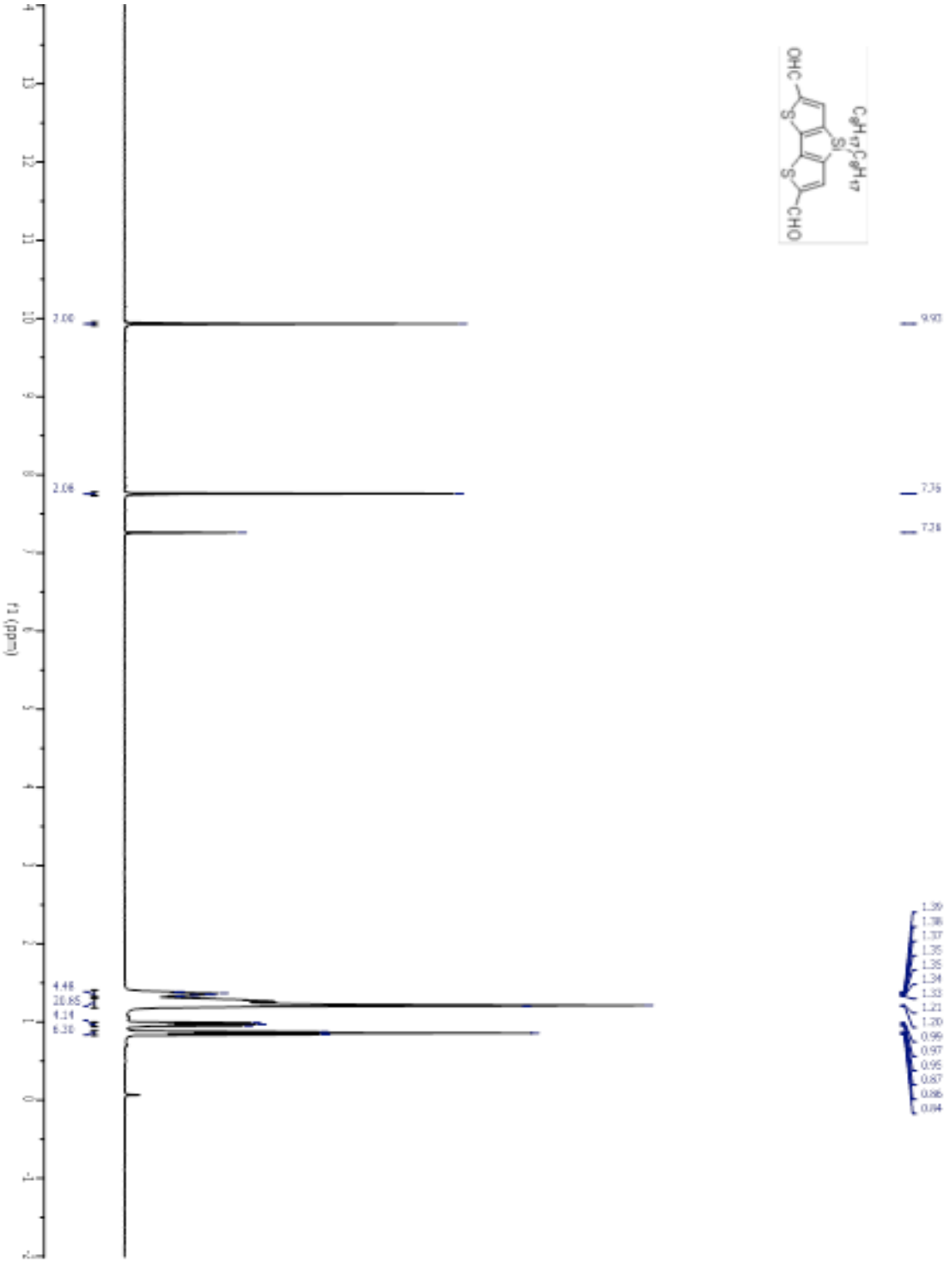

Figure 2.7.23: ^{1}H NMR spectra of compound 10

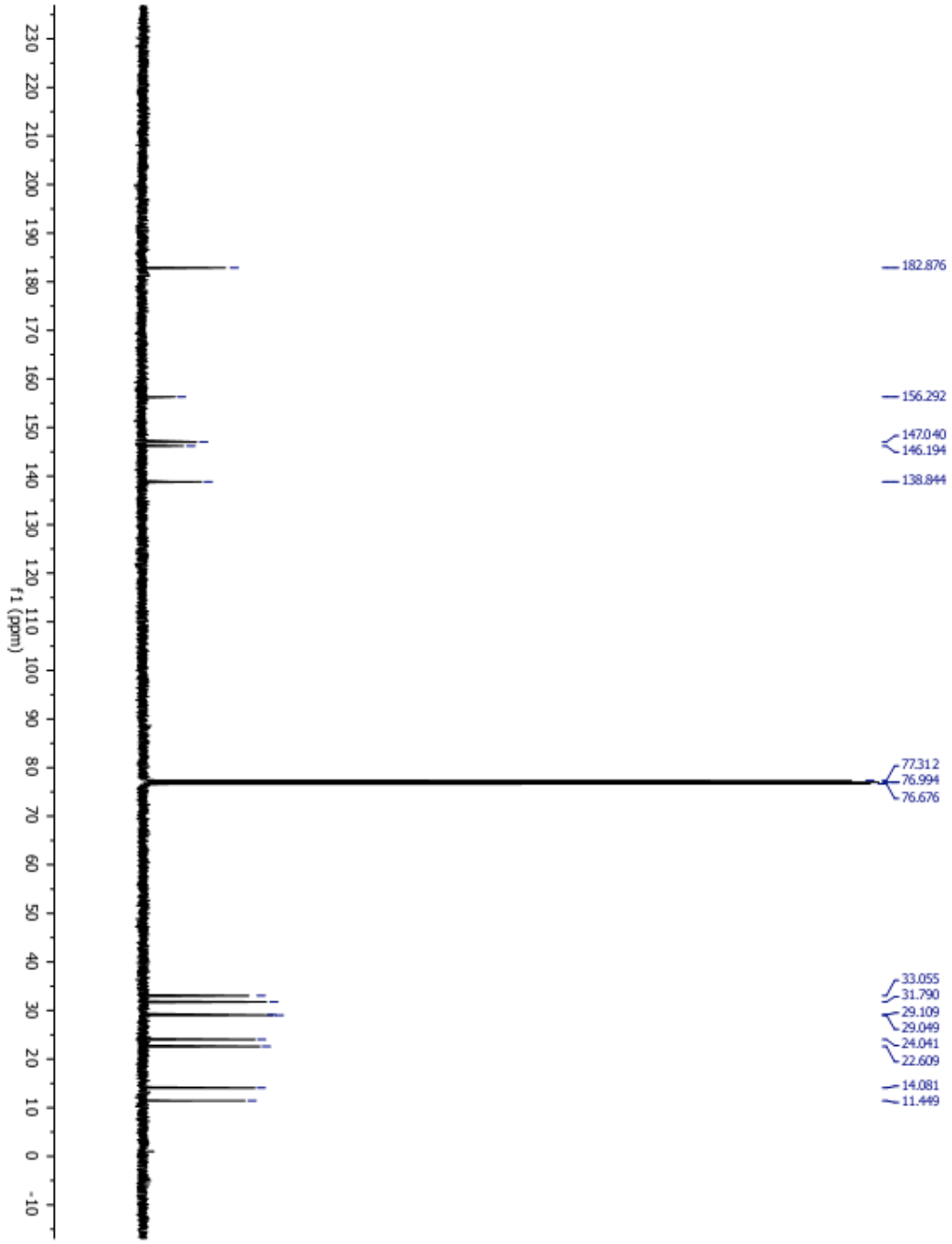

Figure 2.7.24: ^{13}C NMR spectra of compound 10

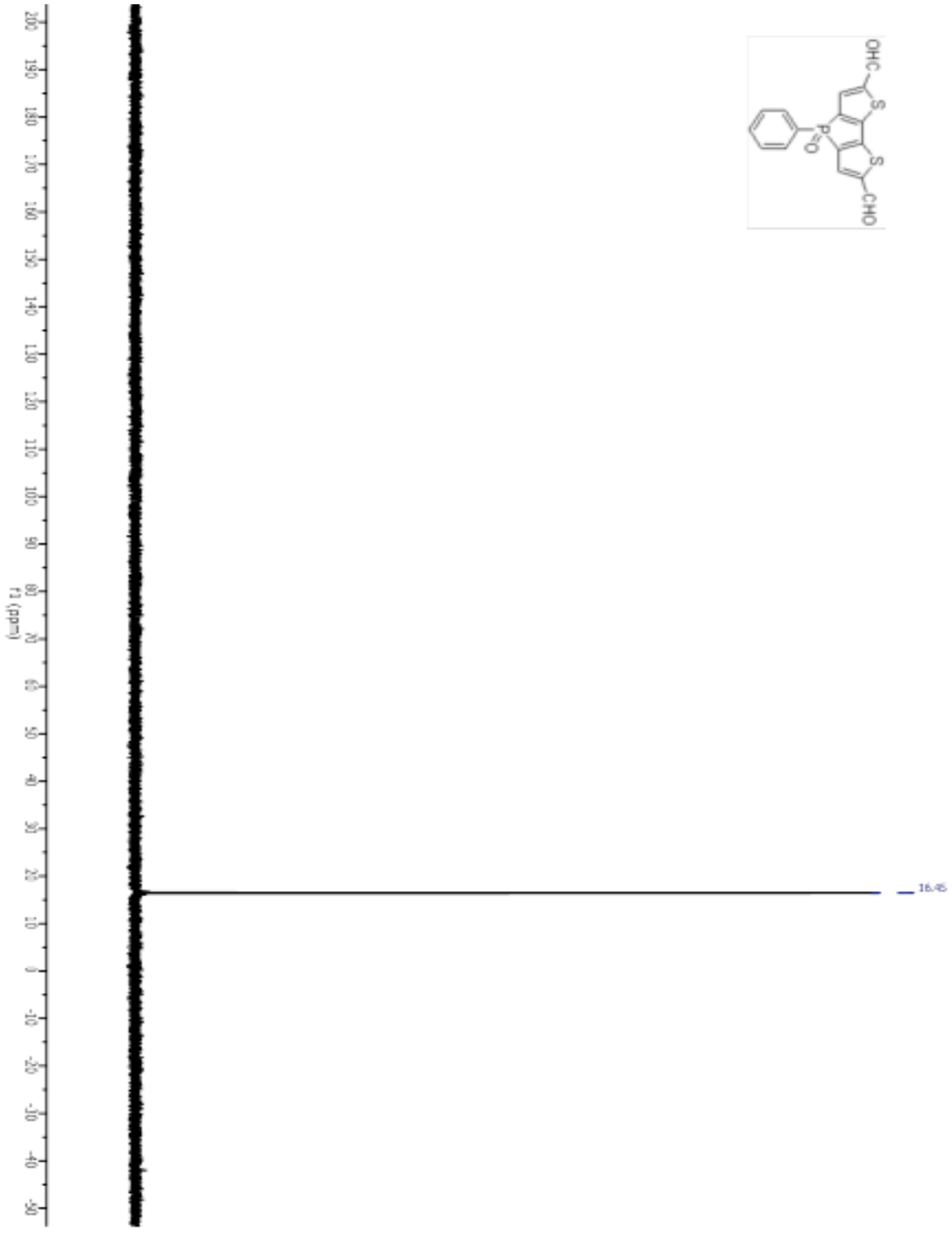

Figure 2.7.25: ^{31}P spectra of compound 11

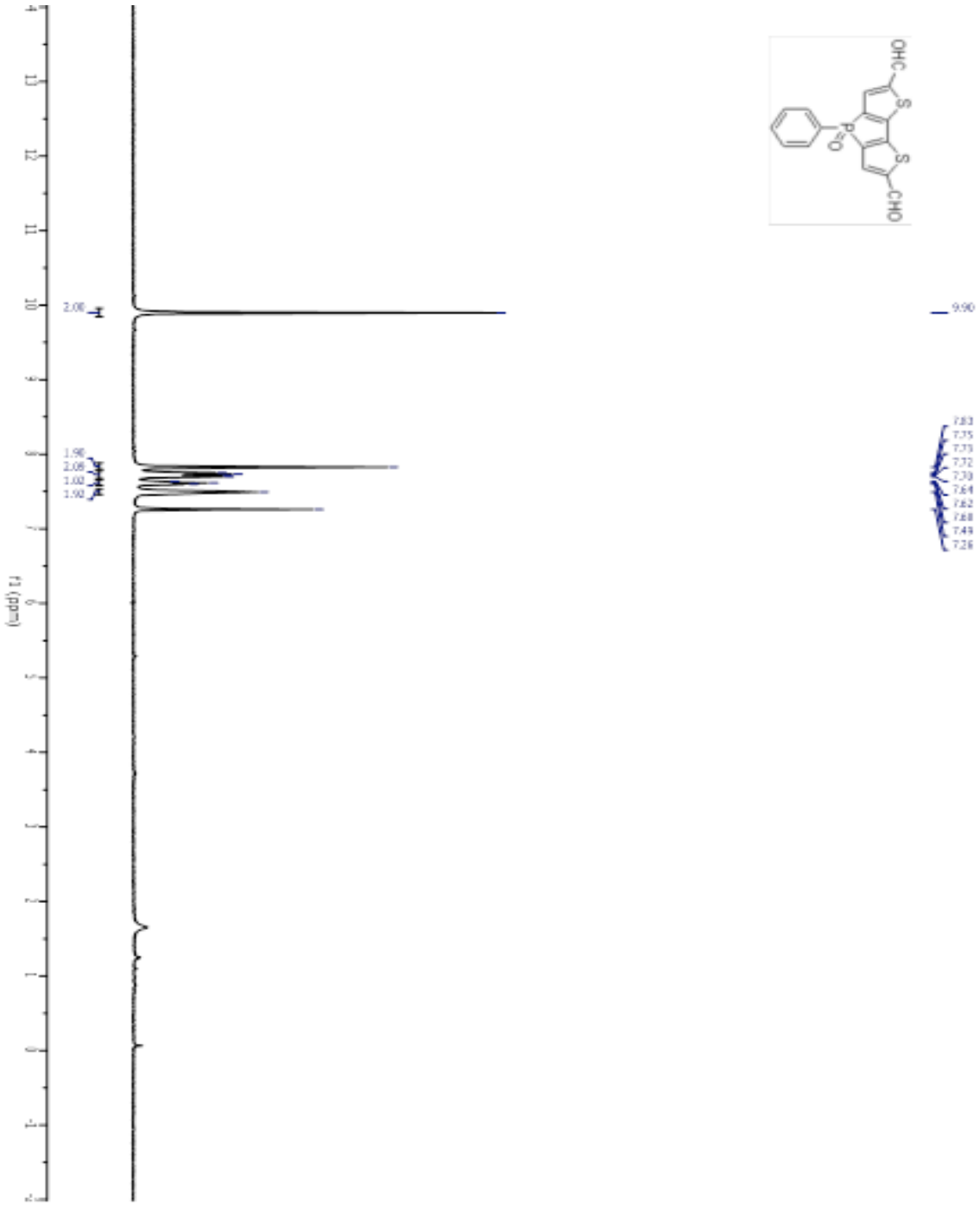

Figure 2.7.26: ^{1}H spectra of compound 11

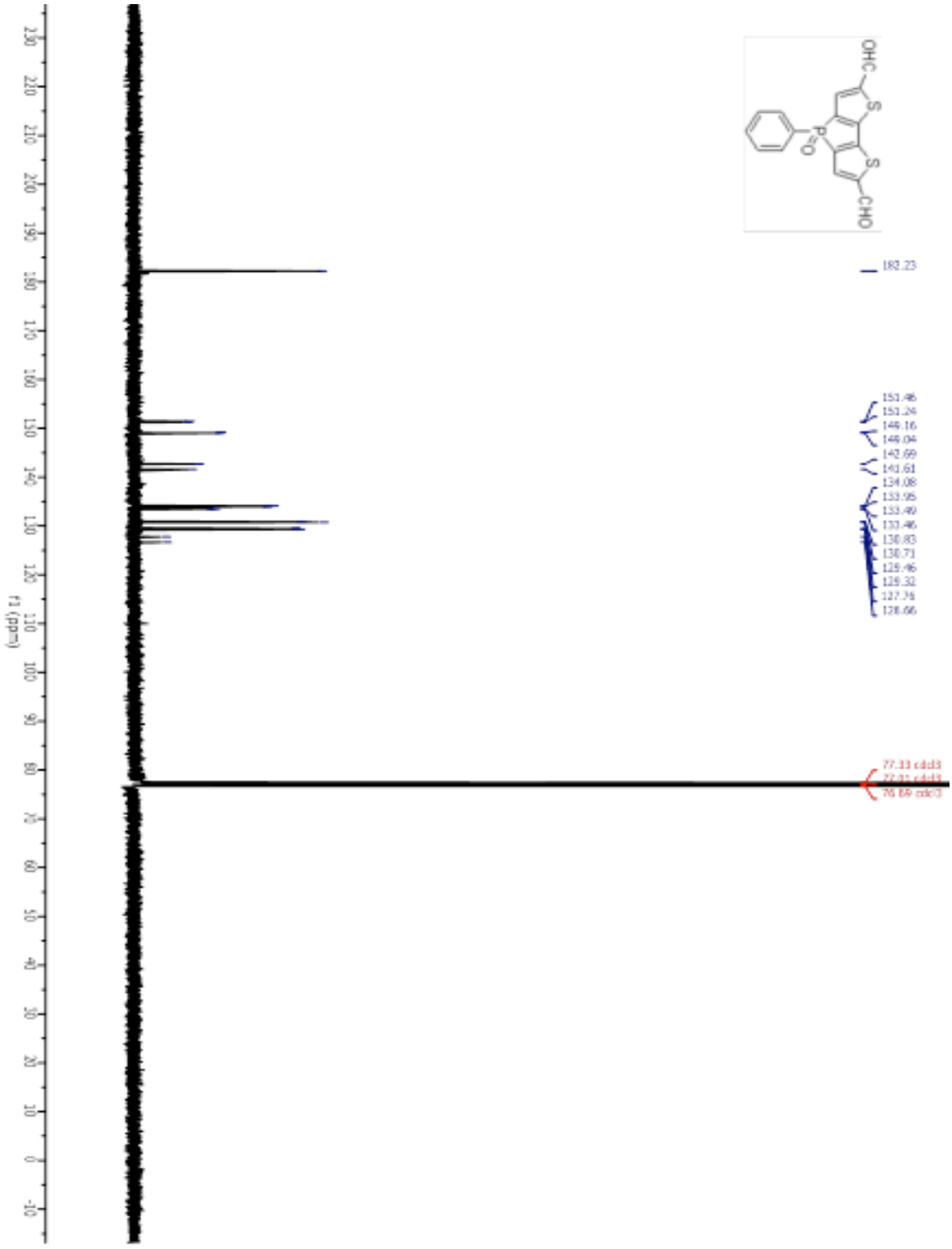

Figure 2.7.27: ^{13}C spectra of compound 11

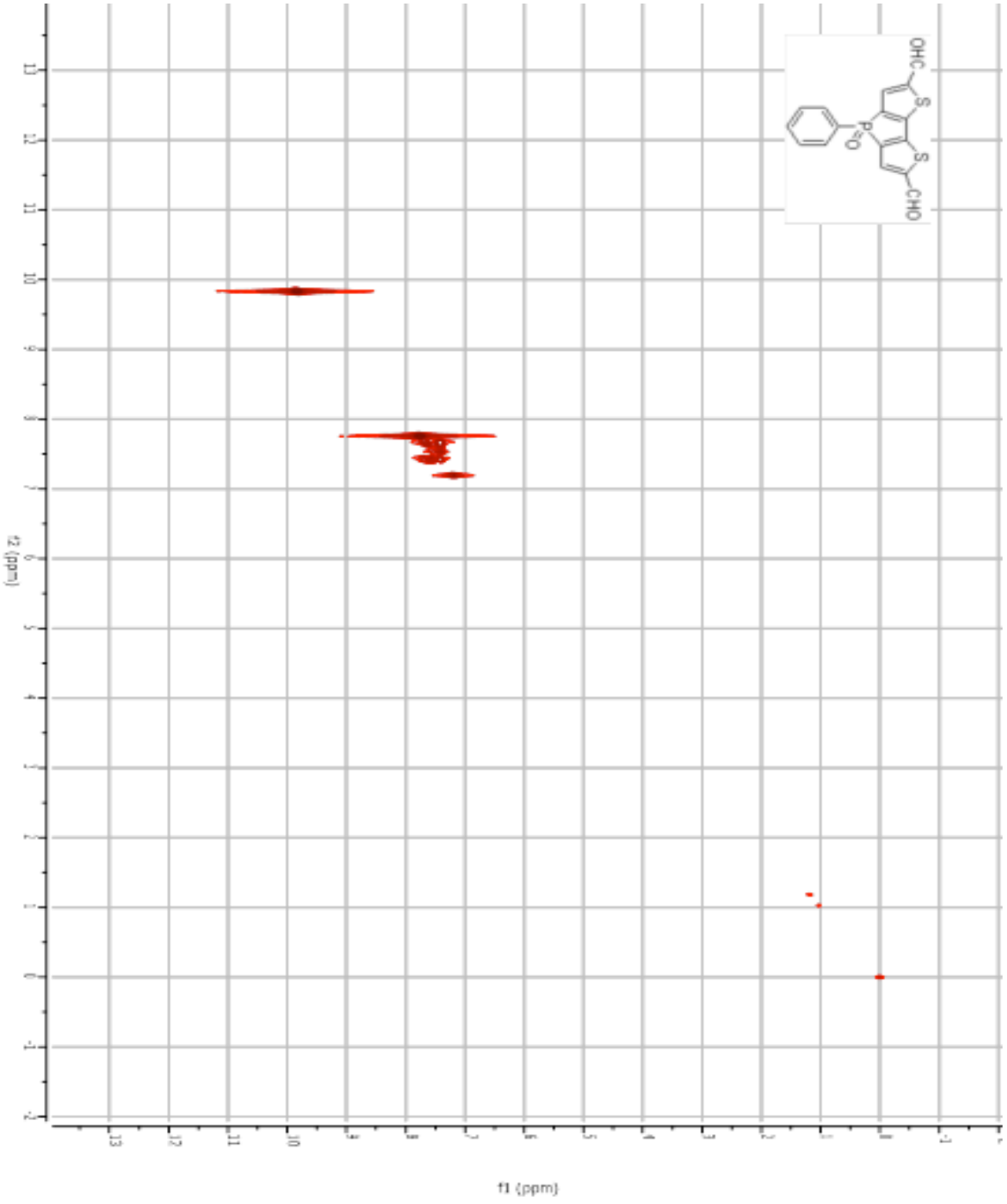

Figure 2.7.28: COSY spectra of compound 11

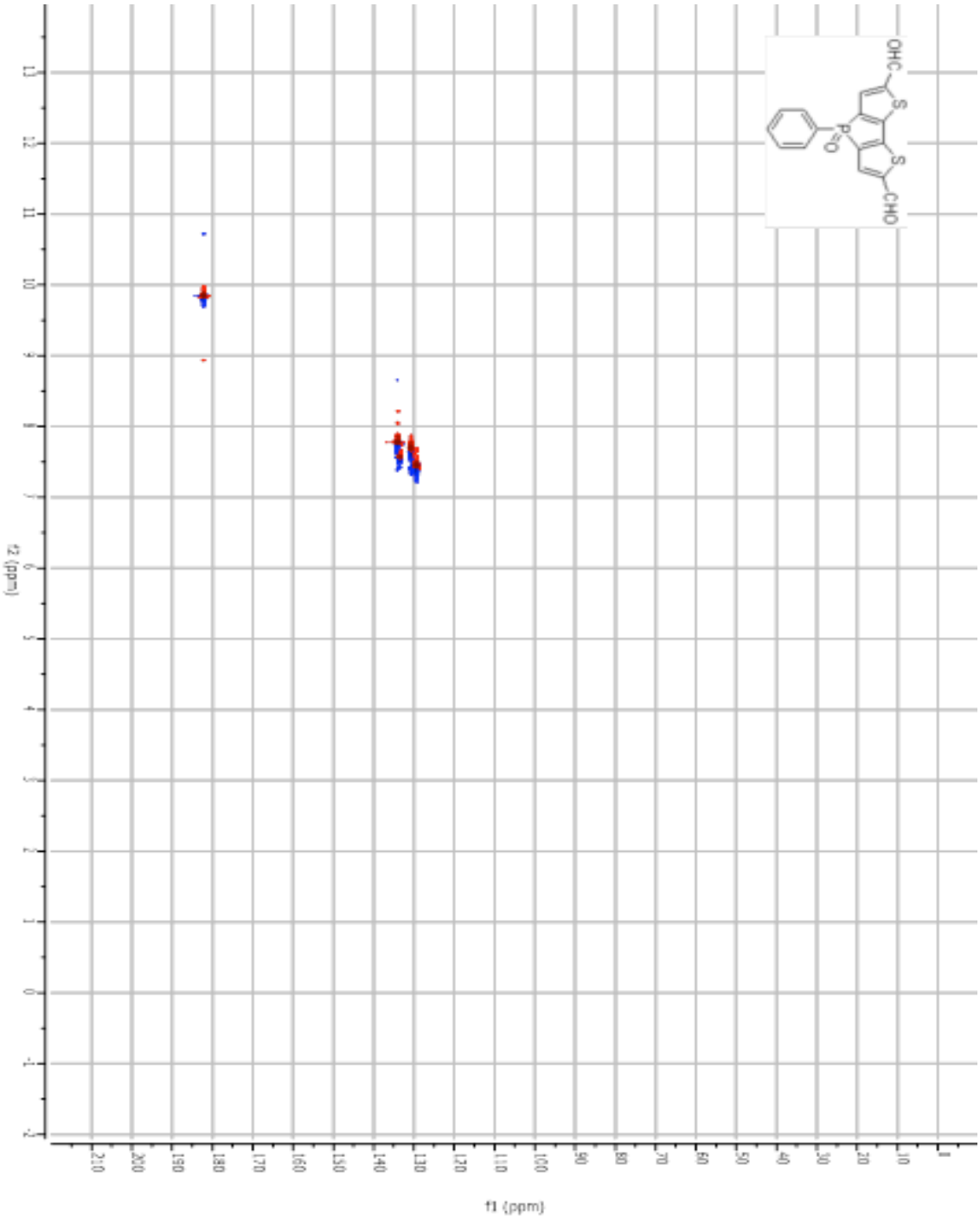

Figure 2.7.29: HSQC spectra of compound 11

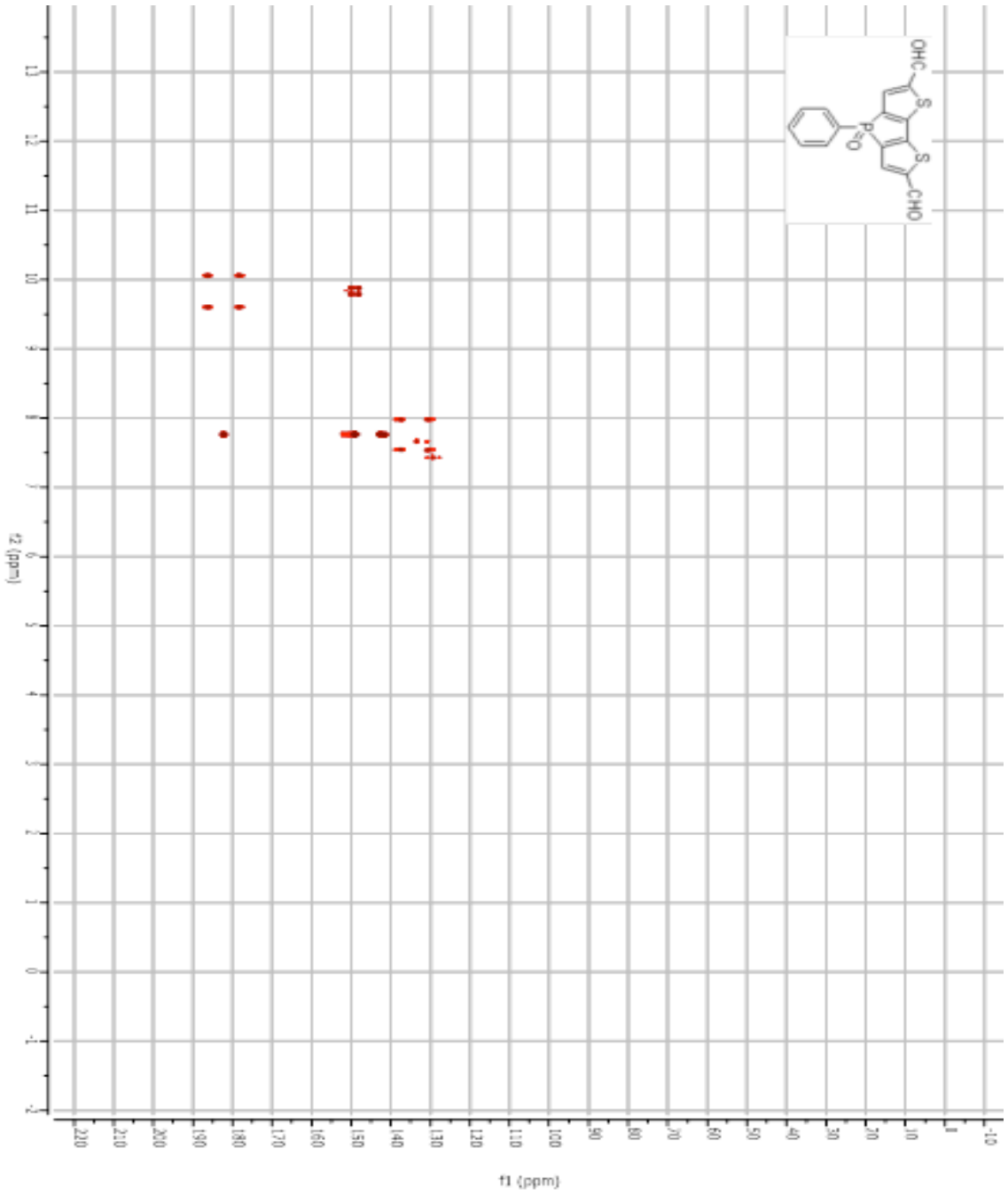

Figure 2.7.30: CIGARAD spectra of compound 11

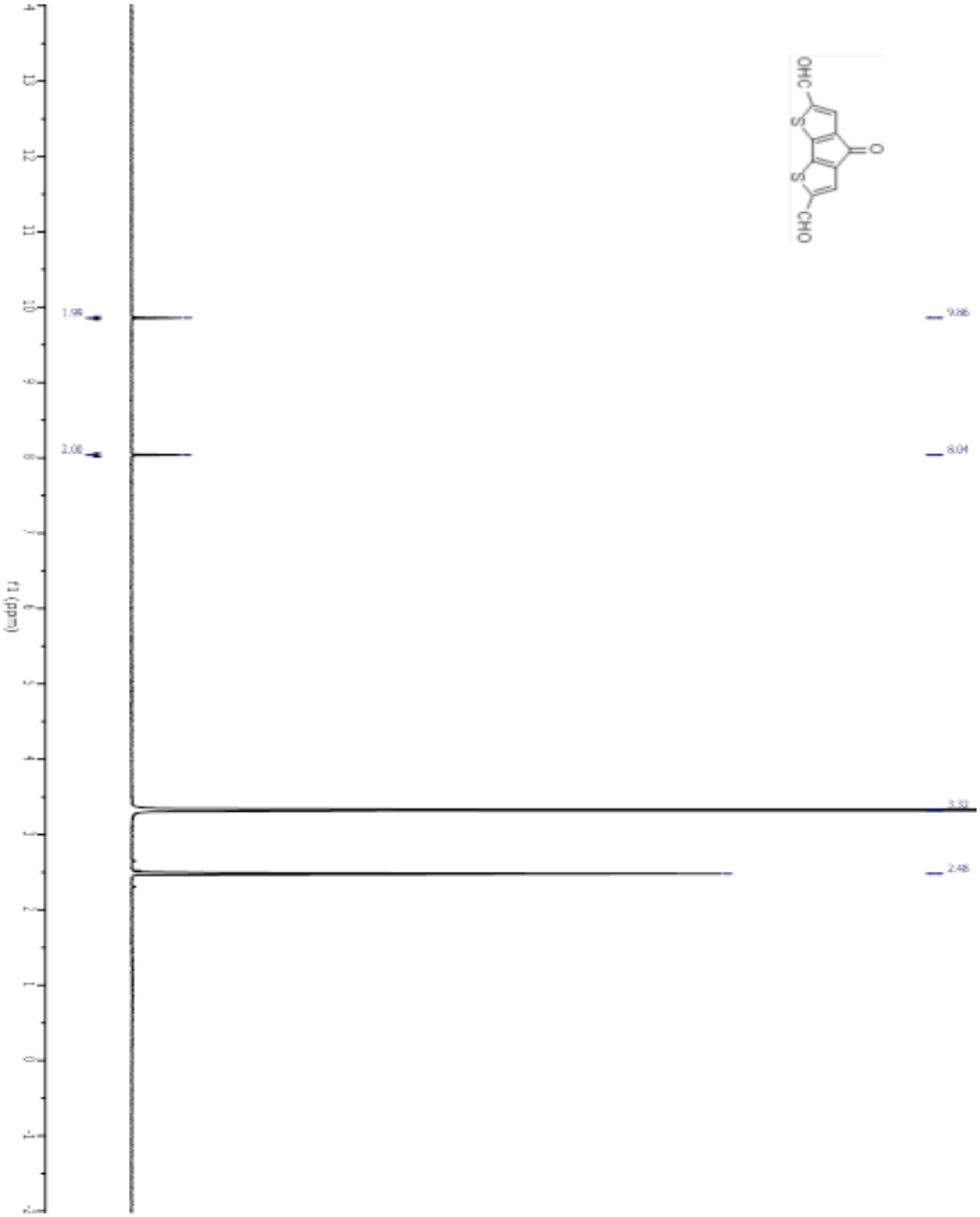

Figure 2.7.31: ^{1}H NMR spectra of compound 12

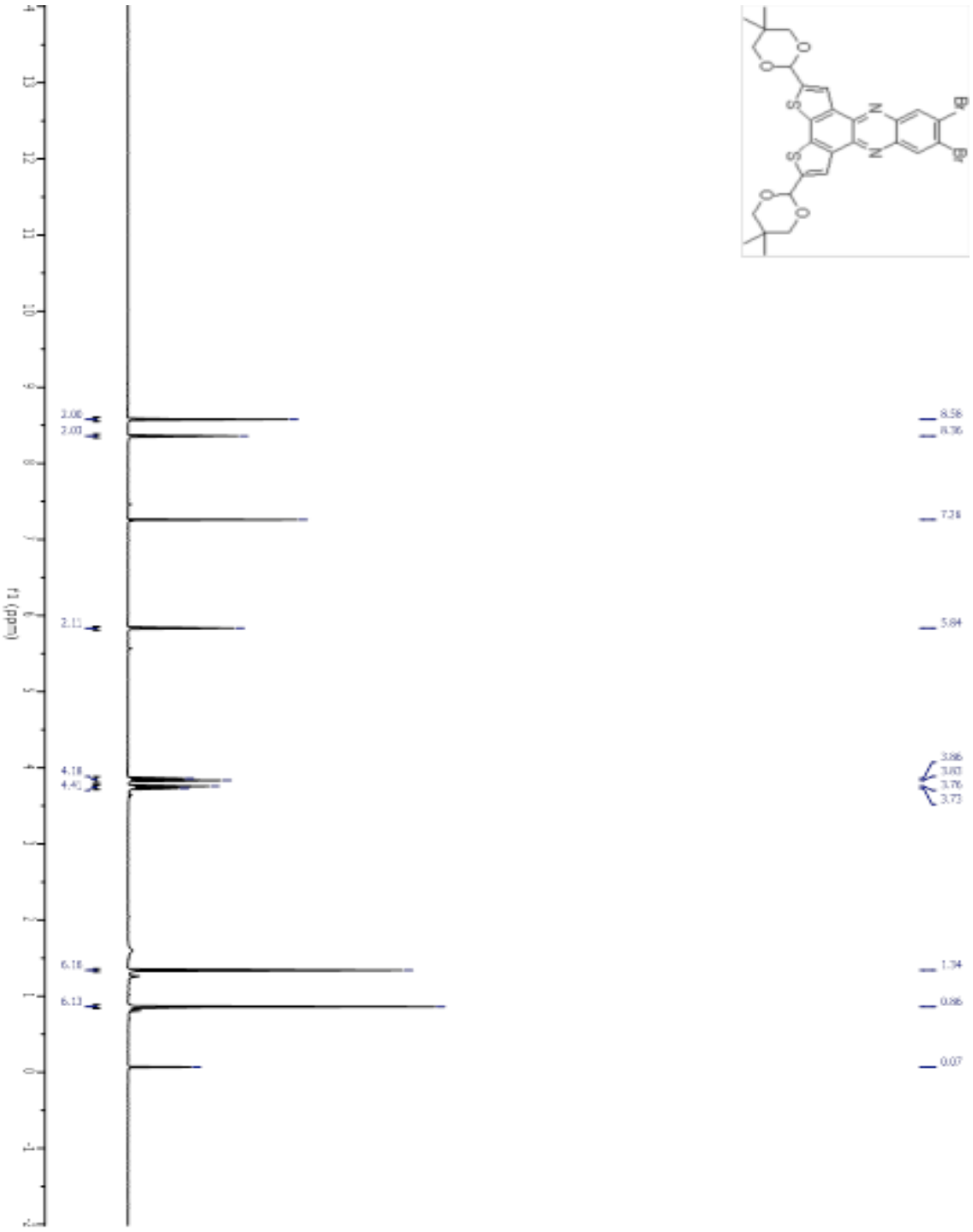

Figure 2.7.32: ^{1}H NMR spectra of compound 13

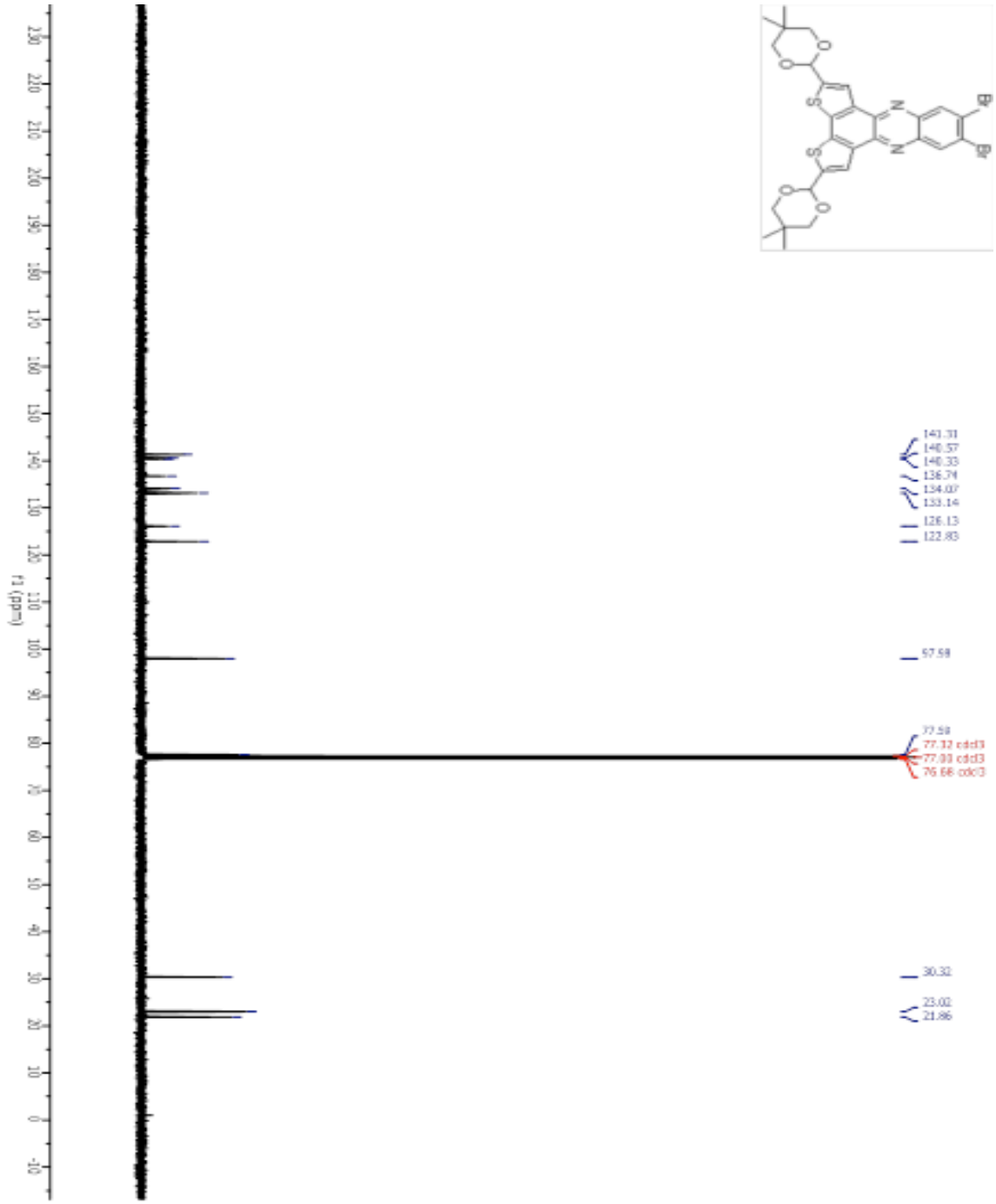

Figure 2.7.33: ^{13}C NMR spectra of compound 13

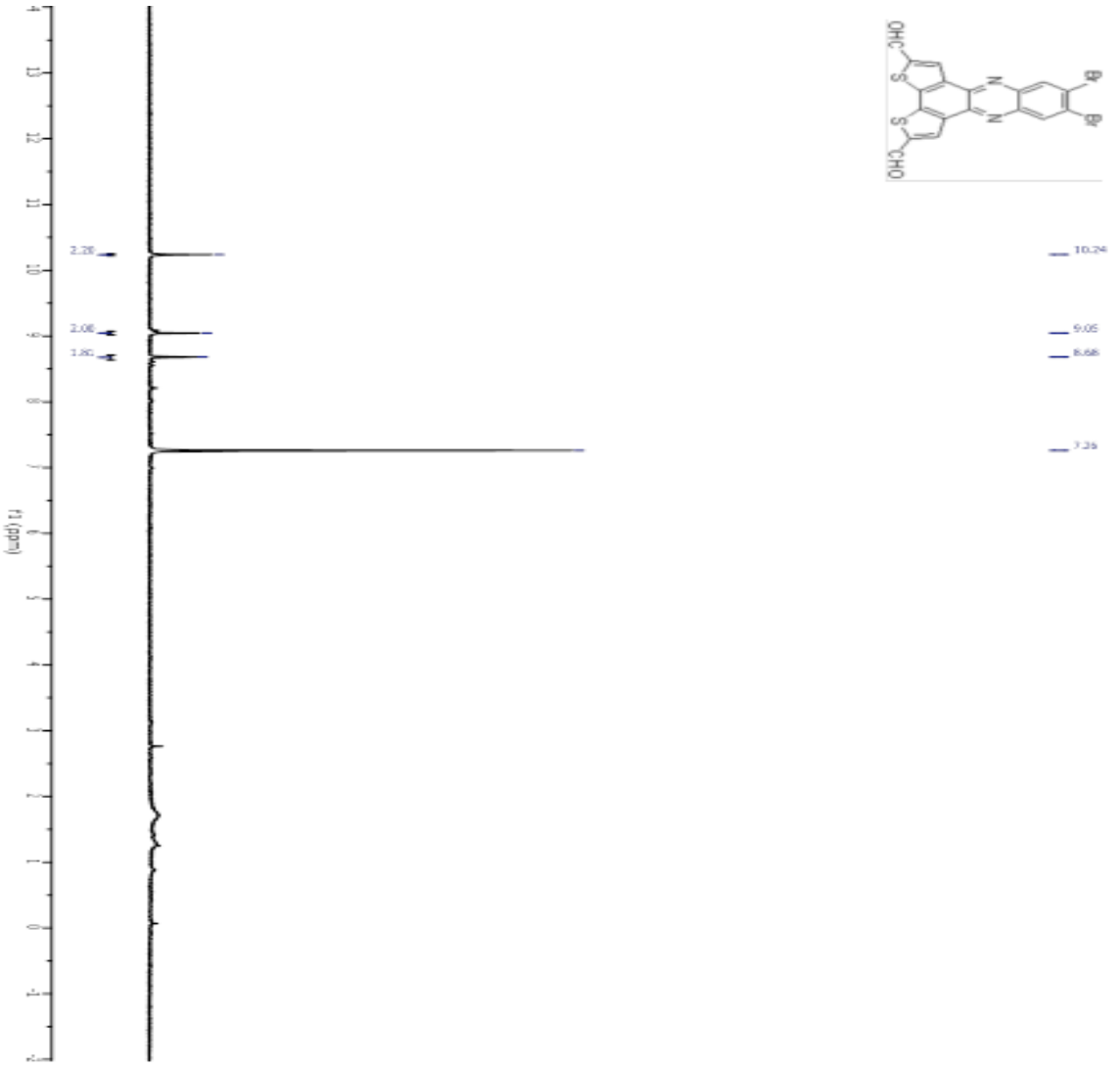

Figure 2.7.34: ^{1}H NMR spectra of compound 14

2.8 NOTES AND REFERENCES

(1) Bao, Z.; Dodabalapur, A.; Lovinger, A. J. *Appl. Phys. Lett.* **1996**, *69*, 4108.
(2) Facchetti, A. *Chem. Mater.* **2011**, *23*, 733.
(3) Burroughes, J. H.; Bradley, D. D. C.; Brown, A. R.; Marks, R. N.; Mackay, K.; Friend, R. H.; Burns, P. L.; Holmes, A. B. *Nature* **1990**, *347*, 539.
(4) Tang, C. W.; VanSlyke, S. A. *Applied Physics Letters* **1987**, *51*, 913.
(5) Grimsdale, A. C.; Leok Chan, K.; Martin, R. E.; Jokisz, P. G.; Holmes, A. B. *Chemical Reviews* **2009**, *109*, 897.
(6) Yu, G.; Gao, J.; Hummelen, J. C.; Wudl, F.; Heeger, A. J. *Science* **1995**, *270*, 1789.
(7) Thompson, B. C.; Frechet, J. M. J. *Angewandte Chemie International Edition* **2008**, *47*, 58.
(8) Havinga, E. E.; ten Hoeve, W.; Wynberg, H. *Polym. Bull.* **1992**, *29*, 119.

(9) Havinga, E. E.; ten Hoeve, W.; Wynberg, H. *Synth. Met.* **1993**, *55*, 299.
(10) Fei, Z.; Gao, X.; Smith, J.; Pattanasattayavong, P.; Buchaca Domingo, E.; Stingelin, N.; Watkins, S. E.; Anthopoulos, T. D.; Kline, R. J.; Heeney, M. *Chem. Mater.* **2013**, *25*, 59.
(11) Coppo, P.; Turner, M. L. *J. Mater. Chem.* **2005**, *15*, 1123.
(12) Chu, T.-Y.; Lu, J.; Beaupré, S.; Zhang, Y.; Pouliot, J.-R.; Wakim, S.; Zhou, J.; Leclerc, M.; Li, Z.; Ding, J.; Tao, Y. *J. Am. Chem. Soc.* **2011**, *133*, 4250.
(13) Zhang, Y.; Zou, J.; Cheuh, C.-C.; Yip, H.-L.; Jen, A. K. Y. *Macromolecules* **2012**, *45*, 5427.
(14) Ogawa, K.; Rasmussen, S. C. *J. Org. Chem.* **2003**, *68*, 2921.
(15) Steckler, T. T.; Zhang, X.; Hwang, J.; Honeyager, R.; Ohira, S.; Zhang, X.-H.; Grant, A.; Ellinger, S.; Odom, S. A.; Sweat, D.; Tanner, D. B.; Rinzler, A. G.; Barlow, S.; Bredas, J.-L.; Kippelen, B.; Marder, S. R.; Reynolds, J. R. *J. Am. Chem. Soc.* **2009**, *131*, 2824.
(16) Nelson, T. L.; Young, T. M.; Liu, J.; Mishra, S. P.; Belot, J. A.; Balliet, C. L.; Javier, A. E.; Kowalewski, T.; McCullough, R. D. *Adv. Mater.* **2010**, *22*, 4617.
(17) Usta, H.; Lu, G.; Facchetti, A.; Marks, T. J. *J. Am. Chem. Soc.* **2006**, *128*, 9034.
(18) Romero-Nieto, C.; Marcos, M.; Merino, S.; Barberá, J.; Baumgartner, T.; Rodríguez-López, J. *Adv. Funct. Mater.* **2011**, *21*, 4088.
(19) Romero-Nieto, C.; Merino, S.; Rodríguez-López, J.; Baumgartner, T. *Chem. -Eur. J.* **2009**, *15*, 4135.
(20) Mei, J.; Heston, N. C.; Vasilyeva, S. V.; Reynolds, J. R. *Macromolecules* **2009**, *42*, 1482.
(21) Ko, S.; Mondal, R.; Risko, C.; Lee, J. K.; Hong, S.; McGehee, M. D.; Bredas, J.-L.; Bao, Z. *Macromolecules* **2010**, *43*, 6685.
(22) Loewe, R. S.; McCullough, R. D. *Chem. Mater.* **2000**, *12*, 3214.
(23) Intemann, J. J.; Mike, J. F.; Cai, M.; Barnes, C. A.; Xiao, T.; Roggers, R. A.; Shinar, J.; Shinar, R.; Jeffries-El, M. *J. Poly. Sci. A.* **2013**, *51*, 916.
(24) Mike, J. F.; Makowski, A. J.; Mauldin, T. C.; Jeffries-El, M. *Journal of Polymer Science Part A: Polymer Chemistry* **2010**, *48*, 1456.
(25) Yassin, A.; Rousseau, T.; Leriche, P.; Cravino, A.; Roncali, J. *Sol. Energy Mater. Sol. Cells* **2011**, *95*, 462.
(26) Padhy, H.; Sahu, D.; Patra, D.; Pola, M. K.; Huang, J.-H.; Chu, C.-W.; Wei, K.-H.; Lin, H.-C. *J. Poly. Sci. A.* **2011**, *49*, 3417.
(27) Lu, G.; Usta, H.; Risko, C.; Wang, L.; Facchetti, A.; Ratner, M. A.; Marks, T. J. *J. Am. Chem. Soc.* **2008**, *130*, 7670.
(28) Dahlmann, U.; Neidlein, R. *Helv. Chim. Acta* **1996**, *79*, 755.
(29) Arroyave, F. A.; Richard, C. A.; Reynolds, J. R. *Org. Lett.* **2012**, *14*, 6138.
(30) Rasmussen, S. C.; Mulholland, M. E.; Schwiderski, R. L.; Larsen, C. A. *J. Heterocycl. Chem.* **2012**, *49*, 479.
(31) Rasmussen, S. C.; Schwiderski, R. L.; Mulholland, M. E. *Chem. Commun.* **2011**, *47*, 11394.
(32) Shahid, M.; Ashraf, R. S.; Klemm, E.; Sensfuss, S. *Macromolecules* **2006**, *39*, 7844.
(33) Zhou, H.; Yang, L.; Liu, S.; You, W. *Macromolecules* **2010**, *43*, 10390.

(34) Meyer, A.; Sigmund, E.; Luppertz, F.; Schnakenburg, G.; Gadaczek, I.; Bredow, T.; Jester, S.-S.; Höger, S. *Beilstein Journal of Organic Chemistry* **2010**, *6*, 1180.
(35) Guo, X.; Wang, S.; Enkelmann, V.; Baumgarten, M.; Müllen, K. *Organic Letters* **2011**, *13*, 6062.
(36) Krebs, F. C.; Jørgensen, M. *Macromolecules* **2003**, *36*, 4374.
(37) Koeckelberghs, G.; De Cremer, L.; Vanormelingen, W.; Dehaen, W.; Verbiest, T.; Persoons, A.; Samyn, C. *Tetrahedron* **2005**, *61*, 687.
(38) Chen, C.-H.; Hsieh, C.-H.; Dubosc, M.; Cheng, Y.-J.; Hsu, C.-S. *Macromolecules* **2009**, *43*, 697.
(39) Baumgartner, T.; Neumann, T.; Wirges, B. *Angewandte Chemie International Edition* **2004**, *43*, 6197.
(40) Getmanenko, Y. A.; Risko, C.; Tongwa, P.; Kim, E.-G.; Li, H.; Sandhu, B.; Timofeeva, T.; Brédas, J.-L.; Marder, S. R. *The Journal of Organic Chemistry* **2011**, *76*, 2660.

CHAPTER 3

QUATERTHIOPHENE – BENZOBISAZOLE COPOLYMERS FOR PHOTOVOLTAIC CELLS: EFFECT OF HETEROATOM PLACEMENT AND SUBSTITUTION ON THE OPTICAL AND ELECTRONIC PROPERTIES

Macromolecules, **2011**, *44* (24), pp 9611–9617

DOI: 10.1021/ma202133e

*Achala Bhuwalka,[1] Jared F. Mike,[1] Meng He,[2,3] Jeremy J. Intemann,[1] Toby Nelson,[4] Monique D. Ewan[1], Robert A. Roggers,[1] Zhiqun Lin[2,5] and Malika Jeffries-EL[1]**

[1]Department of Chemistry, Iowa State University, Ames IA 50011. [2] Department of Materials Science and Engineering, Iowa State University, Ames, IA 50011. [3]The Key Laboratory of Molecular Engineering of Polymers, Ministry of Education, Department of Macromolecular Science, Fudan University, Shanghai 200433, China. [4]Department of Chemistry, Carnegie Mellon University, Pittsburgh, PA 15213. [5]School of Materials Science and Engineering, Georgia Institute of Technology, Atlanta, GA 30332.

3.1 Abstract:

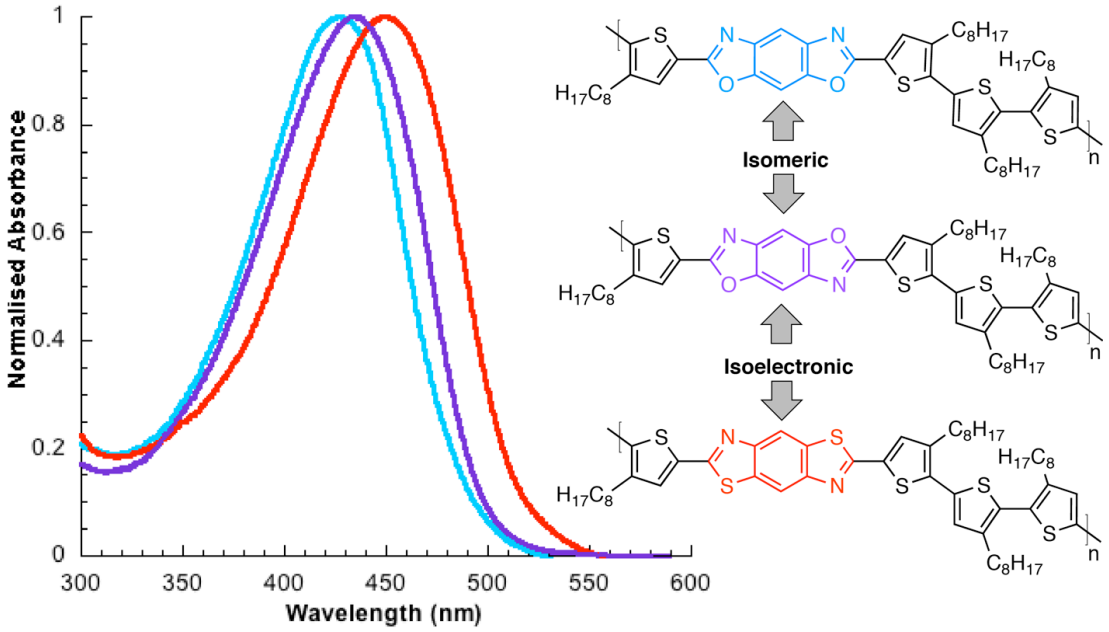

Three new donor-acceptor conjugated polymers were synthesized by combining electron-donating 3-octylthiophenes with various electron-accepting benzobisazoles. The influence of the structural differences of the three benzobisazoles on the electrochemical, optical, and photovoltaic properties of the polymers composed from them was investigated. According to our results, changing the arrangement of the oxygen atoms of the benzobisoxzoles from the *cis* to *trans* orientation slightly stabilized both the HOMO and LUMO levels, whereas replacing the oxygen atoms in *trans*-BBO with sulfur atoms only stabilized the HOMO level. Bulk heterojunction photovoltaic devices were fabricated by using the copolymers as electron donors and $PC_{71}BM$ ([6,6]-phenyl C_{71}-butyric acid methyl ester). It was found that open circuit voltages (V_{oc}s) as high as 0.86 V, and power conversion efficiencies (PCEs) up to 1.14%, were obtained under simulated AM 1.5 solar irradiation of 100 mW/cm^2. Field-effect transistors based on these polymers

exhibited hole mobilities as high as of 4.9 x 10^{-3}cm^2/Vs with the *trans*-BBO polymer giving the best performance in both devices.

3.2 Introduction

In recent years, conjugated polymers have generated a large amount of interest as potential replacements for inorganic semiconductors in applications such as organic light emitting diodes (OLEDs),[1-3] photovoltaic cells[4-6] (PVCs) and field-effect transistors (FETs).[7] It is generally understood that organic semiconductors have several major advantages over their inorganic counterparts including: the opportunity to fabricate lightweight flexible devices, the ability to make large area devices using low-cost solution-based techniques, and the variety of optical and electronic properties that can be attained through chemical synthesis.[8-12] Currently, a popular strategy for tailoring of the properties of conjugated polymers is through the synthesis of materials composed of alternating electron-donating and electron-accepting groups.[13-15] This approach has produced a number of useful materials resulting in charge carrier mobilities exceeding 0.1 cm^2 V^{-1} s^{-1} in FETs and record performances of greater than 8% in PVCs.[15-21] Although conjugated polymer PVCs are rapidly approaching the minimum 10% efficiency required for commercial viability,[5] the development of new materials with improved properties and easy synthetic routes remains a challenge.[16-20]

Based on the aforementioned considerations, we became interested in the development of new materials based on the benzobisoxazole and benzobisthiazole moieties. Collectively known as benzobisazoles,[22] these planar, electron-deficient

heterocycles were initially used for the synthesis of rigid-rod polymers with excellent tensile strength and thermal stability.[23-25] As a result of their origins as high-performance materials, the requisite starting materials for the synthesis of benzobisazoles are readily prepared on a large scale and in good yield.[23, 24, 26, 27] Although the incorporation of benzobisazoles into conjugated materials is known to enhance the electron transport,[28, 29] photoluminescence,[30-33] and third-order nonlinear optical properties,[34-37] until recently their use has been hindered by poor solubility and the harsh conditions used for their synthesis.[38-50] This is particularly problematic for the synthesis of materials based on benzo[1,2-*d*; 4,5-*d*']bisoxazole (*trans*-BBO), as the starting material for its synthesis, 2,5-diaminohydroquinone readily decomposes.[39]

Previous research on the optical and electronic properties of benzo[1,2-*d*; 5,4-*d*']bisoxazole (*cis*-BBO), and benzo[1,2-*d*; 4,5-*d*']bisthiazole (*trans*-BBZT), indicates that replacing oxygen with the less electronegative sulfur atom increases the delocalization within the π-orbitals. [10-12, 15] Additionally, the empty *d*-orbitals of the sulfur atom can contribute to the molecular π-orbitals, decreasing the energy of the π-π* transition.[28-37, 49, 51-54] However, since materials containing the analogous *trans*-BBO had not been synthesized, the influence of the heteroatom position on the optical and electronic properties of materials containing benzobisoxazoles has not been investigated. Varying the arrangement of the oxygen atoms around the central benzene ring impacts the planarity of the benzobisoxazoles, their symmetry and also their dipole moments.[44, 55] In order to investigate the influence of these modifications on the properties of the resulting polymers, we have synthesized three new alternating copolymers containing *trans*-BBO, *cis*-BBO, and the analogous sulfur compound, (*trans*-BBZT) as the accepting group and

an electron donating 3,3''',4'-tetraoctyl-2,2':5',2'':5'',2'''-quaterthiophene unit. The thiophene-based co-monomer was used to improve the solubility and hole mobility of the resulting copolymers.

3.3 Results and Discussion

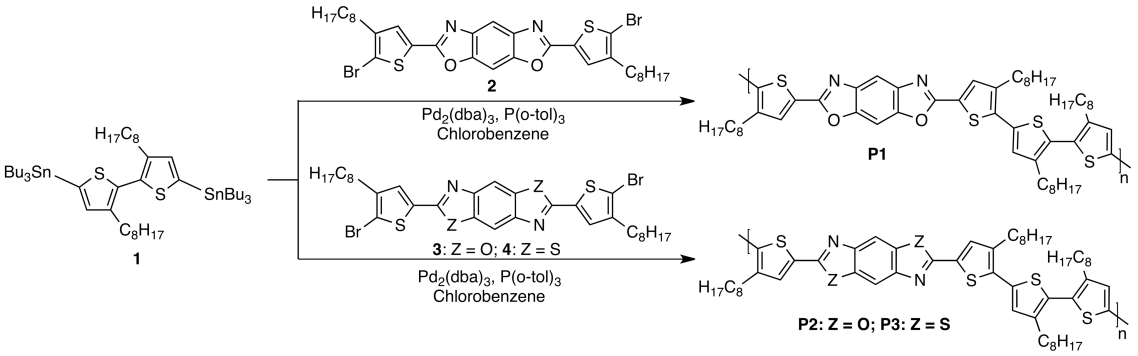

Scheme 3.1. Synthesis of Thiophene-Benzobisazole Copolymers.

3.3.1 Synthesis

The chemical structures and synthetic routes toward the three polymers are outlined in Scheme 1. We elected to first synthesize monomers where the benzobisazole moiety is positioned between two thiophene rings as this building block allows for polymerization to be performed using transition metal-catalyzed cross coupling reactions, instead of condensation polymerization. The requisite monomers 2,6-bis(4-octylthiophen-2-yl)benzo[1,2-*d*; 5,4-*d*']bisoxazole **(2)**, 2,6-bis(4-octylthiophen-2-yl)benzo[1,2-*d*; 4,5-*d*']bisoxazole **(3)**, and 2,6-bis(4-octylthiophen-2-yl)benzo[1,2-*d*; 4,5-*d*']bisthiazole **(4)** were synthesized in high yields (78 – 84%) according to the literature procedure.[56] Unfortunately, we are unable to synthesize the fourth derivative, 2,6-bis(4-octylthiophen-2-yl)-benzo[1,2-*d*; 5,4-*d*']bisthiazole, which contains the *cis*-BBZT moiety due to the lack of protocols for the synthesis of the required starting material 4,6-diaminobenzene 1,3-

dithiol. There are no reports for the synthesis of this compound in the modern literature and all attempts to develop a new approach were unsuccessful.

The Stille cross-coupling polymerization of monomers **2**, **3** or **4** with (3,3'-dioctyl-2,2'-bithiophene-5,5'-diyl)bis(tributylstannane), **(1)** afforded the polymers **P1**, **P2** and **P3** respectively. All polymers were obtained in 55 – 65% yields after purification by Soxhlet extraction with methanol to remove residual catalyst followed by hexanes to remove the lower molecular weight material. The polymer was then obtained using THF as the extraction solvent. The solvent was evaporated and the polymer so obtained was used for further analysis.. All polymers are soluble in standard organic solvents, such as THF, *m*-cresol and chloroform at room temperature, facilitating characterization using ^{1}H NMR spectroscopy and gel permeation chromatography (GPC). The ^{1}H NMR spectra for all polymers were in agreement with the proposed polymer structures (Figures 3.7.10 – 3.7.12 ESI).

Table 3.1. Physical properties of thiophene-benzobisazole copolymers

Polymer	M_n[a]	% yield	PDI	T_d (ºC)[b]	T_g (ºC)[c]
P1	9900	60%	1.37	374	84.2
P2	8200	65%	1.39	401	84.6
P3	5000	55%	1.69	324	80.8

[a] Determined by GPC in THF using polystyrene standards. [b] 5% weight loss temperature by TGA in air.[c] Data from second scan reported, heating rate 15 ºC/min under N_2.

The number averaged degree of polymerization (DP_n) ranged from 8 – 14 and, despite the modest molecular weights, all of the polymers showed excellent film-forming ability. Thermogravimetric analysis (TGA) revealed that all polymers were thermally stable with 5% weight loss onsets occurring above 340 °C under air (Figure 3.7.2). All polymers exhibited weak glass transitions as measured by differential scanning calorimetry (DSC) (Figure 3.7.3). The results are summarized in Table 3.1.

3.3.2 Optical and Electrochemical Properties.

The normalized absorbance spectra of the polymer solutions in THF and in the solid state are shown in Figures 3.1 and 3.2, respectively, and the data is summarized in Table 3.2. In solution, the UV spectra for all three polymers exhibit a single, featureless absorbance band. As a result of changing the arrangement of the oxygen atoms, the absorption maximum for **P2** was red-shifted 7 nm relative to the absorbance maximum for **P1**. Substituting sulfur for oxygen results in a 16 nm red-shift (relative to **P2)** in the absorption maximum of **P3** (and 23 nm relative to **P1**).

As thin films, the absorbance spectra for all polymers are significantly broader, resulting in bathochromic shifts in the absorption maximum, indicating increased backbone planarization and π-stacking in the solid state.[57] Interestingly, the spectra of **P1** and **P2** are significantly broader than that of **P3** and they also exhibit a small shoulder at higher wavelengths, which is indication of strong interchain interactions in the solid state.[47] The presence of long-range order in the solid state is also supported by X-ray analysis, which shows that thin films of all polymers show periodicity (Figure 3.7.14).

The diminished impact of the solid-state interactions within films of **P3** may be a result of its lower molecular weight.

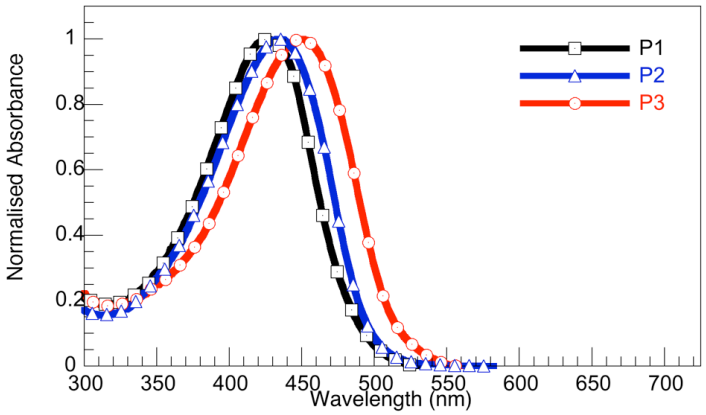

Figure 3.1. UV-Vis absorption spectra of thiophene-benzobisazole copolymers in THF.

Jenekhe also observed differences in the solid-state absorption spectra for the related copolymer composed of 2,6-Bis(5-bromo-3-Octylthiophen-2-yl)benzo[1,2-*d*; 4,5-*d*']bisthiazole and (4,4'-dioctyl-2,2'-bithiophene-5,5'-diyl)bis(trimethylstannane) (PBTOT) when the molecular weight of the polymer was increased.[47] The λ^{abs}_{max} of the benzobisthiazole polymer **P3** is also blue-shifted relative to the λ^{abs}_{max} reported previously for the related polymer PBTOT (λ^{abs}_{max} 540 - 551 nm).[47] This is most likely due to the different substitution pattern of the 3-alkylthiophene comonomers as PBTOT contains a tail-to-tail orientation of alkylthiophenes within the quaterthiophene unit, whereas **P3** contains a head-to-head defect. Such defects are known the decrease planarity, disrupting conjugation and resulting in an increase in the optical band gaps within poly(3-alkylthiophene)s.[58-60]

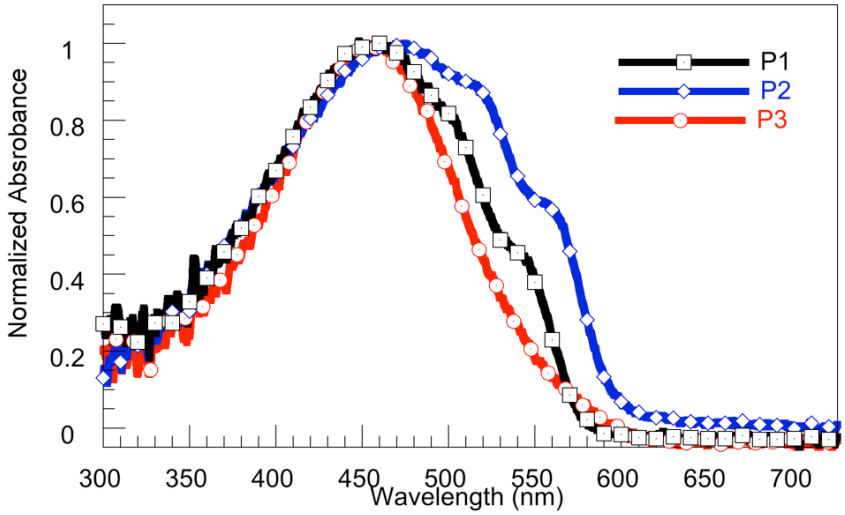

Figure 3.2. UV-vis absorption spectra of the thiophene-benzobisazole copolymers in the solid state. Thin films were spun from solutions of the polymers in *o*-DCB (2 mg/mL).

The optical band gaps of the benzobisazole polymers ranged from 2.1 to 2.2 eV, and are larger than the 1.9 eV reported for the homopolymer poly(3-octylthiophene) (P3OT). [58]The fact that the donor-acceptor copolymer has a larger optical band gap than the homopolymer suggests that there is no significant intramolecular charge transfer within the polymer backbone.[61] The bandgaps of the benzobisoxazole polymers **P1** and **P2** are similar to the reported values for the related poly(thiophenevinylene-co-benzobisoxazole)s (2.0 – 2.2 eV), which were demonstrated to have limited distribution of electron density along the polymer backbone using density functional theory at the B3LYP/6-31G* level.[44] The poly(thiophenevinylene-co-benzobisoxazole)s also exhibited broader spectra with λ^{abs}_{max} that are significantly red-shifted relative to **P1** and **P2** (solution λ^{abs}_{max} 470 - 480 nm; film λ^{abs}_{max} 527 - 556 nm),[44] which is not surprising as the

vinylene linkage minimizes steric interactions between consecutive aromatic rings, planarizing the polymer backbone and extending the π-conjugation, which can produce a more broadly absorbing material.[62, 63]

Table 3.2. Electronic and optical properties of quaterthiophene-benzobisazole copolymers.

	Solution			Film					
Polymer	λ_{abs} (nm)	λ_{abs} (nm)	λ_{onset} (nm)	E_g^{opt} (eV)[a]	E^{ec}_g (eV)	E_{onset}^{ox}	E_{onset}^{red}	LUMO (eV)	HOMO (eV)
P1	427	460	580	2.2	2.4	0.54	-1.88	-2.9[b]/-3.3[c]	-5.1[d]/-5.3[e]
P2	434	475	597	2.1	2.3	0.57	-1.94	-3.1[b]/-3.2[c]	-5.2[d]/-5.4[e]
P3	450	462	560	2.2	2.3	0.62	-1.97	-3.1[b]/-3.2[c]	-5.3[d]/-5.4[e]

[a] Estimated from the optical absorption edge. [b] LUMO = HOMO(obtained from UPS) + E_g^{opt} (eV). [c] LUMO = -4.8- (E^{red}_{onset}) (eV). [d] Obtained using ultraviolet photoelectron spectroscopy. [e] HOMO = -4.8- (E^{ox}_{onset}) (eV). Electrochemical properties were measured using a three-electrode cell (electrolyte: 0.1 mol/L $TBAPF_6$ in acetonitrile) with an Ag/Ag^+ reference electrode, a platinum auxiliary electrode, and a platinum button electrode as the working electrode. Reported values are referenced to Fc/Fc^+. Polymer films were drop cast from an *o*-DCB solution of the polymers on to the working electrode. All differential pulse voltammetry experiments were recorded at a scan rate of 50 mV/s.

The electronic properties of the polymers were investigated by ultraviolet photoelectron spectroscopy (UPS) and differential pulse voltammetry (DPV). The onsets were internally referenced to Fc/Fc^+. In comparison to CV, DPV is more sensitive to oxidation and reduction potential onsets.[63, 64] The electrochemical results are shown in Figures 3.7.3, and summarized in Table 3.2. All of the polymers exhibit measureable and

reproducible oxidation and reduction processes. The HOMO levels were also determined using UPS, which accurately determines the HOMO level by bombarding an organic thin film with ultraviolet photons and measuring the kinetic energies of the ejected valence electrons.[65] In all cases, the values obtained for the HOMO levels using UPS match well with the values obtained using DPV. According to the UPS data, **P1**, **P2**, and **P3** exhibit HOMO levels of -5.1 eV, -5.2 eV and -5.3 eV respectively. These values are all lower than the reported HOMO of regioregular poly(3-hexylthiophene) (rr-P3HT) under the same conditions (-4.89 eV),[66] which means that these polymers are more stable against oxidation than rr-P3HT. Based on the UPS data, changing the position of the oxygen atoms from the *cis*- configuration to the *trans*- configuration stabilizes both the HOMO and LUMO levels, although the LUMO is influenced to a greater extent and thus **P2** has a smaller band gap than **P1**. The higher LUMO level of *cis*-BBO can be attributed to its inability to form a stable quinoidal state. Substituting sulfur atoms for the oxygen atoms in benzobisazoles stabilizes the HOMO but has no effect on the LUMO level, and thus **P3** has a larger band gap than **P2**. Since both *trans*-BBO and *trans*-BBZT can form stable quinoidal forms, the LUMO is unaffected by heteroatom substitution. However, since the sulfur atom is less electronegative than oxygen, *trans*-BBZT is more aromatic than *trans*-BBO. Thus there is a greater delocalization of the electrons, resulting in a deeper HOMO. Overall the *trans*-BBO based **P2** had the smallest bandgap of all of the polymers, whereas the *trans*-BBZT based **P3** has the deepest HOMO level. The HOMO of the benzobisthiazole polymer **P3** is slightly lower than that reported previously for the related PBTOT (HOMO = -5.2 eV); however, **P3** has a slightly higher LUMO level (-3.2 eV) and thus a wider band gap.[47] These variances can be attributed to the different

arrangement of the alkyl chains on the thiophene comonomers used in **P1** – **P3** and the error associated with cyclic voltammetry measurements.[58, 67]

3.3.3 Field-Effect Transistors.

The FET characteristics of the benzobisazole-quaterthiophene copolymers were studied using a bottom-gate, top-contact thin film transistor configuration. Several different channel lengths were measured for each polymer and the best results are summarized in Table **3.7.2**. Before polymer deposition, the SiO_2 surface was treated with octyltrichlorosilane (OTS), which is a surface treatment that can improve the molecular ordering and enhance FET performance.[68] The details of the device fabrication are described in the experimental section. Overall, the FETs based on **P2** gave the best performance with a maximum observed hole mobility, $\mu h = 4.8 \times 10^{-3}$ cm^2/Vs, and an average hole mobility $\mu h = 3.6 \times 10^{-3}$ cm^2/Vs. **P3** exhibited the poorest performance, which is not surprising as FET performance can be correlated to the nanostructure of the polymer.[69] This has been shown to be somewhat dependent on the molecular weight of the polymer.

Table 3.3. OFET Characteristics of Benzobisazole-Quarterthiophene Copolymers.

Polymer	on/off ratio	μh^{max} cm^2 /Vs	V_T (V)
P1	10^4	4.8×10^{-5}	-48
P2	10^2	8.9×10^{-5}	-30
P3	10^4	1.0×10^{-4}	-30

3.3.4 Photovoltaic Properties.

Photovoltaic devices with a configuration of ITO/PEDOT:PSS/ Polymer:$PC_{71}BM$/Ca/Al were fabricated at different weight ratios of polymer to $PC_{71}BM$ in order to identify the best donor-acceptor mixing ratios for these newly designed donor-acceptor copolymers. The area of the photovoltaic devices was 0.10±0.01 cm^2. The current density-voltage (J-V) curves of **P1**/$PC_{71}BM$, **P2**/$PC_{71}BM$, and **P3**/$PC_{71}BM$ photovoltaic devices under AM 1.5 G illumination (100 mW/cm^2) are shown in Figure 3.3. The photovoltaic performances are summarized in Table 3.3. For devices based on **P2**/$PC_{71}BM$ and **P3**/$PC_{71}BM$, the highest power conversion efficiencies (PCE) were obtained using polymer/$PC_{71}BM$ weight ratios of 1:2, with PCEs of 0.61% and 1.14%, respectively. For devices based on **P1**/$PC_{71}BM$, the best performance was obtained using polymer/$PC_{71}BM$ weight ratios of 1:3, with a PCE of 0.98%. These results indicate that the donor/acceptor networks formed within blended films of 1:2 or 1:3 wt/wt ratio of these thiophene-benzobisazole copolymers transported holes more efficiently than in 1:1 P3HT/PCBM blends.[70, 71] Interestingly, the benzobisoxazole polymers **P1** and **P2** both exhibited higher open circuit voltage, V_{oc} > 0.70 V than both **P3** and rr-P3HT. In fact, although **P3** had the lowest-lying HOMO level of all of the polymers, it had the worst performance of all of the benzobisazole polymers. Overall, the highest PCE of 1.14% was obtained in **P2**/$PC_{71}BM$ based device with V_{oc} of 0.73 V, J_{sc} of 5.13 mA/cm^2 and fill factor (FF) of 30.6%. The improved performance of the *trans*-BBO based polymers can be attributed to its higher hole mobility, smaller band gap and broader and red-shifted absorption spectra relative to the other benzobisazoles.

Table 3.4. Summary of photovoltaic performances of **P1**/$PC_{71}BM$, **P2**/$PC_{71}BM$, and **P3**/$PC_{71}BM$ solar cells with different blending ratios under AM 1.5 G illumination at 100 mW/cm^2

Polymer	$PC_{71}BM$ ratio (w/w)	V_{oc} (V)	J_{sc} ($mAcm^{-2}$)	FF (%)	PCE (%)
P1	1:0.5	0.86	1.61	26.38	0.36
	1:1	0.73	4.10	31.49	0.94
	1:2	0.75	2.94	26.71	0.59
	1:3	0.74	4.22	31.48	0.98
	1:4	0.76	2.09	24.49	0.39
P2	1:0.5	0.72	1.90	31.95	0.44
	1:1	0.73	3.92	32.86	0.94
	1:2	0.73	5.13	30.59	1.14
	1:3	0.72	4.20	33.56	1.01
	1:4	0.72	3.43	31.89	0.79
P3	1:0.5	0.48	3.66	30.75	0.54
	1:1	0.28	4.30	29.25	0.35
	1:2	0.53	3.52	32.62	0.61
	1:3	0.57	2.39	29.50	0.40
	1:4	0.54	2.65	28.03	0.40

The low-lying HOMO level of the thiophene-benzobisazole copolymers was expected to improve performance by increasing the V_{oc}. Unfortunately, the overall performance was limited by the relatively wide band gaps of the polymers.

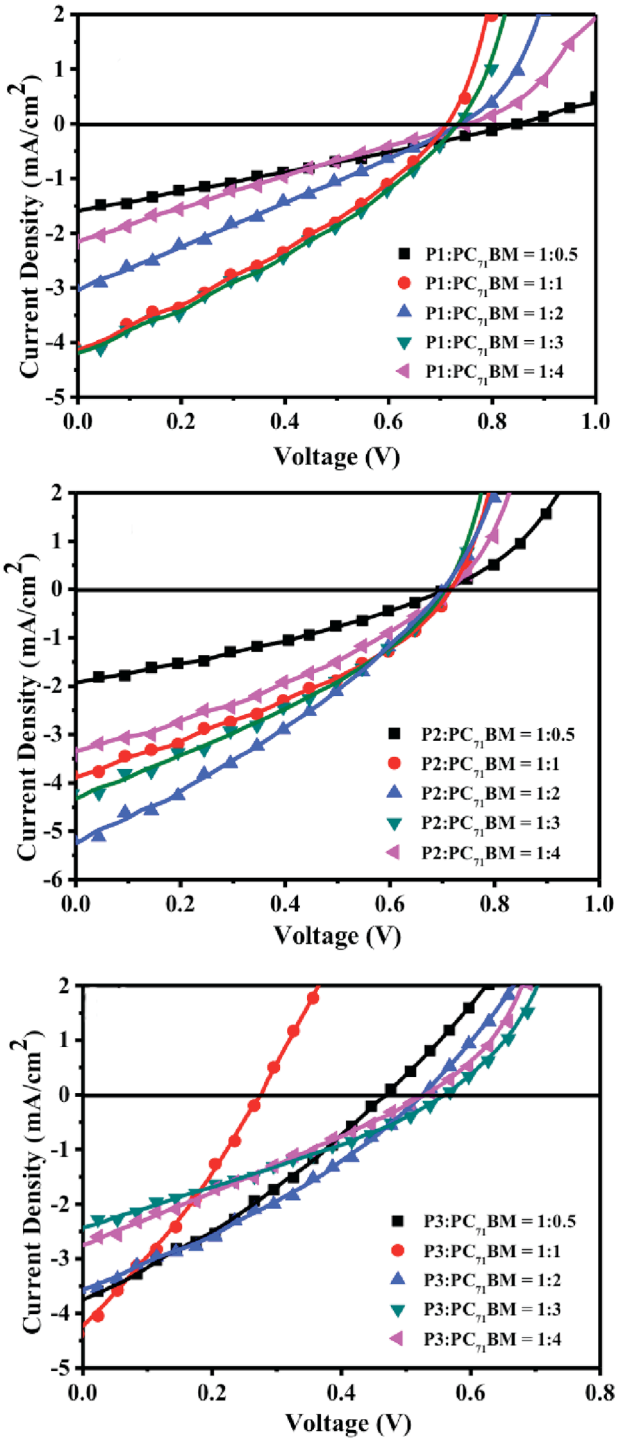

Figure 3.3. J-V curves of bulk heterojunction solar cells fabricated from (a) **P3**/$PC_{71}BM$, (b) **P1**/$PC_{71}BM$, and (c) **P2**/$PC_{71}BM$ solar cells under AM 1.5 G illumination at 100 mW/cm^2. All the polymers and $PC_{71}BM$ were blended at different weight ratios (i.e., 1:0.5, 1:1, 1:2, 1:3, and 1:4).

The relatively low FF for the devices (< 60%) indicates that poor bulk-heterojunction nanostructures formed in the blends. Since the morphology of the polymer:$PC_{71}BM$ blend greatly impacts the overall performance of bulk heterojunction solar cells, we examined the morphology of blends of the best performing polymer, **P2** and $PC_{71}BM$ using atomic force microscopy (AFM). The height and phase images of the blends **P2** and various weight ratios of $PC_{71}BM$ are shown in Figure 3.4. Although there are slight variations in the PVC performance of the different blends, they all formed fairly smooth films with small root- mean-square (rms) roughness of (0.37, 0.43, 0.30, and 0.40 nm), for the 1:1, 1:2, 1:3 and 1:4 **P2**:$PC_{71}BM$ ratios respectively. The 3D AFM images also indicate that the polymers form slightly rounded grains, resulting in a slightly irregular film surface. However, since AFM only indicates the properties of surface-morphology of the active layers, the degree of vertical phase segregation of the two components in these samples is unknown.[62] In order to improve performance, we must first improve the film morphology of these new polymer blended with fullerenes. Future studies will investigate the influence of side chain modifications and solvent additives both of which have been demonstrated to be promising in optimizing the film morphology in such donor-acceptor copolymers and could improve J_{sc} and *FF* in **P1** and **P2** based devices.[72] It is worth noting that thermal annealing treatments under different temperatures (i.e., 100 ℃, 120 ℃, 140 ℃ and 160 ℃) were carried out to improve the film morphology of the blend films. However, the performances of the PVCs decreased after thermal annealing as summarized in Table 3.7.1 in Supporting Information.

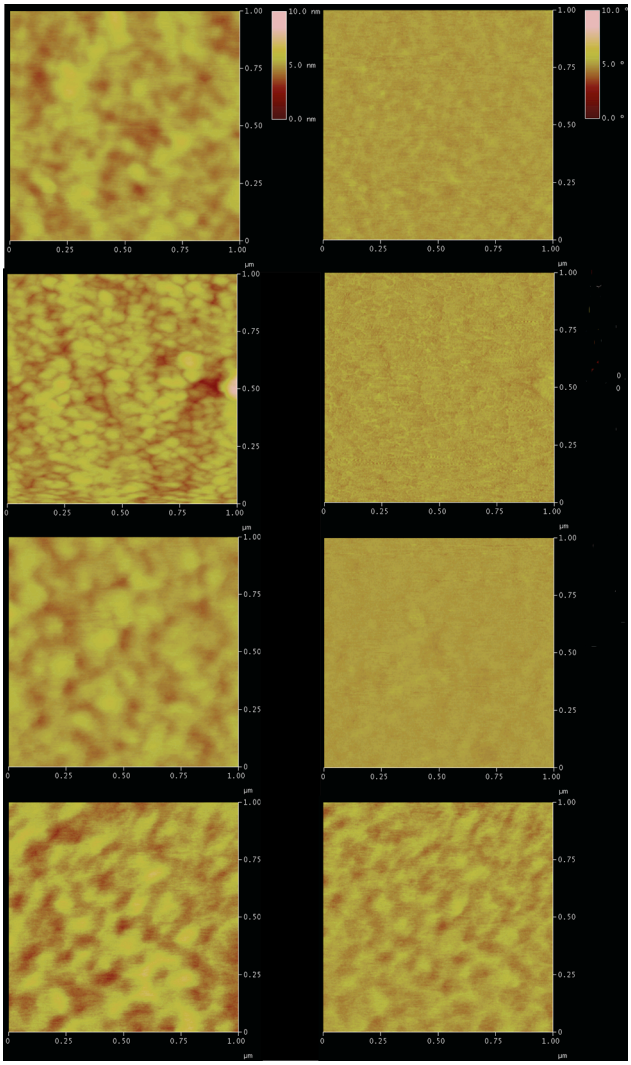

Figure 3.4. AFM Height (left) and Phase (right column) images of devices with various **P2**:$PC_{71}BM$ blends. From top to bottom: 1:1, 1:2, 1:3 and 1:4 **P2**: $PC_{71}BM$ ratios.

3.4 Conclusions

In summary, we have reported the synthesis of three related benzobisazoles-containing polymers. The benzobisazole monomers were prepared in high yields and can be readily polymerized with bithiophene monomers via the Stille cross-coupling reaction.

The octyl side chains on the thiophene rings led to good solubility, while maintaining good thermal stability. While the polymers have slightly different HOMO and LUMO levels, polymers based on *trans*-BBO exhibited broader and red-shifted absorption spectra relative to the other benzobisazoles in the solid state. The *trans*-BBO polymer **P2** also had the highest hole mobility of all three polymers. As a result of the ease of synthesis and deep HOMO level, *trans*-benzobisoxazoles have great potential for use in bulk heterojunction PVCs. We are currently synthesizing new derivatives of this polymer in order to improve its performance in photovoltaic cells and field-effect transistors.

3.5 Experimental Methods

3.5.1 Materials and General Experimental Details.

Tetrahydrofuran was dried using an Innovative Technologies solvent purification system. 2,6-Bis(4-octylthiophen-2-yl)benzo[1,2-*d*; 5,4-*d*']bisoxazole **(2)**, 2,6-Bis(4-octylthiophen-2-yl)benzo[1,2-*d*; 4,5-*d*']bisoxazole **(3)**, 2,6-Bis(4-octylthiophen-2-yl)benzo[1,2-*d*; 4,5-*d*']bisthiazole **(4)** and (3,3'-dioctyl-2,2'-bithiophene-5,5'-diyl)bis(tributylstannane) **(1)** were synthesized according to literature procedures. All other compounds were purchased from commercial sources and used without further purification.

3.5.2 General Polymerization Procedure

A mixture of **1** and the respective benzobisazole, 2 mol% tris(dibenzylideneacetone)dipalladium (0), 8 mol% tris-o-tolyphosphine in 12 mL of chlorobenzene was charged in a round bottom flask equipped with a reflux condenser and

an argon inlet. The mixture was allowed to reflux for 66 hours before it was quenched by pouring into 100 mL of methanol containing 2% HCl. The precipitated polymer was filtered into a cellulose extraction thimble and then washed in a Soxhlet extractor with methanol, hexane, and THF The polymer was recovered from the THF fractions after evaporation of the solvent.

Poly(2,6-bis(4-octyl-5-(3,3'-dioctylbithiophen-2-yl)thiophen-2-yl)benzo[1,2-*d*;5,4-*d'*]bisoxazole) (P1) Polymer obtained as bright red solid (0.28 g, 60% yield);

GPC: M_n = 9,900, M_w = 13,600, PDI = 1.37.

Poly(2,6-bis(4-octyl-5-(3,3'-dioctylbithiophen-2-yl)thiophen-2-yl)benzo[1,2-*d*;5,4-*d'*]bisoxazole)] (POBTtBBO) (P2). Polymer obtained as a deep red solid (0.30 g, 65% yield); GPC: M_n = 8,200, M_w = 11,400, PDI =1.39.

Poly(2,6-bis(4-octyl-5-(3,3'-dioctylbithiophen-2-yl)thiophen-2-yl)benzo[1,2-*d*;5,4-*d'*]bisthiazole)] (P3). Polymer obtained as a deep red solid (0.27 g, 55% yield);

GPC: M_n = 5,000, M_w = 8,500, PDI = 1.69.

3.5.3 Device Fabrication and Characterization.

3.5.3.1 Photovoltaic Cells.

ITO-coated glass substrates were cleaned sequentially by ultrasonication in acetone, methanol and isopropanol, followed by O_2 plasma exposure for 5 min. PEDOT:PSS aqueous solution was passed through a 0.45 μm PTFE filter, and then spin-coated on the ITO substrate at 4000 rpm for 60 s and dried in a vacuum oven at 120 °C for 1 h. The thickness of PEDOT:PSS layer was approximately 40 nm.

All devices were fabricated in a glove box filled with argon. 50 mg/ml $PC_{71}BM$ in *o*-DCB was prepared by ultrasonic mixing for 1 h and filtered with a 0.45 μm PTFE filter prior to use. The polymers **P1**, **P2**, and **P3** were dissolved in *o*-DCB at 90°C to yield 10 mg/ml polymer/*o*-DCB solution. The hot solution was quickly filtered with a 0.45 μm PTFE filter before cooling down to room temperature. Subsequently, the polymer and $PC_{71}BM$ in *o*-DCB solutions at different weight ratios of polymer to $PC_{71}BM$ (i.e., 1:0.5, 1:1, 1:2, 1:3, and 1:4) were thoroughly mixed, and spin-coated on the PEDOT:PSS surface at 1100 rpm for 40 s. A cathode was prepared by sequentially depositing a Ca film (50 nm) and a Al film (100 nm) through a shadow mask. The photovoltaic devices had an area of 0.10±0.01 cm^2 and were tested under simulated AM 1.5 G irradiation (100 $mWcm^{-2}$, calibrated with Daystar Meter) using a SoLux Solar Simulator, and the current-voltage (*I*~*V*) curves were measured using a Keithley 2400 multisource meter.

3.5.3.2 Atomic force microscopy

All measurement were performed on film cast as described above; electrodes were not attached to these samples. A Veeco Digital Instruments atomic force microscope was used to perform the analysis.

3.5.3.3 Field Effect Transistors

Organic field-effect transistors were fabricated in the bottom gate, bottom contact configuration on heavily-doped n-type Si substrates as the gate and a thermally grown 250 nm silicon dioxide as the dielectric layer (Silicon Quest, dry oxide). The source and drain electrodes were patterned using standard photolithography and were deposited on

SiO_2 by sputter deposition of ~5 nm of titanium and 50 nm of gold. Prior to use, the devices were cleaned for 20 minutes by exposure to UV light in air (Novascan PSD-UVT) and heat (hot plate, 60 to 120 ºC). The devices were surface treated with OTS in a glovebox for 2 hours by immersion in a ~30 mM solution of OTS in anhydrous trichloroethylene. The devices were then cleaned by rinsing with HPLC grade toluene, and dried under nitrogen flow followed by vacuum overnight. **P2** films were spincasted from a 5 mg/mL solution at 1500 RPM under N_2 and then annealed at 130 ºC in glovebox. **P1** and **P3** films were deposited in air by drop casting 5 mL of a 1 mg mL^{-1} solution in $CHCl_3$, and allowed to dry in a glass Petri dish saturated with $CHCl_3$. After film formation, the devices were further dried overnight in a desiccator under vacuum. FET mobility measurements were performed under a flow of Ar using an Agilent 4155C Semiconductor parameter analyzer and a Micromanipulator S6 probe station. When measuring current-voltage curves and transfer curves, V_G were scanned from -80V to +40V. The field-effect mobilities were obtained from the transfer curves in the saturation regime at V_{DS}=-80V. A line drawn through the linear part of an $I_{DS}^{1/2}$ vs V_G plot allowed extraction of threshold voltage and field-effect mobilities using the square-law equation for the saturation regime. The average mobilities were obtained from 3 or 4 transistors per polymer film with channel lengths (L) of 10-150 μm.

3.6 Acknowledgments

We thank the 3M Foundation, and the National Science Foundation (DMR-0846607) for financial support.

3.7 Supplemental Information

3.7.1 General Methods.

Tetrahydrofuran was dried using an Innovative Technologies solvent purification system. 2,2'-bithiophene,[76] and 3,3',5,5'-tetrabromo-2,2'-bithiophene (S2), [77] were prepared according to literature procedures. All other compounds were purchased from commercial sources and used without further purification. Chromatographic separation was performed using silica gel 60, using the eluents indicated.

3.7.2 Instrumentation

Nuclear magnetic resonance spectra were obtained on a 400 MHz spectrometer (^{1}H at 400 MHz and ^{13}C at 100 MHz). ^{1}H NMR samples were referenced internally to residual protonated solvent ^{13}C NMR are referenced to the middle carbon peak of $CDCl_3$. In both instances chemical shifts are given in δ relative to solvent. Gel permeation chromatography (GPC) measurements were performed on a Viscotek GPC Max 280 separation module equipped with three 5μm I-gel columns connected in a series (guard, HMW, MMW and LMW) with a refractive index detector. Analyses were performed at 35 °C using THF as the eluent with the flow rate at 1.0 mL/min. Calibration was based on polystyrene standards. and UV-Visible spectroscopy were obtained using polymer solutions in THF, and thin films were spun from *o*-DCB. The films were made by spin-coating 25 x 25 x 1mm glass slides, using a solution of 2 mg of polymer per 1 mL *o*-DCB at a spin rate of 800 rpms on a Spin-Coater. Thermal gravimetric analysis measurements were made within the temperature interval of 30 ºC - 900 ºC, with a heating rate of 20 ºC/minute, under ambient atmosphere. Electrochemical properties were measured on an

eDaq e-corder 410 potentiostat using a three-electrode cell (electrolyte: 0.1 mol/L $TBAPF_6$ in acetonitrile) with an Ag/Ag^+ reference electrode, a platinum auxiliary electrode, and a platinum button electrode as the working electrode. Polymer films were made by drop coating an *o*-DCB solution of the polymers on to the working electrode. All films were annealed at 140 ºC for 2 hours prior to use. All differential pulse voltammetry experiments were carried out under argon atmosphere and were recorded at a scan rate of 50 mV/s. UPS was obtained using a Model AC-2 Photoelectron Spectrometer, manufactured by Riken Keiki. X-ray diffraction data was obtained on a Rigaku Ultima IV powder diffractometer using Cross Beam Optic in parallel beam mode to eliminate the need for a knife edge collimator. An accelerating voltage and current of 40 kV and 44 mA, respectively was used. Samples were placed on an MPA-U4 multipurpose Eulerian cradle to facilitate fine alignment between the beam and the top of the film.

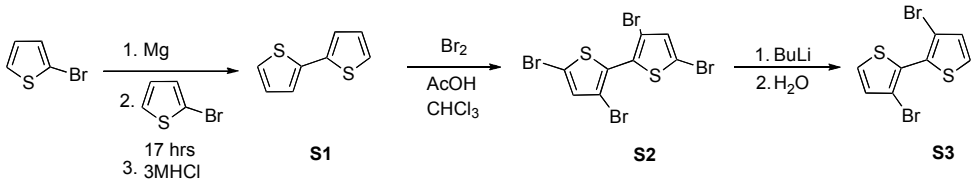

2,2'-bithiophene (S1).[76] This compound was prepared from 2-bromothiophene in 94% yield according to the literature procedure.

3,3',5,5'-tetrabromo-2,2'-bithiophene (S2).[77] This compound was prepared in 70% yield according to the literature procedure. ^{1}H NMR (300MHz; DMSO-d6; d ppm) 7.51 (s, 4H)

3,3'-Dibromo-2,2'-bithiophene (S3). A solution of **S2** (12.0 g, 24.90 mmols) in 150 mL of dry THF was cooled to -78˚C using dry ice/acetone bath. Then a 2.5M solution of *n*-butyl lithium in hexanes (21 mL, 52.5 mmols) was added dropwise over 30 mins. The resulting dianion was stirred for 2 hrs at -78˚C and then allowed to slowly warm to room temperature and stirred at that temperature for 30 mins. The reaction was then quenched with 1M HCl. The organic solvents were removed by rotary evaporation and 60 mL of water was added. The mixture was then extracted with diethyl ether, and the combined extracts were washed with water, dried over anhydrous $MgSO_4$, filtered, and the solvent was removed via rotary evaporation. The crude product was recrystallized from hexane to give light brown crystals (5.7g, yield 71%). ^{1}H NMR (300MHz; $CDCl_3$; d ppm) 7.428-7.410 (d,2H); 7.102- 7.083 (d, 2H).

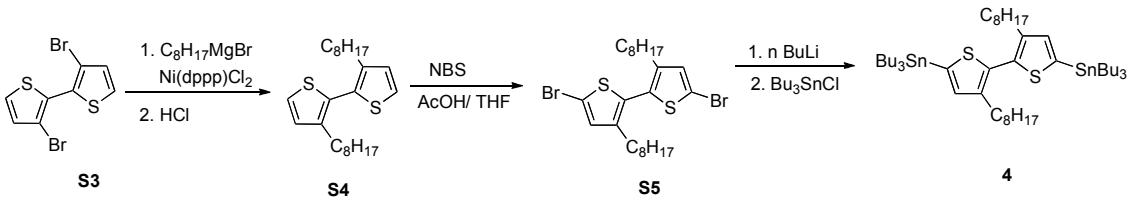

3,3'-Dioctyl-2,2'-bithiophene (S4) [78] To a stirred mixture of activated magnesium (2.94 g) in ether (100 ml), 1-bromooctane (18 g, 93.20 mmol) was added dropwise over 1 h. After refluxing for 2 hrs, the resulting Grignard reagent was added via cannula to a stirred solution of (**S3**) (10g, 30.86 mmol) and $NiCl_2(dppp)_2$ (167.27 mg, 0.31 mmol), in ether

(100 ml), at 0 °C. The resulting solution was refluxed for 17 hrs, after which the reaction was quenched with hydrochloric acid (2 M). The organic layer was washed with water, separated and dried over $MgSO_4$, filtered, and the solvent removed via rotary evaporation. Purification by distillation afforded (**S4**) as a clear oil (7.2g, 60% yield). ^{1}H NMR (300MHz; $CDCl_3$; d ppm): 7.30 – 7.28 (d, 2H); 6.98 – 6.96(d, 2H); 2.52- 2.47 (t, 4H); 1.54 – 1.51 (m, 2H); 1.23 (s, 22H); 0.89-0.85 (t, 6H).

3, 3'-dioctyl-5, 5'-dibromo-2, 2'-bithiophene (S5). [78] To a solution of **S4** (3.0 g, 7.68 mmols) in a 1:1 AcOH: Chloroform mixture (16 mL), NBS (3.28g, 18.43 mmols) was added in one portion and the reaction was allowed to stir at room temperature overnight. The solvent was removed via rotary evaporation, the reaction mass was dissolved in hexanes and filtered through a silica gel plug to remove any unreacted NBS. The solvent was then removed via rotary evaporation to yield the product as thick light-yellow oil in 94% yield. This product was used without any further purification. ^{1}H NMR (300MHz; $CDCl_3$; d ppm): 6.92 (s, 2H); 2.45- 2.40 (t, 4H); 1.45 (m, 2H); 1.237 (s, 22H); 0.90 – 0.85(t, 6H).

(3,3'-dioctyl-2,2'-bithiophene-5,5'-diyl)bis(tributylstannane) (1) [79]

A solution of **S5** (1.64g, 3.00 mmols) in 30mL of degassed THF was cooled to -78˚C using a dry ice/acetone bath. Then a 2.5M solution of *n*-butyl lithium in hexanes (3 mL, 7.5 mmols) was added dropwise. The solution was stirred for 60 mins at -78˚C then it was warmed slowly to room temperature and stir at that temperature for 30 mins. The reaction was then cooled back down to -78˚C and tributyltin chloride (96% wt; 1.70 mL,

6.06 mmols) was added. The solution was then allowed to warm to room temperature overnight. The reaction was washed with water followed by 1M KF and then extracted with ether. The organic layer was dried over $MgSO_4$, then filtered over celite and the solvent was removed via rotary evaporation to yield pure product as brown oil in 75% yield. ^1H NMR (400MHz; $CDCl_3$, d ppm): 6.99 (s, 2H); 2.534 – 2.753 (t, 4H); 1.64 – 1.56 (m, 16H).

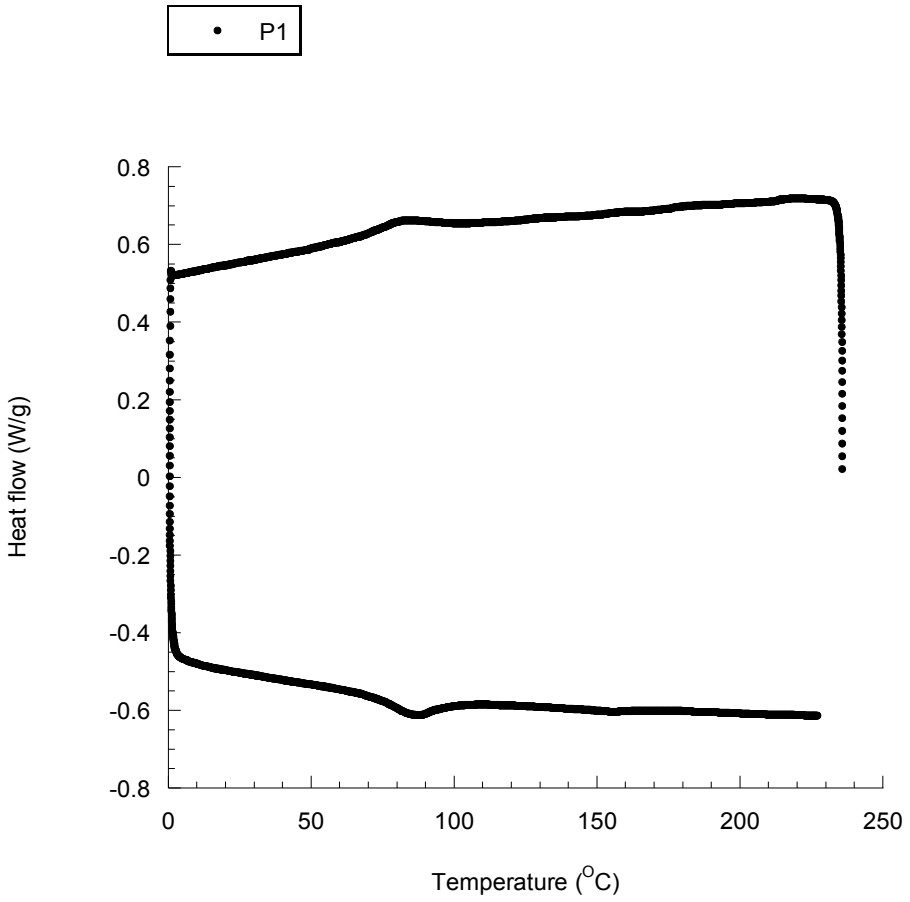

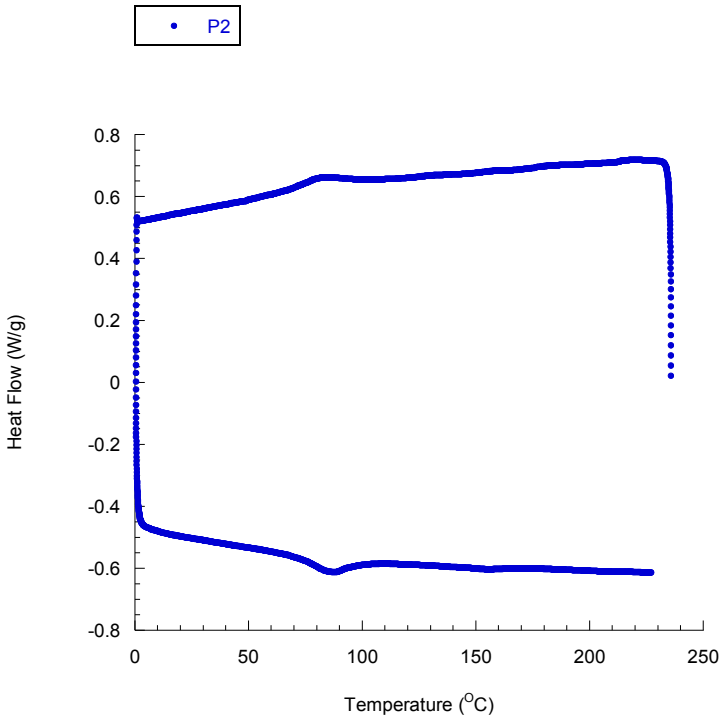

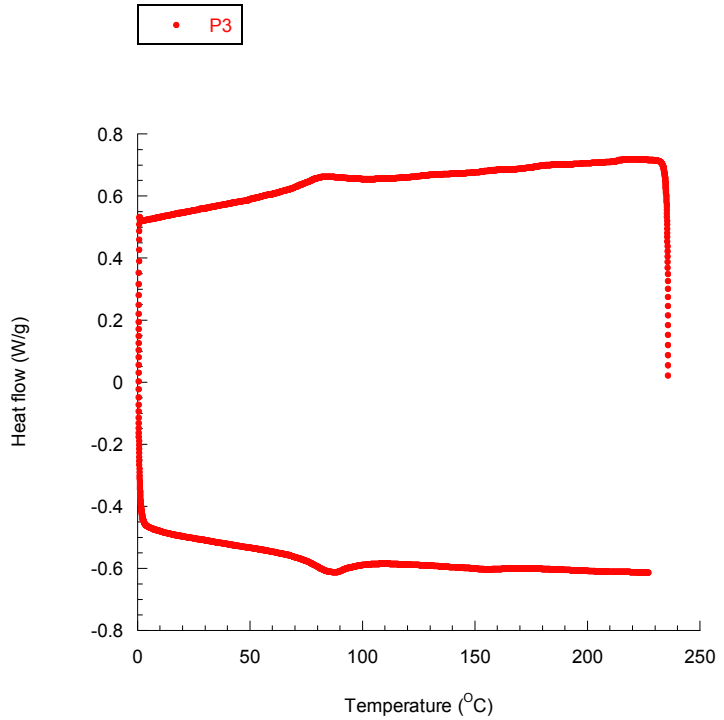

Figure 3.7.1. DSC curves of P1, P2 and P3

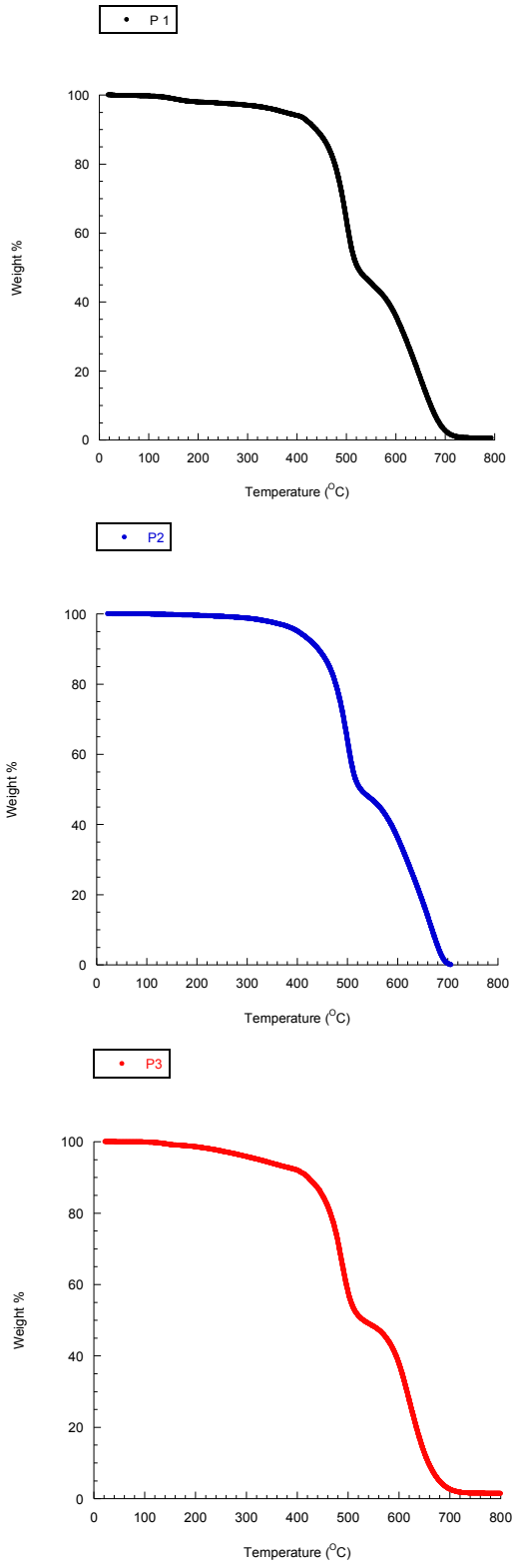

Figure 3.7.2: TGA curves of P1, P2 and P3

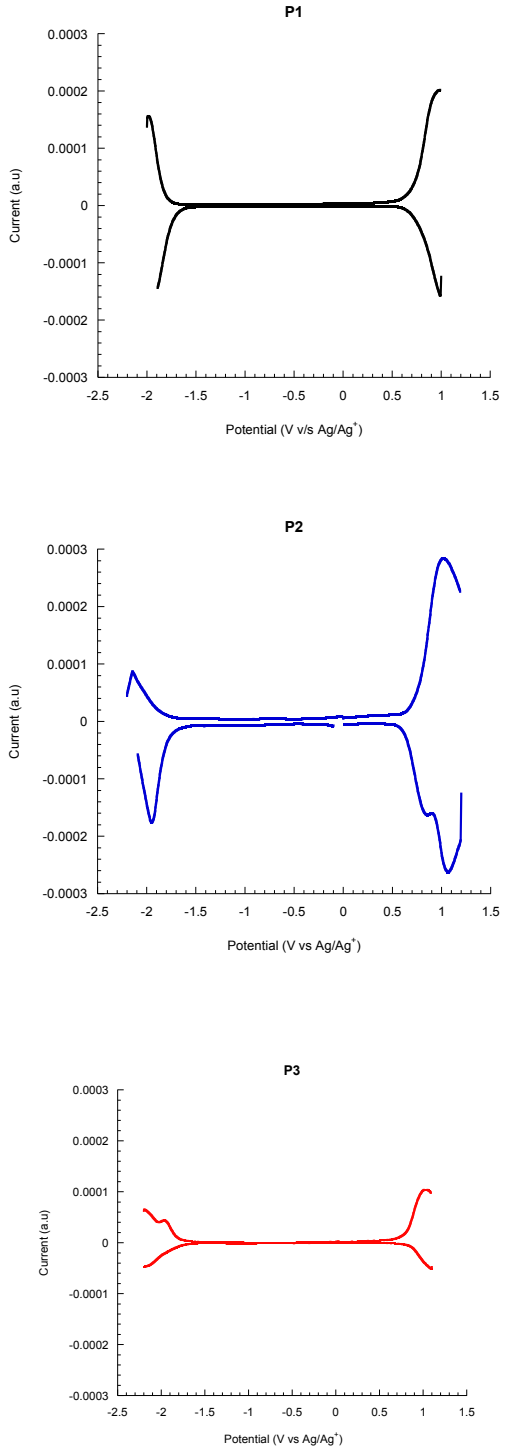

Figure 3.7.3. Differential Pulse Voltammetry of P1, P2 and P3

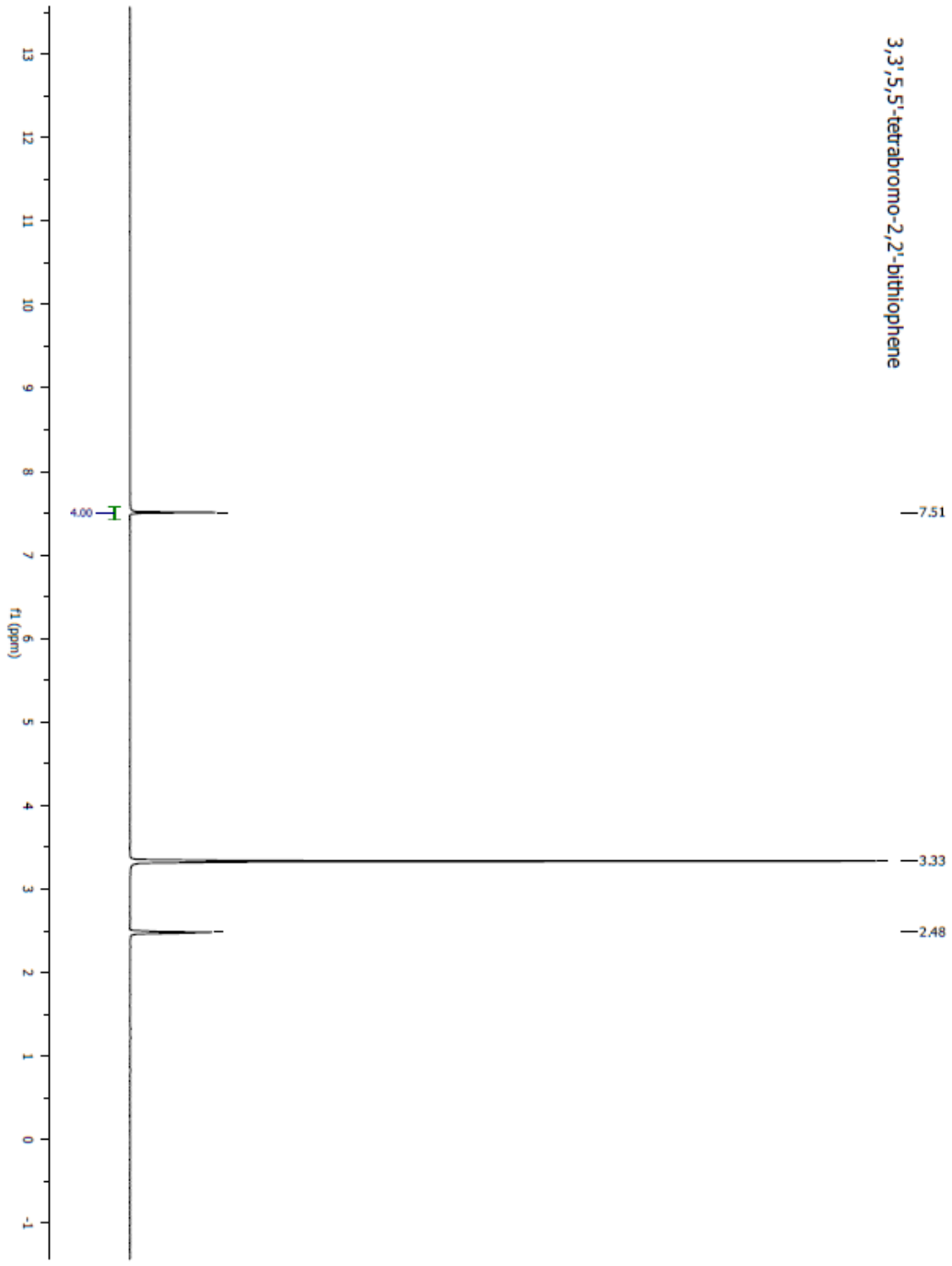

Figure 3.7.4. ^{1}H NMR spectrum of **S2**

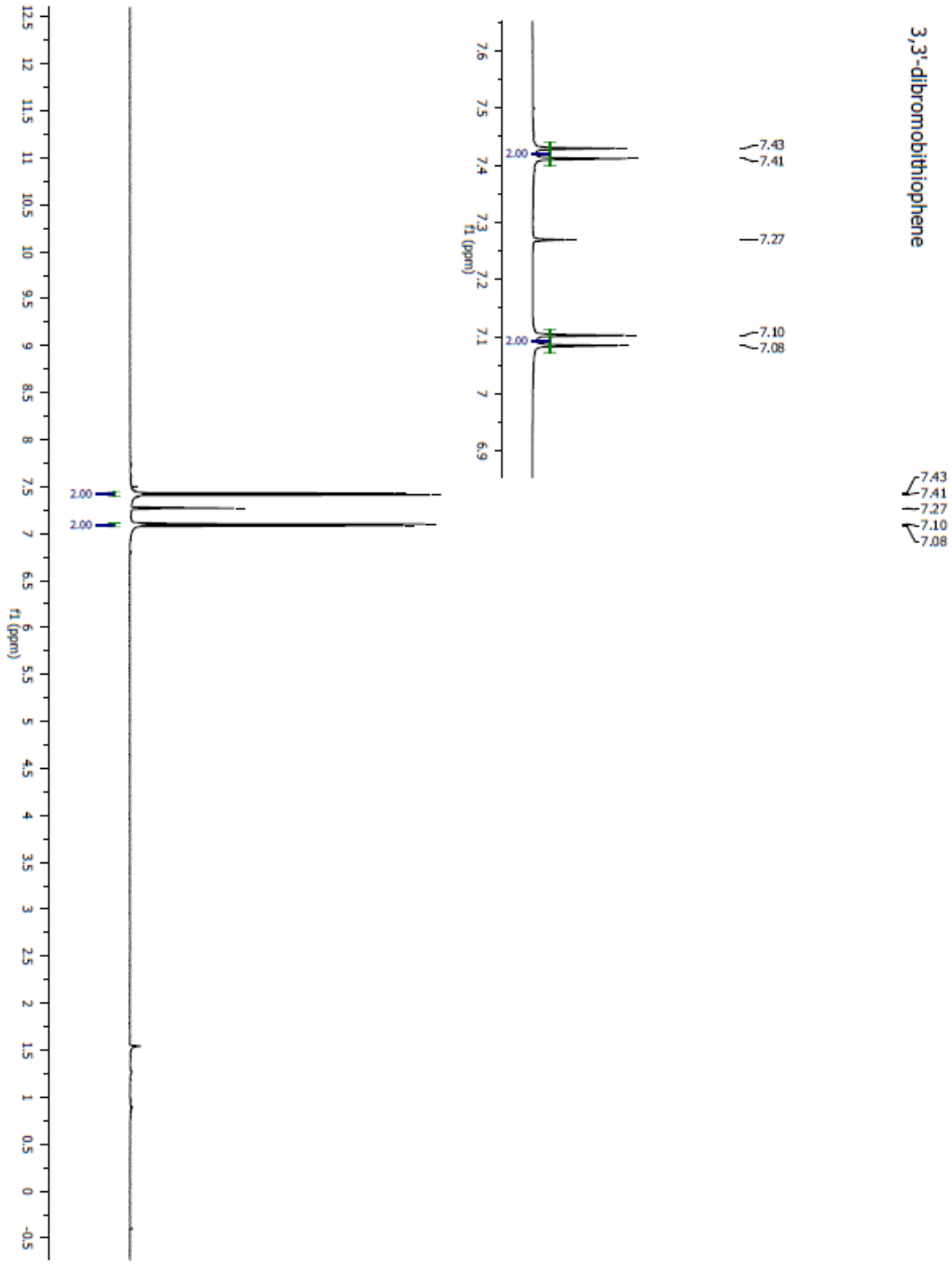

Figure 3.7.5. ^{1}H NMR spectrum of **S3**

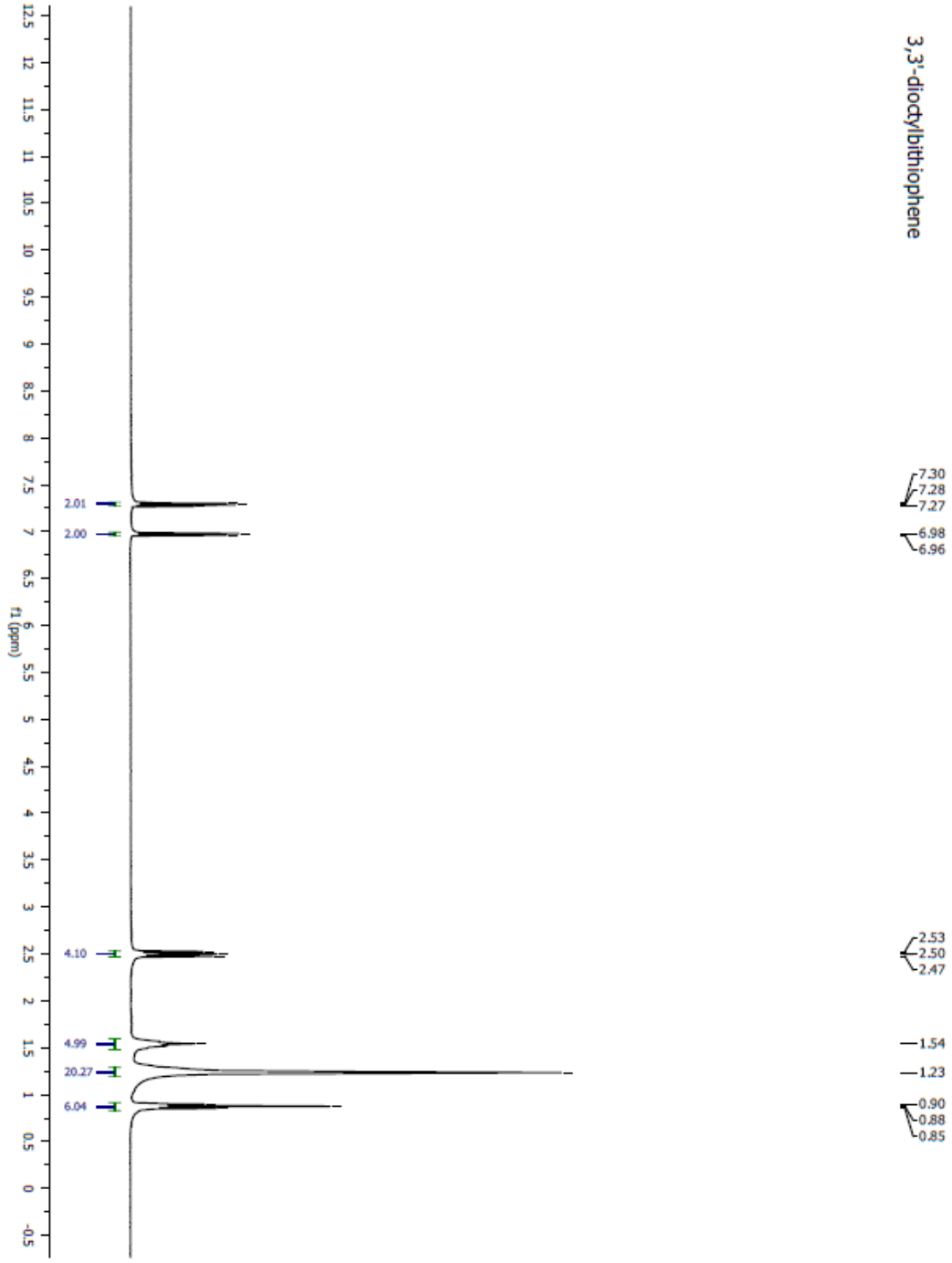

Figure 3.7.6. ^{1}H NMR spectrum of **S4**

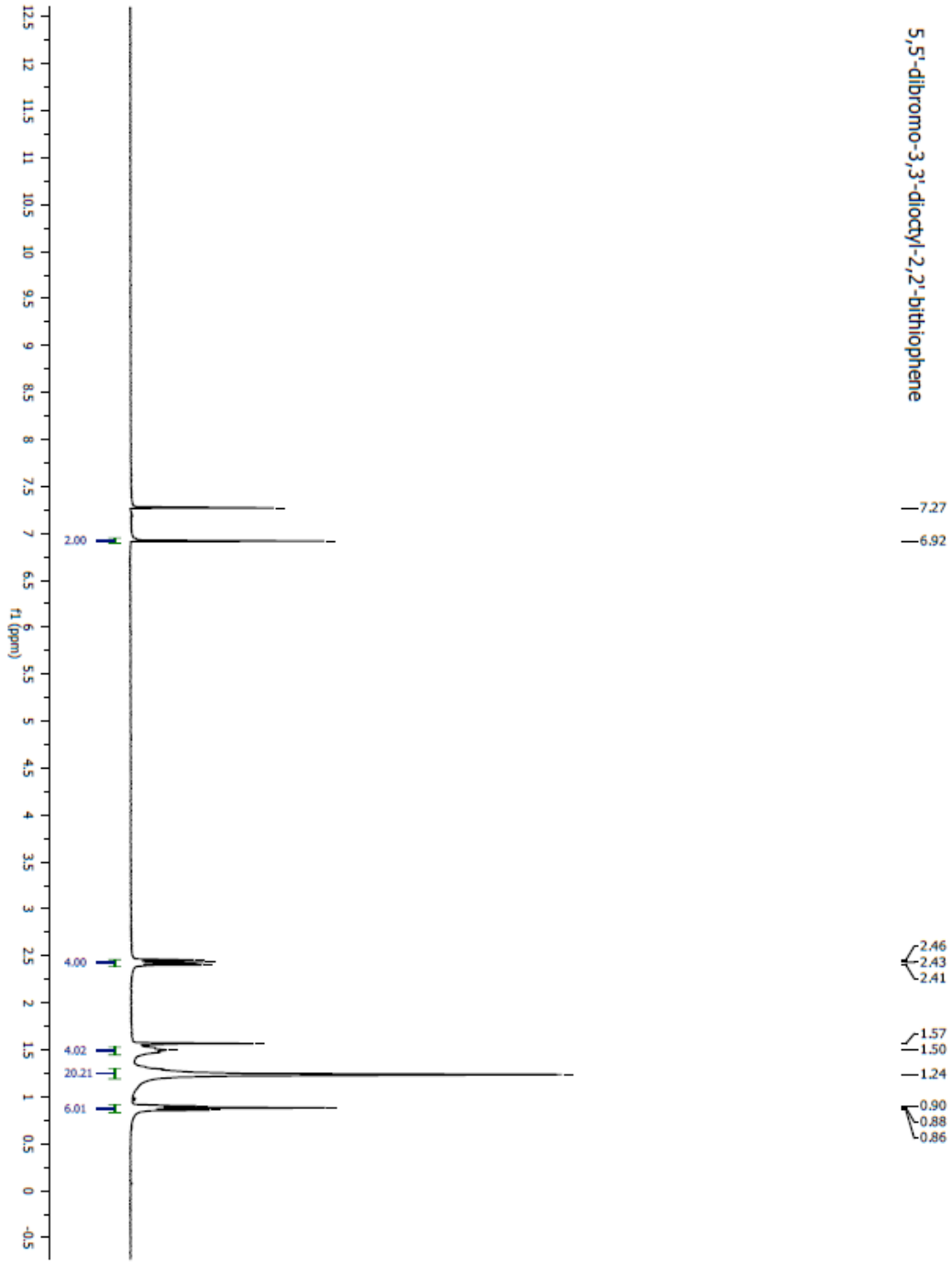

Figure 3.7.7. ^{1}H NMR spectrum of **S5**

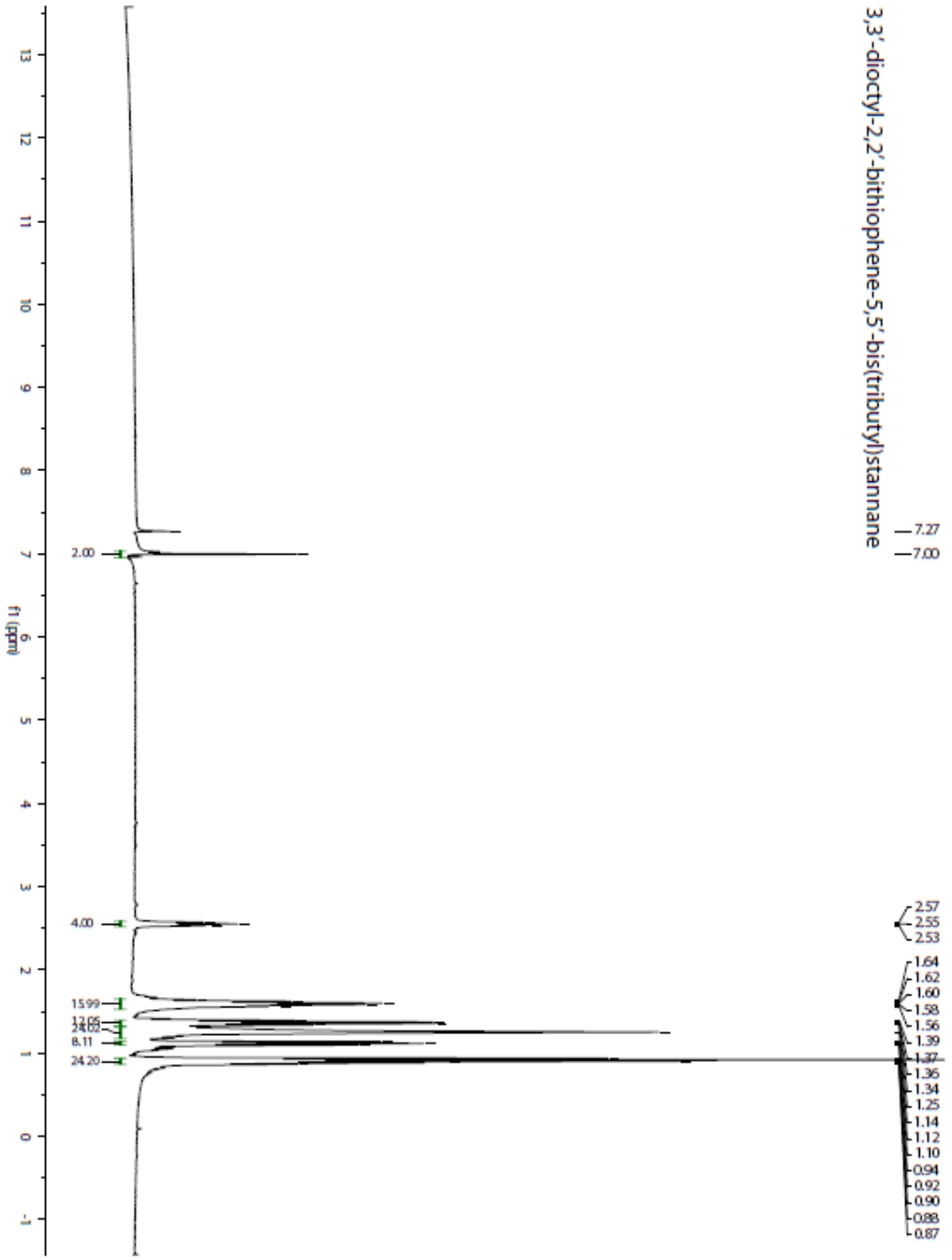

Figure 3.7.8. ^{1}H NMR spectrum of **1**

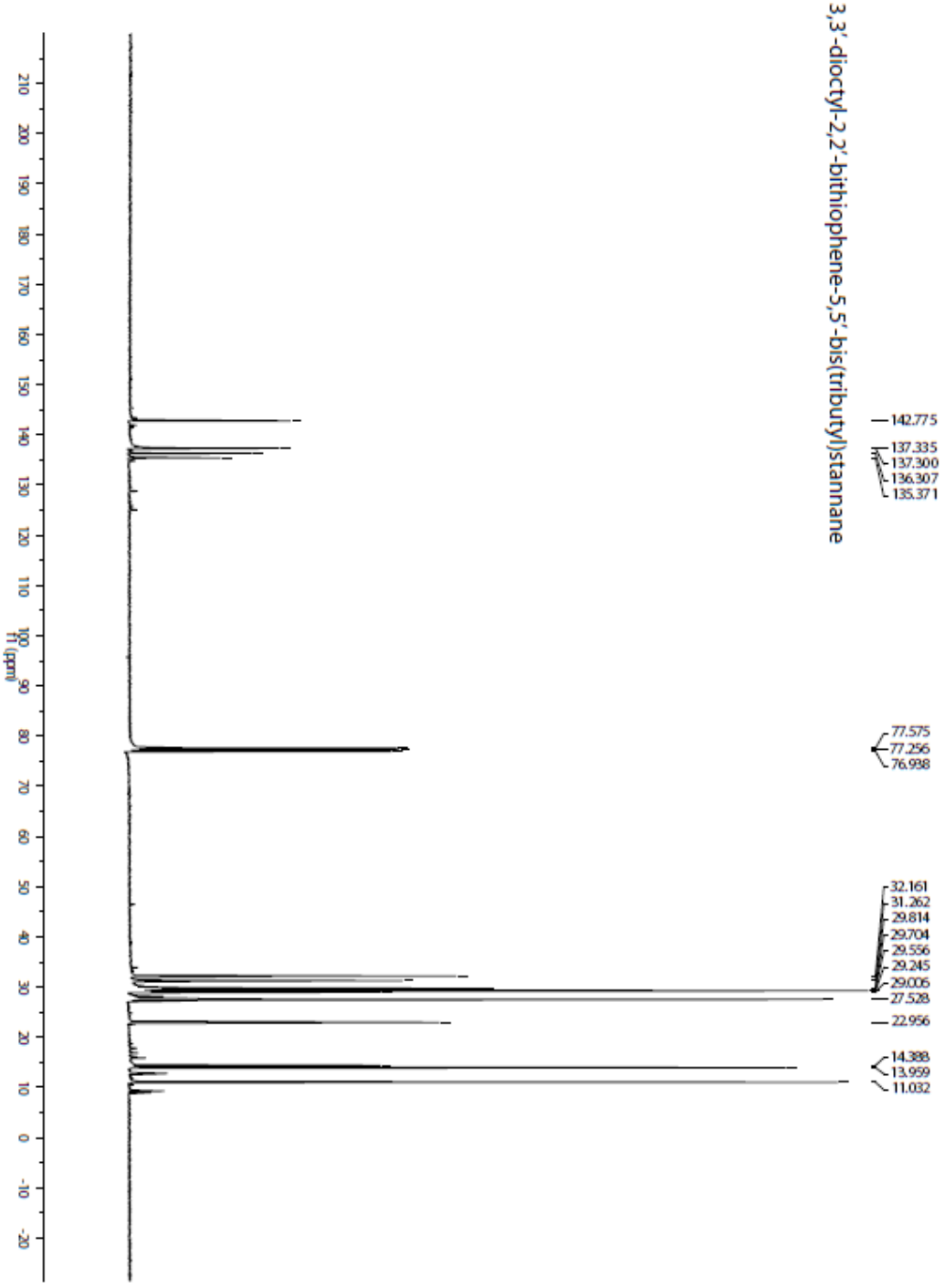

Figure 3.7.9. ^{13}C-NMR spectrum of **1**

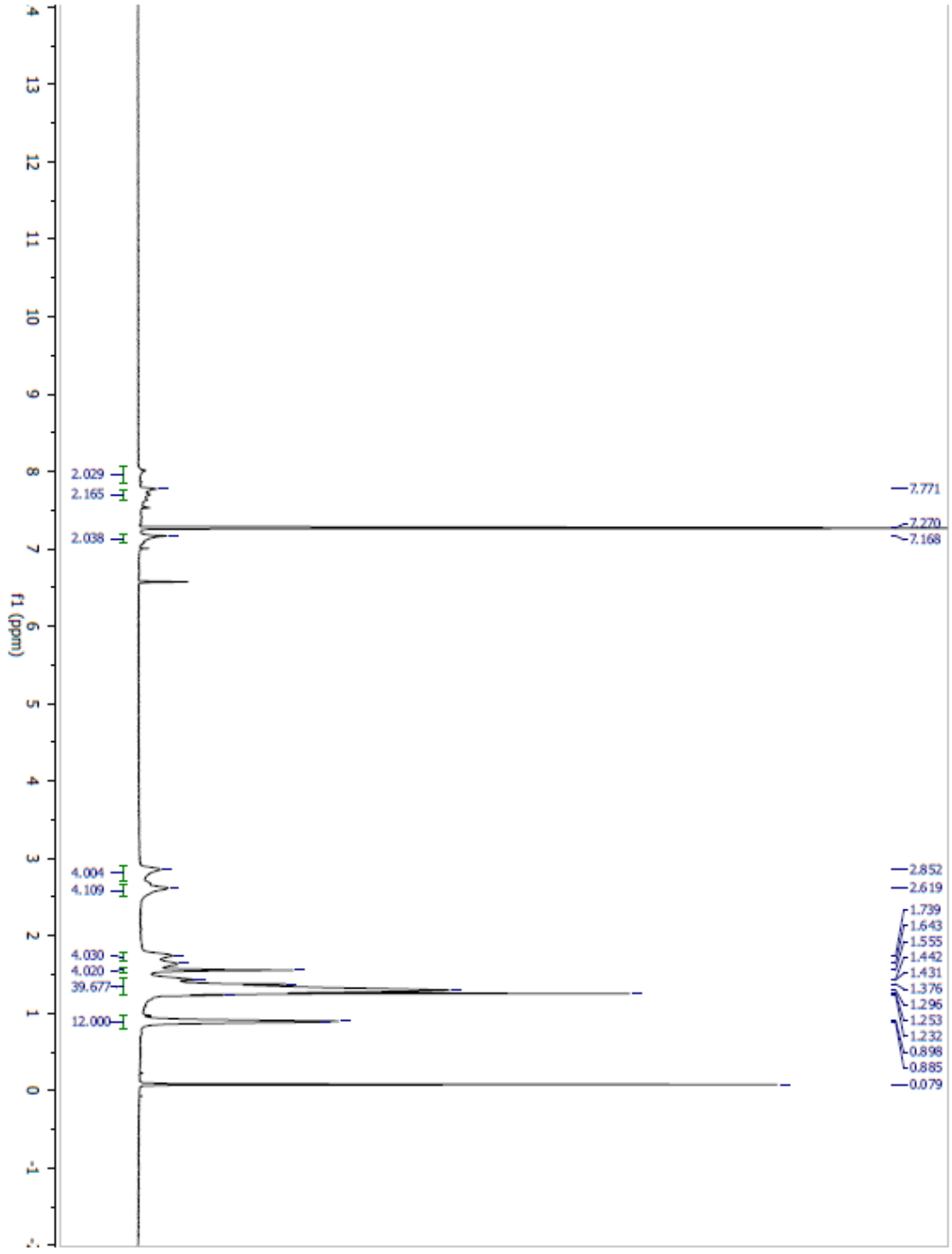

Figure 3.7.10. ^{1}H NMR spectrum of **P1**

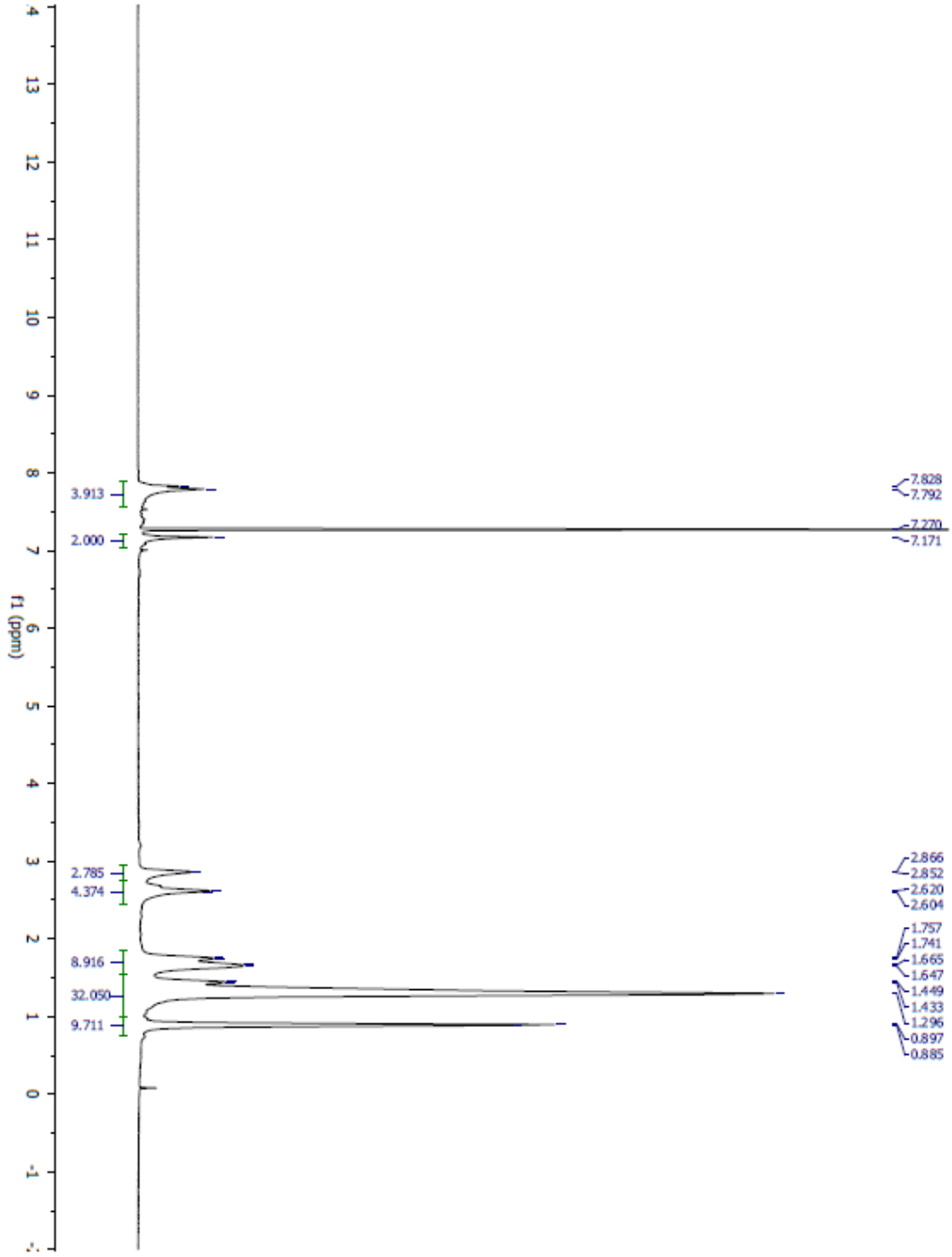

Figure 3.7.11. ^{1}H NMR spectrum of **P2**

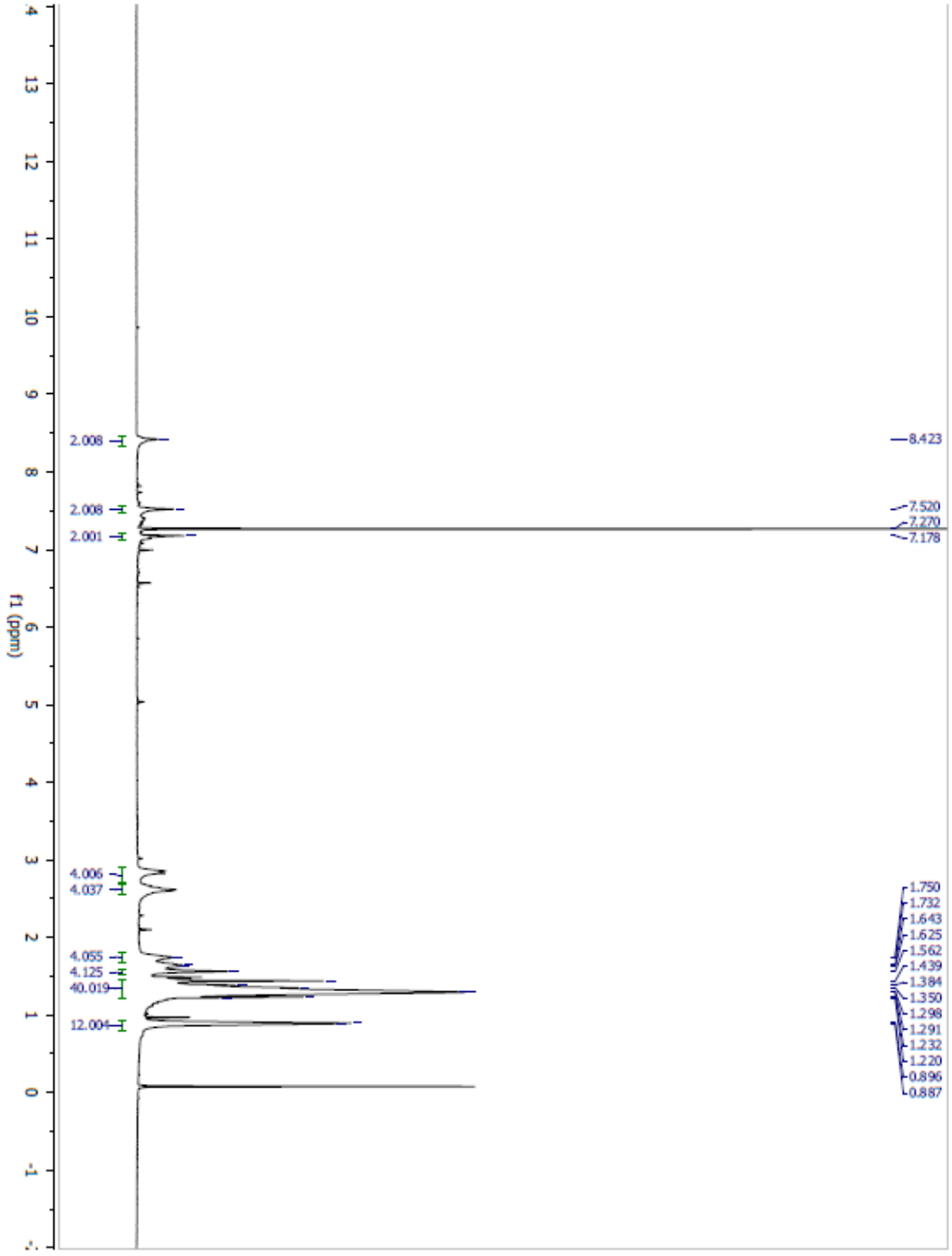

Figure 3.7.12. ^{1}H NMR spectrum of **P3**

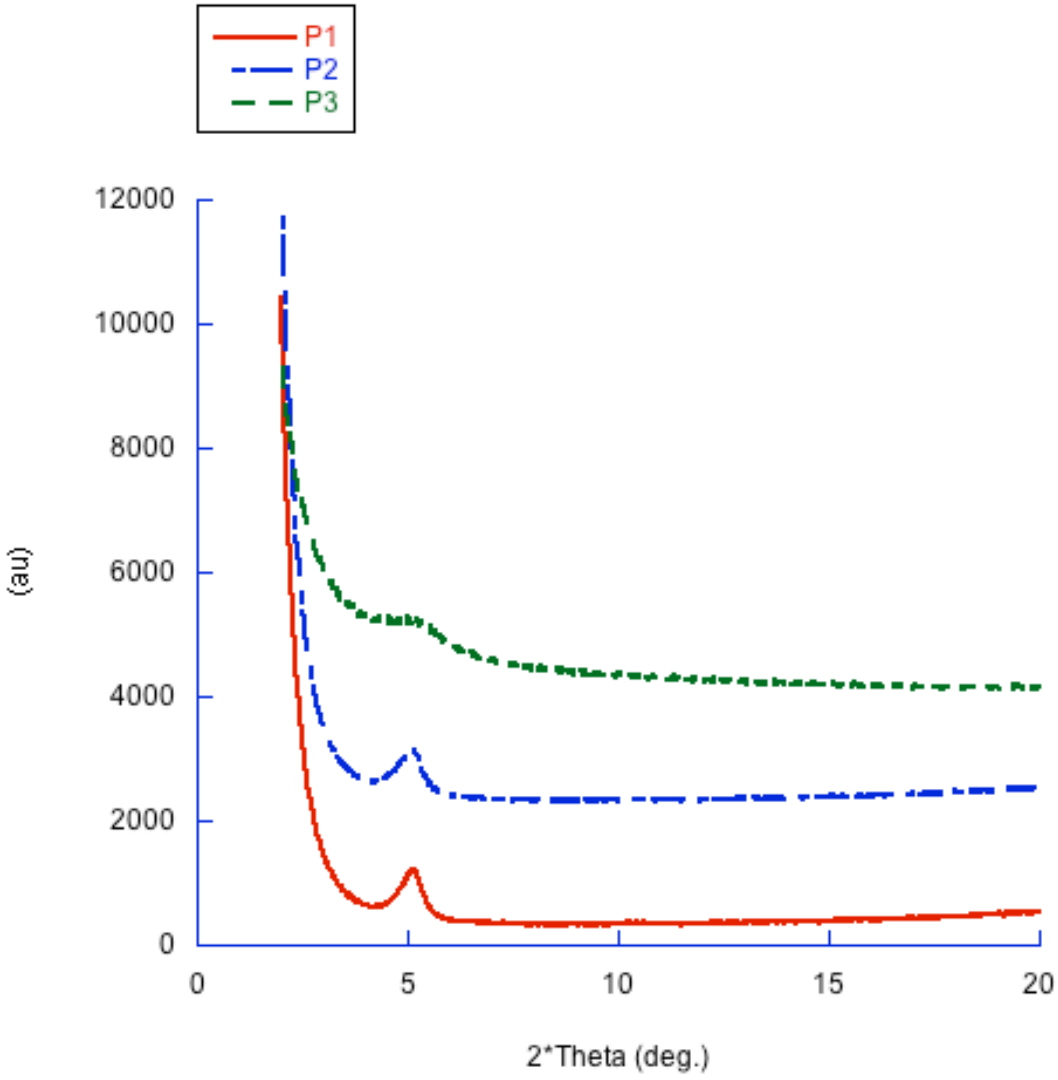

Figure 3.7.13. X-ray diffraction patterns of thin films spun on borosilicate glass slides. The peak appearing at 5 degrees 2*theta is associated with interchain separation of polymers by approximately 1.7 nm. Oscillations in the diffraction patterns from 2 to 4 degrees are caused by internal reflectance of X-rays by the films. Sample data are offset and the intensity data for sample AB-3-1 has been multiplied by a factor of 3 in order to distinguish the peak at 5^{o}.

Table 3.7.1. Impact of thermal annealing on PVC performance

	Thermal-annealing Temperature/°C	***V_{oc}*/ V**	***J_{sc}*/mAcm^{-2}**	***FF*/%**	***PCE* /%**
P1	without	0.74	4.22	31.48	0.98
	100	0.67	2.76	27.57	0.51
	120	0.63	2.25	27.48	0.39
	140	0.60	1.76	32.57	0.34
	160	0.59	1.69	31.01	0.31
P2	without	0.73	5.13	30.59	1.14
	100	0.69	3.09	30.09	0.64
	120	0.66	2.67	32.45	0.57
	140	0.63	2.58	33.04	0.54
	160	0.60	2.32	32.31	0.44

Table 3.7.2. FET Mobilities of polymers using different channel lengths.

P1	**15 (µm)**	**20 (µm)**	**25 (µm)**	**30 (µm)**		**On/Off ratio**	**V_T (V)**
Bare Si/SiO_2	7.1×10^{-5}	7.0×10^{-5}	8.9×10^{-5}	5.0×10^{-5}		10^3 - 10^4	-48[a]
P2 OTS-treated	**5 (µm)**	**10 (µm)**	**15 (µm)**	**25 (µm)**	**30 (µm)**	**On/Off ratio**	**V_T (V)**
	0.008 (0.0104)[a]	0.0036 (0.0049)[a]	0.0037 (0.0048)[a]	0.0027 (0.0032)[a]	0.0006 (0.0007)[a]	10^3 - 10^4	-48[a]
Bare Si/SiO_2	n/a	0.0003	0.0045	n/a	0.006	10	65
P3	**10 (µm)**	**15 (µm)**	**20 (µm)**	**25 (µm)**	**40 (µm)**	**On/Off ratio**	**V_T (V)**
Bare Si/SiO_2	1.5×10^{-4}	7.3×10^{-5}	6.6×10^{-5}	1.0×10^{-4}	8.8×10^{-5}	$10^1 - 10^2$	-30[a]

[a]Max hole mobility. [b]Average values for threshold voltage.

3.8 REFERENCES

1. Tang, C. W.; VanSlyke, S. A. *Appl. Phys. Lett.* **1987,** *51*, 913.
2. Burroughes, J. H.; Bradley, D. D. C.; Brown, A. R.; Marks, R. N.; Mackay, K.; Friend, R. H.; Burns, P. L.; Holmes, A. B. *Nature* **1990,** *347*, 539.
3. Grimsdale, A. C.; Leok Chan, K.; Martin, R. E.; Jokisz, P. G.; Holmes, A. B. *Chem. Rev.* **2009,** *109*, 897.
4. Tang, C. W. *Appl. Phys. Lett.* **1986,** *48*, 183.
5. Scharber, M.; Mühlbacher, D.; Koppe, M.; Denk, P.; Waldauf, C.; Heeger, A.; Brabec, C. *Adv. Mater.* **2006,** *18*, 789.
6. Thompson, B. C.; Frechet, J. M. J. *Angew, Chem. Int. Ed.* **2008,** *47*, 58.
7. Facchetti, A. *Chem. Mater.* **2010,** *23*, 733.
8. Brabec, C. J.; Cravino, A.; Meissne, D.; Sariciftci, N. S.; Fromherz, T.; Rispens, M. T.; Sanchez, L.; Hummelen, J. C. *Adv. Fun. Mater.* **2001,** *11*, 374.

9. Brabec, C. J.; Gowrisanker, S.; Halls, J. J. M.; Laird, D.; Jia, S.; Williams, S. P. *Adv. Mater.* **2010,** *22*, 3839.
10. Yu, G.; Gao, J.; Hummelen, J. C.; Wudl, F.; Heeger, A. J. *Science* **1995,** *270*, 1789.
11. Gunes, S.; Neugebauer, H.; Sariciftci Niyazi, S. *Chem. Rev.* **2007,** *107*, 1324.
12. Coakley, K. M.; McGehee, M. D. *Chem. Mater.* **2004,** *16*, 4533.
13. van Mullekom, H. A. M.; Vekemans, J. A. J. M.; Havinga, E. E.; Meijer, E. W. *Mater. Sci. Eng., R* **2001,** *32*, 1.
14. Boudreault, P.-L. T.; Najari, A.; Leclerc, M. *Chem. Mater.* **2010,** *23*, 456.
15. Zou, Y.; Najari, A.; Berrouard, P.; Beaupre, S.; Reda Aiàch, B.; Tao, Y.; Leclerc, M. *J. Am. Chem. Soc.* **2010,** *132*, 5330.
16. Liang, Y.; Xu, Z.; Xia, J.; Tsai, S.-T.; Wu, Y.; Li, G.; Ray, C.; Yu, L. *Adv. Mater.* **2010,** *22*, E135.
17. Chu, T.-Y.; Lu, J.; Beauprea, S.; Zhang, Y.; Pouliot, J.-R.; Wakim, S.; Zhou, J.; Leclerc, M.; Li, Z.; Ding, J.; Tao, Y. *J. Am. Chem. Soc.* **2011,** *133*, 4250.
18. Liang, Y.; Feng, D.; Wu, Y.; Tsai, S.-T.; Li, G.; Ray, C.; Yu, L. *J. Am. Chem. Soc.* **2009,** *131*, 7792.
19. Piliego, C.; Holcombe, T. W.; Douglas, J. D.; Woo, C. H.; Beaujuge, P. M.; Frechet, J. M. J. *J. Am. Chem. Soc.* **2010,** *132*, 7595.
20. Price, S. C.; Stuart, A. C.; Yang, L.; Zhou, H.; You, W. *J. Am. Chem. Soc.* **2011,** *133*, 4625.
21. Tsao, H. N.; Cho, D. M.; Park, I.; Hansen, M. R.; Mavrinskiy, A.; Yoon, D. Y.; Graf, R.; Pisula, W.; Spiess, H. W.; MuÃàllen, K. *J. Am. Chem. Soc.* **2011,** *133*, 2605.
22. Wolfe, J. F., Polybenzothiazoles and Polybenzoxazoles. In *Encyclopedia of Polymer Science and Engineering*, John Wiley and Sons: New York, NY, 1988; Vol. 11, pp 601.
23. Wolfe, J. F.; Arnold, F. E. *Macromolecules* **1981,** *14*, 909.
24. Wolfe, J. F.; Loo, B. H.; Arnold, F. E. *Macromolecules* **1981,** *14*, 915.
25. Choe, E. W.; Kim, S. N. *Macromolecules* **1981,** *14*, 920.
26. Inbasekaran, M.; Strom, R. *OPPI Briefs* **1994,** *23*, 447.
27. Schmitt, R. J.; Ross, D. S.; Hardee, J. R.; Wolfe, J. F. *J. Org. Chem.* **1988,** *53*, 5568.
28. Alam, M. M.; Jenekhe, S. A. *Chem. Mater.* **2002,** *14*, 4775.
29. Intemann, J. J.; Mike, J. F.; Cai, M.; Bose, S.; Xiao, T.; Mauldin, T. C.; Roggers, R. A.; Shinar, J.; Shinar, R.; Jeffries-El, M. *Macromolecules* **2011,** *44*, 248.
30. Huang, W.; Yin, J. *Polym. Bull.* **2006,** *57*, 269.
31. Jenekhe, S. A.; Osaheni, J. A. *Chem. Mater.* **1994,** *6*, 1906.
32. Osaheni, J. A.; Jenekhe, S. A. *J. Am. Chem. Soc.* **1995,** *117*, 7389.
33. Osaheni, J. A.; Jenekhe, S. A. *Macromolecules* **1993,** *26*, 4726.
34. Jenekhe, S. A.; Osaheni, J. A.; Meth, J. S.; Vanherzeele, H. *Chem. Mater.* **1992,** *4*, 683.
35. Reinhardt, B. A.; Unroe, M. R.; Evers, R. C. *Chem. Mater.* **1991,** *3*, 864.
36. Osaheni, J. A.; Jenekhe, S. A. *Chem. Mater.* **1992,** *4*, 1282.
37. Babel, A.; Jenekhe, S. A. *J. Phys. Chem. B.* **2002,** *106*, 6129.
38. Guo, P.; Wang, S.; Wu, P.; Han, Z. *Polymer* **2004,** *45*, 1885.

39. Kricheldorf, H. R.; Domschke, A. *Polymer* **1994,** *35*, 198.
40. Liu, X.; Xu, X.; Zhuang, Q.; Han, Z. *Polym. Bull.* **2008,** *60*, 765.
41. Wang, S.; Lei, H.; Guo, P.; Wu, P.; Han, Z. *Eur. Polym. J.* **2004,** *40*, 1163.
42. Roberts, M. F.; Jenekhe, S. A. *Chem. Mater.* **1993,** *5*, 1744.
43. Mike, J. F.; Makowski, A. J.; Mauldin, T. C.; Jeffries-El, M. *J. Poly. Sci. A.* **2010,** *48*, 1456.
44. Mike, J. F.; Nalwa, K.; Makowski, A. J.; Putnam, D.; Tomlinson, A. L.; Chaudhary, S.; Jeffries-El, M. *Phys. Chem. Chem. Phys.* **2011,** *13*, 1338.
45. Mike, J. F.; Inteman, J. J.; Ellern, A.; Jeffries-El, M. *J. Org. Chem.* **2010,** *75*, 495.
46. Mike, J. F.; Makowski, A. J.; Jeffries-EL, M. *Org. Lett.* **2008,** *10*, 4915.
47. Ahmed, E.; Kim, F. S.; Xin, H.; Jenekhe, S. A. *Macromolecules* **2009,** *42*, 8615.
48. Osaka, I.; Takimiya, K.; McCullough, R. D. *Adv. Mater.* **2010,** *22*, 4993.
49. Belfield, K. D.; Yao, S.; Morales, A. R.; Hales, J. M.; Hagan, D. J.; Van Stryland, E. W.; Chapela, V. M.; Percino, J. *Polym. Adv. Technol.* **2005,** *16*, 150.
50. Ahmed, E.; Subramaniyan, S.; Kim, F. S.; Xin, H.; Jenekhe, S. A. *Macromolecules* **2011,** *44*, 7207.
51. McEntee, G. J.; Vilela, F.; Skabara, P. J.; Anthopoulos, T. D.; Labram, J. G.; Tierney, S.; Harrington, R. W.; Clegg, W. *J. Mater. Chem.* **2011,** *21*, 2091.
52. Mamada, M.; Nishida, J.-i.; Tokito, S.; Yamashita, Y. *Chem. Lett.* **2008,** *37*, 766.
53. Pang, H.; Vilela, F.; Skabara, P. J.; McDouall, J. J. W.; Crouch, D. J.; Anthopoulos, T. D.; Bradley, D. D. C.; de Leeuw, D. M.; Horton, P. N.; Hursthouse, M. B. *Adv. Mater.* **2007,** *19*, 4438.
54. Wolfe, J. F. *Proceedings of SPIE-The International Society for Optical Engineering* **1987,** *682*, 70.
55. Tsai, H.-H. G.; Chou, L.-C.; Lin, S.-C.; Sheu, H.-S.; Lai, C. K. *Tetrahedron Lett.* **2009,** *50*, 1906.
56. Mike, J. F.; Intemann, J. J.; Cai, M.; Xiao, T.; Shinar, R.; Shinar, J.; Jeffries-EL, M. *Polym. Chem.* **2011,** *2*, 2299.
57. Kokubo, H.; Sato, T.; Yamamoto, T. *Macromolecules* **2006,** *39*, 3959.
58. McCullough, R. D.; Lowe, R. D.; Jayaraman, M.; Anderson, D. L. *J. Org. Chem.* **1993,** *58*, 904.
59. McCullough, R. D.; Tristam-Nagle, S.; Williams, S. P.; Lowe, R. D.; Jayaraman, M. *J. Am. Chem. Soc.* **1993,** *115*, 4910.
60. Liu, J.; Zhang, R.; Sauve, G.; Kowalewski, T.; McCullough, R. D. *J. Am. Chem. Soc.* **2008,** *130*, 13167.
61. Guo, X.; Kim, F. S.; Jenekhe, S. A.; Watson, M. D. *J. Am. Chem. Soc.* **2009,** *131*, 7206.
62. Ko, S.; Mondal, R.; Risko, C.; Lee, J. K.; Hong, S.; McGehee, M. D.; Bredas, J.-L.; Bao, Z. *Macromolecules* **2010,** *43*, 6685.
63. Mei, J.; Heston, N. C.; Vasilyeva, S. V.; Reynolds, J. R. *Macromolecules* **2009,** *42*, 1482.
64. Beaujuge, P. M.; Amb, C. M.; Reynolds, J. R. *Acc. Chem. Res.* **2010,** *43*, 1396.
65. Miyamae, T.; Yoshimura, D.; Ishii, H.; Ouchi, Y.; Miyazaki, T.; Koike, T.; Yamamoto, T.; Muramatsu, Y.; Etori, H.; Maruyama, T.; Seki, K. *Synth. Met.* **1997,** *84*, 939.

66. Koster, L. J. A.; Mihailetchi, V. D.; Blom, P. W. M. *Appl. Phys. Lett.* **2006,** *88*, 093511.
67. Cardona, C. M.; Li, W.; Kaifer, A. E.; Stockdale, D.; Bazan, G. C. *Adv. Mater.* **2011,** *23*, 2367.
68. Li, Y.; Wu, Y.; Ong, B. S. *Macromolecules* **2006,** *39*, 6521.
69. Zhang, R.; Li, B.; Iovu, M. C.; Jeffries-El, M.; Sauve, G.; Cooper, J.; Jia, S.; Tristram-Nagle, S.; Smilgies, D. M.; Lambeth, D. N.; McCullough, R. D.; Kowalewski, T. *J. Am. Chem. Soc.* **2006,** *128*, 3480.
70. Li, G.; Shrotriya, V.; Huang, J. S.; Yao, Y.; Moriarty, T.; Emery, K.; Yang, Y. *Nature Mater* **2005,** *4*, 864.
71. Park, S. H.; Roy, A.; Beaupre, S.; Cho, S.; Coates, N.; Moon, J. S.; Moses, D.; Leclerc, M.; Lee, K.; Heeger, A. J. *Nature Photonics* **2009,** *3*, 297.
72. Boudreault, P. L. T.; Najari, A.; Leclerc, M. *Chem Mater* **2011,** *23*, 456.
73. Ranger, M.; Rondeau, D.; Leclerc, M. *Macromolecules* **1997,** *30*, 7686.
74. Kannan, R.; He, G. S.; Lin, T.-C.; Prasad, P. N.; Vaia, R. A.; Tan, L.-S. *Chem. Mater.* **2004,** *16*, 185.
75. Mike, J. F.; Makowski, A. J.; Mauldin, T. C.; Jeffries-El, M. *J. Poly. Sci. A.* **2010,** *48*, 1456.
76. Tamao, K.; Kodama, S.; Nakajima, I.; Kumada, M.; Minato, A.; Suzuki, K. *Tetrahedron* **1982,** *38*, 3347.
77. Usta, H.; Lu, G.; Facchetti, A.; Marks, T. J. *J. Am. Chem. Soc.* **2006,** *128*, 9034.
78. (a) Khor, E.; Ng, S. C.; Li, H. C.; Chai, S. *Heterocycles* **1991,** *32*, 1805; (b) Xu, J.; Ng, S. C.; Chan, H. S. O. *Tetrahedron Lett.* **2001,** *42*, 5327.
79. Salhi, F.; Collard, D. M. *Adv. Mater. (Weinheim, Ger.)* **2003,** *15*, 81.

CHAPTER 4

IMPROVING THE ORGANIC PHOTOVOLTAIC CELL PERFORMANCE OF BENZOBISAZOLE COPOLYMERS.

Manuscript under review for publication in Polymer chemistry, Royal Society of Chemistry

*Achala Bhuwalka[a] Monique D. Ewan,[a] Jared F. Mike,[a] Moneim Elshobaki,[b] Sumit Chaudhary,[c] and Malika Jeffries-EL[a]**

[a]Department of Chemistry, Iowa State University, Ames IA 50011.

[b]Department of Materials Science and Engineering Department, Iowa State University, and Department of Physics, Mansoura University, Mansoura, 35516, Egypt

[c] Department of Electrical and Computer Engineering, Iowa State University, USA

4.1 Abstract

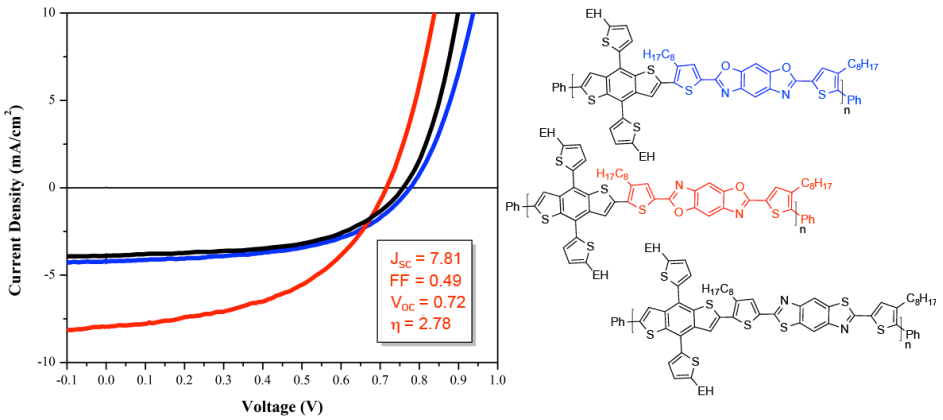

In an effort to design efficient low cost polymers for use in organic photovoltaic cells we combined the easily prepared donor-acceptor-donor triad of a either cis-benzobisoxazole, trans-benzobisoxazole or trans-benzobisthiazole flanked by two thiophene rings with the electron-rich 4,8-bis(5-(2-ethylhexyl)-thien-2-yl)-benzo[1,2-b:4,5-b']dithiophene. The electrochemical, optical, morphological, charge transport and photovoltaic properties of the resulting terpolymers were investigated. Although the polymers differed in the arrangement and/or nature of the chalcogens, they all had similar HOMO energy levels (-5.2 to -5.3 eV) and optical band gaps (2.1 to 2.2 eV). However, the LUMO energy levels ranged from -3.1 to -3.5 eV. When the polymers were used as electron donors in bulk heterojunction photovoltaic devices with PC71BM ([6,6]-phenyl C71-butyric acid methyl ester) as the acceptor, the trans-benzobisoxazole polymer had the best performance with a power conversion efficiency of 2.8%. This is the highest reported photovoltaic performance to date for a benzobisoxazole- based polymer to date.

4.2 Introduction

Organic photovoltaic cells (OPVs) continue to garner a large amount of interest due to their potential for use in the development of lightweight, large area panels for efficient solar energy conversion. Currently, the most efficient OPVs are based on the bulk-heterojunction concept in which an electron accepting material, such as a functionalized fullerene, is blended with an electron donating conjugated polymer.[1] Achieving high power conversion efficiency (PCE) in these systems requires concurrent optimization of several parameters including the nanoscale morphology of the polymer

film formed upon blending with the donor conjugated polymers the fullerene acceptor and the alignment of energy levels of these two components.[2] In an effort to optimize the properties of the donor polymers, there has been extensive research on the design and synthesis of new materials. A popular approach is the synthesis of polymers composed of alternating electron rich and electron poor moieties as the intramolecular charge transfer (ICT) between these groups can be modified by adjusting the strength of the two monomers, thereby enabling tuning of the polymer's highest occupied molecular orbital (HOMO) and lowest unoccupied molecular orbital (LUMO) levels.[3] Although there are many known donor-acceptor conjugated polymers, only a few combinations have resulted in high PCEs. Moreover, many of these polymers utilize complex heterocycles that are challenging to synthesize and purify on large scale.[2, 4]

Accordingly, benzo[1,2-*d*;5,4-*d*']bisoxazole (*cis*-BBO), benzo[1,2-*d*;4,5-*d*']bisoxazole (*trans*-BBO), and benzo[1,2-*d*;4,5-*d*']bisthiazole (*trans*-BBZT), are particularly promising for the development low- cost solution processible OPVs. Collectively referred to as the benzobisazoles, these electron deficient heterocycles are present in a variety of materials including high performance rigid-rod polymers,[5] non-linear optical materials,[6] emissive polymers for use in organic light emitting diodes,[7] electron transporting layers,[8] field-effect transistors (OFET)s,[9] and OPVs.[9c, 10] Benzobisazoles have planar conjugated structure that facilitates π–π stacking, improving charge carrier mobility.[8, 9d] Additionally, polybenzobisazoles are among some of the most thermally and environmentally stable materials known, which is benefical for long term device stability.[5] As a result of their origins as high performance materials, the monomers required for the synthesis of benzobisazoles can be prepared in large quantities, and

purified without the use of column chromatography, making scale-up feasible.[5a, b, 11] Historically, the use of polybenzobisazoles was hampered by their poor solubility and the harsh conditions used for their synthesis. However, new synthetic methods have enabled the development of solution processable polybenzobisazoles.[7f, 9c, 10a]

Previously, we reported the synthesis and photovoltaic properties of copolymers comprising a donor-acceptor-donor triad of a benzobisazole flanked by two thiophene rings and 3,3'-dioctylbithiophene.[10c] These copolymers exhibited hole mobilities as high as 4.9 x 10^{-3}cm^2 V^{-1} s^{-1} when used in OFETs and modest PCEs up to 1.14%, with the *trans*-BBO polymer giving the best performance in both devices. In an effort to improve upon the performance of these polymers we replaced the bithiophenes with benzo[1,2-*b*:4,5-*b'*]dithiophene (BDT). This electron rich building block has a planar structure that facilitates π–π stacking thus improving hole mobility.[12] As a result there are several copolymers comprised of BDT and various electron-deficient moieties with reported PCEs approaching the 10% PCE sought after for commercial viability.[13] In this work, we have utilized the two dimensional donor moiety 4,8-bis(5-(2-ethylhexyl)thien-2-yl)-benzo[1,2-*b*:4,5-*b'*]dithiophene. Replacing the electron rich alkoxy-side chains with thiophene rings lowers the HOMO level of the resulting polymers, while the extended conjugation created by the flanking thiophene rings increases absorption. As a result polymers made from thiophene substituted BDTs often have better OPV performance than their alkoxy substituted analogs.[14] This selection proved to be advantegous as when the polymers were used as electron donors in BH photovoltaic devices with $PC_{71}BM$ as the acceptor, the *trans*-benzobisoxazole polymer had the best performance with a PCE of 2.8%. This nearly a three-fold increase over the previously reported devices.

4.3 Results and Discussion

4.3.1 Synthesis and physical charecterization

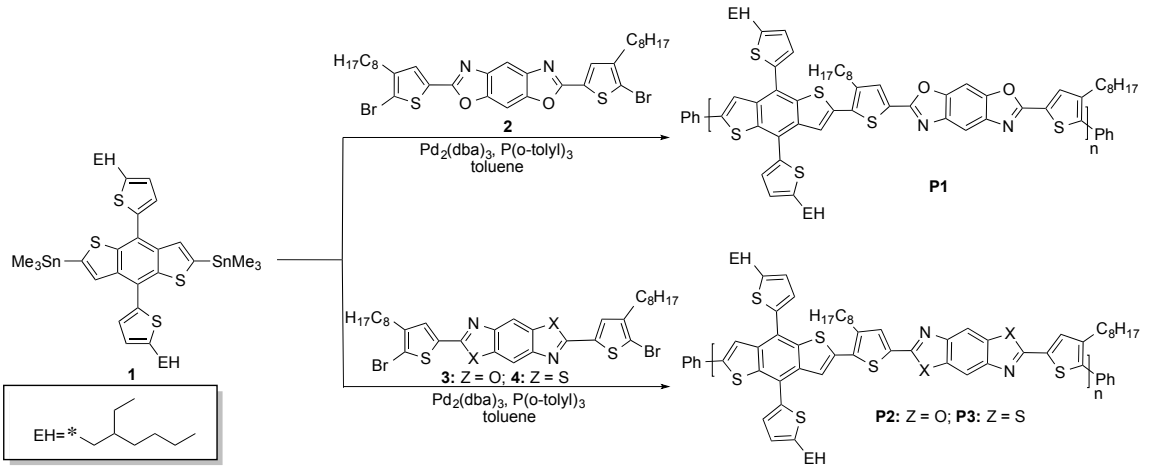

Scheme 4.1. Synthesis of benzodithiophene-thiophene-benzobisazole copolymers.

The synthesis of the polymers is shown in Scheme 4.1. The required monomers 4,8-bis(5-(2-ethylhexyl) thien-2-yl)-benzo[1,2-*b*:4,5-*b*′]dithiophene **1**,[15] 2,6-bis(4-octylthiophen-2-yl)-benzo[1,2-*d*; 5,4-*d*′]bisoxazole **2**,[7f] 2,6-bis(4-octylthiophen-2-yl)-benzo[1,2-*d*; 4,5-*d*']bisoxazole **3**,[7f] and 2,6-bis(4-octylthiophen-2-yl)-benzo[1,2-*d*; 4,5-*d*']bisthiazole **4**[7f] were synthesized according to the literature procedure. The use of the thiophene-benzobisazole-thiophene triad prevents ring opening side reactions at the 2- and 6-positions of the benzobisazole ring during the cross-coupling reaction.[16] The Stille cross-coupling polymerization of monomer **1** with **2**, **3,** or **4** with afforded polymers **P1**, **P2** and **P3** respectively in yields ranging from 60 – 76% after purification by Soxhlet extraction. All polymers are soluble in common organic solvents, such as THF, *m*-cresol, and chloroform at room temperature, facilitating characterization via gel permeation

chromatography (GPC) as shown in Table 1 and figure 4.7.7 – 4.7.9. The reported molecular weight of **P3** appears to be half that of **P1** and **P2** due to the reduced solubility of the sulfur containing polymer. We also believe that the limited solubility of **P3** has impeded its analysis as only the fraction soluble in chloroform at room temperature was evaluated. Nonetheless, all of the polymers showed excellent film-forming abilities. Thermogravimetric analysis (TGA) revealed that all polymers were thermally stable with 5% weight loss onsets occurring above 240 °C under air (Figure 4.7.6). The results are summarized in Table 5.1.

Table 4.1: Physical properties of **P1- P3**

Polymer	Yield (%)[a]	M_n[b] (kDa)	PDI	DP_n	T_d[c] (°C)
P1	76	15.9	1.9	17	387
P2	71	10.9	2.1	12	246
P3	60	5.3	1.5	4	250

[a] determined by GPC in chloroform using polystyrene standards. [b] 5% weight loss temperature by TGA in air.

4.3.2 Optical and electrochemical Properties

The normalized absorbance spectra of the polymer solutions in chloroform and in the solid state are shown in Figures 4.1 and 4.2, respectively, and the data is summarized in Table 4.2. In solution the UV-Visible spectrum for **P2** has a single, featureless absorbance band, whereas vibronic coupling is seen in the spectra of **P1** and **P3**. The absorption maximum for **P2** is hypsochromically shifted 26 nm relative to the absorbance

maximum for its isomer, **P1**, whereas the absorption maximum of **P3** is red-shifted 87 nm relative to the isoelectronic **P2**.

Table 4.2 Electronic and optical properties of poly(arylenebenzobisazoles)

	Solution		Film						
Polymer	λ_{max}^{abs} (nm)	λ_{max}^{abs} (nm)	λ_{onset} (nm)	E_g^{opt} (eV)[a]	E_g^{EC} (eV)[a]	E_{onset}^{ox} (eV)[b]	E_{onset}^{red} (eV)[b]	HOMO (eV)	LUMO (eV)
P1	451	490	565	2.2	2.1	0.42	-1.70	-5.2	-3.1
P2	425	487	575	2.2	2.1	0.46	-1.59	-5.3	-3.2
P3	513	518	600	2.1	1.7	0.35	-1.35	-5.2	-3.5

[a] Estimated from the optical absorption edge. [b] HOMO = -4.8 - (E^{ox}_{onset}) (eV). [c] LUMO = -4.8 - (E^{red}_{onset}) (eV). Electrochemical properties were measured using a three-electrode cell (electrolyte: 0.1 mol/L $TBAPF_6$ in acetonitrile) with an Ag/Ag^+ reference electrode, a platinum auxiliary electrode, and a platinum-button working electrode. Reported values are referenced to Fc/Fc^+. Polymer films were drop cast from an ortho-dichlorobenzene (*o*DCB) solution of the polymers on to the working electrode. All cyclic voltammetry experiments were recorded at a scan rate of 50 mV/s.

All of the spectra are fairly broad and lack a second low-energy absorption seen when intermolecular charge transfer between the electron donating and electron accepting units is occuring.[3c] As thin films, the absorbance maximum for all of the polymers are bathochromically shifted indicating increased backbone planarization and π-stacking in the solid state.[17] Interestingly, the absorbance maxima of **P1** and **P2** in thin film are significantly red-shifted relative to their solution spectra, while the absorbance maxima of **P3** is only slightly red-shifted relative to its solution spectra. The difference is likely a result of the lower molecular weight of **P3**. Despite the lower molecular weight of the

polymer, **P3** exhibited the most red-shifted absorbance maximum of the series. Overall, the absorption maxima for these polymers is also red-shifted relative to the analogous quarter thiophene benzobisazoles, which had absorption maxima of 460, 475, and 462 nm for the *cis*-BBO, *trans*-BBO, and *trans*-BBZT polymers, respectively and similar molecular weights.[10c]

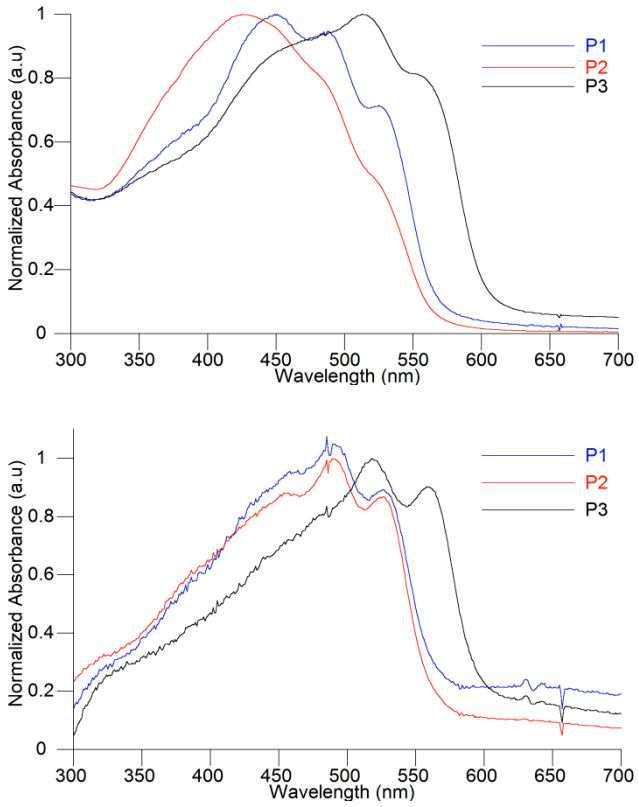

Figure 4.1. UV-Vis absorption spectra of benzodithiophene-thiophene-benzobisazole terpolymers **P1 – P3** in chloroform (top) and film bottom. Thin films were spun from 2 mg/mL solutions of the polymers in *o*-DCB

Although the optical band gaps for both series of polymers were similar, the red-shifted absorption in this series of polymers is beneficial in improving the photovoltaic properties of the polymers.

The electrochemical properties of the polymers were evaluated by cyclic voltammetry. All three polymers exhibit measureable and reproducible oxidation and reduction processes (Figure 4.7.5). The HOMO and LUMO levels were estimated from the onset of oxidation and reduction using the absolute energy level of ferrocene/ferrocenium (Fc/Fc^{+}) as 4.8 eV under vacuum and are summarized in Table 4.2.[18] The HOMO levels ranged from -5.2 to -5.3 eV, all of which are deep enough to guarantee good air stability.[19]

The LUMO levels ranged from -3.1 to -3.5 eV, with the *trans*-BBZT being the lowest. As a result, **P3** had the smallest electrochemical band gap of the series. The electrochemical band gaps for **P1** and **P2** are both similar to their optical band gaps, whereas the electrochemical band gap of **P3** is significantly smaller than its optical band gap. We note that the current of the cyclic voltammogram of **P3** is also smaller than that of the other polymers and this difference is likely a result of morphology of the polymer film on the electrodes surface. This data demonstrates that changing the position of the oxygen atoms from the *cis*- configuration to the *trans*- configuration has no impact on the HOMO level and a negligible impact on the LUMO level. However, replacing the oxygen atoms of *trans*-BBO with sulfur had a slight impact on the HOMO level, while reducing the LUMO level by ~0.3 eV. As a result the benzobisthiazole polymer has the smallest bandgap.

Previously, we were able to evaluate the energy levels using both CV and

ultraviolet photoelectron spectroscopy (UPS) and saw good correlation between both measurements. Generally UPS provides a more accurate values for the HOMO level.[20] Based on the UPS measurements switching the orientation of oxygen within benzobisoxzole from *cis* to *trans* lowered the HOMO level by 0.1 eV, and substituting the oxygen atoms in *trans*-BBO with sulfur atoms had no effect on the HOMO level. Conversely, switching the orientation within benzobisoxzole from *cis* to *trans* lowered the LUMO level by 0.1 eV, whereas replacing the oxygen atoms in *trans*-BBO with sulfur atoms raised the LUMO level by 0.1 eV. The LUMO levels of **P1** and **P2** are both 0.2 eV lower that those reported previously for the analogous quarterthiophene benzobisoxazole polymers (-2.9 eV) and the HOMO levels are both 0.1 eV higher (-5.3 and -5.4 eV).[10c] However, **P3** has a significantly lower LUMO level than its quarterthiophene analog (-3.1 eV) and the HOMO level is 0.2 eV higher (-5.4 eV).[10c] This suggests that there may be some error in the values obtained via CV for **P3**.

4.3.3 Evaluation of Charge Carrier Mobility and Photovoltaic Properties.

The performance of all three polymers in OPVs were evaluated using $PC_{71}BM$ as the electron acceptor with a device configuration of ITO/PEDOT:PSS/polymer:$PC_{71}BM$/Ca/Al. Photovoltaic devices with this configuration were fabricated using different polymer/ $PC_{71}BM$ weight ratios and are summarized in table S1. The active layer was deposited from 21 mg/mL *o*-DCB solutions, using processing conditions selected to yield a thickness of about 100 nm. In all cases the best performance was obtained using a 1:2.5 weight ratio of polymer to $PC_{71}BM$.

The current density-voltage (*J-V*) curves of **P1**:$PC_{71}BM$, **P2**:$PC_{71}BM$, and **P3**:$PC_{71}BM$ photovoltaic devices at this weight ratio under AM 1.5 G illumination (100 mW/cm^2) are shown in Figure 4.3. These devices were evaluated with and without the solvent additive, 1,8-diiodooctane (DIO). The resultant photovoltaic performances including short circuit current density (J_{SC}), open circuit voltage (V_{OC}), fill factor (FF) and PCE are shown in Table 4.3.

Overall, the devices based on **P2** gave the highest PCE at 2.78% without the use of solvent additives. The devices made from **P1** and **P3** had lower efficiencies with values of 1.75% and 1.62%, respectively. Although all of the polymers had similar V_{oc} and FF, **P2** had the highest photocurrent, and as a result, the highest PCE. This is almost a three-fold improvement over the previously reported poly(quarterthiophene benzobisoxazole).[10c] Interestingly, the **P1**- and **P3**-based devices had gave similar performances with respective values of 1.85% and 1.62%, despite the significantly lower molecular weight of **P3**, which can negatively affect film formation and charge carrier mobility.[21]

The OPV performance of **P3** is comparable to that reported by Jenekhe et al. for a related benzobisthiazole polymer, poly[(4,8-bis(2-hexyldecyl)oxy)benzo[1,2-*b*:4,5-*b*']dithiophene)-2,6-diyl-alt-(2,5-bis(3-dodecylthiophen-2-yl)benzo[1,2-*d*;4,5-*d*']bisthiazole)] (PBTHDDT), which had a PCE of 1.76%, that improved to 2.96% with the use of additives.[10a] We also evaluated the use of DIO as a solvent additive,[22] but only observed a nominal improvement in the PCE for **P1**, and a decrease in the performance of

P2 and **P3**. However, PBTHDDT differs from our polymer in the placement and nature of the substituents on both the thiophenes and benzodithiophene. This suggests that additional optimization of our system could yield an even higher PCE. The hole mobility of the polymers was examined using the space-charge-limited current (SCLC) method with a hole only device structure of ITO/PEDOT:PSS/Polymer/Al.[23]

The mobilites were calculated according to the equation 1:

$$J_{SCLC} = \frac{9\varepsilon_0\varepsilon_r\mu_h V^2}{8L^3} \qquad (1)$$

where $\varepsilon_0\varepsilon_r$ is the permittivity of the polymer, μ_h is the carrier mobility, and L is the device thickness.[24]

The hole mobilities were determined to be 2.19 x 10^{-5}, 2.18 x 10^{-5}, and 6.58 x 10^{-5} cm ^{2} V^{-1} s^{-1} for **P1**, **P2**, and **P3**, respectively. Intriguingly, **P1**and **P2** had similar mobilities, yet **P2** gave a significantly higher PCE, whereas **P3** gave the poorest performance, but the highest hole mobility. This suggests that the difference in the PCE of the polymers is not a function of their charge carrier mobility.

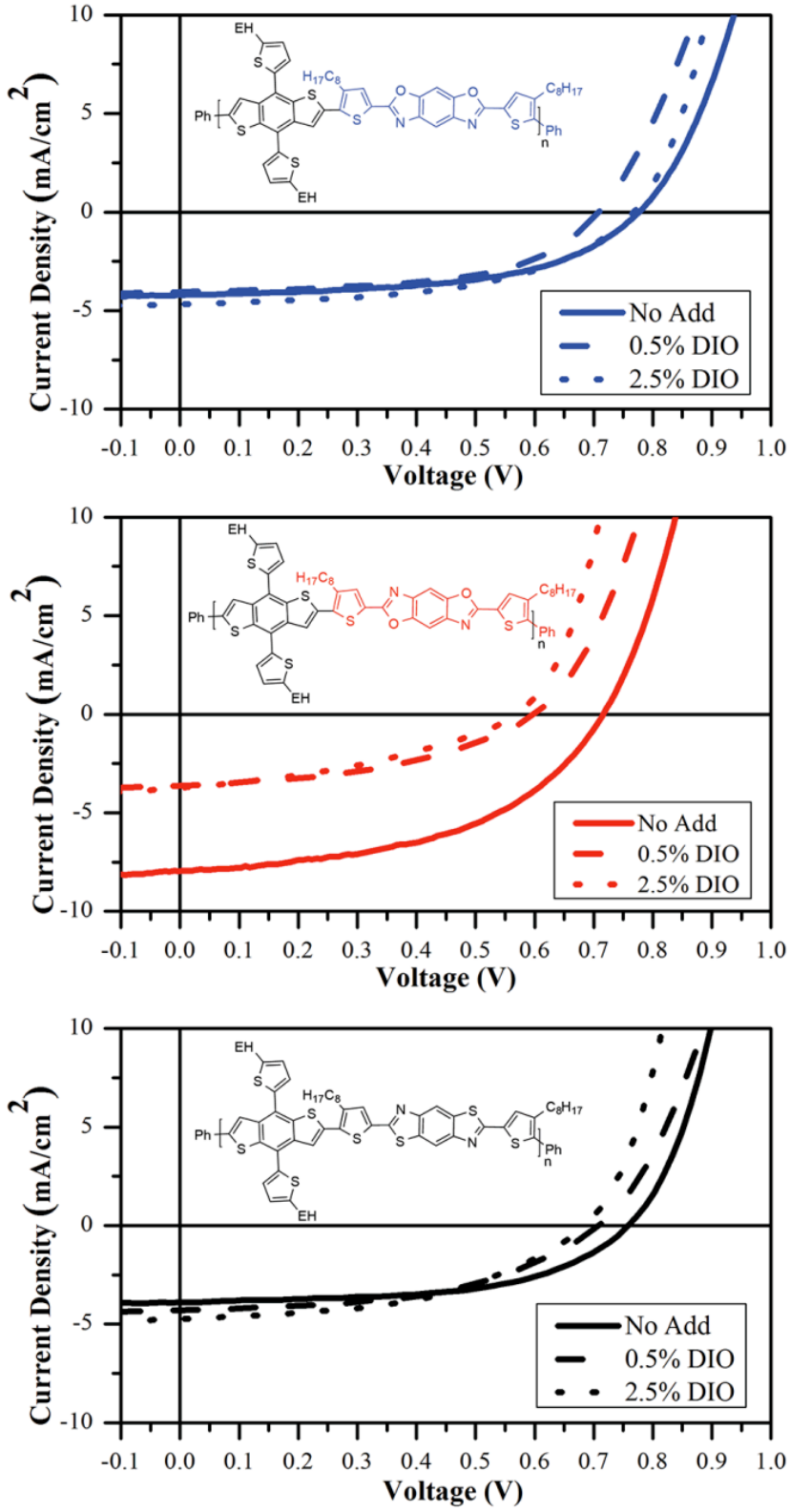

Figure 4.3. Current voltage characteristics of **P1 – P3** OPV devices.

Further investigation of the active layer blends using atomic force microscopy (AFM) revealed differences in surface morphology (Figure 4.4). The AFM height images revealed that both the **P1**:$PC_{71}BM$ and **P2**:$PC_{71}BM$ blend films have large domain sizes, manifesting root-mean square surface roughness (RMS) values of 2.94 nm and 1.20 nm, respectively. Whereas, the **P3**:$PC_{71}BM$ blend film has smaller domains (RMS = 0.78 nm). Visual inspection of the AFM phase images also indicate that there is a higher

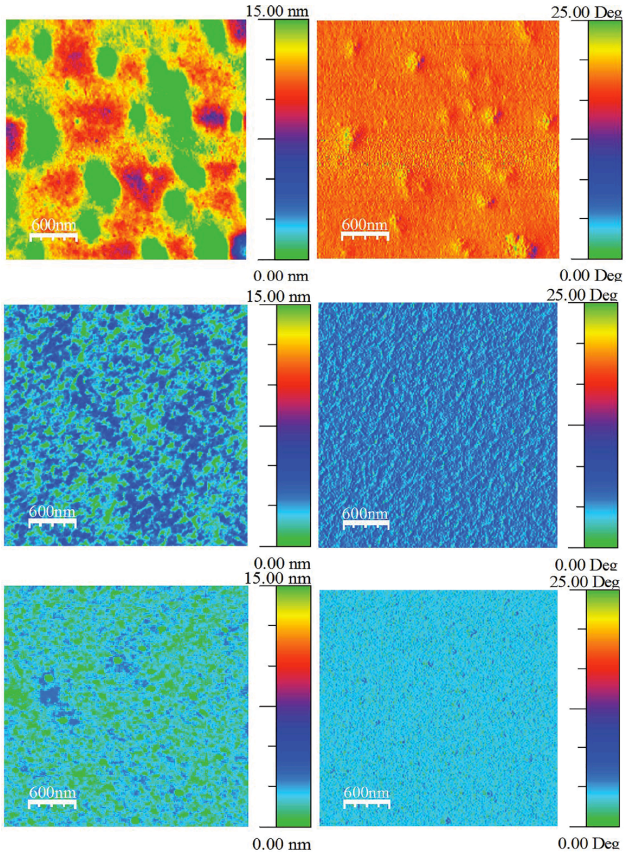

Figure 4.4. AFM height (left) and phase (right) images at 3 µm x 3 µm of devices with polymer:$PC_{71}BM$ blends at a 1:2.5 weight ratio. From top to bottom: **P1**:$PC_{71}BM$, **P2**:$PC_{71}BM$ and **P3:**$PC_{71}BM$

degree of intermixing between the polymer and the fullerene in the **P2**:$PC_{71}BM$ film. This phase segregation can enhance exciton dissociation. Conversely, films of the **P1**:$PC_{71}BM$ and **P3**:$PC_{71}BM$ blend exhibit vertical phase separation, similar to a bilayer type structure, reducing overall efficiency. Our previous X-ray diffraction studies on poly(quarter thiophene benzobisazoles) indicate that the structural differences in the materials do not significantly impact the packing of the polymer chains.[10c] Therefore, the differences in the morphology of these polymers are likely a result of their molecular weights as **P1** has the highest molecular weight and a greater tendency to aggregate in solution, while **P3** has a significantly lower molecular weight as a result of its reduced solubility.

4.4 Conclusions

Three terpolymers composed of thiophene, benzodithiophene and benzobisazoles were prepared in an effort to develop efficient materials for use in photovoltaic cells. The benzobisoxazole polymers had good solubility in various organic solvents,whereas the *trans*-benzobisthiazole polymer had limited solubility preventing the synthesis of high molecular weight polymer. All of the polymers had similar HOMO levels, but different LUMO levels and fairly wide band gaps. The *trans*-benzobisthiazole polymer, **P3,** exhibited slightly broader and red-shifted absorption spectra relative to the other benzobisazoles in the solid state. Furthermore, this polymer also had the highest hole mobility of all three polymers. However, these properties did not translate into better performance in OPVs as the polymer based on *trans*-benzobisoxazole gave the best performance of the series at 2.78%. This is the highest reported values for a

benozbisoxazole OPV and represents a near three-fold improvement over previous reports. The poor performance of the *trans*-benzobisthiazole polymer is likely a result of the negative impact the molecular weight has on the active layer film morphology. At the same time the OPV performance of all these polymers is limited due to the wide band gap and relatively high-lying HOMO level. Given the overall ease of synthesis, benzobisazoles are still promising building blocks for the development of OPV materials. However, additional improvements in solubility, processing and electronic properties are needed. Accordingly, we are actively pursuing the synthesis of new derivatives to address the wide band gap and processibility of these polymers.

4.5 Experimental Methods

4.5.1 Materials.

Toluene was dried using an Innovative Technologies solvent purification system. All other chemical reagents were purchased from commercial sources and used without further purification unless otherwise noted. 4,8-bis(5(2-ethylhexyl) thien-2-yl)-benzo[1,2-*b*:4,5-*b'*]dithiophene (**1**),[15] 2,6-bis(4-octylthiophen-2-yl)benzo[1,2-*d*; 5,4-*d*']bisoxazole **(2)**,[7f] 2,6-bis(4-octylthiophen-2-yl)benzo[1,2-*d*; 4,5-*d*']bisoxazole **(3)**,[7f] and 2,6-bis(4-octylthiophen-2-yl)benzo[1,2-*d*; 4,5-*d*']bisthiazole **(4)**[7f] were synthesized according to literature procedures. All other compounds were purchased from commercial sources and used without further purification.

4.5.2 Characterization

Nuclear magnetic resonance (NMR) spectra were carried out in $CDCl_3$ and recorded on Varian VXR (300 MHz), Varian MR (400 MHz) or a Bruker Avance III (600 MHz). ^1H NMR spectra were internally referenced to the residual protonated solvent peak. In all spectra, chemical shifts are given in ppm (δ) relative to the solvent. Gel permeation chromatography (GPC) measurements were performed on a separation module equipped with two 10 μm AMGPC-gel columns (crosslinked styrene-divinyl benzene copolymer) connected in series (guard, 10,000 Å, 1,000 Å pore size) with a UV-Vis detector. Analyses were performed at 40 °C temperature using chloroform as the eluent with a flow rate of 1.0 mL min^{-1}. Calibration was based on polystyrene standards. Thermogravimetric analysis measurements were performed over an interval of 30 - 850 °C at a heating rate of 20 °C min^{-1} under ambient atmosphere. Cyclic voltammetry was performed using a e-DAQ e-corder 410 potentiostat with a scanning rate of 100 mV s^{-1}. The polymer solutions (1-2 mg mL^{-1}) were drop-cast onto a platinum electrode. Ag/Ag^+ was used as the reference electrode and a platinum wire as the auxiliary electrode. The reported values are referenced to Fc/Fc^+ (-4.8 eV versus vacuum). All electrochemistry experiments were performed in deoxygenated CH_3CN under an argon atmosphere using 0.1 M tetrabutylammonium hexafluorophosphate as the electrolyte. Absorption spectra were obtained on a photodiode-array Agilent 8453 UV-visible spectrophotometer using polymer solutions in $CHCl_3$ and thin films. The films were made by spin-coating 25 x 25 x 1 mm glass slides using solutions of polymer (2 mg/mL) in $CHCl_3$/*o*-dichlorobenzene at a spin rate of 1200 rpm on a Headway Research, Inc. PWM32 spin-coater.

4.5.3 Fabrication of photovoltaic devices.

All devices were produced via a solution-based, spin-casting fabrication process. All polymers were mixed with $PC_{71}BM$ (SES Research) (mixed 1:2.5 with a total solution concentration of 21 mg mL^{-1} for $PC_{71}BM$) then dissolved in *o*-dichlorobenzene and stirred at 90 °C for 48 hours. ITO (20 – 25.2 Ω) coated glass slides (Delta Technologies) were cleaned by consecutive 10 minute sonications in (i) Mucasol™ detergent (dissolved in deionized water), 2x, (ii) deionized water, (iii) acetone, and then (iv) isopropanol. The slides were then dried in an oven for at least 3 hours and cleaned with air plasma (Harrick Scientific plasma cleaner) for 10 minutes. Filtered (0.45 μm) PEDOT:PSS (Clevios P™) was spin-coated onto the prepared substrates (2000 rpm/60 sec) after first being stirred for 10 minutes at room temperature. The PEDOT:PSS films were annealed at 150 °C for 30 minutes. After cooling, the substrates were transferred to an argon-filled glovebox. After 48 hours of mixing, the polymer:$PC_{71}BM$ solutions were filtered (0.45 μm pore, GS-Tek) and simultaneously dropped onto the PEDOT:PSS-coated substrates and spin-cast at 1000 rpm for 60 seconds. The films were dried under vacuum overnight. Ca (20 nm) and Al (100 nm) were successively thermally evaporated through a shadow mask (area = 0.06 cm^{-2}) under vacuum of 10^{-6} mbar to complete the devices. *J-V* data was generated by illuminating the devices using an ETH quartzline lamp at 1 sun (calibrated using a crystalline silicon photodiode with a KG-5 filter). The hole mobility was extracted from the SCLC measurement using keithley 2400 source/meter in the dark under ambient condition.

4.5.4 Atomic force microscopy.

All measurements were performed on films cast as described above; electrodes were not attached to these samples. A Veeco Digital Instruments atomic force microscope was used to perform the analysis. The tapping-mode AFM was carried out using TESPA tip with scan rate of 0.5 μm sec^{-1} and scan size of 3 μm x 3 μm Synthesis

4.5.5 General procedure for the synthesis of copolymers.

A mixture of 1 and the respective benzobisazole, 2 mol % tris(dibenzylideneacetone)dipalladium(0), 8 mol % tris-*o*-tolyphosphine in 7 mL of deoxygenated toluene was charged in a round bottom flask equipped with a reflux condenser and an argon inlet. The mixture was allowed to reflux for 18 - 72 hours before it was end capped by addition of triphenylmethyltin followed by iodobenzene. The polymer was precipitated by pouring into 100 mL of cold methanol. The precipitated polymer was filtered into a cellulose extraction thimble and purified by Soxhlet extraction with methanol to remove residual palladium followed by hexanes to remove the lower molecular weight material. The polymers were then extracted $CHCl_3$. Functionalized silica (SiliaMetS® Cysteine) was added to the chloroform fractions and the solutions were allowed to stir overnight at 50 ˚C. The chloroform fractions were then filtered through a bed of Celite and the solvent was removed under reduced pressure. The polymers were further purified by passing them through a pad of silica using chloroform as the eluent. They were then precipitated in methanol, filtered and dried under vacuum.

Synthesis of P1. Following the general polymerization procedure using compounds 1 (200 mg, 0.22 mmol) and 2 (156 mg, 0.22 mmol) and a reaction time of 72 hours afforded a dark solid (154 mg, 76%). GPC ($CHCl_3$, 40 °C): M_n = 15.9 kDa, PDI = 1.9.

Synthesis of P2. Following the general polymerization procedure using compounds 1 (200 mg, 0.22 mmol) and 3 (156 mg, 0.22 mmol) and a reaction time of 72 hours afforded a dark solid (143 mg, 71%). GPC ($CHCl_3$, 40 °C): M_n = 10.9 kDa, PDI = 2.1

Synthesis of P3. Following the general polymerization procedure using compounds 1 (80 mg, 0.09 mmol) and 4 (65 mg, 0.09 mmol) and a reaction time of 18 hours afforded a dark solid (70 mg, 60%). GPC ($CHCl_3$, 40 °C): M_n = 5.3 kDa, PDI = 1.5

4.6 Acknowledgements

We thank the National Science Foundation (DMR-0846607) for partial support of this work. We also thank the National Science Foundation Materials Research Facilities Network (DMR-0820506) and Polymer-Based Materials for Harvesting Solar Energy, an Energy Frontier Research Center funded by the U.S. Department of Energy, Office of Science, Office of Basic Energy Sciences under Award Number DE-SC0001087 for support of the device fabrication. The Iowa State University (ISU), the Institute for Physical Research and Technology provided MDE with a Catron Fellowship. Some of the OPV work was performed at the ISU Microelectronics Research Center. ME thanks the financial support from the Egyptian government (scholarship # GM915). We thank Mr. Michael Zenner for thermal analysis.

4.7 Supplementary Information

Materials and General Experimental Details. Tetrahydrofuran was dried using an Innovative Technologies solvent purification system. 2,2'-bithiophene, and 3,3',5,5'-tetrabromo-2,2'-bithiophene (1), were prepared according to literature procedures. All other compounds were purchased from commercial sources and used without further purification. Chromatographic separation was performed using silica gel 60, using the eluents indicated.

Instrumentation

Nuclear magnetic resonance spectra were obtained on a 400 MHz/300MHz spectrometer (^{1}H at 300MHz or 400 MHz and ^{13}C at 100 MHz). ^{1}H NMR samples were referenced internally to residual protonated solvent ^{13}C NMR are referenced to the middle carbon peak of $CDCl_3$. In both instances chemical shifts are given in δ relative to solvent. Gel permeation chromatography (GPC) measurements were performed on a Shimadzu GPC, model number RID – 10A equipped with two 10μm AM-gel columns connected in a series (guard, HMW and LMW) with a UV-Vis detector. Analyses were performed at 40 °C using chloroform as the eluent with the flow rate at 1.0 mL/min. Calibration was based on polystyrene standards. UV-Visible spectroscopy was obtained using polymer solutions in chloroform, and thin films were spun from *o*-DCB. The films were made by spin-coating 25 x 25 x 1mm glass slides, using a solution of 2 mg of polymer per 1 mL *o*-DCB at a spin rate of 800 rpms on a Spin-Coater. Thermal gravimetric analysis measurements were made within the temperature interval of 30 ºC - 800 ºC, with a heating rate of 20 ºC/minute, under ambient atmosphere. Electrochemical properties were

measured on an eDaq e-corder 410 potentiostat using a three-electrode cell (electrolyte: 0.1 mol/L $TBAPF_6$ in acetonitrile) with an Ag/Ag^+ reference electrode, a platinum auxiliary electrode, and a platinum button electrode as the working electrode. Polymer films were made by drop coating an *o*-DCB solution of the polymers on to the working electrode. All films were annealed at 140 ºC for 2 hours prior to use. All differential pulse voltammetry experiments were carried out under argon atmosphere and were recorded at a scan rate of 50 mV/s.

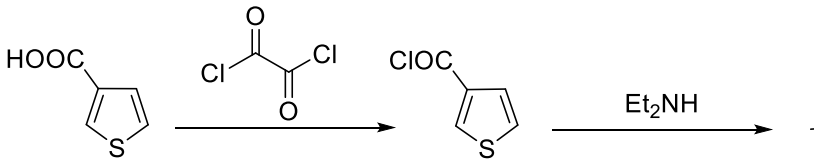

Scheme 4.7.1: Synthesis of N,N-diethylthiophene-3-carboxamide

***N,N*-diethylthiophene-3-carboxamide (S1).** Thiophene-3-carboxylic acid (11.77 g, 91.8 mmol) was dissolved in 21 mL of anhydrous DCM in a flame-dried round bottom flask. The solution was cooled to 0 °C in an ice bath. Oxalyl chloride (16.3 mL, 193 mmol) was added dropwise. The solution was allowed to warm to room temperature overnight. Unreacted oxalyl chloride was removed under reduced pressure.

To a flame-dried round bottom flask, diethyl amine (23.7 mL, 229 mmol) in 15 mL of anhydrous DCM was added. The solution was cooled to 0 °C in an ice bath. Crude thiophene-3-carbonyl chloride dissolved in 21 mL of anhydrous DCM was added dropwise. The solution was stirred at room temperature for 4 h. The reaction was quenched by addition of water. The organic layer was separated and rinsed with brine and dried over $MgSO_4$. The solvent was removed under reduced pressure. Purification via

distillation yielded 16.11 g (96%) of S1 as a pale yellow oil. ^{1}H NMR (400 MHz, $CDCl_3$) δ 7.47 (dd, *J* = 2.8, 1.1 Hz, 1H), 7.31 (dd, *J* = 5.0, 2.9 Hz, 1H), 7.18 (dd, *J* = 5.1, 1.2 Hz, 1H), 3.42 (s, 4H), 1.19 (s, 6H)

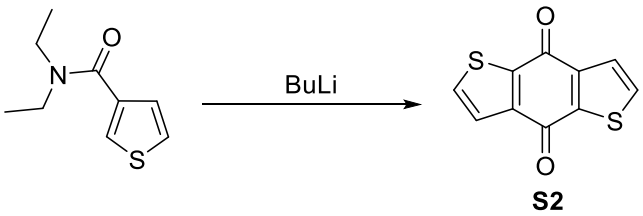

Scheme 4.7.2: Synthesis of benzo[1,2-*b*:4,5-*b*′]dithiophene-4,8-dione

Benzo[1,2-*b*:4,5-*b*′]dithiophene-4,8-dione (S2). S1 (5.66 g, 31 mmol) was dissolved in 50 mL of anhydrous THF in a flame-dried round bottom flask. The solution was cooled to 0 °C in an ice bath. *n*-butyllithium (14.2 mL, 2.5 M in hexanes) was added dropwise. The resulting solution was allowed to warm to room temperature overnight. The reaction was quenched by addition of 1M HCl. The resulting solid was then filtered and washed with water followed by methanol and then hexanes. It was recrystallized from glacial acetic acid to give 2.2 g (65%) of S2 as yellow solid. ^{1}H NMR (400 MHz, DMSO-d_6) δ 8.14 (d, *J* = 5.0 Hz, 2H), 7.61 (d, *J* = 5.0 Hz, 2H).

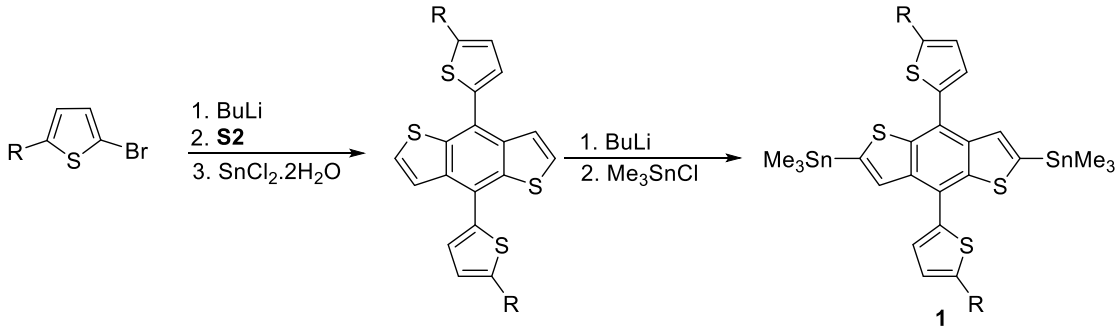

Scheme 4.7.3: Synthesis of **1**

4,8-bis(5-(2-ethylhexyl)thiophen-2-yl)benzo[1,2-*b*:4,5-*b*′]dithiophene (1). 2-bromo-5-(2-ethylhexyl)thiophene (4.00 g, 14.5 mmol) was dissolved in 12 mL of anhydrous THF in a flame-dried round bottom flask. The solution was cooled to 0 °C in an ice bath. *n*-butyllithium (6.4 mL, 2.5 M in hexanes) was added dropwise. The resulting anion was warmed to 50 °C and stirred at that temperature for 2 h. The solution was then cooled to 0 °C in an ice bath. Benzo[1,2-*b*:4,5-*b*′]dithiophene-4,8-dione (0.8 g, 3.6 mmol) was added in one portion. The solution was heated to 50 °C and stirred at that temperature for 1 h. The reaction was then cooled to room temperature. A solution of 6.55g tin chloride dihydrate in 10 % HCl (10 mL) was slowly added. The reaction was stirred at room temperature for 2 h before it was poured into ice-water. The product was extracted with hexanes, washed with water, and dried over Na_2SO_4. The solvent was removed under reduced pressure. The crude product was purified by column chromatography using hexanes as the eluent to give a yellow solid in 87% yield.

^{1}H NMR (400 MHz, CDCl3) δ 7.64 (d, *J* = 5.7 Hz, 2H), 7.45 (d, *J* = 5.7 Hz, 2H), 7.29 (d, *J* = 3.4 Hz, 2H), 6.89 (d, *J* = 3.5 Hz, 2H), 2.86 (d, *J* = 6.8 Hz, 4H), 1.73 – 1.64 (m, 2H), 1.35 (td, *J* = 8.7, 4.9 Hz, 16H), 1.05 – 0.84 (m, 12H).

(4,8-bis(5-(2-ethylhexyl)thiophen-2-yl)benzo[1,2-*b*:5,4-*b*′]dithiophene-2,6-diyl)bis (trimethy lstannane) (1). 4,8-bis(5-(2-ethylhexyl)thiophen-2-yl)benzo[1,2-*b*:4,5-*b*′]dithiophene (1.8 g, 3.1 mmol) was dissolved in 30 mL of anhydrous THF in a flame-dried round bottom flask. The solution was cooled to 0 °C in an ice bath. *n*-butyllithium (2.8 mL, 2.5 M in hexanes) was added dropwise. The resulting dianion was stirred at

room temperature for 2 h. Trimethyltin chloride (7.8 mL, 1 M in THF) was added. The reaction was stirred for an additional 2 h at room temperature. The reaction was quenched by addition of water. The product was extracted with hexanes. The organic layer was washed with 1M KF followed by water and brine, and dried over Na_2SO_4. The solvent was removed under reduced pressure. Recrystallization from isopropanol afforded 2.27 g (81 %) of pure product as a yellow solid.

^{1}H NMR (600 MHz, CDCl3) δ 7.75 (s, 2H), 7.37 (d, J = 3.5 Hz, 2H), 6.95 (d, J = 3.6 Hz, 2H), 2.92 (t, 4H), 1.78 – 1.71 (m, 2H), 1.53 – 1.33 (m, 18H), 0.99 (m, 13H), 0.45 (t, 17H).

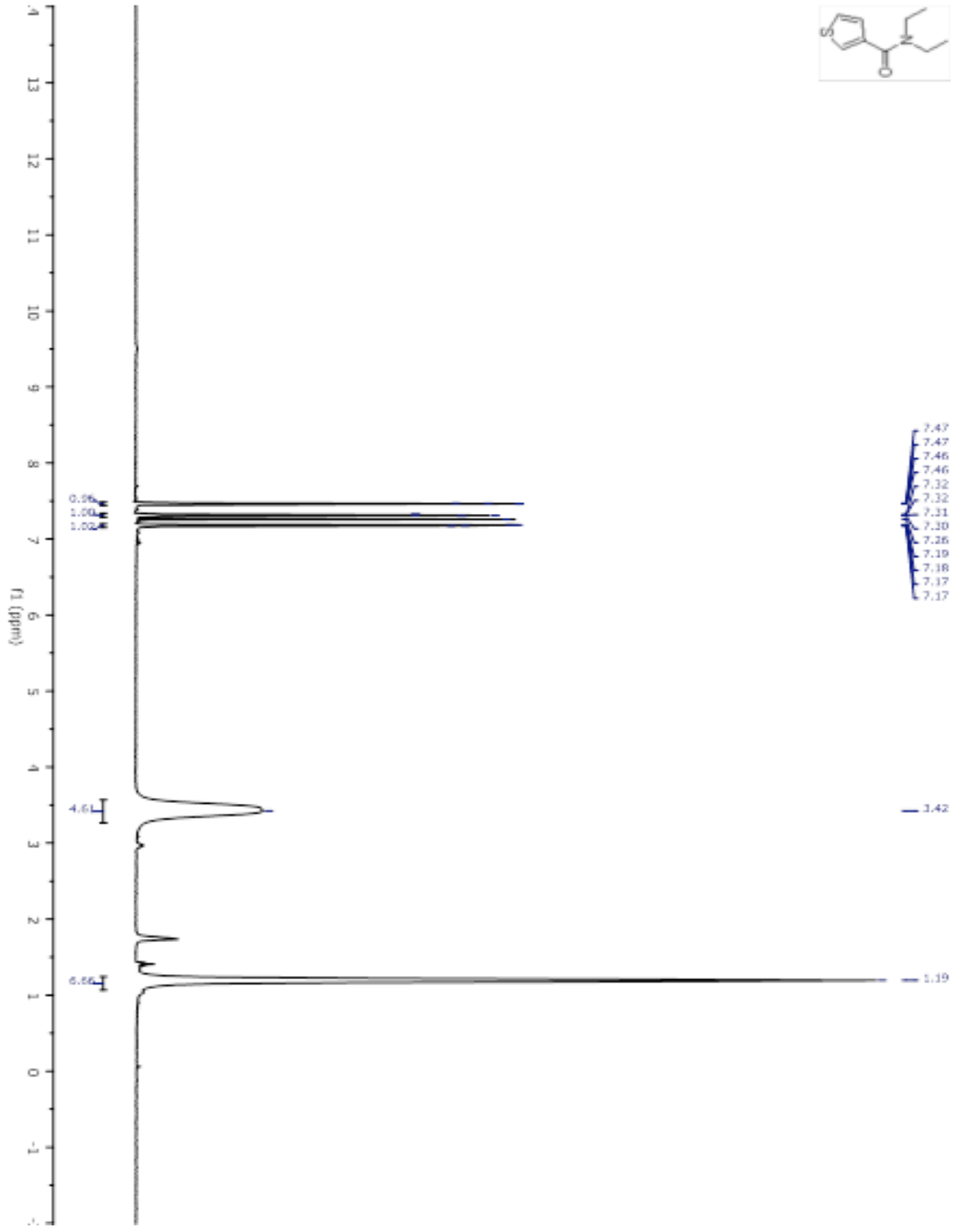

Figure 4.7.1: ^{1}H NMR spectra of N,N-diethylthiophene-3-carboxamide

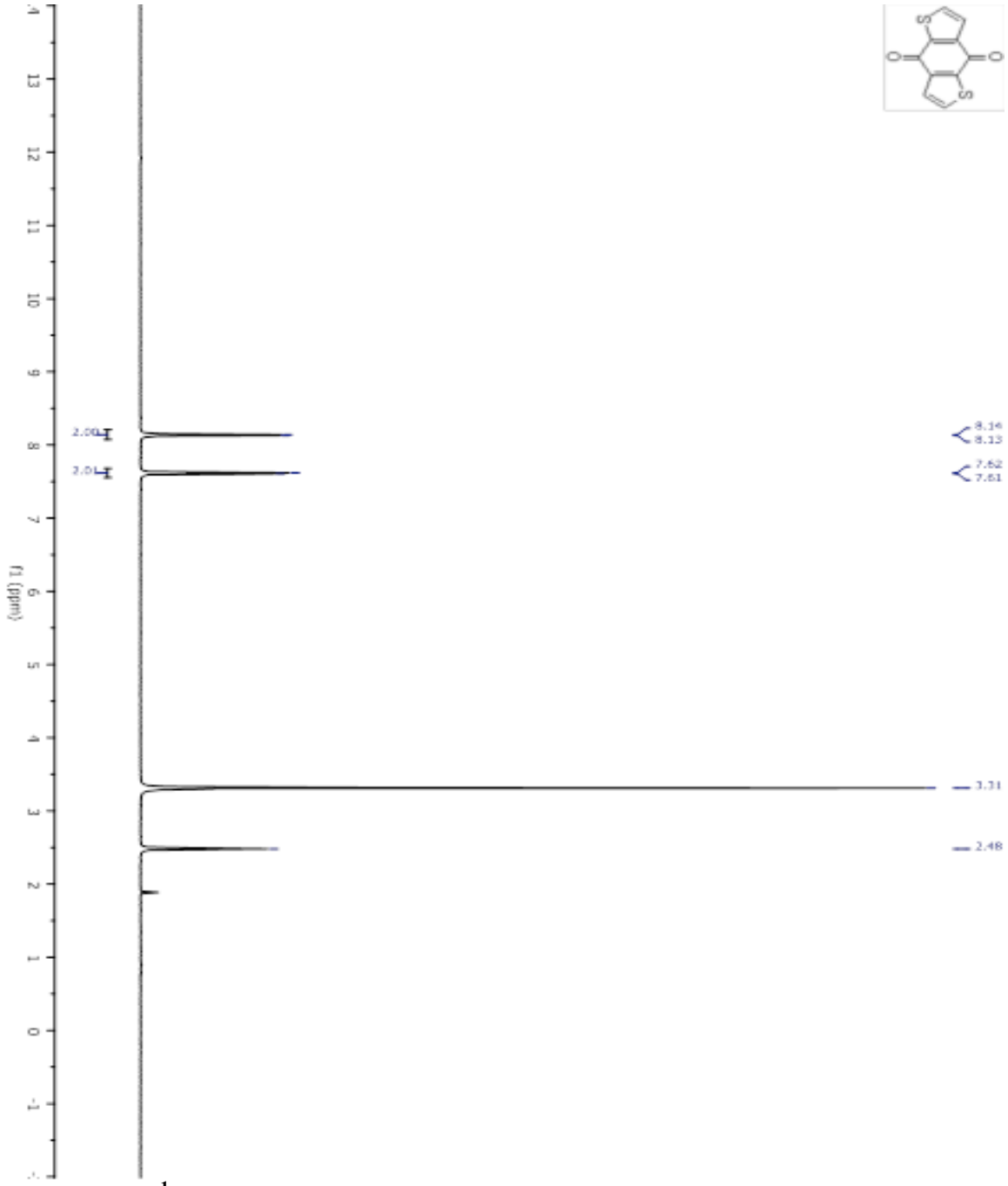

Figure 4.7.2: ^{1}H NMR spectra of Benzo[1,2-b:4,5-b']dithiophene-4,8-di

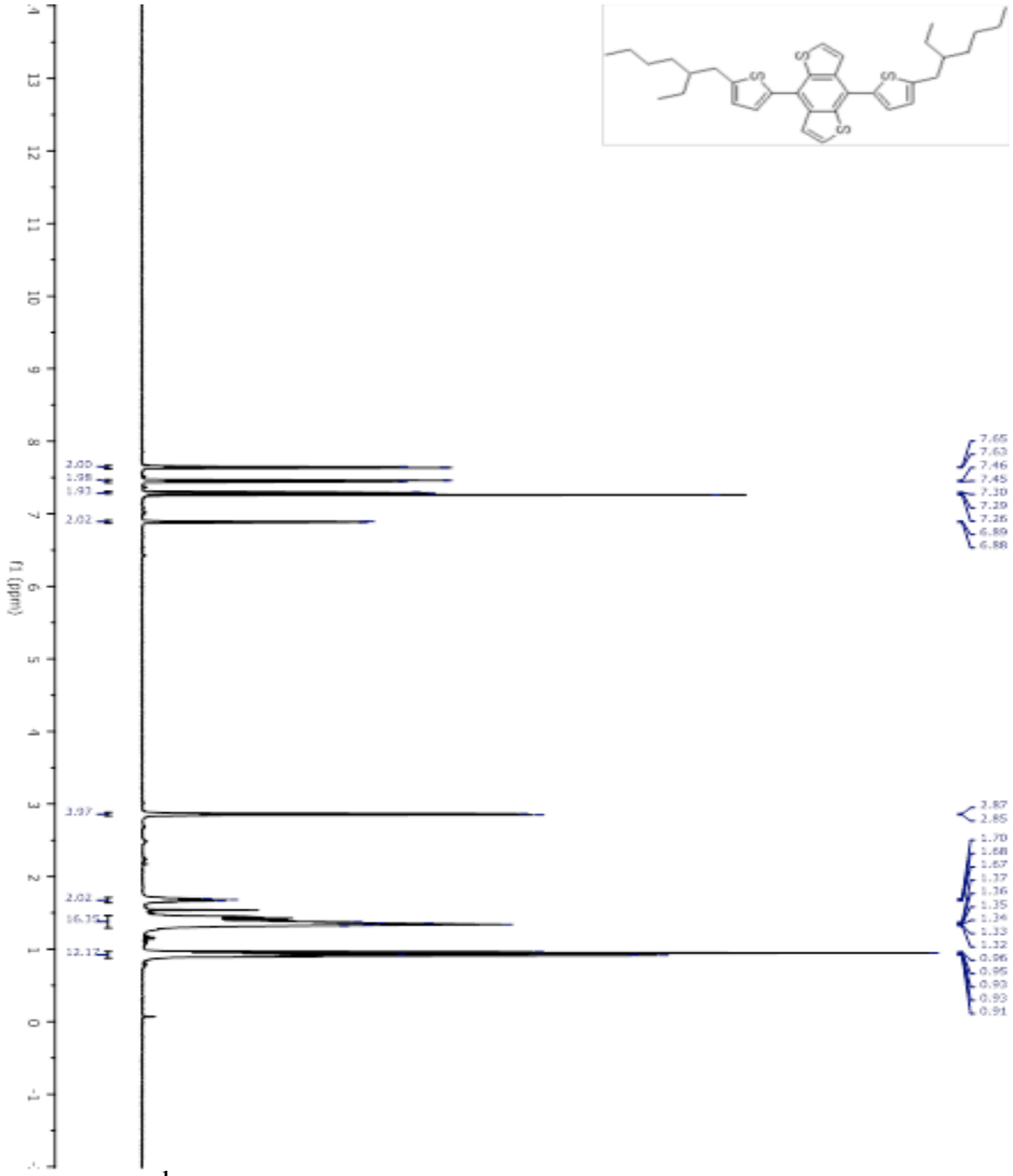

Figure 4.7.3: ^{1}H NMR spectra of 4,8-bis(5-(2-ethylhexyl)thiophen-2-yl)benzo[1,2-b:4,5-b']dithiophene

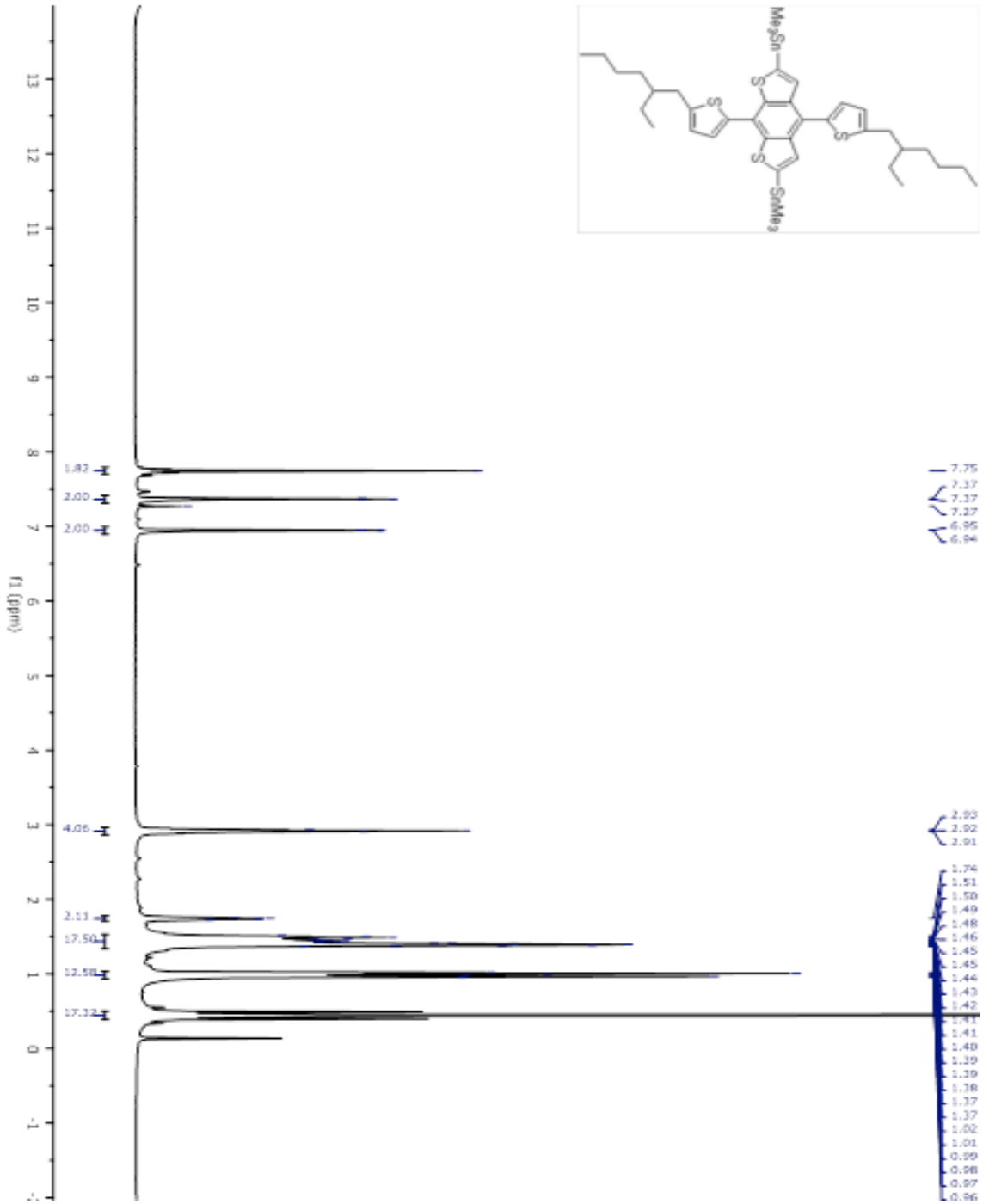

Figure 4.7.4: ^{1}H NMR spectra of (4,8-bis(5-(2-ethylhexyl)thiophen-2-yl)benzo[1,2-b:5,4-b']dithiophene-2,6-diyl)bis (trimethylstannane) (1)

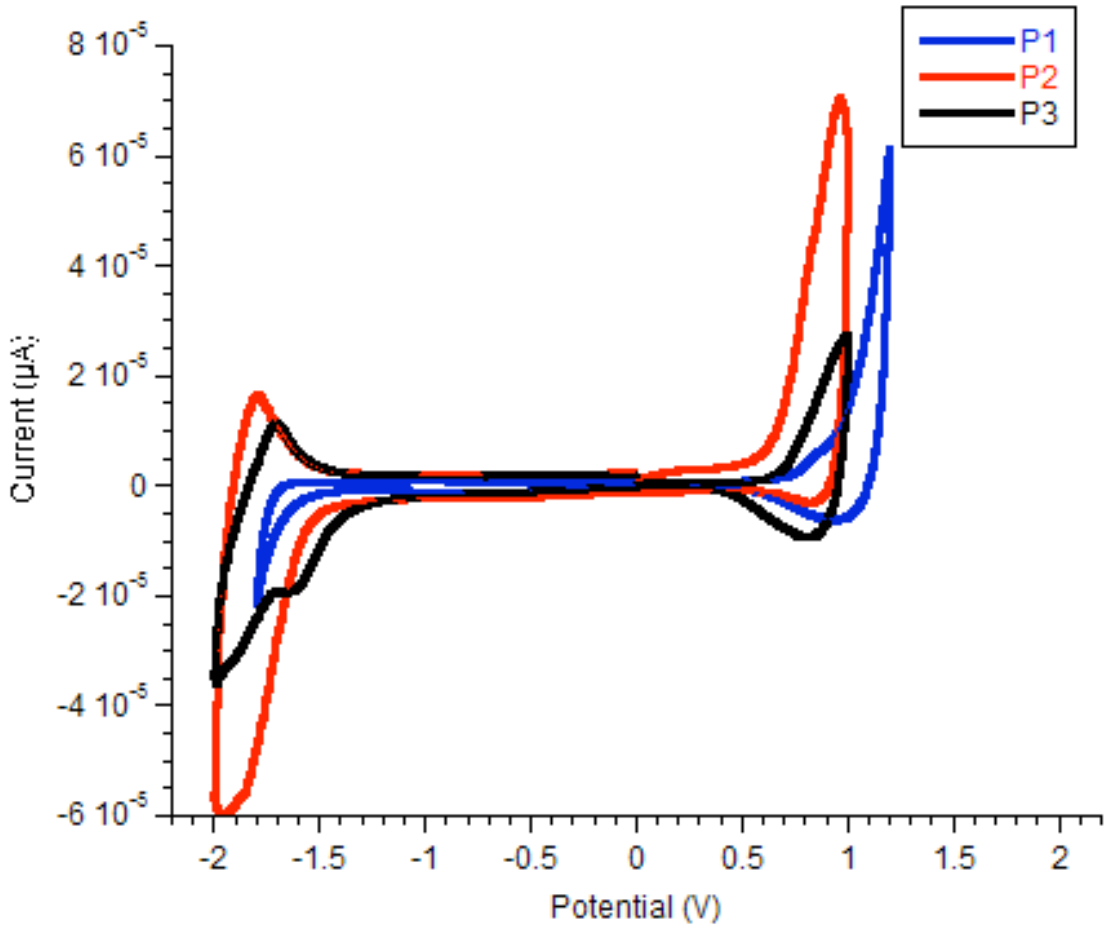

Figure 4.7.5: CV curves for P1 - P3

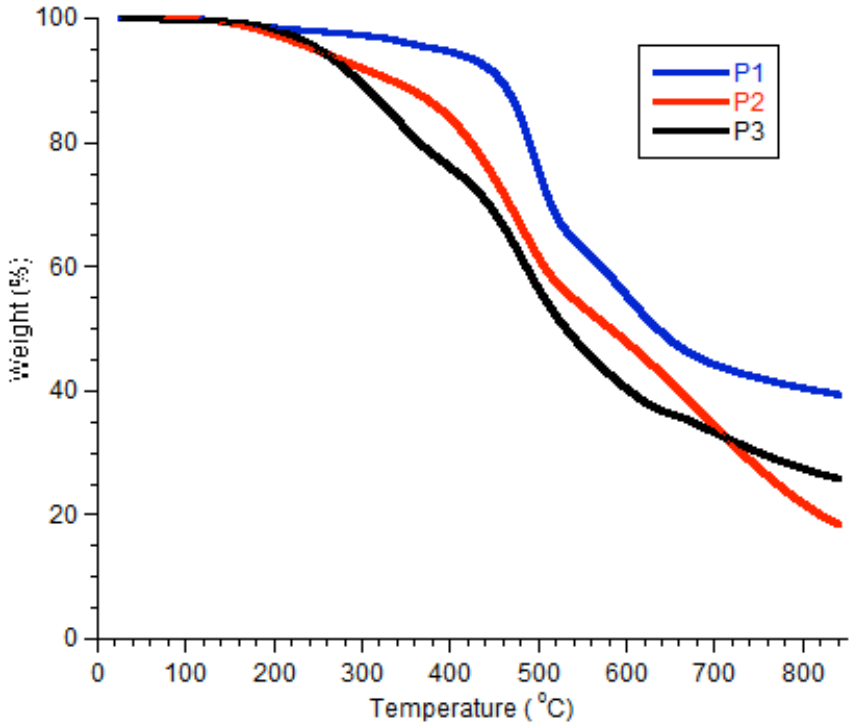

Figure 4.7.6: TGA plots for P1 - P3

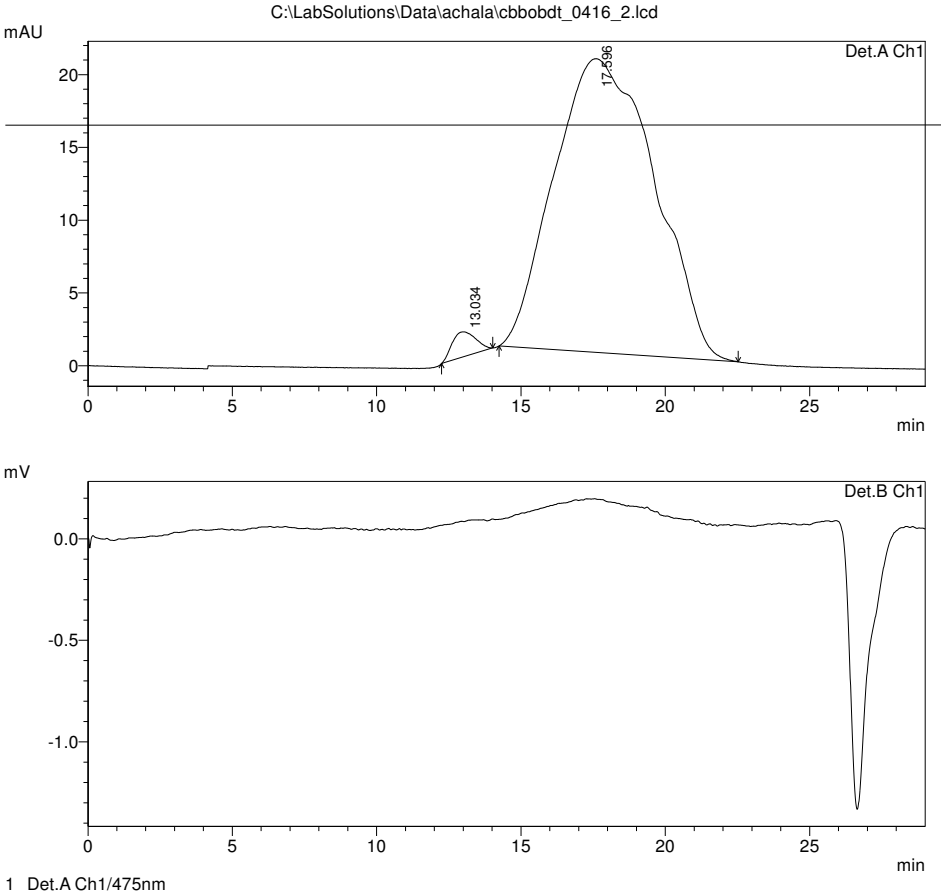

GPC Results

Peak#:1 (Detector A Ch1)	
[Average Molecular Weight]	
Number Average Molecular Weight(Mn)	624985
Weight Average Molecular Weight(Mw)	711444
Mw/Mn	1.13834
Peak#:2 (Detector A Ch1)	
[Average Molecular Weight]	
Number Average Molecular Weight(Mn)	15929
Weight Average Molecular Weight(Mw)	33759
Mw/Mn	2.11937

C:\LabSolutions\Data\achala\cbbobdt_0416_2.lcd

Figure 4.7.7: GPC trace of P1

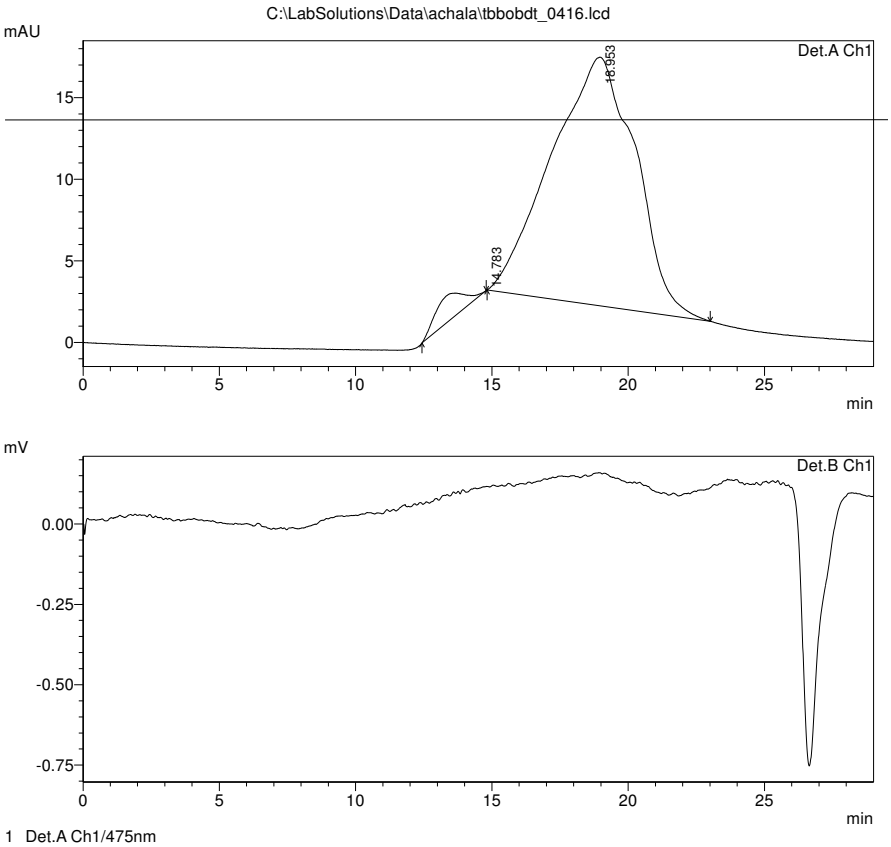

GPC Results

Peak#:1 (Detector A Ch1)	
[Average Molecular Weight]	
Number Average Molecular Weight(Mn)	411776
Weight Average Molecular Weight(Mw)	488151
Mw/Mn	1.18548
Peak#:2 (Detector A Ch1)	
[Average Molecular Weight]	
Number Average Molecular Weight(Mn)	10976
Weight Average Molecular Weight(Mw)	22730
Mw/Mn	2.07087

C:\LabSolutions\Data\achala\tbbobdt_0416.lcd

Figure 4.7.8: GPC trace of P2

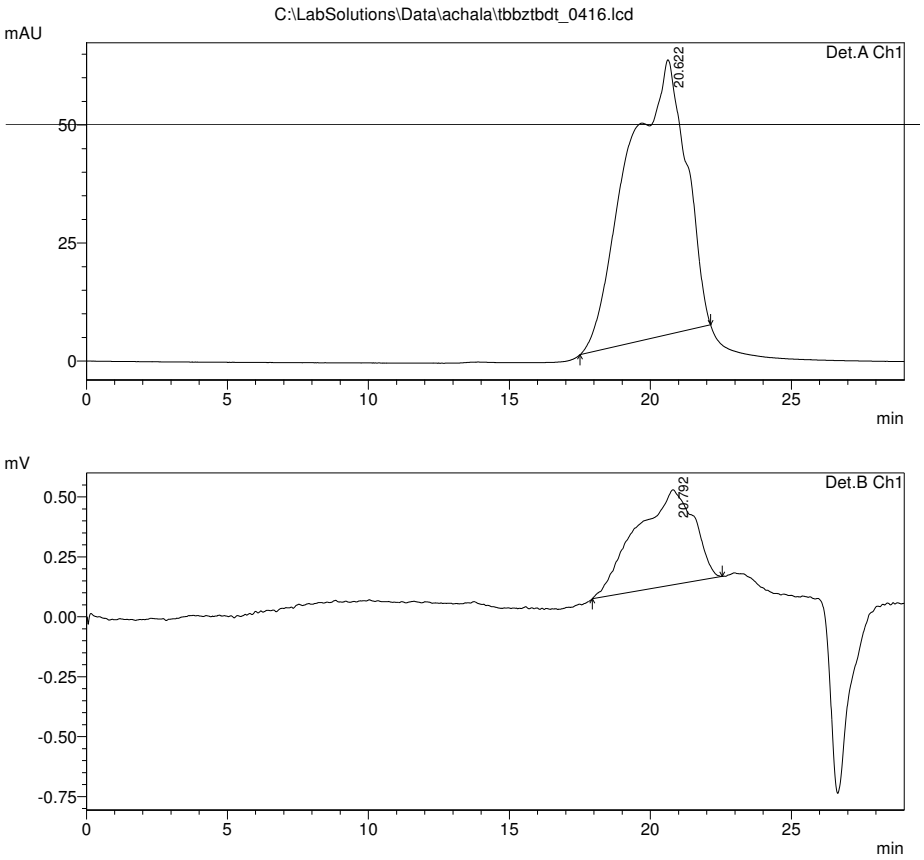

GPC Results

Peak#:1 (Detector A Ch1)	
[Average Molecular Weight]	
Number Average Molecular Weight(Mn)	5321
Weight Average Molecular Weight(Mw)	7874
Mw/Mn	1.47986
Peak#:1 (Detector B Ch1)	
[Average Molecular Weight]	
Number Average Molecular Weight(Mn)	4861
Weight Average Molecular Weight(Mw)	7272
Mw/Mn	1.49595

C:\LabSolutions\Data\achala\tbbztbdt_0416.lcd

Figure 4.7.9: GPC trace of P3

Polymer	Polymer:$PC_{71}BM$ Ratio	V_{OC} (V)	J_{SC} (mA cm^{-2})	FF	PCE (%)
P1	1:1.5	0.769	3.53	0.55	1.50
	1:2	0.790	3.54	0.54	1.51
	1:2.5	0.776	4.20	0.54	1.75
P2	1:1.5	0.619	4.10	0.41	1.03
	1:2	0.703	3.75	0.48	1.27
	1:2.5	0.715	7.95	0.49	2.78
P3	1:1.5	0.741	3.20	0.55	1.3
	1:2	0.735	3.58	0.56	1.50
	1:2.5	0.758	3.87	0.55	1.62

Table 4.7.1: Photovoltaic performance of polymers P1 – P3 using different polymer:$PC_{71}BM$ blends

4.8 REFERENCES

1. G. Yu, J. Gao, J. C. Hummelen, F. Wudl and A. J. Heeger, *Science*, 1995, **270**, 1789.
2. H. Zhou, L. Yang and W. You, *Macromolecules*, 2012, **45**, 607.
3. a) H. A. M. van Mullekom, J. A. J. M. Vekemans, E. E. Havinga and E. W. Meijer, *Mater. Sci. Eng., R*, 2001, **32**, 1; b) E. E. Havinga, W. ten Hoeve and H. Wynberg, *Polymer Bulletin*, 1992, **29**, 119; c) P. M. Beaujuge, C. M. Amb and J. R. Reynolds, *Acc. Chem. Res.*, 2010, **43**, 1396.
4. a) C. M. Amb, S. Chen, K. R. Graham, J. Subbiah, C. E. Small, F. So and J. R. Reynolds, *J. Am. Chem. Soc.*, 2011, **133**, 10062; b) A. Facchetti, *Chem. Mater.*, 2011, **23**, 733.
5. a) J. F. Wolfe and F. E. Arnold, *Macromolecules*, 1981, **14**, 909; b) J. F. Wolfe, B. H. Loo and F. E. Arnold, *Macromolecules*, 1981, **14**, 915; c) E. W. Choe and S. N. Kim, *Macromolecules*, 1981, **14**, 920.
6. S. A. Jenekhe, J. A. Osaheni, J. S. Meth and H. Vanherzeele, *Chem. Mater.*, 1992, **4**, 683.
7. a) J. A. Osaheni and S. A. Jenekhe, *Macromolecules*, 1993, **26**, 4726; b) J. Intemann, J. Mike, M. Cai, S. Bose, T. Xiao, T. Mauldin, R. Roggers, J. Shinar,

R. Shinar and M. Jeffries-EL, *Macromolecules*, 2011, **44**, 248; c) J. J. Intemann, J. F. Mike, M. Cai, C. A. Barnes, T. Xiao, R. A. Roggers, J. Shinar, R. Shinar and M. Jeffries-EL, *J. Polym. Sci., Part A*, 2013, **51**, 916; d) J. J. Intemann, E. S. Hellerich, B. C. Tlach, M. D. Ewan, C. A. Barnes, A. Bhuwalka, M. Cai, J. Shinar, R. Shinar and M. Jeffries-El, *Macromolecules*, 2012, **45**, 6888; e) E. S. Hellerich, J. J. Intemann, M. Cai, R. Liu, M. D. Ewan, B. C. Tlach, M. Jeffries-El, R. Shinar and J. Shinar, *J. Mater. Chem. C*, 2013, **1**, 5191; f) J. F. Mike, J. J. Intemann, M. Cai, T. Xiao, R. Shinar, J. Shinar and M. Jeffries-EL, *Polym. Chem.*, 2011, **2**, 2299.

8. M. M. Alam and S. A. Jenekhe, *Chem. Mater.*, 2002, **14**, 4775.
9. a) I. Osaka, K. Takimiya and R. D. McCullough, *Adv. Mater.*, 2010, **22**, 4993; b) E. Ahmed, A. L. Briseno, Y. Xia and S. A. Jenekhe, *J. Am. Chem. Soc.*, 2008, **130**, 1118; c) E. Ahmed, F. S. Kim, H. Xin and S. A. Jenekhe, *Macromolecules*, 2009, **42**, 8615; d) H. Pang, F. Vilela, P. J. Skabara, J. J. W. McDouall, D. J. Crouch, T. D. Anthopoulos, D. D. C. Bradley, D. M. de Leeuw, P. N. Horton and M. B. Hursthouse, *Adv. Mater.*, 2007, **19**, 4438.
10. a) E. Ahmed, S. Subramaniyan, F. S. Kim, H. Xin and S. A. Jenekhe, *Macromolecules*, 2011, **44**, 7207; b) A. V. Patil, H. Park, E. W. Lee and S.-H. Lee, *Synth. Met.*, 2010, **160**, 2128; c) A. Bhuwalka, J. F. Mike, M. He, J. J. Intemann, T. Nelson, M. D. Ewan, R. A. Roggers, Z. Lin and M. Jeffries-El, *Macromolecules*, 2011, **44**, 9611.
11. M. Inbasekaran and R. Strom, *OPPI Briefs*, 1994, **23**, 447.
12. a) J. G. Laquindanum, H. E. Katz, A. J. Lovinger and A. Dodabalapur, *Adv. Mater.*, 1997, **9**, 36; b) J. Hou, M.-H. Park, S. Zhang, Y. Yao, L.-M. Chen, J.-H. Li and Y. Yang, *Macromolecules*, 2008, **41**, 6012; c) P. Sista, M. C. Biewer and M. C. Stefan, *Macromol. Rapid Commun.*, 2012, **33**, 9; d) Y. Liang, Z. Xu, J. Xia, S.-T. Tsai, Y. Wu, G. Li, C. Ray and L. Yu, *Adv. Mater.*, 2010, **22**, E135; e) A. Najari, S. Beaupré, P. Berrouard, Y. Zou, J.-R. Pouliot, C. Lepage-Pérusse and M. Leclerc, *Adv. Funct. Mater.*, 2011, **21**, 718.
13. a) K. Li, Z. Li, K. Feng, X. Xu, L. Wang and Q. Peng, *J. Am. Chem. Soc.*, 2013, **135**, 13549; b) L. Dou, J. You, J. Yang, C.-C. Chen, Y. He, S. Murase, T. Moriarty, K. Emery, G. Li and Y. Yang, *Nat Photon*, 2012, **6**, 180; c) Y. Liang, D. Feng, Y. Wu, S.-T. Tsai, G. Li, C. Ray and L. Yu, *J. Am. Chem. Soc.*, 2009, **131**, 7792; d) H.-C. Chen, Y.-H. Chen, C.-C. Liu, Y.-C. Chien, S.-W. Chou and P.-T. Chou, *Chem. Mater.*, 2012, **24**, 4766; e) Z. He, C. Zhong, S. Su, M. Xu, H. Wu and Y. Cao, *Nat Photon*, 2012, **6**, 591; f) S. Zhang, L. Ye, W. Zhao, D. Liu, H. Yao and J. Hou, *Macromolecules*, 2014, **47**, 4653.
14. a) L. Huo, J. Hou, S. Zhang, H.-Y. Chen and Y. Yang, *Angew. Chem., Int. Ed.*, 2010, **49**, 1500; b) L. Ye, S. Zhang, L. Huo, M. Zhang and J. Hou, *Acc. Chem. Res.*, 2014, **47**, 1595.
15. J. Yuan, Z. Zhai, H. Dong, J. Li, Z. Jiang, Y. Li and W. Ma, *Adv. Funct. Mater.*, 2013, **23**, 885.
16. R. S. Sanchez and F. A. Zhuravlev, *J. Am. Chem. Soc.*, 2007, **129**, 5824.
17. H. Kokubo, T. Sato and T. Yamamoto, *Macromolecules*, 2006, **39**, 3959.
18. C. M. Cardona, W. Li, A. E. Kaifer, D. Stockdale and G. C. Bazan, *Adv. Mater.*, 2011, **23**, 2367.

19. B. C. Thompson, Y.-G. Kim and J. R. Reynolds, *Macromolecules*, 2005, **38**, 5359.
20. W. R. Salaneck, *Journal of Electron Spectroscopy and related Phenomena*, 2009, **174**, 3.
21. a) R. J. Kline, M. D. McGehee, E. N. Kadnikova, J. Liu, J. M. J. Frechet and M. F. Toney, *Macromolecules*, 2005, **38**, 3312; b) R. Zhang, B. Li, M. C. Iovu, M. Jeffries-El, G. Sauve, J. Cooper, S. Jia, S. Tristram-Nagle, D. M. Smilgies, D. N. Lambeth, R. D. McCullough and T. Kowalewski, *J. Am. Chem. Soc.*, 2006, **128**, 3480.
22. J. K. Lee, W. L. Ma, C. J. Brabec, J. Yuen, J. S. Moon, J. Y. Kim, K. Lee, G. C. Bazan and A. J. Heeger, *J. Am. Chem. Soc.*, 2008, **130**, 3619.
23. V. D. Mihailetchi, J. Wildeman and P. W. M. Blom, *Phys. Rev. Lett.*, 2005, **94**, 126602.
24. V. Shrotriya, Y. Yao, G. Li and Y. Yang, *Appl. Phys. Lett.*, 2006, **89**, 063505.

CHAPTER 5

SYNTHESIS, CHARACTERIZATION AND PHOTOVOLTAIC PROPERTIES OF DITHIENYLBENZOBISAZOLE-DITHIENYLSILOLE COPOLYMERS

Manuscript under review for publication in Journal of Polymer Science Part A: Polymer Chemistry, Royal Society of Chemistry

Achala Bhuwalka,[1] Monique D. Ewan,[1] Jared F. Mike, [1] Moneim Elshobaki,[2,3] Brandon Kobilka,[1] Sumit Chaudhary,[2] Malika Jeffries-EL[1]

[1]Department of Chemistry, Iowa State University, Ames IA 50011.

[1]Department of Materials Science and Engineering Department, Iowa State University

[2]Materials Science & Engineering Department, Iowa State University, Ames, IA, USA.

[3]Physics Department, Mansoura University, Mansoura, 35516, Egypt.

5.1 Abstract

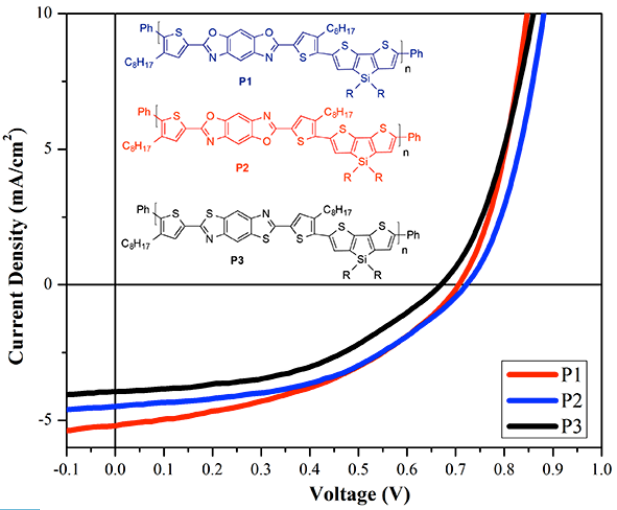

Three conjugated polymers comprised of dioctyl-dithieno-[2,3-*b*:2',3'-*d*]silole and a donor-acceptor-donor triad of either *cis*-benzbisoxazole, *trans*-benzobisoxazole or *trans*-benzobisthiazole were synthesized via the Stille cross-coupling reaction. The impact of varying the heteroatoms and/or the location within the benzobisazole moiety on the optical and electronic properties of the resulting polymers was evaluated via cyclic voltammetry and UV-Visible spectroscopy. All of the polymers have similar optical band-gaps of ~1.9 eV and highest occupied molecular orbital levels of -5.2 eV. Interestingly, when the polymers were used as donor materials in bulk-heterojunction photovoltaic cells with $PC_{71}BM$ as the electron-acceptor, the benzobisoxazole-based polymers gave slightly better results than the benzobisthiazole-containing polymers with power conversion efficiencies up to 1.55 %. These results indicate that benzobisoxazoles are promising materials for use in OPVs.

5.2 Introduction

Nowadays conjugated polymers (CP)s have become ubiquitous in applications such as field-effect transistors,[1] light emitting diodes,[2] photovoltaic cells,[3] and sensors.[4] CPs offer several advantages over their inorganic counterparts including solution processability to reduce fabrication costs, and the ability to tune their properties via organic synthesis, which enables optimization for use in specific applications. Currently, one of the most effective strategies for tuning the optical and electronic properties of CPs is through the incorporation of alternating electron donating and electron accepting comonomers within the polymer backbone.[5] This approach has afforded many materials with narrow band-gaps suitable for effective harvesting of solar energy. However, in

most organic photovoltaic cells (OPV)s a bulk heterojunction is formed by using the CP as a donor material and blending it with a fullerene acceptor, such as $PC_{61}BM$ or $PC_{71}BM$. Thus, the energy levels of both materials must be well aligned for efficient electron transfer between the two materials.[6] Additionally, the morphology of the polymer/PCBM blend should favor charge carrier formation and facilitate the disassociation of hole-electron pairs by providing a path for migration toward the electrodes. Although CP based OPVs are rapidly approaching the 10 % power conversion efficiency (PCE) recommended for them to be competitive commercially, the development of new materials remains an important area of research.[7] In particular the development of efficient donor materials that address practical aspects of commercialization such as facile synthesis and purification of monomers, and enhanced thermal and environmental stability of the resulting material are still needed.[8]

Polybenzobisazoles are a class of polymers that are known for their exceptional thermal stability and high tensile strength of fibers spun from them.[9] For example, poly(*p*-phenylene-2,6-benzobisoxazole) is a liquid crystalline polymer based on benzo[1,2-*d*; 4,5-*d*']benzobisoxazole that is spun into fibers commercially sold under the name Zylon®.[9b] Due to the previous use of polybenzobisazoles in high performance applications, all of the necessary monomers can be synthesized on industrial scale, and purified without the use of column chromatography. This is advantageous for large-scale synthesis. Furthermore, the benzobisazole ring system is electron-deficient and planar, which leads strong intermolecular interactions and good charge transport properties within polymer films.[10] Despite these advantages, the use of benzobisazoles in optoelectronic materials has been nominal due to the harsh reaction conditions used for

their synthesis and their poor solubility. Traditionally, benzobisazoles are synthesized by an acid catalyzed condensation reaction at high temperatures.[9c,d] Such reaction conditions not only limit the types of substituents that can be on the monomer but residual acid also results in undesirable doping of the polymer and can also catalyze the degradation of the material in sunlight.[11] To address these limitations, our group has developed a mild high yielding synthesis of functional benzobisazoles via an orthoester condensation reaction.[12]

To date, there are only a few reports on the synthesis and photovoltaic properties of donor-acceptor polymers comprising benzobisazoles.[13] Jenekhe and coworkers reported a PCE of 2.1 % for a quarterthiophene benzobisthiazole polymer.[13a] Our group reported a PCE of only 0.6 % for a related benzobisthiazole polymer, but obtained a PCE of 1.1 % for the isoelectronic benzobisoxazole polymer.[13c] Although all of these polymers exhibited good charge carrier mobilities, they had relatively wide band gaps (1.9 – 2.1 eV), limiting the harvesting of solar energy. To improve on the properties of this system, we decided to evaluate the electron rich dithienosilole (DTS) moiety. This silicon bridged fused bithiophene system features two alkyl chains that impart excellent solubility to the resulting polymer, while the long C-Si bonds move the alkyl chains away from the ring system, thereby allowing for improved π-stacking. Additionally, the σ*-orbital in DTS is able to interact with the π*-orbital of the bithiophene, giving a conjugated, planar system further increasing π-stacking interactions and the long-range order.[14] Furthermore, DTS has a lower-lying (LUMO) and highest occupied molecular orbital (HOMO) than other bithiophene derivatives, which can reduce the polymer band gap and increase the open circuit voltage (V_{oc}) of the devices fabricated from them affording PCEs as high as 7.3 %.[15] Jenekhe and coworkers reported a PCE of 2.1 % for a

BHJ device using a dithienosilole-dithienylbenzobisthiazole polymer as the donor and $PC_{71}BM$ as the acceptor.[13b] Since, our previous results indicate that polymers incorporating the benzobisoxazole moiety exhibited higher V_{oc} and PCE in comparison to the analogous benzobisthiazole polymers, we set out to evaluate the optical and electronic properties of a series of polymers containing DTS and the isomeric benzo[1,2-*d*; 5,4-*d*′]bisoxazole (*cis*-BBO) and benzo[1,2-*d*; 4,5-*d*′]bisoxazole (*trans*-BBO) and the isoelectronic benzo[1,2-*d*; 4,5-*d*′]bisthiazole (*trans*-BBZT). Unfortunately, we cannot include *cis*-BBZT in our studies as to date, all efforts to synthesize the starting material have been unsuccessful.

5.3 Experimental

5.3.1 Materials and General Experimental Details. Tetrahydrofuran and toluene were dried using an Innovative Technologies solvent purification system. Air and moisture sensitive reactions were performed using standard Schlenk techniques. Solvents used for palladium-catalyzed reactions were deoxygenated prior to use by bubbling a stream of argon through the solvent with vigorous stirring for 30-60 minutes. All chemical reagents were purchased from commercial sources and used without further purification unless otherwise noted. SiliaMetS® Cysteine was purchased from SiliCycle, Inc. 4,4-Dioctyl-2,6-bis(trimethylstannyl)-4*H*-silolo[3,2-*b*:4,5-*b*′]dithiophene **(1)**,[16] 2,6-bis(4-octylthiophen-2-yl)benzo[1,2-*d*; 5,4-*d*′]bisoxazole **(2)**, 2,6-Bis(4-octylthiophen-2-yl)benzo[1,2-*d*; 4,5-*d*′]bisoxazole **(3)**, and 2,6-Bis(4-octylthiophen-2-yl)benzo[1,2-*d*; 4,5-*d*′]bisthiazole **(4)** were synthesized according to literature procedures.[12b]

5.3.2 **General Polymerization Procedure.** A mixture of **1** and the respective benzobisazole, 2 mol% tris(dibenzylideneacetone)dipalladium(0), 8 mol % tris-o-tolyphosphine in 7 mL of degassed toluene was added to a round bottom flask equipped with a reflux condenser and an argon inlet. The mixture was allowed to reflux for 12 - 36 h before it was end capped by addition of trimethylphenyl tin followed by iodobenzene. The reaction was then quenched by pouring into 100 mL of cold methanol. The precipitated polymer was filtered into a cellulose extraction thimble and purified by Soxhlet extraction with methanol to remove residual palladium followed by acetone and hexanes to remove the lower molecular weight material. The polymers were then obtained using $CHCl_3$ as the extraction solvent. Functionalized silica (SiliaMetS® Cysteine) was added to the chloroform fraction and the solution was allowed to stir overnight at 50 ˚C. The chloroform fraction was then filtered through a bed of Celite and the solvent was removed under vacuum. The polymer was then reprecipitated in methanol, filtered and dried in the vacuum oven overnight.

Poly(2-(5-(4,4-dioctyl-4*H*-silolo[3,2-*b*:4,5-*b′*]dithiophen-2-yl)-4-octylthiophen-2-yl)-6-(4-octylthiophen-2-yl)benzo[1,2-*d*:5,4-*d′*]bis(oxazole))(P1) Polymer was obtained as dark red solid (298 mg, 89% yield) starting with 2,6-bis(5-bromo-4-octylthiophen-2-yl)benzo[1,2-*d*:5,4-*d′*]bis(oxazole) (237 mg, 0.33 mmol) and 4,4-dioctyl-2,6-bis(trimethylstannyl)-4*H*-silolo[3,2-*b*:4,5-*b′*]dithiophene (250 mg, 0.33 mmol); GPC: Mn =11.6 kDa, Mw = 26.2kDa, PDI = 2.3

Poly(2-(5-(4,4-dioctyl-4*H*-silolo[3,2-*b*:4,5-*b′*]dithiophen-2-yl)-4-octylthiophen-2-yl)-6-(4-octylthiophen-2-yl)benzo[1,2-*d*:4,5-*d′*]bis(oxazole))(P2). Polymer obtained as a deep red solid (275 mg, 83% yield) starting with 2,6-bis(5-bromo-4-octylthiophen-2-yl)benzo[1,2-*d*:4,5-*d′*]bis(oxazole) (237 mg, 0.33 mmol) and 4,4-dioctyl-2,6-bis(trimethylstannyl)-4*H*-silolo[3,2-*b*:4,5-*b′*]dithiophene (250 mg, 0.33 mmol); GPC: Mn = 12.4 kDa, Mw = 31.7 kDa, PDI = 2.6.

Poly(2-(5-(4,4-dioctyl-4*H*-silolo[3,2-*b*:4,5-*b′*]dithiophen-2-yl)-4-octylthiophen-2-yl)-6-(4-octylthiophen-2-yl)benzo[1,2-*d*:4,5-*d′*]bis(thiazole))(P3). Polymer obtained as a deep red-purple solid (273 mg, 79% yield) starting with 2,6-bis(5-bromo-4-octylthiophen-2-yl)benzo[1,2-*d*:4,5-*d′*]bis(thiazole) (248 mg, 0.33 mmol) and 4,4-dioctyl-2,6-bis(trimethylstannyl)-4*H*-silolo[3,2-*b*:4,5-*b′*]dithiophene (250 mg, 0.33 mmol); GPC: Mn = 9.5 kDa, Mw = 20.8 kDa, PDI = 2.2.

5.3.3 Device Fabrication and Characterization.

ITO-coated glass substrates were cleaned sequentially by ultrasonication in acetone, methanol and isopropanol, followed by O_2 plasma exposure for 5 minutes. PEDOT:PSS aqueous solution was passed through a 0.45 μm PVDF filter, and then spin-coated on the ITO substrate at 4000 rpm for 60 seconds and dried in a vacuum oven at 120 °C for 1 hour. The thickness of PEDOT:PSS layer was approximately 40 nm. All devices were fabricated in a glove box filled with argon. 50 mg/mL $PC_{71}BM$ in *o*-DCB was prepared by ultrasonic mixing for 1 h and filtered with a 0.45 μm PTFE filter prior to use. The polymers **P1**, **P2**, and **P3** were dissolved in *o*-DCB at 90 °C to yield 10 mg/mL polymer/*o*-DCB solution. The hot solution was quickly filtered with a 0.45 μm PTFE

filter before cooling down to room temperature. Photovoltaic devices with a configuration of ITO/PEDOT:PSS/ Polymer:$PC_{71}BM$/Ca/Al were fabricated at a 1:2 weight ratio of polymer to $PC_{71}BM$ and a total solution concentration of 21 mg/mL. These devices were evaluated with and without the solvent additive, 1,8-diiodooctane (DIO). A cathode was prepared by sequentially depositing a Ca film (50 nm) and a Al film (100 nm) through a shadow mask. The photovoltaic devices had an area of 0.10±0.01 cm^2 and were tested under simulated AM 1.5 G irradiation (100 $mWcm^{-2}$, calibrated with Daystar Meter) using a SoLux Solar Simulator, and the current-voltage (*I-V*) curves were measured using a Keithley 2400 multisource meter.

5.4 Results and Discussion

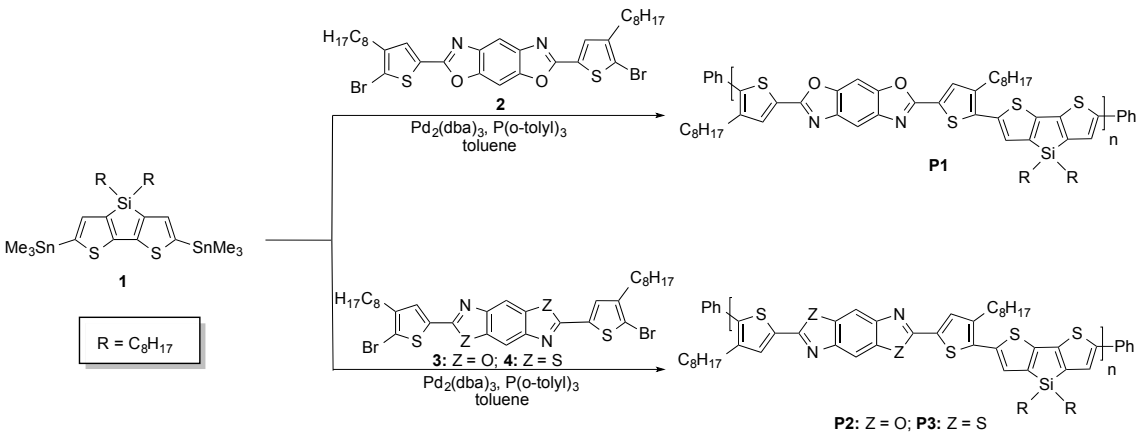

Scheme 5.1. Synthesis of benzobisazole-thiophene-dithienosilole terpolymers

5.4.1 Synthesis. We utilized a monomer composed of a benzobisazole moiety placed between two brominated thiophene rings with the alkyl chains facing away from the benzene core for the polymer synthesis. The thiophene rings serve as π spacers whereas the octyl chains aid solubility. The halogens on the thiophene rings provide a handle for

transition metal catalyzed cross-coupling reactions, while avoiding potential ring opening reactions that can occur during palladium insertion at the 2-position of benzazoles.[17] The synthetic routes toward the polymers are outlined in Scheme 5.1. The Stille cross-coupling polymerization of 4,4-dioctyl-2,6-bis(trimethylstannyl)-4*H*-silolo[3,2-*b*:4,5-*b'*]bithiophene **1**[16] with either 2,6-bis(4-octylthiophen-2-yl)-benzo[1,2-*d*; 5,4-*d'*]bisoxazole **2**, 2,6-bis(4-octylthiophen-2-yl)-benzo[1,2-*d*; 4,5-*d'*]bisoxazole **3**, or 2,6-bis(4-octylthiophen-2-yl)-benzo[1,2-*d*; 4,5-*d'*]bisthiazole **4**[12b] afforded polymers **P1**, **P2** and **P3**, respectively. All the polymers exhibited reasonable solubility (~10 mg/mL) in standard organic solvents, such as THF, *m*-cresol and chloroform at room temperature, enabling characterization by gel permeation chromatography (GPC). The weight-averaged (M_w), number-averaged (M_n) molecular weights and polydispersity index (PDI) as estimated using GPC are summarized in Table 5.1. The number averaged degree of polymerization (DP_n) for the polymers was determined to range from 9-12. Unfortunately, the limited solubility of the polymers and disproportionate ratio of alkyl to aryl protons prevented analysis by ^{1}H NMR spectroscopy. Thermogravimetric analysis (TGA) revealed that all polymers were thermally stable with 5 % weight loss onsets occurring above 300 °C under air (Figure 5.7.2). None of the polymers exhibited any glass transitions as shown by differential scanning calorimetry (DSC) (Figure 5.7.7). The results are summarized in Table 5.1.

Table 5.1. Physical characterization of **P1 – P3**.

Polymer	Yield[a] (%)	M_n[b] (kDa)	PDI[b]	DP_n	T_d (°C)[c]
P1	89	11.6	2.3	12	308
P2	83	12.4	2.6	12	306
P3	55	9.5	2.2	9	315

[a] Isolated yield [b]Determined by GPC in $CHCl_3$ using polystyrene standards.. [c] 5% weight loss temperature by TGA in air.

5.4.2 Optical and Electrochemical Properties. The optical properties of the polymers were investigated using UV-Visible absorption spectroscopy in solution and solid state. The normalized absorbance spectra of the polymer solutions in dilute chloroform solution and in the solid state are shown in Figures 5.1 and 5.2, respectively. The data is summarized in Table 5.2. In solution, the λ_{max} of all the polymers are similar. However, **P1** and **P2** have small shoulders arising from aggregation in polymer backbone,[13a] whereas **P3** exhibits a single, featureless absorbance band. As thin films, the λ_{max} values for **P1**, **P2** and **P3** are 524 nm, 536 nm and 549 nm respectively. These absorbance spectra are slightly broader than the corresponding solution spectra, resulting in bathochromic shifts of 2 nm – 30 nm in the absorption maximum. This suggests a slight increase in the backbone planarization and π- stacking in the solid state.[18] The film λ_{max} of **P3** is the same as that reported by Jenekhe for a similar polymer which had branched alkyl chains on the dithienosilole unit and the alkyl chain on the thiophenes flanking the benzobisthiazole moiety was facing inwards.[13b] The solution and thin film λ_{max} values of **P1 – P3** are bathochromically shifted by 70 – 95 nm relative to our previous reported polymers which employed bithiophene as the donor.[13c] This can be attributed to the fused dithienosilole ring system which can lead to a more rigid, coplanar backbone thereby

increasing the effective π-conjugation length, decreasing the band gap and red-shifting the absorbance spectra.

The optical band gaps for **P1 – P3** were estimated from the onset wavelength of the polymers films and range from 1.9 – 2.0 eV. As expected, these band-gaps are slightly narrower than those reported previously for the benzobisazole-quarterthiophene system which ranged from 2.1 eV – 2.2 eV.[13c] This further demonstrates that using a stronger fused electron-donating comonomer was beneficial in narrowing the band gap.

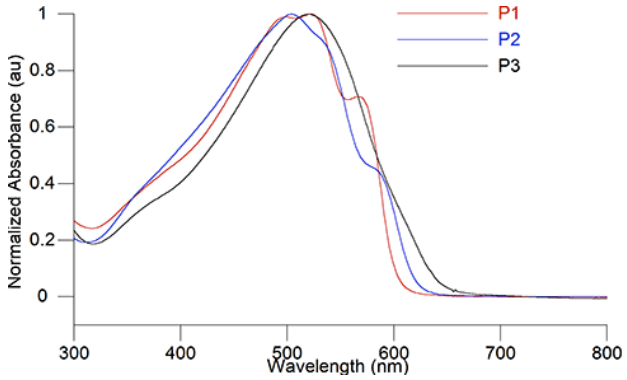

Figure 5.1. UV-Vis absorption spectra of **P1 – P3** in dilute chloroform solutions.

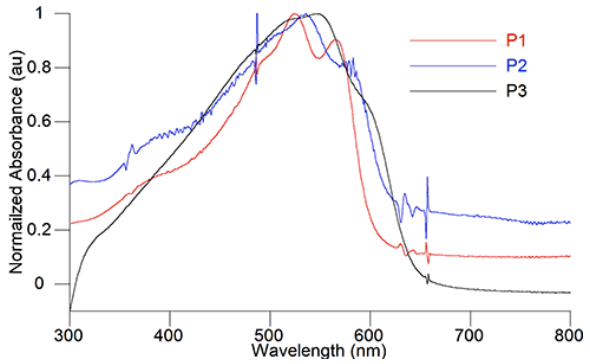

Figure 5.2. UV-Vis absorption spectra of **P1 – P3** as thin films. Thin films were spun from polymer solutions in 1:1 (v/v) $CHCl_3$:*o*DCB (2 mg/mL).

Using cyclic voltammetry, the electrochemical properties of the polymers were evaluated and the results are summarized in Table 5.2. **P1** and **P2** showed reproducible oxidation and reduction processes, whereas **P3** only showed a clear wave during the oxidation cycle (Figure 5.7.5). The HOMO levels were all ranged from -5.2 to -5.3 eV

Table 5.2. Electronic and optical properties of benzobisazole-thiophene-dithienosilole terpolymers.

Polymer	Solution	Film							
	λ_{max}^{soln} (nm)	λ_{max}^{film} (nm)	λ_{onset} (nm)	E_g^{opt} (eV)[a]	E_g^{EC} (eV)[b]	E_{ons}^{ox}	E_{ons}^{red}	LUMO (eV)[c]	HOMO (eV)[d]
P1	522	524	610	2.0	2.2	0.4	-1.8	-3.0	-5.2
P2	505	536	640	1.9	2.0	0.4	-1.6	-3.2	-5.2
P3	520	549	650	1.9	--	0.5	---	---	-5.2

[a] Estimated from the optical absorption edge. [b] Estimated from HOMO-LUMO. [c] LUMO = -4.8- (E^{red}_{onset}) (eV). [d] HOMO = -4.8- (E^{ox}_{onset}) (eV). Electrochemical properties were measured using a three-electrode cell (electrolyte: 0.1 mol/L $TBAPF_6$ in acetonitrile) with an Ag/Ag^+ reference electrode, a platinum auxiliary electrode, and a platinum button electrode as the working electrode. Reported values are referenced to Fc/Fc^+. Polymer films were drop cast on to the working electrode from an *o*-DCB solution of **P1** – **P3**. No reduction peak was seen for **P3.**

and were estimated using the absolute energy level of ferrocene/ferrocenium (Fc/Fc^+) as 4.8 eV under vacuum and the onsets of oxidation.[19] These are deep enough to provide good air stability.[6b] Similarly, the LUMO levels of -3.0 eV and -3.2 eV were estimated using the onsets of reduction for the BBO polymers **P1** and **P2**, respectively. The *trans*-BBZT polymer **P3** did not exhibit a measurable reduction wave. These results indicate that the HOMO level of these polymers are unaffected by changing the configuration of the oxygen atoms or replacing them with sulphur. In contrast, switching the oxygen from the *cis*- to the *trans*- configuration reduced the LUMO level by ~0.2 eV. The LUMO levels for all of the polymers are also lower than those of their quarterthiophene

counterparts.[13c] Thus replacing the bithiophene with DTS was beneficial. The difference between the electrochemical band gaps of **P1** and **P2** and their optical band gaps is typical for these measurements due to the energy barrier associated with the interface of the polymer film and the electrode surface.[19-20]

5.4.3 Photovoltaic Properties. The OPV performances of the polymers was evaluated using photovoltaic devices with a configuration of ITO/PEDOT:PSS/**Polymer**:$PC_{71}BM$/Ca/Al and a 1:2 weight ratio of polymer to $PC_{71}BM$ with a total solution concentration of 21 mg/mL. These devices were evaluated with and without the solvent additive, DIO. The details of the OPV studies including short circuit current density (J_{SC}), open circuit voltage (V_{OC}), fill factor (*FF*) and power conversion efficiency (PCE) are listed in Table 5.3. The current density-voltage (*J-V*) curves of **P1**/$PC_{71}BM$, **P2**/$PC_{71}BM$, and **P3**/$PC_{71}BM$ photovoltaic devices under AM 1.5 G illumination (100 mW/cm^2) are shown in Figure 5.3. We were able to obtain maximum PCE values of 2.47, 3.51 and 2.15 for **P1**, **P2**, and **P3**, respectively. However, we were unable to obtain these values reproducible in subsequent runs. This indicative of the difficulty in obtaining ideal nanoscale morphology within the polymer:fullerene blends. On average the devices based on the benzobisoxazole polymers **P1** and **P2** had similar performance with PCEs of ~1.5 % without the use of solvent additives. Whereas, the performance of the devices made from the benzobisthiazole polymer **P3** were slightly lower with a PCEs of 1.22 %. We also evaluated the use of DIO as a solvent additive,[21] but only observed a nominal improvement in the PCE for **P3**, and a minor decrease in the performance of **P1** and **P2**. In general, the performances of these devices were modest as

a result of both J_{SC} and V_{OC} and moderate *FF*. The external quantum efficiency (EQE) curves for the best devices are shown in figure 5.4. All of the devices had broad photoresponses between 400 to 690 nm, with a maximum EQE of 79% at 400nm, 83% at 400nm, and 73% at 400nm, for **P1**, **P2**, and **P3**, respectively. These overall performance of these polymers represent a modest improvement over our previously results on poly(quarterthiophene benzobisazoles), in which the best performance was a PCE of 1.14 % for the *trans*-BBO polymer.[13c] The OPV performance of **P3** is comparable to that reported by Jenekhe *et al* for a related benzobisthiazole polymer, poly[(4,4' -bis(2- **P3** ethylhexyl)dithieno[3,2-*b*:2' ,3' -*d*]silole)-2,6-diyl-alt- (2,5-bis(3-dodecylthiophen-2-yl)benzo[1,2-*d*;4,5-*d'*]bisthiazole)] (PBTEHS), which had a PCE of 1.24 % that increased to 2.02 % with the use of additives.[13b] Although PBTEHS and PBTHDDT have different substituents on both the flanking thiophenes and benzodithiophene, the similarities in their initial performance but different behavior upon the addition of the co-solvents suggest that the polymers' structure has a negative impact on the morphology of the blends thin film.

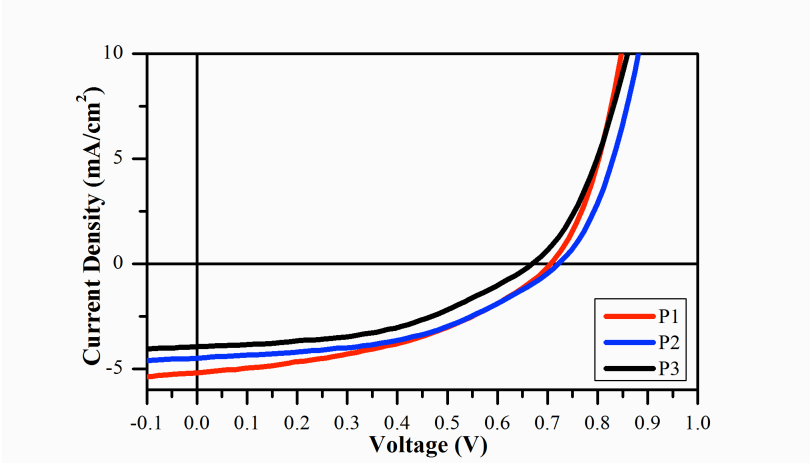

Figure 5.3. Current density-voltage *(J-V)* curves of polymer:$PC_{71}BM$, photovoltaic devices under AM 1.5 G illumination (100 mW cm^{-2}).

The hole mobilities of the polymers were examined using the space-charge-limited current (SCLC) method with a hole only device structure of ITO/PEDOT:PSS/Polymer/Al and are summarized in Table 5.4.[22] The mobilites were calculated according to equation 1:

$$J_{SCLC} = \frac{9\varepsilon_0\varepsilon_r\mu_h V^2}{8L^3} \qquad (1)$$

in which $\varepsilon_0\varepsilon_r$ is the permittivity of the polymer, μ_h is the carrier mobility, and L is the device thickness.[23] The mobilities of the polymers were on the same order of magnitude as each other, with **P3** having the lowest mobility. This is consistent with the OPV data, with **P3** giving the worst performance, by only by a small margin.

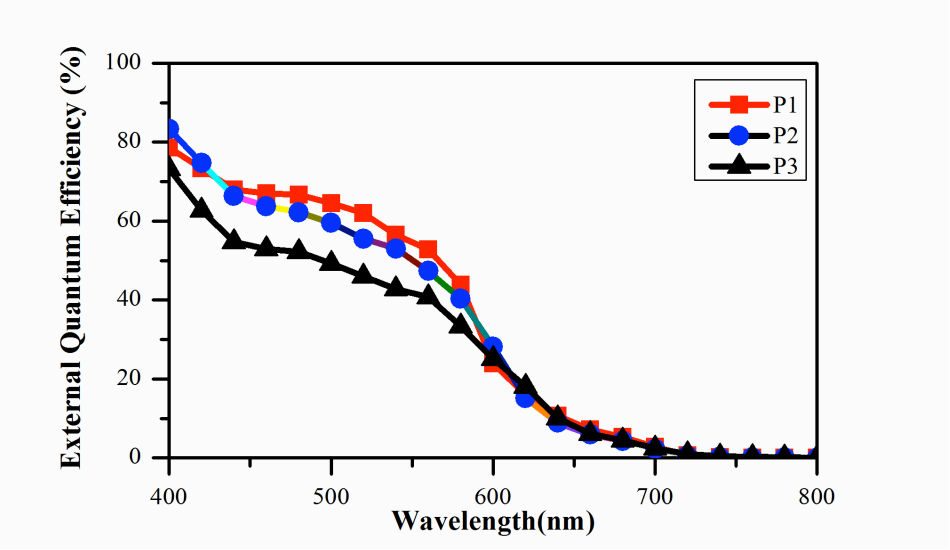

Figure 5.4. The external quantum efficiency of polymer:$PC_{71}BM$, photovoltaic devices under AM 1.5 G illumination (100 mW cm^{-2}).

Using atomic force microscopy (AFM) we investigated the surface morphology of the active layer blends (Figure 5.5). The AFM height images revealed that all of the

blends have small domain sizes, with root-mean square (RMS) surface roughness values that were no larger than 1.30 nm. In the AFM phase images of the **P3**:$PC_{71}BM$ film it is evident that vertical phase separation is occurring.

Table 5.3. Photovoltaic device performance of **P1 - P3** with $PC_{71}BM$.

Polymer	Additive (% DIO)	J_{SC} (mA/cm^2)	V_{OC} (V)	*FF*	PCE (%)	Max PCE (%)	R_{SH} (Ω cm^2)
P1	None	8.07±8.83	0.69±0.04	0.40±0.1	2.01±1.50	3.51	457±383
P1	0.5	3.14±0.07	0.69±0.02	0.49±0.2	1.08±0.03	1.11	1,656±145
P1	2.5	4.00±0.15	0.65±0.03	0.46±0.1	1.20±0.14	1.34	982±95
P2	None	5.13±3.04	0.71±0.01	0.46±0.1	1.67±0.90	2.57	818±370
P2	0.5	4.47±0.08	0.71±0.01	0.46±0.1	1.43±0.02	1.45	792±20
P2	2.5	4.80±0.04	0.69±0.01	0.42±0.1	1.39±0.02	1.42	708±46
P3	None	5.27±4.55	0.66±0.01	0.44±0.2	1.44±0.71	2.15	944±729
P3	0.5	3.78±0.13	0.68±0.02	0.46±0.1	1.17±0.04	1.21	970±40
P3	2.5	4.23±0.16	0.67±0.01	0.43±0.1	1.22±0.03	1.25	835±150

Photovoltaic devices with a configuration of ITO/PEDOT:PSS/Polymer:$PC_{71}BM$/Ca/Al were fabricated at a 1:2 weight ratio of polymer to $PC_{71}BM$ and a total solution concentration of 21mg /mL. DIO was used as the additive (% v/v).

This bilayer morphology diminishes exciton formation and device performance. However, both the **P1**:$PC_{71}BM$ and **P2**:$PC_{71}BM$ blend films show a more uniform distribution of the polymer and the fullerene. This bicontinuous interpenetrating network enhances exciton dissociation and device performance. From our previous studies on poly(quarter thiophene benzobisazoles) we know that the structural differences in the materials do not significantly impact the packing of the polymer chains.[13c] Given the bulky nature of the side chains on these polymers, it is unlikely that benzobisazole structure is impacting the chain packing within these systems. Historically, the BBZT containing polymers have poorer solubility than the BBO based ones.[12b,13c] It is most likely that the film formation is affected by the reduced solubility and the potential increased tendency for aggregation of **P3** relative to **P1** and **P2**.

Table 5.4. Mobility of **P1 - P3** hole only devices and AFM data of polymer: $PC_{71}BM$ blends.

Polymer	μ_h ($cm^2 V^{-1} s^{-1}$)	RMS Roughness (nm)	RMS Phase (Deg)
P1	8.04E-06	1.08	2.12
P2	5.06E-06	0.97	2.39
P3	2.34E-06	1.30	0.43

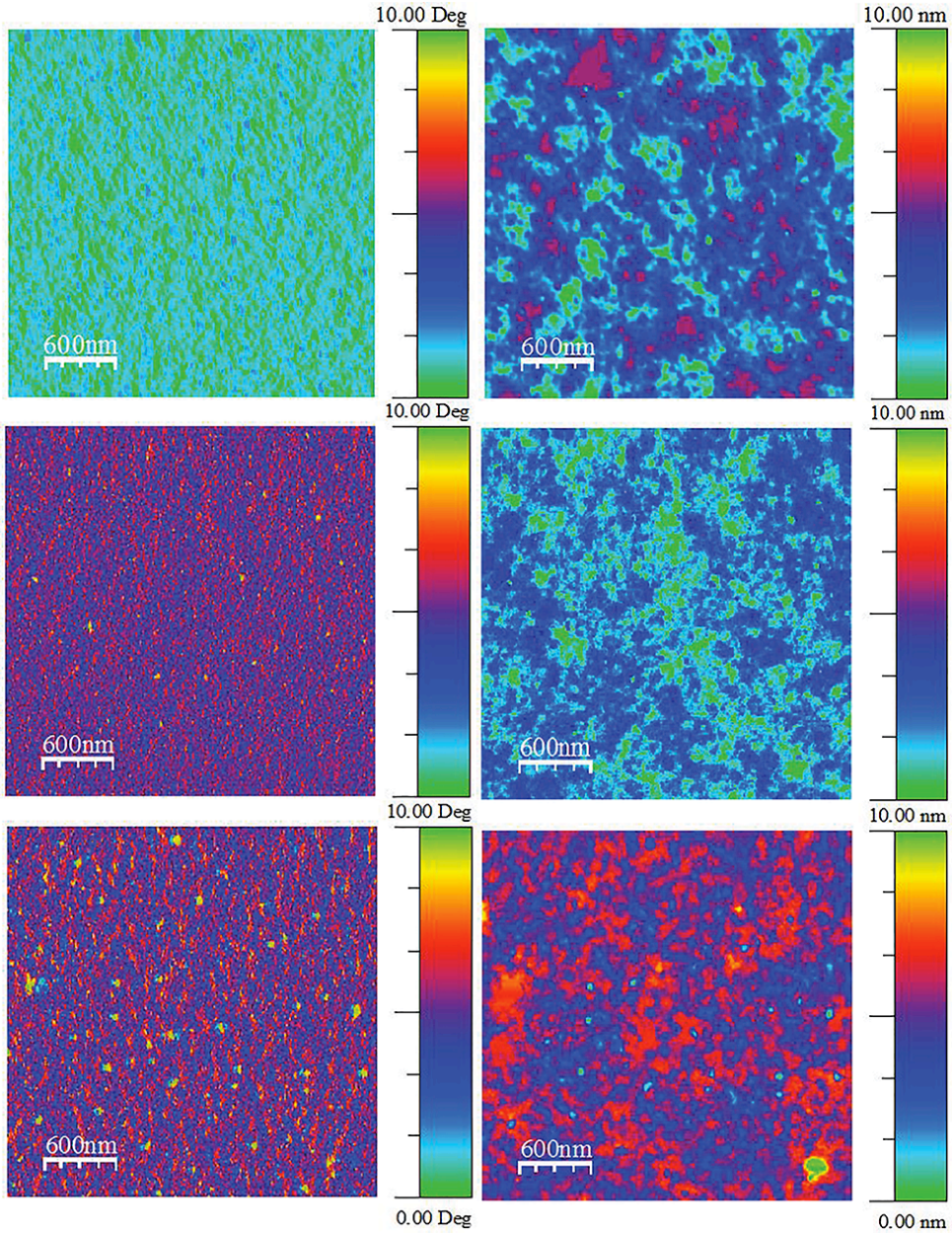

FIGURE 5.5. AFM phase (left) and height (right) images at 3 mm x 3 mm of devices with polymer:$PC_{71}BM$ blends at a 1:2 weight ratio. From top to bottom: **P1**:$PC_{71}BM$, **P2**:$PC_{71}BM$ and **P3:**$PC_{71}BM$

5.5 Conclusions

In summary, a series of donor-acceptor copolymers based on dithienylbenzobisazole and dithieno[3,2-*b*:2' ,3' -*d*]silole were synthesized in an effort to improve the OPV performance

of benzobisazole polymers. Although the polymers differed in the location and/or nature of the heteroatoms within the benzobisazole moiety they had identical HOMO levels (- 5.2 eV) and fairly similar LUMO levels (-3.0 to 3.2 eV).The use of the DTS monomer had only a moderate effect on the band gap of these polymers. However, these materials did outperform our previously reported benzobisazoles. Furthermore our data indicates that among this series, benzobisoxazole based polymers are the most promising due to improved solubility and thin film formation. Research is ongoing in our lab to further improve upon the properties of this class of polymers.

5.6 Acknowledgements

We thank the National Science Foundation (DMR-0846607) for support of this work. The Iowa State University (ISU), the Institute for Physical Research and Technology provided MDE with a Catron Fellowship. Some of the OPV work was performed at the ISU Microelectronics Research Center. ME thanks the financial support from the Egyptian government (scholarship # GM915).

5.7 Supplemetary Information

Materials and General Experimental Details. Tetrahydrofuran was dried using an Innovative Technologies solvent purification system. 2,2'-bithiophene, and 3,3',5,5'-tetrabromo-2,2'-bithiophene (1), were prepared according to literature procedures. All other compounds were purchased from commercial sources and used without further purification. Chromatographic separation was performed using silica gel 60, using the eluents indicated.

Instrumentation

Nuclear magnetic resonance spectra were obtained on a 400 MHz/300MHz spectrometer (^{1}H at 300MHz or 400 MHz and ^{13}C at 100 MHz). ^{1}H NMR samples were referenced internally to residual protonated solvent ^{13}C NMR are referenced to the middle carbon peak of $CDCl_3$. In both instances chemical shifts are given in δ relative to solvent. Gel permeation chromatography (GPC) measurements were performed on a Viscotek GPC Max 280 separation module equipped with three 5μm I-gel columns connected in a series (guard, HMW, MMW and LMW) with a refractive index detector. Analyses were performed at 35 °C using THF as the eluent with the flow rate at 1.0 mL/min. Calibration was based on polystyrene standards. and UV-Visible spectroscopy were obtained using polymer solutions in THF, and thin films were spun from *o*-DCB. The films were made by spin-coating 25 x 25 x 1mm glass slides, using a solution of 2 mg of polymer per 1 mL *o*-DCB at a spin rate of 800 rpms on a Spin-Coater. Thermal gravimetric analysis measurements were made within the temperature interval of 30 ºC - 900 ºC, with a heating rate of 20 ºC/minute, under ambient atmosphere. Electrochemical properties were measured on an eDaq e-corder 410 potentiostat using a three-electrode cell (electrolyte: 0.1 mol/L $TBAPF_6$ in acetonitrile) with an Ag/Ag^{+} reference electrode, a platinum auxiliary electrode, and a platinum button electrode as the working electrode. Polymer films were made by drop coating an *o*-DCB solution of the polymers on to the working electrode. All films were annealed at 140 ºC for 2 hours prior to use. All differential pulse voltammetry experiments were carried out under argon atmosphere and were recorded at a scan rate of 50 mV/s. UPS was obtained using a Model AC-2 Photoelectron Spectrometer, manufactured by Riken Keiki. X-ray diffraction data was obtained on a Rigaku Ultima IV powder diffractometer using Cross Beam Optic in parallel

beam mode to eliminate the need for a knife edge collimator. An accelerating voltage and current of 40 kV and 44 mA, respectively was used. Samples were placed on an MPA-U4 multipurpose Eulerian cradle to facilitate fine alignment between the beam and the top of the film.

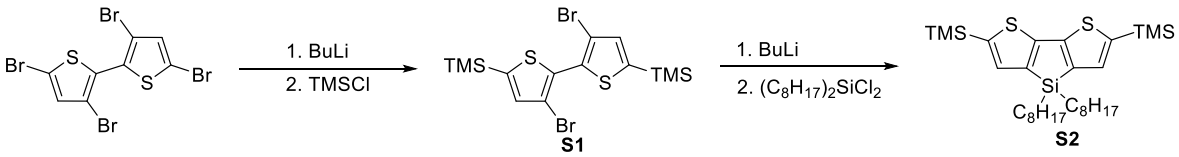

Scheme S1: Synthesis of 4,4-dioctyl-2,6-bis(trimethylsilyl)-4*H*-silolo[3,2-*b*:4,5-*b'*]dithiophene

(3,3'-dibromo-[2,2'-bithiophene]-5,5'-diyl)bis(trimethylsilane) (S1). 3,3',5,5'-tetrabromo-2,2'-bithiophene (20.0 g, 41.5 mmols, 1 eq) was dissolved in 200 mL anhydrous ethyl ether. The solution was cooled to -78 ˚C in an acetone/dry ice bath. *n*BuLi (1.7 M, 50.0 mL, 85.1 mmols, 2.1 eq) was added dropwise. The resulting dianion was stirred for 2 h at -78 ˚C after which Chlorotrimethylsilane (11.1 mL, 87.2 mmols, 2.10 eq) was added dropwise. The reaction mixture was allowed to warm to room temperature overnight. It was then poured into cold water and extracted three times with ether. The combined organic layers were then washed with brine. The organic and aqueous layers were separated; the organic layer was dried over an $MgSO_4$, filtered and then concentrated under reduced pressure. The crude product was purified by column chromatography using hexanes as the eluent to give 16.5 g (85 %) of **1** as a light yellow solid. ^{1}H NMR (400 MHz, $CDCl_3$) δ: 0.34 (s, 18H), 7.15 (s, 2H).

4,4-dioctyl-2,6-bis(trimethylsilyl)-4*H*-silolo[3,2-*b*:4,5-*b*′]dithiophene (S2):

(3,3'-dibromo-[2,2'-bithiophene]-5,5'-diyl)bis(trimethylsilane) (2.0 g, 4.3 mmol) was dissolved in 30 mL THF. The solution was cooled to -78°C in an acetone/dry ice bath. *n*BuLi (2.0 M, 5.4 mL, 10.7 mmol, 2.5 eq) was added dropwise. The resulting dianion was stirred for 1 h at -78 °C after which dichlorodioctylsilane (4.4 mL, 11.6 mmol, 2.7 eq). The reaction mixture was allowed to warm to room temperature overnight. It was then quenched with water and extracted three times with hexanes. The combined organic layers were dried over anhydrous magnesium sulfate and concentrated. The crude product was purified by column chromatography using hexanes as the eluent to give 1.8 g (75 %) of **S2** as a pale yellow oil ^{1}H NMR (400 MHz, $CDCl_3$, ppm) δ 7.12 (s, 2H), 1.43-1.39 (m, 4H), 1.24- 1.22 (m, 21H), 0.88-0.87 (m, 10H), 0.34 (s, 18 H)

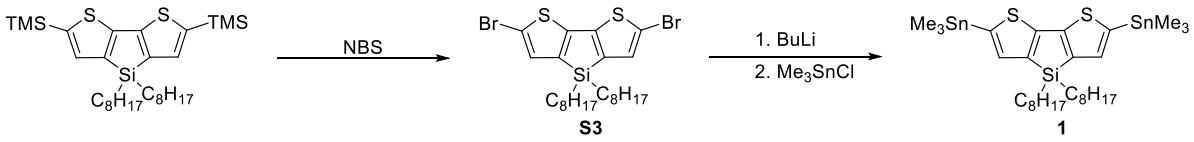

Scheme S2: Synthesis of 4,4-dioctyl-2,6-bis(trimethylstannyl)-4*H*-silolo[3,2-*b*:4,5-*b*′]dithiophene

2,6-dibromo-4,4-dioctyl-4*H*-silolo[3,2-*b*:4,5-*b*′]dithiophene (S3)

S2 (1.30 g, 2.31 mmol) was dissolved in 20 mL THF. NBS (1.03 g, 5.77 mmol) was then added in one portion and the reaction mixture was stirred overnight. It was then quenched with water and extracted three times with hexanes. The combined organic layers were then washed with brine. The organic and aqueous layers were separated; the organic layer was dried over $MgSO_4$, filtered and then concentrated under reduced pressure to give 1.2 g (91

%) of product as a yellow solid. The crude product was used without further purification. ^{1}H NMR (400 MHz, $CDCl_3$, ppm) δ 6.99 (s, 2H), 1.31 -1.21 (m, 24H), 0.89-0.85 (t, 10H).

4,4-dioctyl-2,6-bis(trimethylstannyl)-4*H*-silolo[3,2-b:4,5-b']dithiophene (1)

S3 (0.8 g, 1.39 mmol) was dissolved in 20 mL THF in a flame dried round bottom flask. The solution was cooled to -78°C in an acetone/dry ice bath. *n*BuLi (2.0 M, 1.53 mL, 3.05 mmol, 2.5 eq) was added dropwise. The resulting dianion was stirred for 1 h at -78°C after which trimethyltin chloride (1 M in hexanes, 3.5 mL, 3.5 mmol) was added. The reaction was allowed to warm up to room temperature overnight. The reaction was quenched by addition of water. The product was extracted with hexanes. The organic layer was washed with 1M KF followed by water and brine, and dried over $MgSO_4$. The solvent was removed under reduced pressure to give 0.67 g (65 %) of product as a sticky oil: ^{1}H NMR (400 MHz, $CDCl_3$, ppm) δ : 7.09 (s, 2H), 1.43-1.37 (m, 3H), 1.30-1.22 (m, 20H), 0.92-0.84 (m, 11H), 0.38 (s, 18 H).

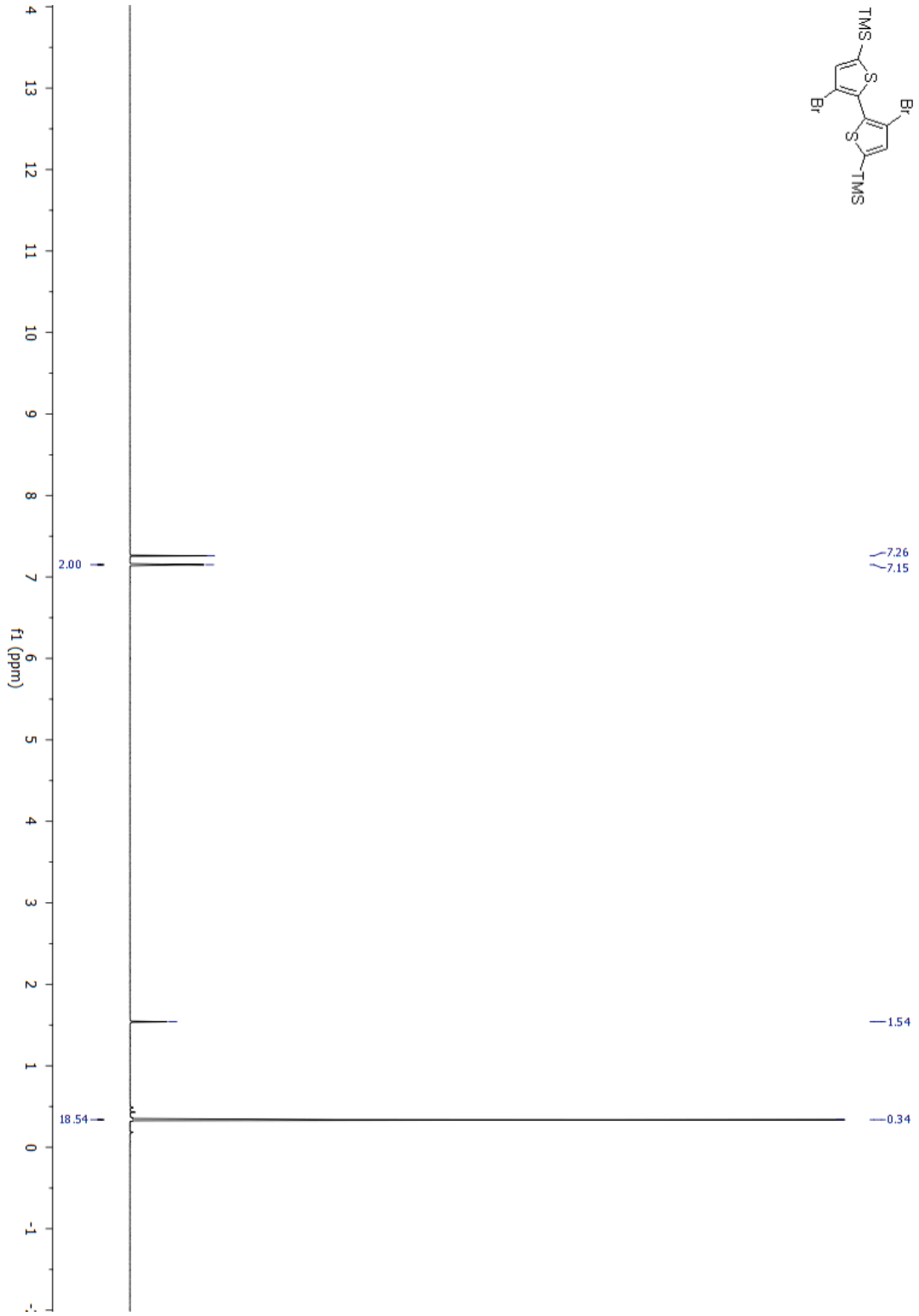

Figure 5.7.1: ^{1}H NMR spectra of (3,3'-dibromo-[2,2'-bithiophene]-5,5'-diyl)bis(trimethylsilane) (S1).

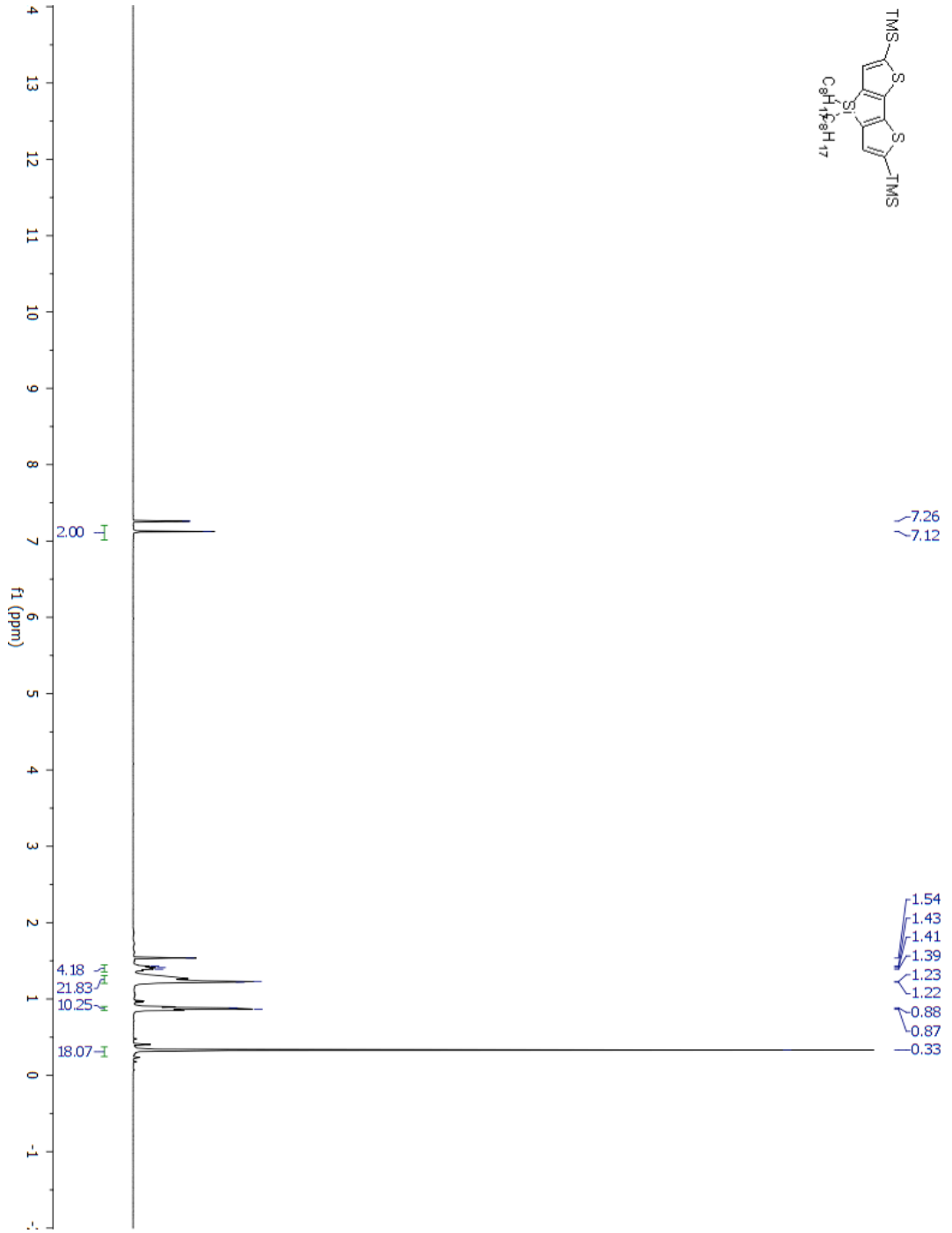

Figure 5.7.2: ^{1}H NMR spectra of 4,4-dioctyl-2,6-bis(trimethylsilyl)-4*H*-silolo[3,2-*b*:4,5-*b'*]dithiophene (S2)

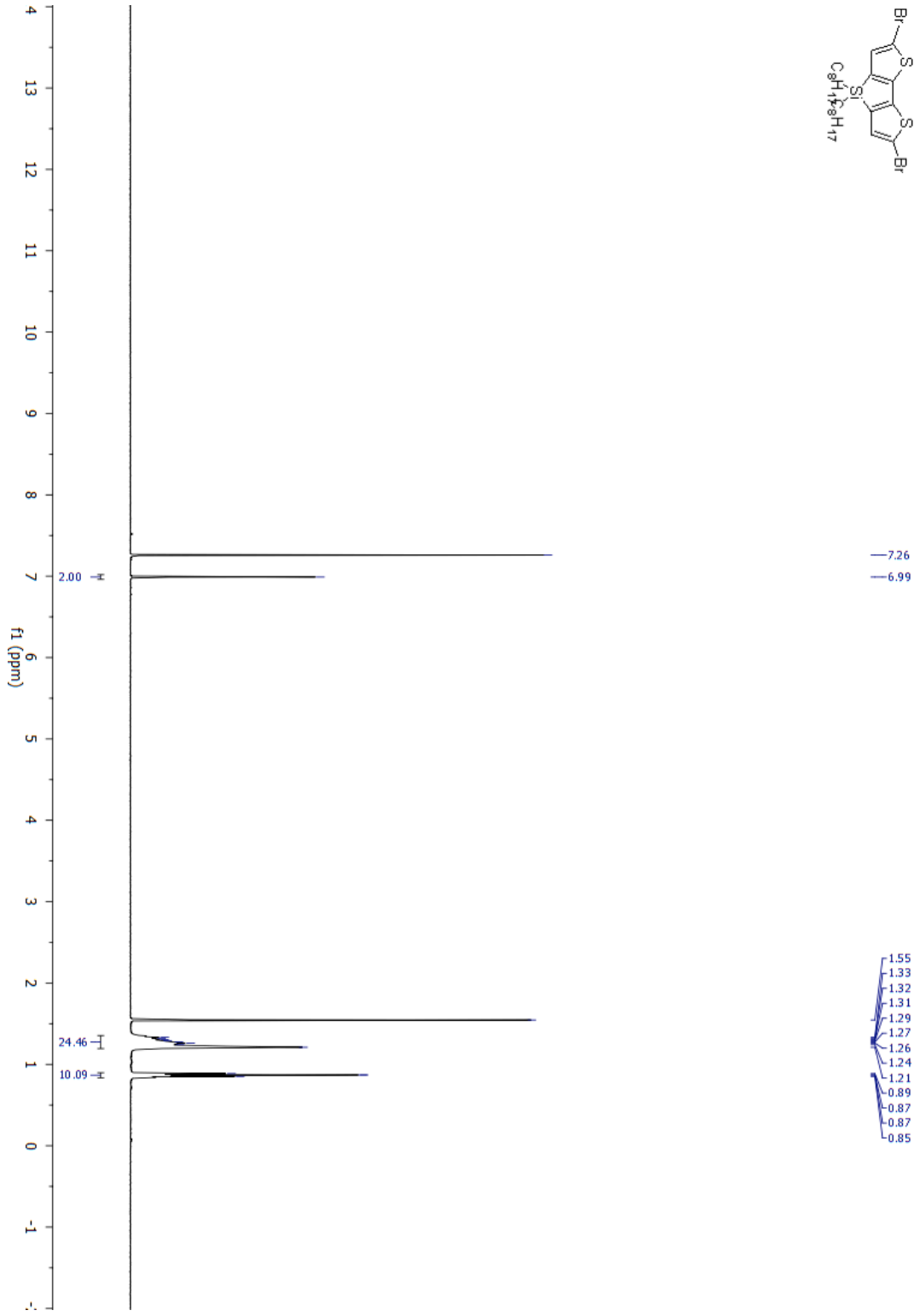

Figure 5.7.3: ^{1}H NMR spectra of 2,6-dibromo-4,4-dioctyl-4*H*-silolo[3,2-*b*:4,5-*b'*]dithiophene (S3)

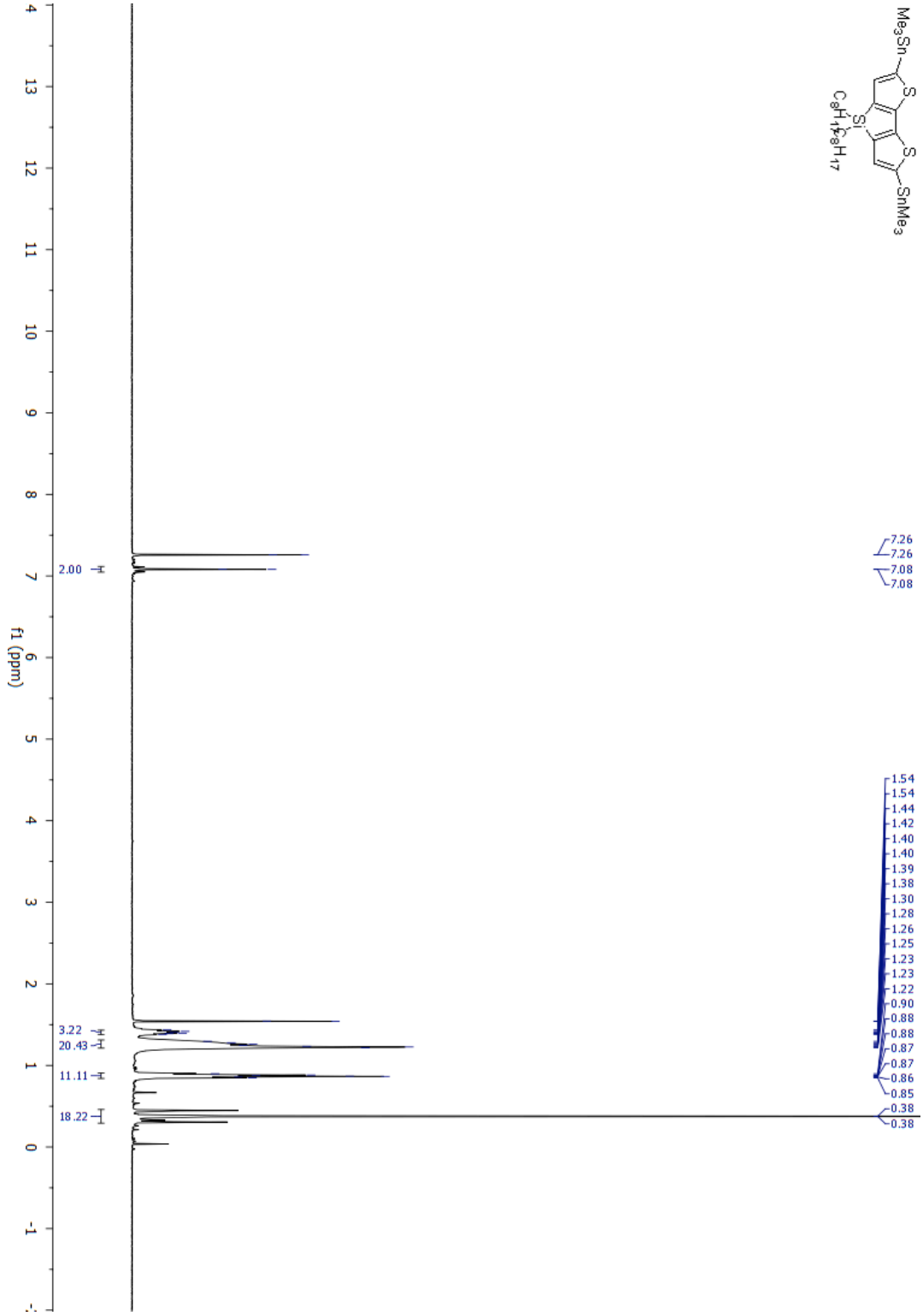

Figure 5.7.4: ^{1}H NMR spectra of 4,4-dioctyl-2,6-bis(trimethylstannyl)-4*H*-silolo[3,2-*b*:4,5-*b*′]dithiophene (1)

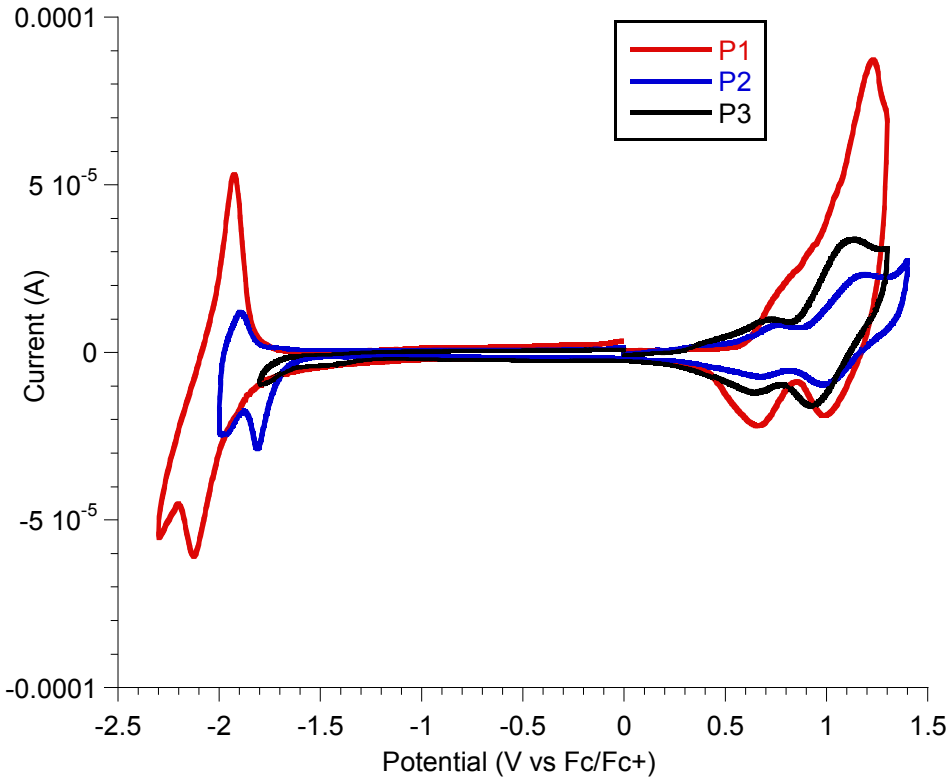

Figure 5.7.5. Cyclic Voltammetry of P1, P2 and P3

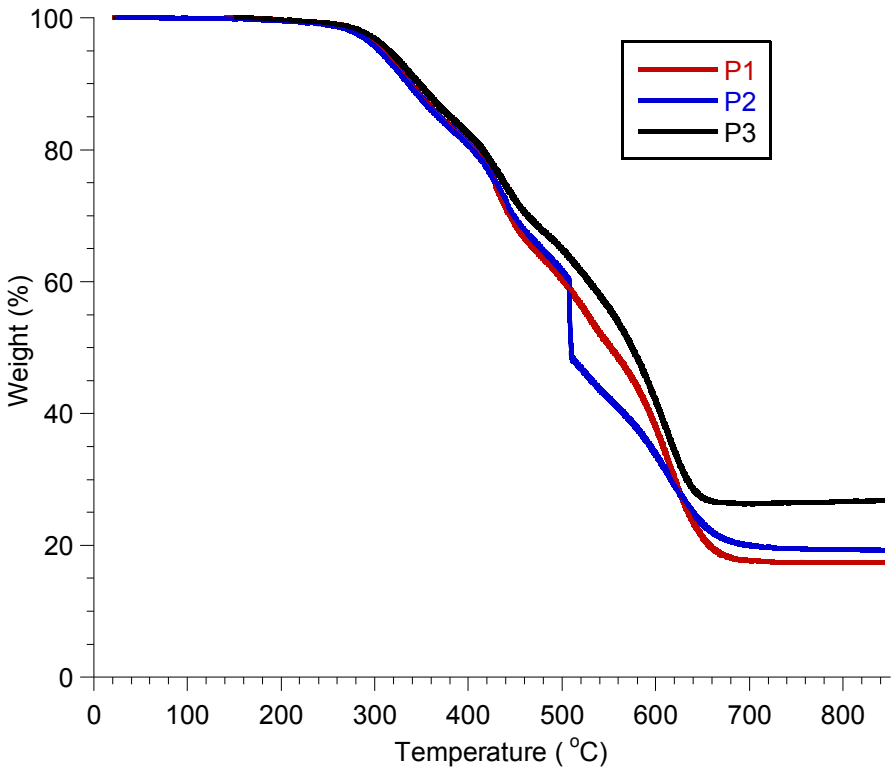

Figure 5.7.6. TGA plot of P1, P2 and P3

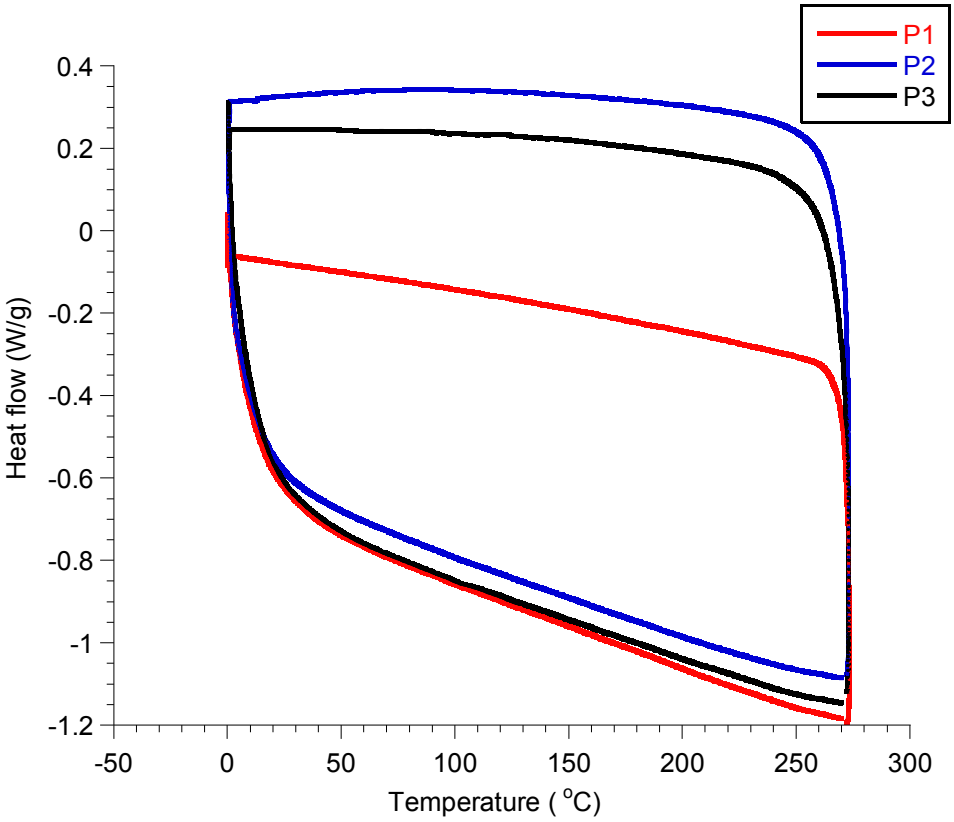

Figure 5.7.7. DSC plot of P1, P2 and P3

C:\LabSolutions\Data\achala\cbbodts_2.lcd

Acquired by	: Jeffries-EL Group
Sample Name	: lcbbotdts
Injection Volume	: 5 uL
Data File Name	: cbbodts_2.lcd
Method File Name	: GPC Run-500 nm.lcm
Data Acquired	: 4/9/2014 3:00:49 PM
Data Processed	: 4/16/2014 5:05:49 PM

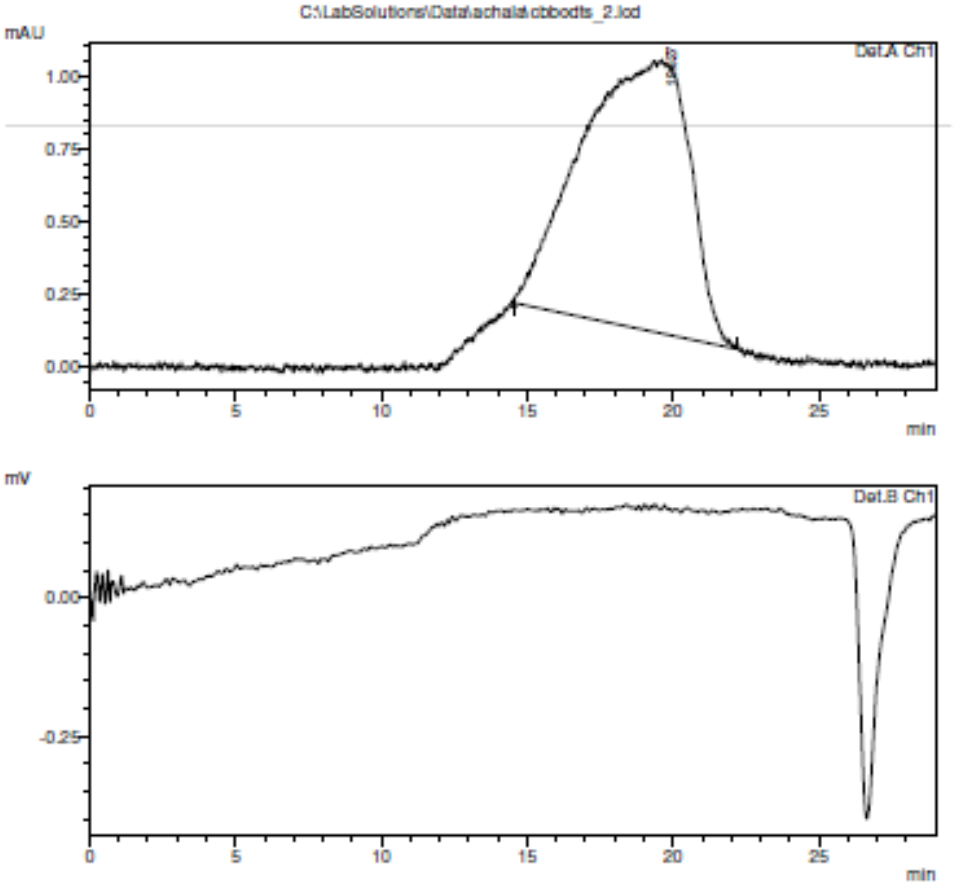

GPC Results

Peak#:1 (Detector A Ch1)

[Average Molecular Weight]

Number Average Molecular Weight(Mn)	11645
Weight Average Molecular Weight(Mw)	26251
Mw/Mn	2.25424

Figure 5.7.8. GPC plot of P1

C:\LabSolutions\Data\achala\tbbodts_2.lcd

Acquired by	: Jeffries-EL Group
Sample Name	: tBBOdts_attempt2
Injection Volume	: 5 uL
Data File Name	: tbbodts_2.lcd
Method File Name	: GPC Run-500 nm.lcm
Data Acquired	: 4/15/2014 1:58:23 PM
Data Processed	: 4/16/2014 11:14:38 AM

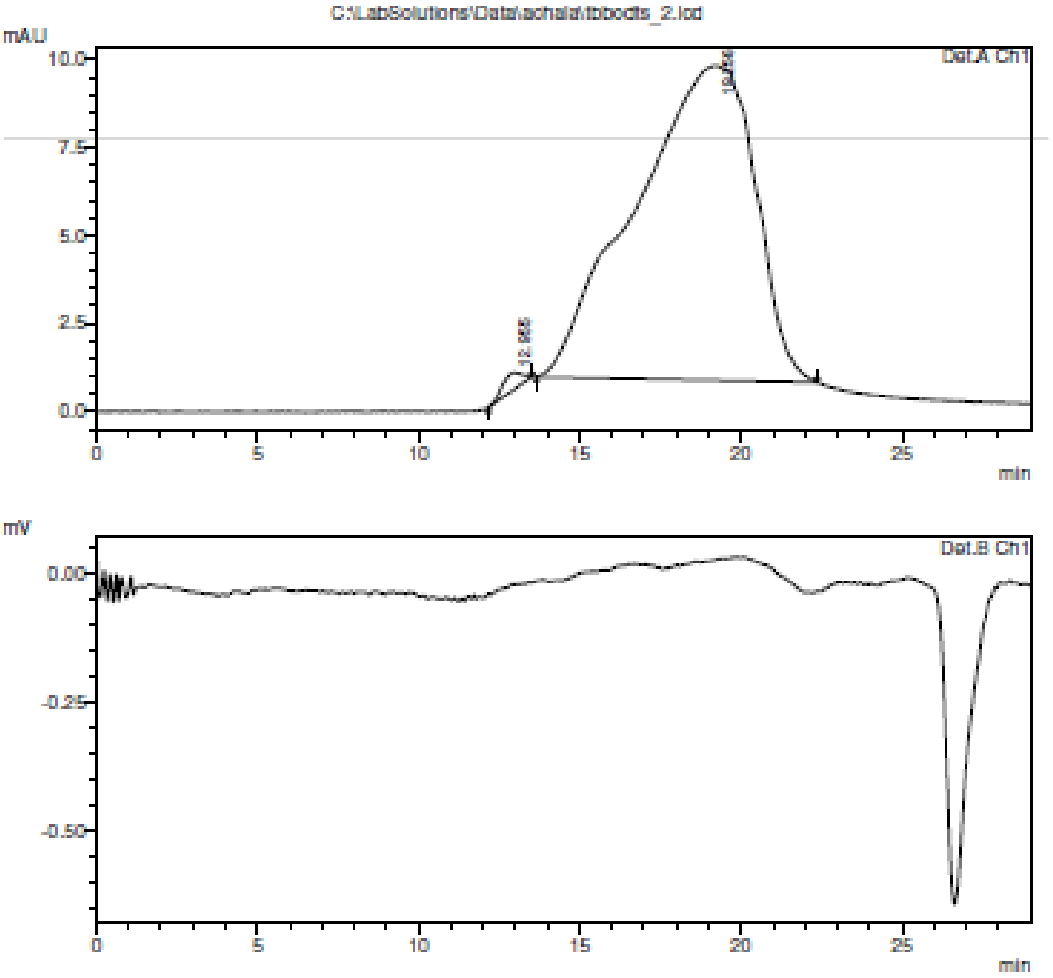

GPC Results

Peak#:1 (Detector A Ch1)	
[Average Molecular Weight]	
Number Average Molecular Weight(Mn)	752760
Weight Average Molecular Weight(Mw)	818382
Mw/Mn	1.08717
Peak#:2 (Detector A Ch1)	
[Average Molecular Weight]	
Number Average Molecular Weight(Mn)	12409
Weight Average Molecular Weight(Mw)	31758
Mw/Mn	2.55932

Figure 5.7.9. GPC plot of P2

C:\LabSolutions\Data\achala\tbbztdts_2.lcd

Acquired by	: Jeffries-EL Group
Sample Name	: tBBZTdts_attempt2
Injection Volume	: 5 uL
Data File Name	: tbbztdts_2.lcd
Method File Name	: GPC Run-500 nm.lcm
Data Acquired	: 4/15/2014 2:27:49 PM
Data Processed	: 4/16/2014 11:28:28 AM

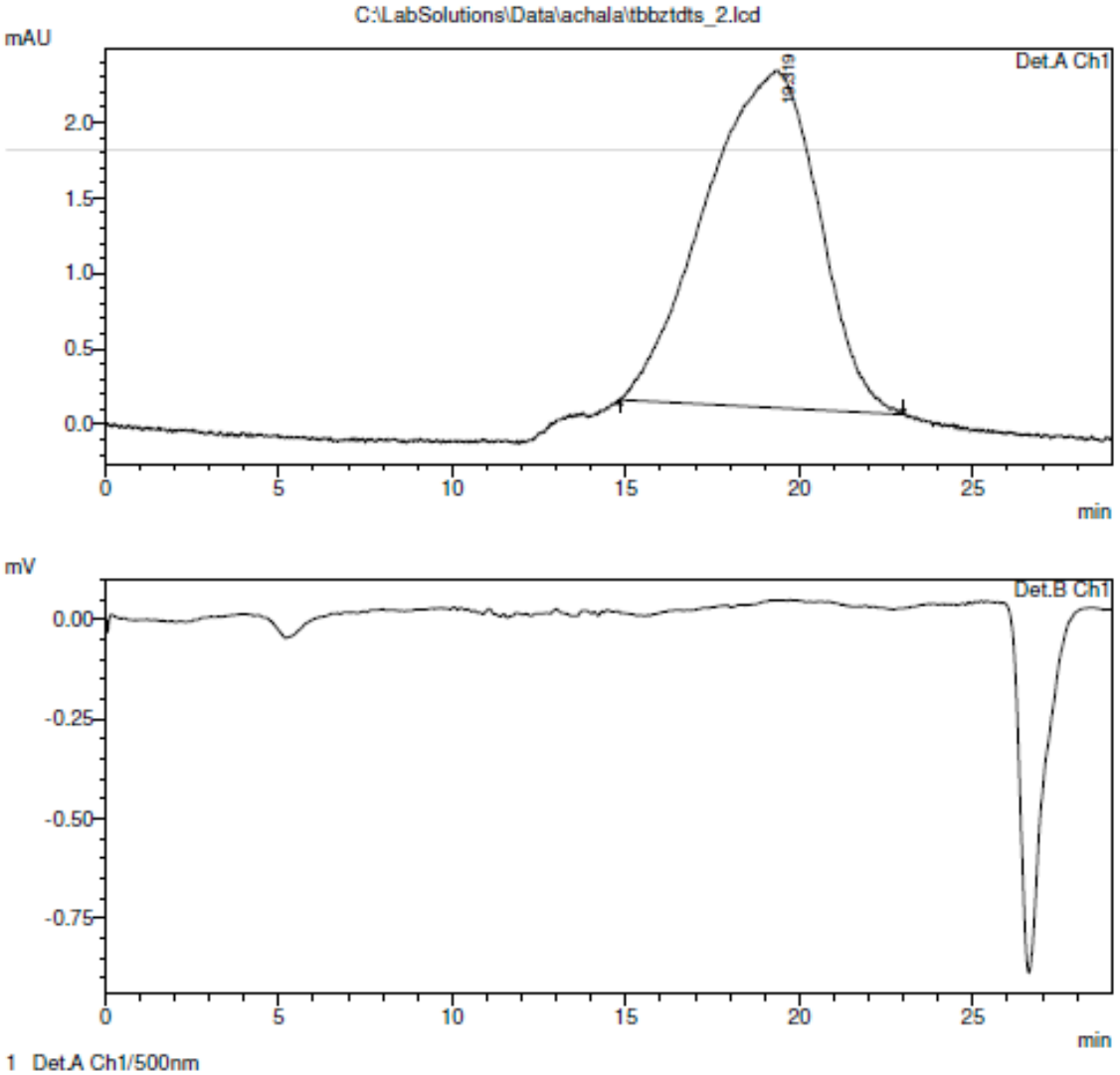

1 Det.A Ch1/500nm
2 Det.B Ch1/

GPC Results

Peak#:1 (Detector A Ch1)
[Average Molecular Weight]

Number Average Molecular Weight(Mn)	9566
Weight Average Molecular Weight(Mw)	20884
Mw/Mn	2.18322

Figure 5.7.10. GPC plot of P3

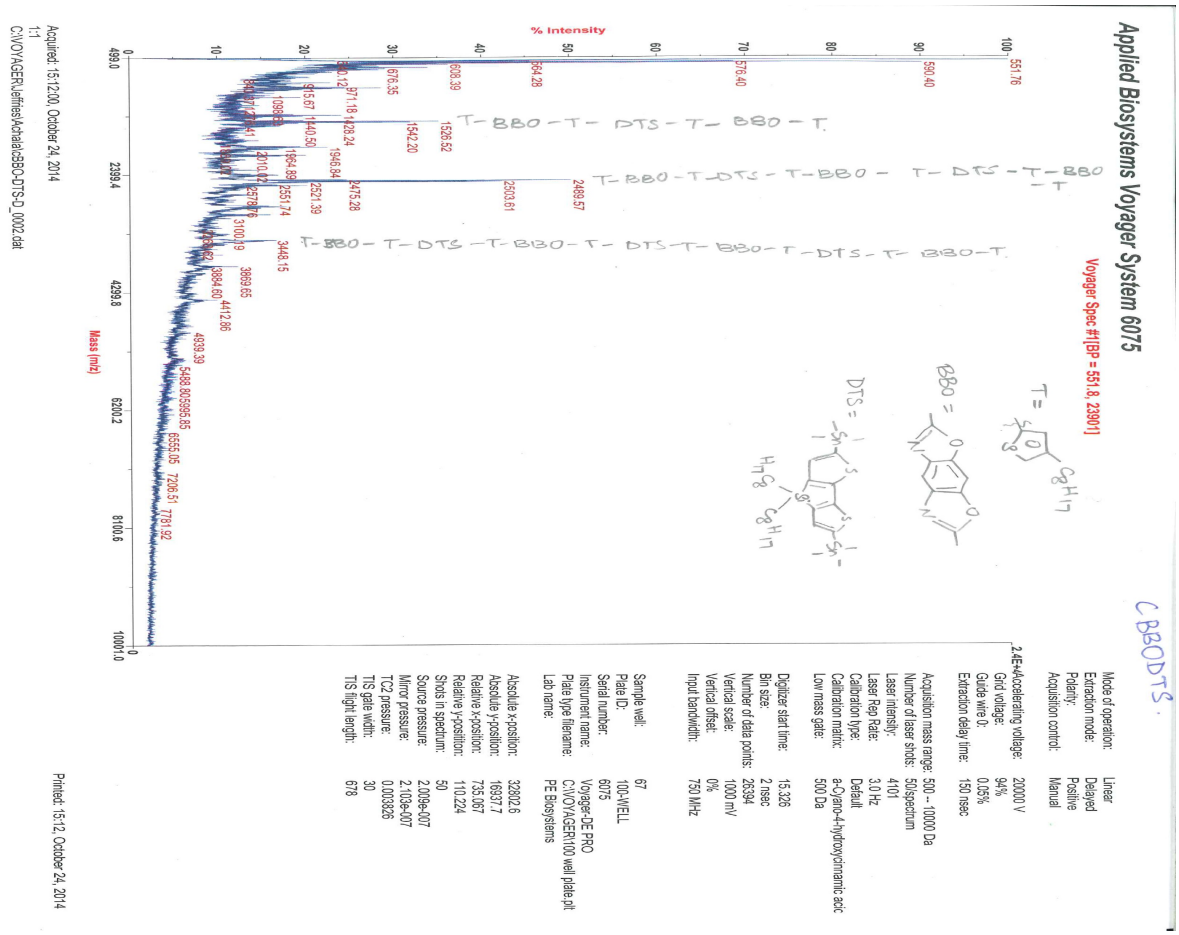

Figure 5.7.11. Maldi of P1

3.8 REFERENCES

(1) a) Facchetti, A. *Mater. Today* **2007**, *10*, 28; b) Bao, Z.; Lovinger, A. J. *Chem. Mater.* **1999**, *11*, 2607.

(2) a) Friend, R. H.; Gymer, R. W.; Holmes, A. B.; Burroughes, J. H.; Marks, R. N.; Taliani, C.; Bradley, D. D. C.; Dos Santos, D. A.; Bredas, J. L.; Logdlund, M.; Salaneck, W. R. *Nature* **1999**, *397*, 121; b) Tang, C. W.; VanSlyke, S. A. *Appl. Phys. Lett.* **1987**, *51*, 913; c) Grimsdale, A. C.; Leok Chan, K.; Martin, R. E.; Jokisz, P. G.; Holmes, A. B. *Chem. Rev.* **2009**, *109*, 897.

(3) a) Tang, C. W. *Appl. Phys. Lett.* **1986**, *48*, 183; b) Facchetti, A. *Chem. Mater.* **2011**, *23*, 733; c) Günes, S.; Neugebauer, H.; Sariciftci, N. S. *Chem. Rev.* **2007**, *107*, 1324.

(4) a) McQuade, D. T.; Pullen, A. E.; Swager, T. M. *Chem. Rev.* **2000**, *100*, 2537; b) Thomas, S. W.; Joly, G. D.; Swager, T. M. *Chem. Rev.* **2007**, *107*, 1339.

(5) a) van Mullekom, H. A. M.; Vekemans, J. A. J. M.; Havinga, E. E.; Meijer, E. W. *Mater. Sci. Eng., R* **2001**, *32*, 1; b) Havinga, E. E.; ten Hoeve, W.; Wynberg, H.

Polymer Bulletin **1992**, *29*, 119; c) Havinga, E. E.; ten Hoeve, W.; Wynberg, H. *Synth. Met.* **1993**, *55*, 299.

(6) a) Koster, L. J. A.; Mihailetchi, V. D.; Blom, P. W. M. *Appl. Phys. Lett.* **2006**, *88*, 093511; b) Thompson, B. C.; Kim, Y.-G.; Reynolds, J. R. *Macromolecules* **2005**, *38*, 5359.

(7) a) Son, H. J.; Carsten, B.; Jung, I. H.; Yu, L. *Energy & Environmental Science* **2012**, *5*, 8158; b) Dennler, G.; Scharber, M. C.; Brabec, C. J. *Adv. Mater.* **2009**, *21*, 1323; c) Kalowekamo, J.; Baker, E. *Solar Energy* **2009**, *83*, 1224.

(8) Po, R.; Bernardi, A.; Calabrese, A.; Carbonera, C.; Corso, G.; Pellegrino, A. *Energy & Environmental Science* **2014**, *7*, 925.

(9) a) Wolak, M. A.; Jang, B. B.; Palilis, L. C.; Kafafi, Z. H. *J. Phys. Chem. B* **2004**, *108*, 5492; b) Wolfe, J. F. In *Encyclopedia of Polymer Science and Engineering*; John Wiley and Sons: New York, NY, 1988; Vol. 11, p 601; c) Wolfe, J. F.; Arnold, F. E. *Macromolecules* **1981**, *14*, 909; d) Wolfe, J. F.; Loo, B. H.; Arnold, F. E. *Macromolecules* **1981**, *14*, 915.

(10) a) Alam, M. M.; Jenekhe, S. A. *Chem. Mater.* **2002**, *14*, 4775; b) Pang, H.; Vilela, F.; Skabara, P. J.; McDouall, J. J. W.; Crouch, D. J.; Anthopoulos, T. D.; Bradley, D. D. C.; de Leeuw, D. M.; Horton, P. N.; Hursthouse, M. B. *Adv. Mater.* **2007**, *19*, 4438; c) Osaka, I.; Takimiya, K.; McCullough, R. D. *Adv. Mater.* **2010**, *22*, 4993.

(11) Song, B.; Fu, Q.; Ying, L.; Liu, X.; Zhuang, Q.; Han, Z. *J. Appl. Polym. Sci.* **2012**, *124*, 1050.

(12) a) Mike, J. F.; Inteman, J. J.; Ellern, A.; Jeffries-El, M. *The Journal of Organic Chemistry* **2009**, *75*, 495; b) Mike, J. F.; Intemann, J. J.; Cai, M.; Xiao, T.; Shinar, R.; Shinar, J.; Jeffries-EL, M. *Polym. Chem.* **2011**, *2*, 2299; c) Mike, J. F.; Makowski, A. J.; Jeffries-El, M. *Org. Lett.* **2008**, *10*, 4915.

(13) a) Ahmed, E.; Kim, F. S.; Xin, H.; Jenekhe, S. A. *Macromolecules* **2009**, *42*, 8615; b) Ahmed, E.; Subramaniyan, S.; Kim, F. S.; Xin, H.; Jenekhe, S. A. *Macromolecules* **2011**, *44*, 7207; c) Bhuwalka, A.; Mike, J. F.; He, M.; Intemann, J. J.; Nelson, T.; Ewan, M. D.; Roggers, R. A.; Lin, Z.; Jeffries-El, M. *Macromolecules* **2011**, *44*, 9611; d) Patil, A. V.; Park, H.; Lee, E. W.; Lee, S.-H. *Synth. Met.* **2010**, *160*, 2128; e) Tsuji, M.; Saeki, A.; Koizumi, Y.; Matsuyama, N.; Vijayakumar, C.; Seki, S. *Adv. Funct. Mater.* **2014**, *24*, 28; f) Saeki, A.; Tsuji, M.; Yoshikawa, S.; Gopal, A.; Seki, S. *J. Mater. Chem. A* **2014**, *2*, 6075.

(14) Chen, H.-Y.; Hou, J.; Hayden, A. E.; Yang, H.; Houk, K. N.; Yang, Y. *Adv. Mater.* **2010**, *22*, 371.

(15) Chu, T.-Y.; Lu, J.; Beaupré, S.; Zhang, Y.; Pouliot, J.-R.; Wakim, S.; Zhou, J.; Leclerc, M.; Li, Z.; Ding, J.; Tao, Y. *Journal of the American Chemical Society* **2011**, *133*, 4250.

(16) Hou, J.; Chen, H.-Y.; Zhang, S.; Li, G.; Yang, Y. *J. Am. Chem. Soc.* **2008**, *130*, 16144.

(17) Sanchez, R. S.; Zhuravlev, F. A. *J. Am. Chem. Soc.* **2007**, *129*, 5824.

(18) Kokubo, H.; Sato, T.; Yamamoto, T. *Macromolecules* **2006**, *39*, 3959.

(19) Cardona, C. M.; Li, W.; Kaifer, A. E.; Stockdale, D.; Bazan, G. C. *Adv. Mater.* **2011**, *23*, 2367.

(20) Admassie, S.; Inganäs, O.; Mammo, W.; Perzon, E.; Andersson, M. R. *Synth. Met.* **2006**, *156*, 614.

(21) Lee, J. K.; Ma, W. L.; Brabec, C. J.; Yuen, J.; Moon, J. S.; Kim, J. Y.; Lee, K.; Bazan, G. C.; Heeger, A. J. *J. Am. Chem. Soc.* **2008**, *130*, 3619.
(22) Mihailetchi, V. D.; Wildeman, J.; Blom, P. W. M. *Phys. Rev. Lett.* **2005**, *94*, 126602.
(23) Shrotriya, V.; Yao, Y.; Li, G.; Yang, Y. *Appl. Phys. Lett.* **2006**, *89*, 063505.

CHAPTER 6

STUDY ON THE SYNTHESIS AND STRUCTURE-PROPERTY RELATIONSHIPS OF THAIZOLOPYRIDINE.

*Achala Bhuwalka,[1] Aimée L. Tomlinson[2], Nia Johnson,[3]Lindsey Hannam,[1] and Malika Jeffries-EL[1]**

[1]Department of Chemistry, Iowa State University, Ames IA 50011.

[2]Department of Chemistry, University of North Georgia, Dahlonega, Georgia 30597

[3]Ames High School, Ames, IA 50011.

6.1 Abstract:

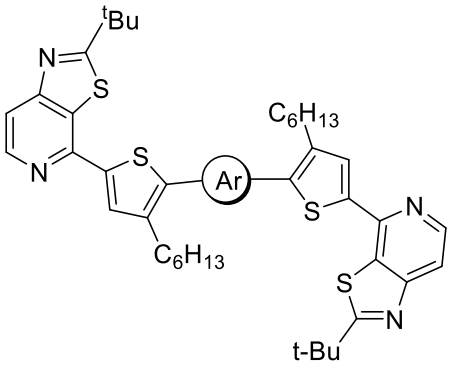

New materials for small molecule organic solar cells comprised of acceptor-donor-acceptor triad or acceptor-π-donor-π-acceptor incorporating thiazolopyridines were synthesized via the Stille cross-coupling reaction. The effect of increasing conjugation on the optical properties of the resulting small molecules was evaluated using UV-Visible spectroscopy. All of the small molecules have similar optical band-gaps of 2.2 - 2.4 eV.

These are comparable to band gaps obtained for donor-acceptor polymers incorporating benzobisazoles previously reported by our group.

6.2 Introduction

Conjugated polymers are currently at the forefront of semiconductor research for organic photovoltaic cells (OPV)s,[1-3] organic light emitting diodes (OLED)s,[4-6] and organic field-effect transistors (OFET)s.[7-9] Organic semiconductors are promising alternatives to their inorganic counterparts since they provide the opportunity to fabricate lightweight flexible devices using low-cost solution-based techniques over large areas. Moreover, their optical and electronic properties can be fine-tuned by chemical synthesis.[10-12] The bulk heterojunction is the most commonly employed device architecture, in which the active material consists of a conjugated polymer as the donor and a functionalized fullerene as the acceptor.[13-15] The conjugated polymer consists of alternating electron-rich and electron-deficient units in its backbone.[15-17] The most commonly used fullerene acceptors are [6,6]-phenyl C_{61} butyric acid methyl ester ($PC_{61}BM$) and [6,6]-phenyl C_{71} butyric acid methyl ester ($PC_{71}BM$).[18-20] Efficiencies over 9% have been achieved in solar cells fabricated in this manner.[21] Although promising, these high efficiencies are not always reproducible for the same set of materials due to polymer batch-to-batch variability.[22] This is one of the biggest challenges being faced by the polymer community. Batch-to-batch variability leads to discrepancies in properties such as the molecular weight and, therefore, solubility of the polymer in organic solvents at a particular temperature, as well as differences in the polydispersity and purity of the resulting materials. Any inconsistencies in these properties lead to different processing

conditions and unreproducible photovoltaic performances.[23] In order to address this, scientists are looking into devices in which small molecule donors and fullerene and non-fullerene acceptors make up the active layer.[24,25] These materials have better molecular precision, which makes them better systems to study structure-property relationships. Moreover, every batch of these materials has the same molecular weight, solubility, PDI, purification, and processing conditions. As a result, the device performance is reproducible. On the other hand, small molecules suffer from poor film-forming ability as compared to their polymeric counterparts, leading to poor fill factors and loss of charge carrier species.[26]

It is important to consider several factors while designing materials for small-molecule organic electronics. Firstly, the donors should be chosen such that they maintain good miscibility with the fullerene acceptor, as well as maintain sufficient crystallinity to form an interpenetrating donor-acceptor network in the active layer.[27] Secondly, the small-molecule must possess a broad absorption spectrum to harvest a large portion of the solar spectrum.[26] Furthermore, the energy levels must be well aligned, and the materials must exhibit high carrier mobility.[22] Using these strategies, power conversion efficiencies over 7% have been achieved for small molecule solar cells.[24,28,29] Nonetheless, development of new materials as well as optimizing device engineering remain extremely crucial for obtaining higher performing organic solar cells.

Thiazolo[5,4-*c*]pyridine is (TP) an electron-deficient heterocycle that has not yet been studied for organic electronic devices. Fusing an electron-deficient thiazole ring to an already electron-deficient pyridine core is expected to impart high electron affinity to this material making it a good electron acceptor. Additionally, since it is asymmetric like

pyridalthiadiazole (PT), TP can be selectively functionalized leading to high yields during

synthesis.[30] Previous reports on PT have shown that incorporating pyridine units in the structural backbone deepen the LUMO and HOMO levels making these materials less prone to oxidation by air.[31] Additionally, linking a strong donor with the acceptor to form an acceptor-donor-acceptor triad leads to strong intramolecular charge transfer and broad absorption profiles.[31,32] Based on the aforementioned findings, we have developed new thiazolopyridine based small molecule acceptor-donor-acceptor triads.

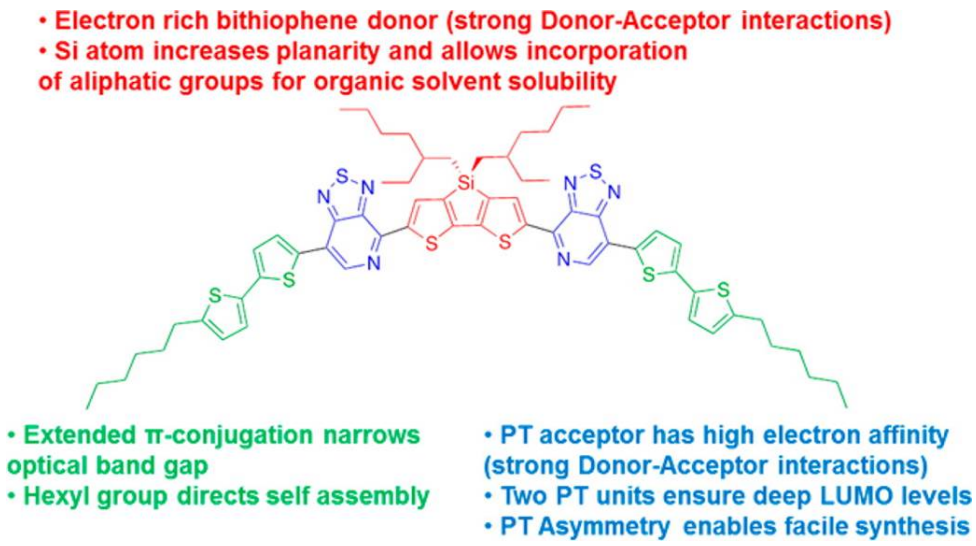

Figure 6.1 Design rules for small molecule donor – acceptor organic solar cells

In order to draw a direct comparison between the TP and PT units, the small molecules were initially designed such that the donor units were flanked on either sides with TP acceptor units, which in turn were directly attached to bithiophene groups on the other side, similar to the ones reported by Bazan et al. **M1** was successfully synthesized with the A-D-A architecture. Unfortunately, all efforts to synthesize A-D-A small

molecules using donors other than thiophene were unsuccessful. In all such attempts, the reaction stopped after coupling between the donor with one TP unit. Therefore, a new set of A-π-D-π-A small molecules were developed with the thiophene π-spacer to enable cross-coupling chemistry with donor units (Figure 6.2) Methods to further extend the conjugation are currently being investigated.

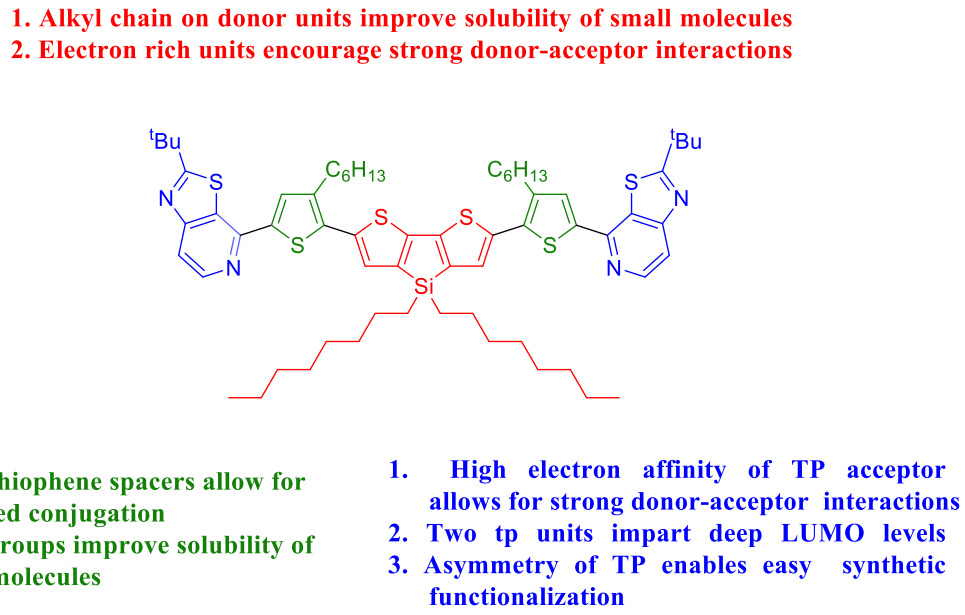

Figure 6.2 TP based A-π-D-π-A small molecules

6.3 Results and Discussion

6.3.1 Synthesis

2-Substituted thiazolo[5,4-*c*]pyridine was prepared by modified literature procedures.[33] 2-(*tert*-butyl)thiazolo[5,4-*c*]pyridine (Scheme 6.1) was chosen as a model substrate due to ease of synthesis and purification. Furthermore, the *tert*-butyl group increased solubility of the materials in common organic solvents.

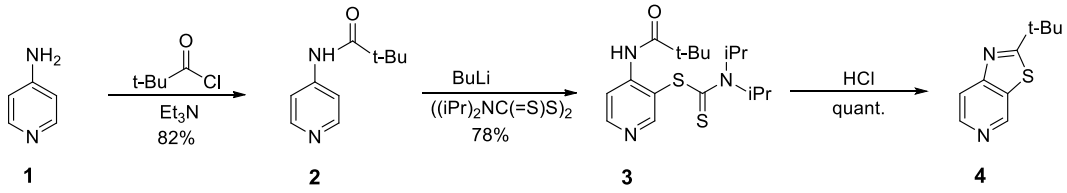

Scheme 6.1 Synthesis of 2-(*tert*-butyl)thiazolo[5,4-*c*]pyridine

2-(*tert*-butyl)thiazolo[5,4-*c*]pyridine was then selectively oxidized and halogenated at the 4-position to yield the 2-(*tert*-butyl)-4-chlorothiazolo[5,4-*c*]pyridine (Scheme 6.2) Both reactions proceed in high yields.

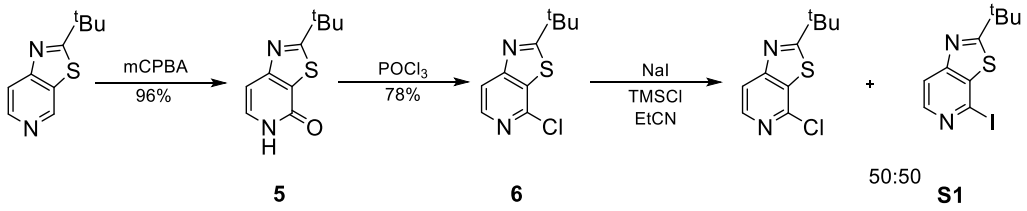

Scheme 6.2 Synthesis of 2-(*tert*-butyl)-4-halothiazolo[5,4-*c*]pyridine

Since bromo- and iodo arenes are more reactive than chloroarenes in typical transition metal catalyzed cross-coupling reactions, we initially elected to synthesize 2-(*tert*-butyl)-4-bromothiazolo[5,4-*c*]pyridine and 2-(*tert*-butyl)-4-iodothiazolo[5,4-*c*]pyridine. However, no conversion of the starting material to the product was observed using the original reaction conditions, with $POBr_3$ instead of $POCl_3$. Several reaction parameters including the brominating reagents, reaction solvents, reaction time, and reaction temperature were screened. In all these attempts, starting material was recovered. In order to obtain 2-(*tert*-butyl)-4-iodothiazolo[5,4-*c*]pyridine, Finkelstein reaction conditions were employed.[34,35] At best, a 1:1 inseparable mixture of 2-(*tert*-butyl)-4-chlorothiazolo[5,4-*c*]pyridine and 2-(*tert*-butyl)-4-iodothiazolo[5,4-*c*]pyridine was

obtained in low yields. It was later found that the chloroarene was reactive enough at the 4-position and formed 2,2'-di-*tert*-butyl-4,4'-bithiazolo[5,4-*c*]pyridine cleanly and in high yields. Therefore, 2-(*tert*-butyl)-4-chlorothiazolo[5,4-*c*]pyridine was used in all further studies.

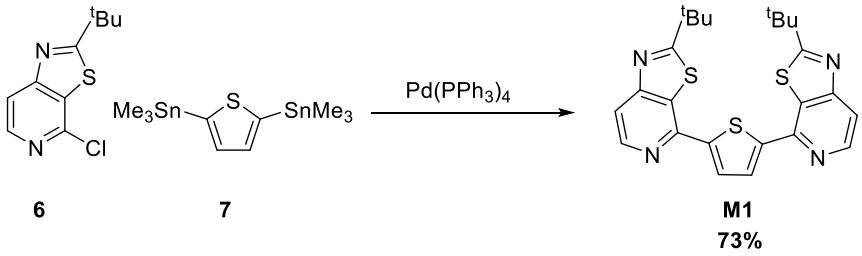

Scheme 6.3 Synthesis of A-D-A small molecule

We then attempted to synthesize the A-D-A triads via a Stille cross coupling reaction between the 2-(*tert*-butyl)-4-chlorothiazolo[5,4-*c*]pyridine and 2,5-bis(trimethylstannyl)thiophene **(7)**, (3,3'-dioctyl-[2,2'-bithiophene]-5,5'-diyl)bis(trimethylstannane) **(9)**, and 4,4-dioctyl-2,6-bis(trimethylstannyl)-4*H*-silolo[3,2-*b*:4,5-*b*']dithiophene **(10)**. Reaction of **6** with **7** yielded disubstituted product 2,5-bis(2-(*tert*-butyl)thiazolo[5,4-*c*]pyridin-4-yl)thiophene **(M1)** in moderate yields. Unfortunately, the reaction of **6** with **9** and **10**, yielded only monosubtitued products, i.e., 2-(*tert*-butyl)-4-(3,3'-dioctyl-[2,2'-bithiophen]-5-yl)thiazolo[5,4-*c*]pyridine **(12)** and 2-(*tert*-butyl)-4-(4,4-dioctyl-4*H*-silolo[3,2-*b*:4,5-*b*']dithiophen-2-yl)thiazolo[5,4-*c*]pyridine **(13)**.

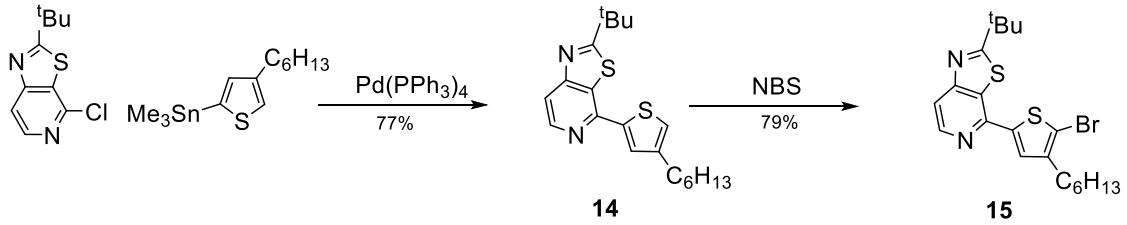

Scheme 6.4 Synthesis of 4-(5-bromo-4-hexylthiophen-2-yl)-2-(*tert*-butyl)thiazolo[5,4-*c*]pyridine.

In order to utilize this to our advantage, **6** was reacted with (4-hexylthiophen-2-yl)trimethylstannane to yield 2-(*tert*-butyl)-4-(4-hexylthiophen-2-yl)thiazolo[5,4-*c*]pyridine **(14)** which was then easily brominated at the 5-position on the thiophene to yield 4-(5-bromo-4-hexylthiophen-2-yl)-2-(*tert*-butyl)thiazolo[5,4-*c*]pyridine **(15).** The bromosubstituted compound was then reacted with compounds **8**, **9** and **10** to yield small molecules **M2**, **M3** and **M4** of A-π-D-π-A architecture respectively. All these small molecules were highly soluble in standard organic solvents, facilitating easy purification via flash chromatography. The materials were characterized using ^{1}H NMR spectroscopy. The ^{1}H NMR spectra for all the small molecules were in agreement with the proposed structures.

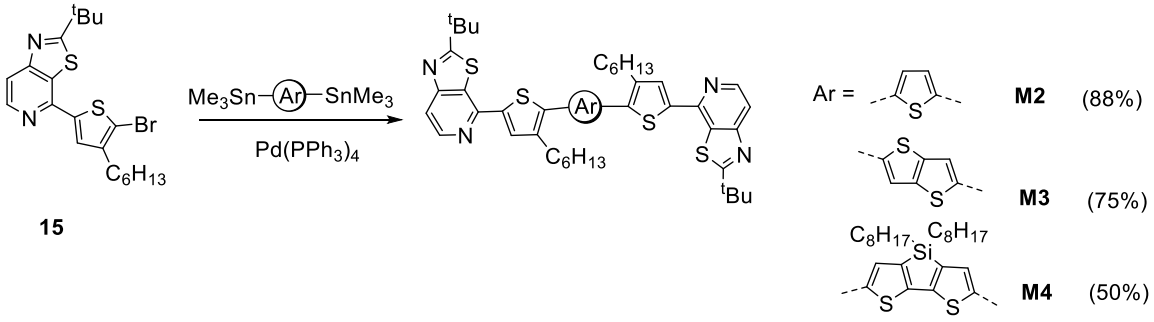

Scheme 6.5 Synthesis of **M2** – **M4**.

6.3.2 Optical and Electronic properties

The normalized solution (Fig. 6.3) as well as thin-film absorption spectra (Fig. 6.4) for **M1** – **M4** were recorded. In solution, the UV-Vis spectra for all the small molecules exhibit a single featureless band. The A-D-A small molecule, **M1**, absorbs mainly in the UV region. The introduction of the π-spacer leads to red shift in the absorption of the small molecules. The λ_{max} of **M2** is bathochromically shifted by 40 nm as compared to **M1**.

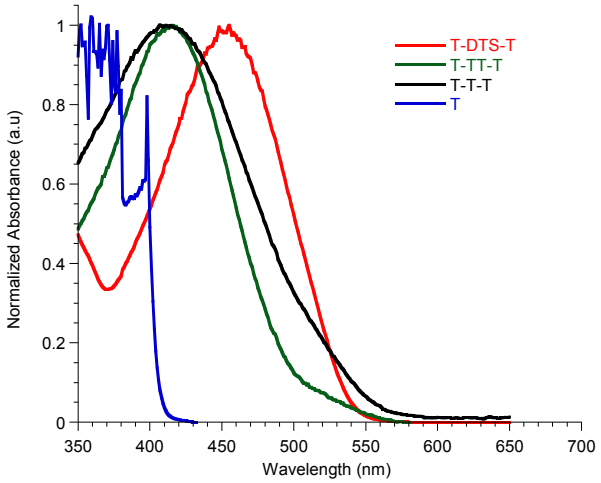

Figure 6.3 Absorbance spectra of **M1**-M4 in chloroform solution

The λ_{max} for **M2** and **M3** are similar at 411 nm and 415 nm respectively. As expected, increasing the donor strength from thiophene to 4,4-dioctyl-4*H*-silolo[3,2-*b*:4,5-*b*']dithiophene results in a further red shift in the absorption spectrum (relative to **M2** and **M3**), with the λ_{max} for **M4** at 455 nm (Table 6.1). Additionally, the planar fused ring system in 4,4-dioctyl-4*H*-silolo[3,2-*b*:4,5-*b*']dithiophene facilitates π-stacking interactions and long-range order.[36]

In the solid state, the absorbance spectra for all the small molecules are significantly broader, resulting in bathochromic shifts in the absorption maximum for **M1**-**M3**. The largest red shift is seen in the case of **M3**, which is shifted by 72 nm (λ_{max} = 487 nm). This is

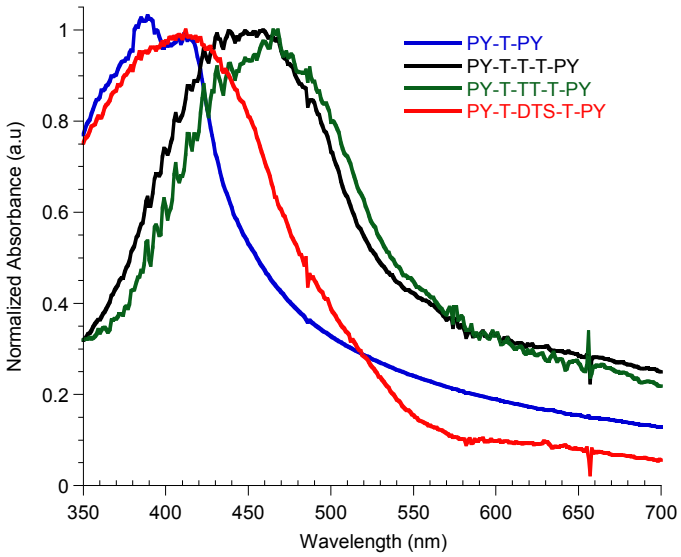

Figure 6.4 Absorbance spectra of **M1** – **M4** in the solid state.

probably as a result of increased π- stacking and backbone planarization in the solid state.[37] The λ_{max} for **M4** is hypsochromically shifted by 43 nm in the solid state as compared to its solution phase. This may be due to disruption in packing caused by the *tert* - butyl groups as well as twisting of the backbone caused by steric interactions between the units in the small molecule backbone.

The optical band gaps for small molecules **M1**-**M4** were obtained from the edge of the respective absorption onsets in the solid state. **M1** had the largest band gap at 2.4 eV. As expected, extending the conjugation from A-D-A in **M1** to A-π-D-π-A in **M2**-

M4, resulted in a decrease in band gap. The observed optical band gap for all the A-π-D-π-A type molecules was the same at 2.2 eV. **M4** showed the greatest agreement in band gap values obtained via theoretical calculations and those observed experimentally.

The energy levels (HOMO and LUMO values) reported in Table 6.1 were obtained via theoretical calculations. As expected, theory suggested an increase in the HOMO energy levels with increasing conjugation and higher donor strength. **M4** is therefore expected to have the highest HOMO level at –4.66 eV. However, this suggests that **M4** may not be oxidatively stable. In further studies, donors with lower lying HOMO will be employed.

Table 6.1 Optical and electronic properties of **M1**-**M4**

Small Molecule	λ_{max}^{soln} (nm)	λ_{max}^{film} (nm)	E_g^{opt} (eV)	$E_g^{theoretical}$ (eV)	HOMO (eV)	LUMO (eV)
M1	371	394	2.4	3.26	-5.52	-1.94
M2	411	459	2.2	2.70	-5.01	-1.97
M3	415	487	2.2	2.69	-5.02	-1.98
M4	455	412	2.2	2.32	-4.66	-2.04

6.4 Conclusions

In summary, four new thiazolo[5,4-*c*]pyridine based small molecules have been synthesized. 2-(*tert*-butyl)-4-chlorothiazolo[5,4-*c*]pyridine was prepared in high yields via modified literature methods and was readily reacted with thiophene based donor molecules via the Stille cross-coupling reaction. The *tert* - butyl side chains on the thiazolo[5,4-*c*]pyridine led to good solubility of the resulting materials in organic solvents at room temperature. The A-π-D-π-A small molecules had a broader and bathochromically shifted absorption spectrum as well as narrower band gaps as compared to the A-D-A small molecule. New small molecules with reactive handles on the pyridine in order to further extend the π-system are being synthesized and studied in order to improve the absorption in the lower energy region of the absorption spectrum.

6.5 Experimental Methods

6.5.1 Materials and General Experimental Details.

Tetrahydrofuran was dried using an Innovative Technologies solvent purification system. 2,5-bis(trimethylstannyl)thiophene **(7)**, (3,3'-dioctyl-[2,2'-bithiophene]-5,5'-diyl)bis(trimethylstannane) **(9)**, and 4,4-dioctyl-2,6-bis(trimethylstannyl)-4*H*-silolo[3,2-*b*:4,5-*b*']dithiophene **(10)** were synthesized according to literature procedures. All other compounds were purchased from commercial sources and used without further purification. All reactions were run under argon at ambient temperature unless otherwise noted. Chromatographic separation was performed using 35-70 μm silica gel, using the eluents indicated.

6.5.2 Instrumentation

Nuclear magnetic resonance spectra were obtained on a Varion MR-400 MHz spectrometer (^{1}H at 400 MHz and ^{13}C at 100 MHz). ^{1}H NMR samples were referenced internally to residual protonated solvent ^{13}C NMR are referenced to the middle carbon peak of $CDCl_3$. UV-Visible spectroscopy were obtained using small molecule solutions in chloroform, and thin films were spun from 1:1 $CHCl_3$:*o*-DCB. The films were made by spin-coating 25 x 25 x1 mm glass slides, using a solution of 2 mg of **M1** – **M4** per 1 mL *o*-DCB and chloroform at a spin rate of 800 rpms on a Spin-Coater. All films were annealed at 140 ºC for 2 hours prior to use.

N-(pyridin-4-yl)pivalamide (2).[33] To a flame-dried 500 mL round bottom flask equipped with a stir bar and argon inlet, a solution of 4-aminopyridine (9.5 g, 101 mmol) and triethylamine (15 mL) in anhydrous DCM (50 mL) was added. The solution was cooled to 0 °C in an ice bath. A solution of pivaloyl chloride (13.1 mL, 105.9 mmol) in 20 mL of anhydrous DCM was added dropwise. The reaction temperature was maintained at 0 °C during the addition. After the addition was complete, the cooling bath was removed and the solution was allowed to warm to room temperature overnight. The reaction was quenched by addition of water and $NaHCO_3$. The organic layer was separated and rinsed with brine and dried over MgSO4. The solvent was removed under reduced pressure. Purification via recrystallization from hexanes/ethyl acetate yielded 14.72 g (82%) of **2** as a buff colored solid. ^{1}H NMR (300 MHz, Chloroform-*d*) δ 8.49 (d, *J* = 6.5 Hz, 2H), 7.49 (d, *J* = 6.4 Hz, 2H), 7.14 (s, 1H, broad), 1.32 (s, 9H).

Tetraisopropylthiuram disulfide (TITD).[33] To a flame-dried 500 mL round bottom flask equipped with a stir bar and addition funnel, was added a solution of diisopropylamine (20 mL, 143 mmol) and 40% aq. sodium hydroxide (5.72 g, 143 mmol in 14.5 mL water). The reaction mixture was cooled to -10 °C in an ice/acetone bath. Carbon disulfide (8.6 mL, 143 mmol) was added dropwise via an addition funnel over a period of 45 minutes while the temperature of the ice/acetone bath was maintained at -10 °C. After the addition was complete, an ice cold solution of potassium ferricyanide (47.5g, 144 mmol in 200 mL water) was added slowly via the addition funnel. The reaction mixture was allowed to stir for 2 h at -10 °C after which the cooling bath was removed. The reaction mixture was allowed to warm up gradually and stir at room temperature for 6 h. Dichloromethane (100 mL) was then added to the reaction flask. The organic and aqueous layers were separated. The organic layer was washed with water and dried over an. Na_2SO_4. The solution was filtered into a pre – weighed round bottom flask and the solvent was removed under reduced pressure. The solid obtained was recrystallized from hexanes/ dichloromethane to yield 14.9 g (60 %) of pure product as a canary yellow solid.

4-pivalamidopyridin-3-yl diisopropylcarbamodithioate (3).[33] N-(pyridin-4-yl)pivalamide (6 g, 33.7 mmol) was dissolved in 50 mL of anhydrous THF in a flame-dried round bottom. The solution was cooled to -78 °C in a dry ice/ acetone bath. *n*-butyllithium (39.3 mL, 1.8 M in hexanes) was added dropwise via an addition funnel. After the addition was complete, the cooling bath was removed and the reaction mixture was allowed to warm rapidly to 0 °C. It was stirred at this temperature for 3 h. An off –

white precipitate was observed. The reaction mixture was then cooled back down to -78 °C in a dry ice/ acetone bath and a solution of TITD (11.9 g, 33.7 mmol) in 55 mL of THF was added dropwise. After the addition was complete, the cooling bath was removed and the reaction mixture was allowed to warm to room temperature. After it turned clear at room temperature, the reaction was quenched by addition of 75 mL of diethyl ether and 75 mL of water. The organic layer was separated and rinsed with brine. It was then dried over an. Na_2SO_4. The solution was filtered into a pre – weighed round bottom flask and the solvent was removed via rotary evaporation. Purification by recrystallization from ethyl acetate yielded 7.10 g (60%) of **3** as a light brown solid. Purification of the filtrate from recrystallization via column chromatography yielded another 3.2 g (27%) of pure product, leading to 10.3 g (87%) of product totally.

^{1}H NMR (400 MHz, Chloroform-*d*) δ 8.60 (d, *J* = 5.7 Hz, 1H), 8.50 (s, 1H), 8.47 (s, 1H), 8.38 (d, *J* = 5.6 Hz, 1H), 1.52 (s, 12H), 1.29 (s, 9H).

2-(*tert*-butyl)thiazolo[*5,4-c*]pyridine (4).[33] 6M HCl (40 mL) was added to a round bottom flask containing **(3)** (2.8 g, 7.92 mmol). The reaction mixture was refluxed for 3 h, after which it was poured into ice. 6 M NaOH was added to the ice cold reaction mixture until the solution was strongly basic. The reaction mixture was extracted with ethyl ether. The organic layer was separated and rinsed with brine. It was then dried over an. Na_2SO_4. The solution was filtered into a pre – weighed round bottom flask. Evaporation of eh solvent under reduced pressure yielded 1.34 g (quant.) of product as a light brown oil. The product obtained was pure by NMR and was used without further

purification. ^{1}H NMR (400 MHz,) δ 9.15 (s, 1H), 8.61 (d, *J* = 5.6 Hz, 1H), 7.87 (d, *J* = 6.5 Hz, 1H).

2-(*tert*-butyl)thiazolo[*5,4-c*]pyridin-4(5*H*)-one (5).[38] 2-(*tert*-butyl)thiazolo[5,4-*c*]pyridine (1.35 g, 7.02 mmol), mCPBA (6.06 g, 35.11 mmol) and 35 mL chloroform was added to a flame dried round bottom flask. The reaction was allowed to stir at room temperature for 6 h after which it was quenched by pouring into water. The organic layer was separated and washed several times with sat. $NaHCO_3$ after which, it was washed with water, followed by brine. The organic layer was dried over an. Na_2SO_4. It was filtered into a pre-weighed round bottom flask and the solvent was removed under reduced pressure. 1.4 g (96%) of product was obtained as a white solid. The crude product was carried forward without further purification.

^{1}H NMR (400 MHz, Chloroform-*d*) δ 8.72 (d, *J* = 1.3 Hz, 1H), 8.23 (dd, *J* = 7.1, 1.8 Hz, 1H), 7.76 (d, *J* = 0.6 Hz, 1H), 1.50 (s, 9H). ^{13}C NMR (101 MHz, Chloroform-*d*) δ ^{13}C NMR (101 MHz , Chloroform-*d*) δ 187.75, 158.19, 145.45, 144.02, 132.17, 117.06, 38.84, 30.66.

2-(*tert*-butyl)-4-chlorothiazolo[5,4-*c*]pyridine (6). 2-(*tert*-butyl)thiazolo[5,4-*c*]pyridin-4(5*H*)-one (1.3 g, 6.24 mmol) was refluxed in 18 mL of $POCl_3$ for 2 h. The reaction mixture was evaporated and extracted with ethyl acetate. The organic layers were washed with $NaHCO_3$ followed water and brine. The organic layer was dried over an. Na_2SO_4. It was filtered into a pre-weighed round bottom flask and the solvent was removed under reduced pressure. The residue was purified by flash column chromatography using

hexanes: ethyl acetate (90:10→ 100:0) as the eluent. 1.1g (78%) of the product was obtained as a white solid.

^{1}H NMR (400 MHz, Chloroform-*d*) δ 8.39 (d, *J* = 5.6 Hz, 1H), 7.78 (d, *J* = 5.5 Hz, 1H), 1.54 (s, 10H).

2-(*tert*-butyl)-4-iodothiazolo[5,4-*c*]pyridine (S1). KI (0.73 g, 4.4mmol) was added to a stirred solution of **6** in dry propionitrile (3 mL) at room temperature. Chlorotrimethylsilane (0.24 mL, 2.20 mmol) was added to the slurry causing it to turn bright yellow. The slurry was refluxed overnight after which it was cooled to room temperature. It was then poured in to NaOH solution in crushed ice. The aqueous phase was extracted with ethyl ether. Organic layer was separated and rinsed with water followed by brine. It was then dried over an. Na_2SO_4 and filtered into a pre-weighed round bottom flask. The solvent was removed under reduced pressure. An inseparable mixture of starting material and product was obtained as evidenced by the NMR. ^{1}H NMR (400 MHz, DMSO-d_6) δ 8.40 (d, *J* = 5.5 Hz, 1H), 8.33 (d, *J* = 5.4 Hz, 1H), 7.95 (d, *J* = 5.6 Hz, 1H), 7.92 (d, *J* = 5.3 Hz, 1H), 1.44 (s, 9H), 1.43 (s, 12H).

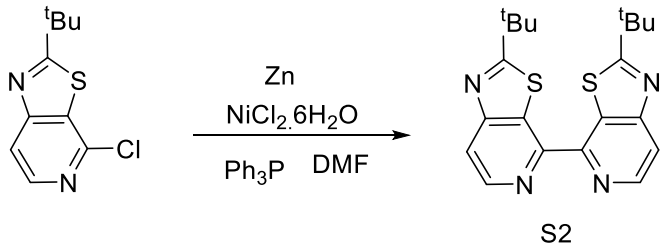

S2

Scheme 6.5.1 Synthesis of 2,2'-di-*tert*-butyl-4,4'-bithiazolo[5,4-*c*]pyridine

2,2'-di-*tert*-butyl-4,4'-bithiazolo[5,4-*c*]pyridine (S2). Zinc powder (0.15 g, 2.21 mmol) was added to a stirred, deep blue solution of $NiCl_2.6H_2O$ (0.53 g, 2.21 mmol) and Ph_3P (2.31 g, 8.82 mmol) in anhydrous DMF under Argon at 50 °C. After 2h, the color of the mixture changed to red – brown. At this point, **6** was added to the reaction mixture. The reaction was stirred overnight at 50 °C. The reaction was cooled to room temperature and quenched by pouring into NH_4OH solution. It was stirred under a stream of air for an additional 30 mins until the mixture turned blue. The solid obtained was filtered and purified by column chromatography using hexanes: chloroform (90:10) as the eluent to yield 0.24g (58%) of product as an off – white solid. NMR shows leftover triphenylphosphine oxide as well as residual DMF.

^{1}H NMR (400 MHz, Chloroform-*d*) δ 8.84 (d, *J* = 5.5 Hz, 2H), 7.95 (d, *J* = 5.4 Hz, 2H), 1.61 (s, 18H).

2,5-bis(2-(*tert*-butyl)thiazolo[5,4-*c*]pyridin-4-yl)thiophene (M1). 2,5-bis(trimethylstannyl)thiophene (0.2 g, 0.59 mmol) and 2-(*tert*-butyl)-4-chlorothiazolo[5,4-*c*]pyridine (0.27 g, 1.17 mmol) were added to a flame - dried round bottom flask. 6 mL of toluene was added. The resulting solution was deoxygenated for 45 min. $Pd(PPh_3)_4$ (68 mg, 0.059 mmol) was added under a stream of inert gas. The reaction mixture was refluxed for 36 h after which it was cooled and poured into water. The organic layer was separated and washed several times with 1M KF. The organic layer was washed with water, followed by brine. It was then dried over an. Na_2SO_4 and filtered into a pre-weighed round bottom flask. The solvent was removed under reduced pressure. Purification by column chromatography using chloroform as the eluent yielded 0.16 g

(73%) of pure product as a light yellow solid. ^{1}H NMR (300 MHz, Chloroform-*d*) δ 8.68 (d, *J* = 5.5 Hz, 2H), 7.98 (s, 2H), 7.83 (d, *J* = 5.5 Hz, 2H), 1.60 (s, 18H). ^{13}C NMR (101 MHz, Chloroform-*d*) δ 159.92, 146.88, 145.27, 127.85, 127.46, 116.09, 115.99, 38.85, 30.66.

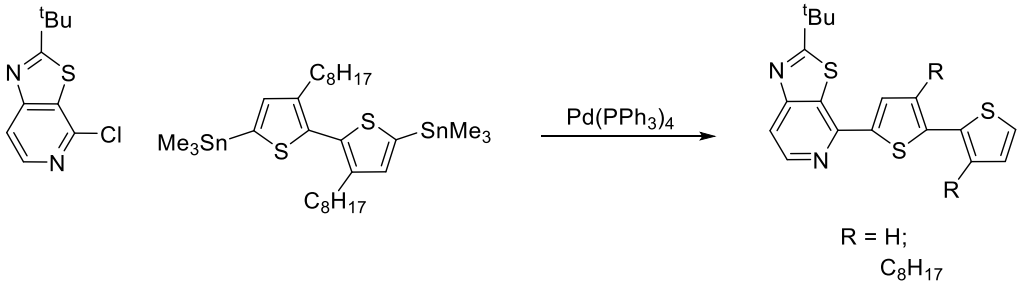

Scheme 6.5.2. Reaction of **6** with (3,3'-disubstituted-[2,2'-bithiophene]-5,5'-diyl)bis(trimethylstannane)

2-(*tert*-butyl)-4-(3,3'-dioctyl-[2,2'-bithiophen]-5-yl)thiazolo[5,4-*c*]pyridine (S3). A solution of **6** (0.3 g, 1.32 mmol) and (3,3'-dioctyl-[2,2'-bithiophene]-5,5'-diyl)bis(trimethylstannane) (0.46 g, 0.63 mmol) in 6 – 8 mL of toluene was degassed for 30 mins. $Pd(PPh_3)_4$ (72.8 mg, 0.06 mmol) was then added under a stream of inert gas. The reaction was refluxed for 36 h, after which it was cooled and poured into water. The organic layer was separated and washed several times with 1M KF. The organic layer was washed with water, followed by brine. It was then dried over an. Na_2SO_4 and filtered into a pre-weighed round bottom flask. The solvent was removed under reduced pressure. The dark oil obtained was purified by column chromatography (1:1 hexanes: DCM → 100% DCM) to give 0.21 g (43%) of 2-(*tert*-butyl)-4-(3,3'-dioctyl-[2,2'-bithiophen]-5-yl)thiazolo[*5,4-c*]pyridine as a light yellow oil. Small amounts of 2-(*tert*-butyl)-4-(5'-(2-(*tert*-butyl)thiazolo[5,4-*c*]pyridin-4-yl)-3,3'-dioctyl-[2,2'-bithiophen]-5-yl)thiazolo[4,5-

c]pyridine was obtained according to the NMR. ^{1}H NMR (400 MHz, Chloroform-*d*) δ 8.90 (s, 1H), 8.61 (d, *J* = 5.5 Hz, 1H), 8.39 (d, *J* = 5.6 Hz, 0.2 H), 7.89 (s, 1H), 7.76 (d, *J* = 5.5 Hz, 1H), 7.66 (s, 1H), 7.33 (d, *J* = 5.2 Hz, 1H), 6.99 (d, *J* = 5.2 Hz, 1H), 2.62 – 2.55 (m, 3H), 1.59 (s, 9H), 1.53 (s, 5H), 1.24 (d, *J* = 4.0 Hz, 19H), 0.86 (t, *J* = 6.6 Hz, 3H), 0.82 (t, *J* = 6.8 Hz, 3H).

2-(*tert*-butyl)-4-(4-hexylthiophen-2-yl)thiazolo[5,4-*c*]pyridine (14). A solution of (4-hexylthiophen-2-yl)trimethylstannane (1.31 g, 3.97 mmol) and **6** (0.9 g, 3.97 mmol) in toluene (10 mL) was degassed for 30 mins. $Pd_2(dba)_3$ (72.7 mg, 0.08 mmol) and P(*o*-tolyl)$_3$ (0.097 g, 0.31 mmol) were then added under a stream of inert gas. The reaction was degassed for an additional 15-20 minutes after which it was refluxed for 36 h. It was the cooled and poured into water. The organic layer was separated and washed several times with 1M KF. The organic layer was washed with water, followed by brine. It was then dried over an. Na_2SO_4 and filtered into a pre-weighed round bottom flask. The solvent was removed under reduced pressure. Purification by column chromatography yielded 1.12 g (79%) of the product as pale yellow oil.

^{1}H NMR (400 MHz, Chloroform-*d*) δ 8.60 (d, *J* = 5.5 Hz, 1H), 7.75 (d, *J* = 5.5 Hz, 1H), 7.60 (s, 1H), 7.10 (s, 1H), 2.69 (t, *J* = 7.7 Hz, 2H), 1.74 – 1.65 (m, 2H), 1.58 (s, 9H), 1.39 – 1.32 (m, 6H, broad), 0.92 – 0.88 (t, 3H).

4-(5-bromo-4-hexylthiophen-2-yl)-2-(*tert*-butyl)thiazolo[5,4-*c*]pyridine (15) NBS (0.58 g, 3.28 mmol) was added portion-wise to a solution of **14** in DMF at room temperature. The reaction was stirred overnight at room temperature after which it was

poured into ice – cold water. It was extracted into hexanes. Organic layer was separated and rinsed with water followed by brine. It was then dried over an. Na_2SO_4 and filtered into a pre-weighed round bottom flask. The solvent was removed under reduced pressure. Recrystallization from 95 % EtOH afforded pure product (1.08 g, 79%) as an off – white solid.

^{1}H NMR (400 MHz, Chloroform-*d*) δ 8.57 (d, *J* = 5.5 Hz, 1H), 7.76 (d, *J* = 5.5 Hz, 1H), 7.43 (s, 1H), 2.67 – 2.61 (m, 2H), 1.66 (q, *J* = 7.4 Hz, 2H), 1.58 (s, 9H), 1.44 – 1.30 (m, 6H), 0.91 (t, 3H).^{13}C NMR (101 MHz, Chloroform-*d*) δ 159.81, 145.27, 143.29, 127.41, 115.71, 38.80, 31.63, 30.66, 29.80, 29.70, 28.89, 22.65, 14.12.

4,4'-(3,3''-dihexyl-[2,2':5',2''-terthiophene]-5,5''-diyl)bis(2-(tert-butyl)thiazolo[5,4-c]pyridine) (M2). 2,5-bis(trimethylstannyl)thiophene (0.085g, 0.21 mmol) and **15** (0.2 g, 0.46 mmol) were added to a flame - dried round bottom flask. 6 mL of toluene was added. The resulting solution was deoxygenated for 45 min. $Pd(PPh_3)_4$ (24 mg, 0.021 mmol) was added under a stream of inert gas. The reaction mixture was refluxed for 36 h after which it was cooled and poured into water. The organic layer was separated and washed several times with 1M KF. The organic layer was washed with water, followed by brine. It was then dried over an. Na_2SO_4 and filtered into a pre-weighed round bottom flask. The solvent was removed under reduced pressure. Purification by column chromatography using hexanes:EtOAc (98:2 + few drops Et_3N) as the eluent yielded 0.12 g (72%) of pure product as a light yellow solid.

^{1}H NMR (400 MHz, Chloroform-*d*) δ 8.62 (d, *J* = 5.5 Hz, 2H), 7.77 (d, *J* = 5.5 Hz, 2H), 7.62 (s, 2H), 7.25 (s, 2H), 2.91 (t, *J* = 8.0 Hz, 4H) 1.77 (q, *J* = 7.9 Hz, 4H), 1.60 (s, 18H), 1.47 (q, *J* = 7.7 Hz, 4H), 1.37 (m, 8H, broad), 0.91 (t, *J* = 8 Hz , 6H)

2,5-bis(5-(2-(*tert*-butyl)thiazolo[5,4-*c*]pyridin-4-yl)-3-hexylthiophen-2-yl)thieno[3,2-*b*]thiophene (M3). 2,5-bis(trimethylstannyl)thieno[3,2-*b*]thiophene (0.13 g, 0.28 mmol) and **15** (0.3 g, 0.62 mmol) were added to a flame - dried round bottom flask. 5 mL of toluene was added. The resulting solution was deoxygenated for 45 min. $Pd_2(dba)_3$ (5.16 mg, 0.05mmol) and P(*o*-tolyl)$_3$ was added under a stream of inert gas. The reaction mixture was refluxed for 36 h after which it was cooled and poured into water. The organic layer was separated and washed several times with 1M KF. The organic layer was washed with water, followed by brine. It was then dried over an. Na_2SO_4 and filtered into a pre-weighed round bottom flask. The solvent was removed under reduced pressure. Purification by column chromatography using hexanes: EtOAc (97:3 → 94:6) and 5% Et_3N as the eluent yielded 0.18 g (75%) of pure product as a light yellow solid.

^{1}H NMR (400 MHz, Chloroform-*d*) δ 8.60 (d, *J* = 5.5 Hz, 2H), 7.76 (d, *J* = 5.5 Hz, 2H), 7.61 (s, 2H), 7.26 (s, 2H), 2.89 (t, *J* = 8.0 Hz, 4H), 1.78 – 1.72 (m, 4H), 1.59 (s, 18H), 1.46 (t, *J* = 7.1 Hz, 6H), 1.32 (t, *J* = 7.3 Hz, 12H).

4,4'-((4,4-dioctyl-4*H*-silolo[3,2-*b*:4,5-*b*']dithiophene-2,6-diyl)bis(4-hexylthiophene-5,2-diyl))bis(2-(*tert*-butyl)thiazolo[5,4-*c*]pyridine) (M4). 4,4-dioctyl-2,6-bis(trimethylstannyl)-4*H*-silolo[3,2-b:4,5-*b*']dithiophene (0.23 g, 0.31 mmol) and **15** (0.3 g, 0.69 mmol) were added to a flame - dried round bottom flask. 5 mL of toluene was

added. The resulting solution was deoxygenated for 45 min. $Pd_2(dba)_3$ (5.71 mg, 0.05mmol) and P(*o*-tolyl)$_3$ (7.61 mg, 0.025 mmol) was added under a stream of inert gas. The reaction mixture was refluxed for 36 h after which it was cooled and poured into water. The organic layer was separated and washed several times with 1M KF. The organic layer was washed with water, followed by brine. It was then dried over an. Na_2SO_4 and filtered into a pre-weighed round bottom flask. The solvent was removed under reduced pressure. Purification by column chromatography using hexanes: EtOAc (97:3 → 94:6) and 5% Et_3N as the eluent yielded 0.14 g (42%) of pure product as light yellow oil.

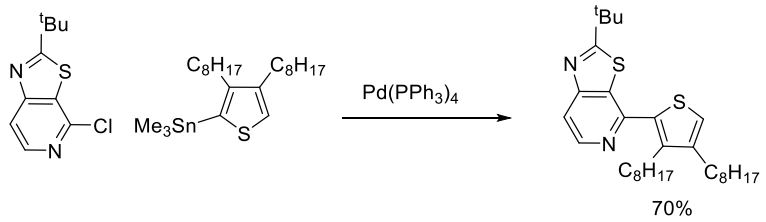

Scheme 6.5.3 Synthesis of 2-(*tert*-butyl)-4-(3,4-dioctylthiophen-2-yl)thiazolo[5,4-*c*]pyridine

2-(*tert*-butyl)-4-(3,4-dioctylthiophen-2-yl)thiazolo[5,4-*c*]pyridine. (3,4-dioctylthiophen-2-yl)trimethylstannane (2.18 g, 4.63 mmol) and **6** (0.3 g, 1.32 mmol) were added to a flame - dried round bottom flask. 7 mL of toluene was added. The resulting solution was deoxygenated for 45 min. $Pd(PPh_3)_4$ (0.15 g, 0.13 mmol) was added under a stream of inert gas. The reaction mixture was refluxed for 36 h after which it was cooled and poured into water. The organic layer was separated and washed several times with 1M KF. The organic layer was washed with water, followed by brine. It was

then dried over an. Na_2SO_4 and filtered into a pre-weighed round bottom flask. The solvent was removed under reduced pressure. Purification by column chromatography using hexanes: EtOAc (97:3 → 95:5) as the eluent afforded 0.4 g (61%) of pure product as light yellow oil. ^{1}H NMR (400 MHz, Chloroform-*d*) δ 8.66 (d, *J* = 5.4 Hz, 1H), 7.78 (d, *J* = 8 Hz, 1H), 7.05 (s, 1H), 2.81 (t, *J* = 8 Hz, 2H), 2.58 (t, *J* = 5.4 Hz, 2H), 1.69 (m, 2H), 1.53 (s, 9H), 1.47 – 1.24 (m, 14H), 1.09 (s, 8H), 0.89 (t, *J* = 6.7 Hz, 3H), 0.83 (t, *J* = 7.1 Hz, 3H).

2-(*tert*-butyl)-4-(5-iodo-3,4-dioctylthiophen-2-yl)thiazolo[*5,4-c*]pyridine. NIS (0.11 g, 0.46 mmol) was added portion-wise to a solution of 2-(*tert*-butyl)-4-(3,4-dioctylthiophen-2-yl)thiazolo[5,4-*c*]pyridine (0.21 g, 0.42 mmol) in chloroform (4 mL) and AcOH (3 mL) at room temperature. The reaction was stirred overnight at room temperature after which it was poured into ice – cold water. It was extracted into hexanes. Organic layer was separated and rinsed with water followed by brine. It was then dried over an. Na_2SO_4 and filtered into a pre-weighed round bottom flask. The solvent was removed under reduced pressure. The crude product (0.20 g, 80%) was carried forward without further purification.

^{1}H NMR (400 MHz, Chloroform-*d*) δ 8.66 (d, *J* = 5.6 Hz, 1H), 7.80 (d, *J* = 5.4 Hz, 1H), 2.85 (t, *J* = 8 Hz, 2H), 2.58 (t, *J* = 8 Hz, 2H), 1.54 (s, 9H), 1.34 – 1.27 (m, 16H), 1.09 (s, 8H), 0.89 (t, *J* = 6.8 Hz, 3H), 0.83 (t, *J* = 7.2 Hz, 3H).

7-bromo-2-(*tert*-butyl)-4-(5-iodo-3,4-dioctylthiophen-2-yl)thiazolo[*5,4-c*]pyridine.

Bromine (57 mg, 0.35 mmol) was added to a solution of 2-(*tert*-butyl)-4-(5-iodo-3,4-dioctylthiophen-2-yl)thiazolo[5,4-*c*]pyridine (0.2 g, 0.32 mmol) in 3 mL AcOH and 5 mL chloroform. The reaction was stirred at room temperature overnight. The reaction was quenched by addition of water and sodium bisulfite after which it was extracted with hexanes. Organic layer was separated and rinsed with water followed by brine. It was then dried over an. Na_2SO_4 and filtered into a pre-weighed round bottom flask. The solvent was removed under reduced pressure. Purification via column chromatography using chloroform as the eluent afforded pure product (0.09 g) as a pale yellow oil in 40% yield.

^{1}H NMR (400 MHz, Chloroform-*d*) δ 8.73 (s, 1H), 2.79 (t, *J* = 8.0 Hz, 2H), 2.58 (t, *J* = 8.0 Hz, 2H), 1.37 (m, 4H), 1.34 – 1.24 (m, 20H), 1.12 (s, 9H), 0.97 – 0.82 (m, 6H).

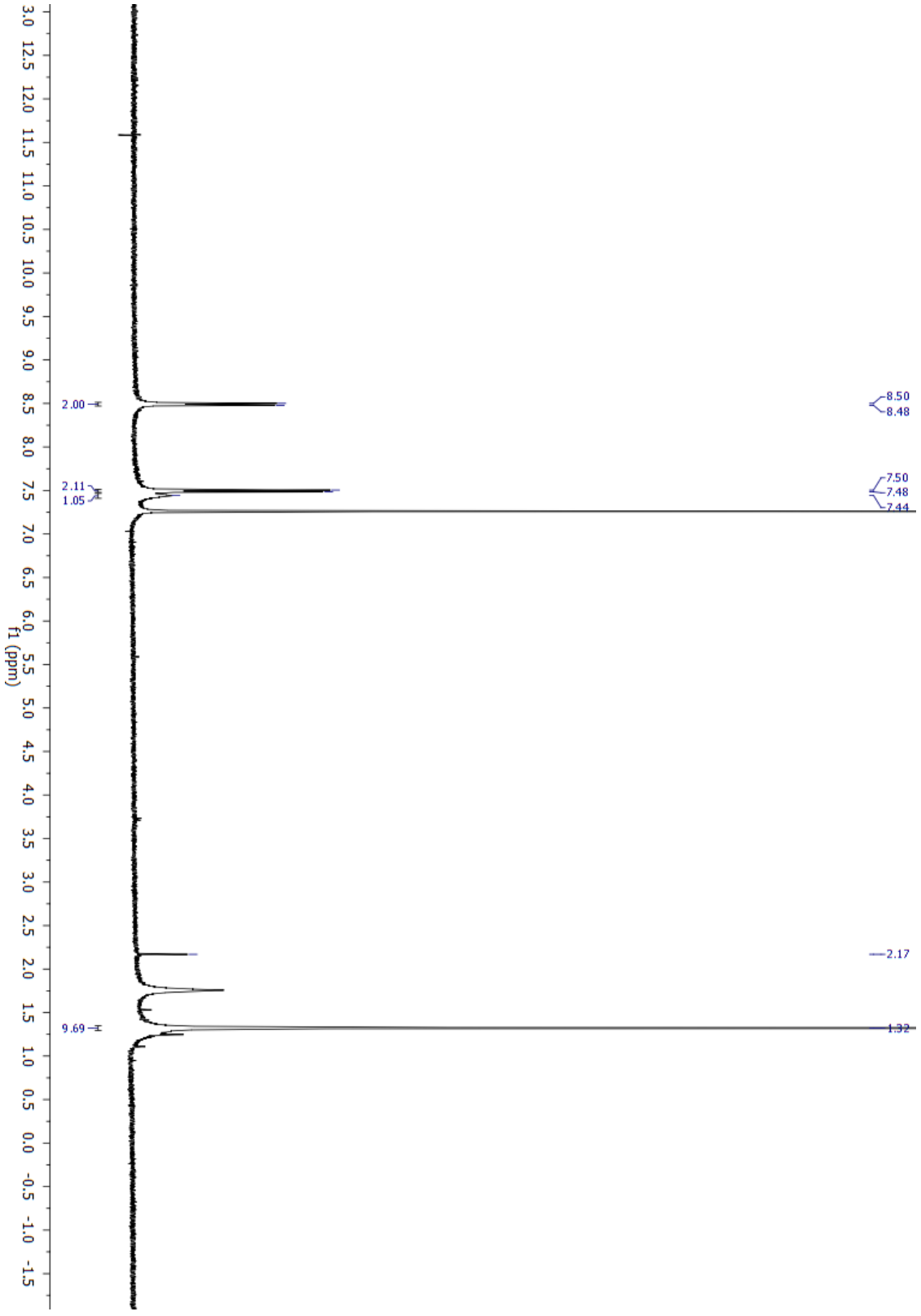

Figure 6.5.1 ^{1}H NMR of N-(pyridin-4-yl)pivalamide

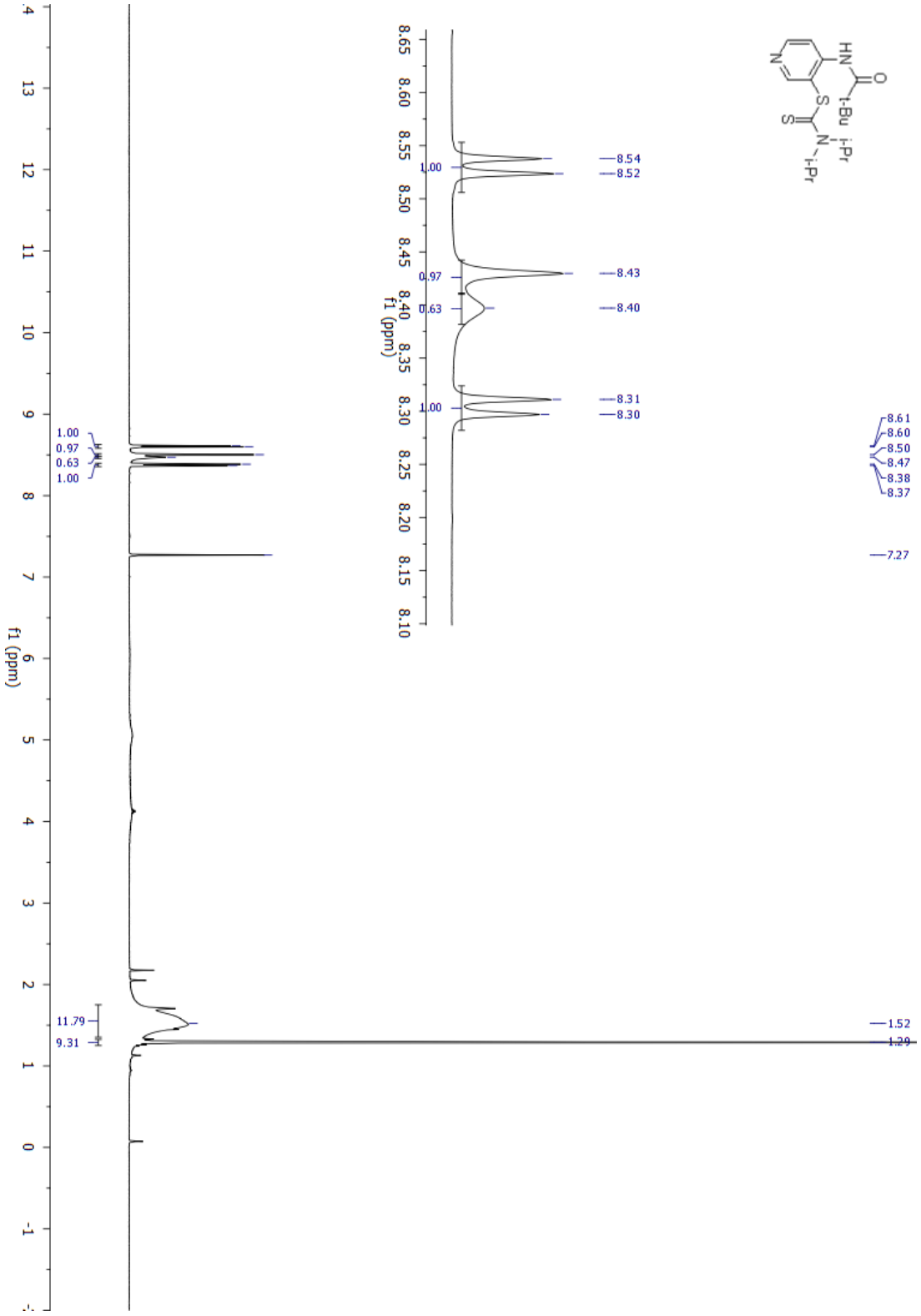

Figure 6.5.2 ^{1}H NMR of 4-pivalamidopyridin-3-yl diisopropylcarbamodithioate

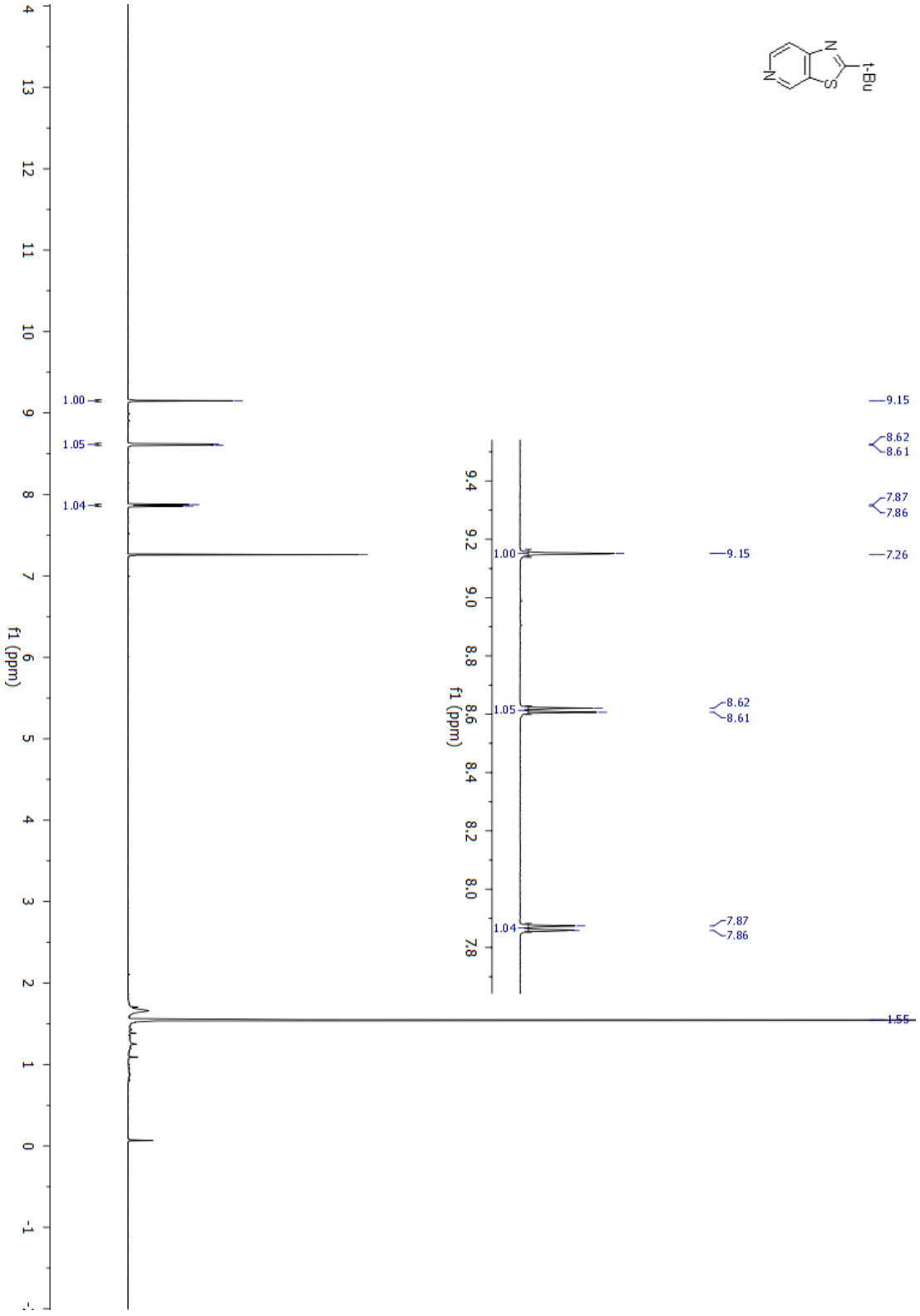

Figure 6.5.3 ^{1}H NMR of 2-(*tert*-butyl)thiazolo[5,4-*c*]pyridine

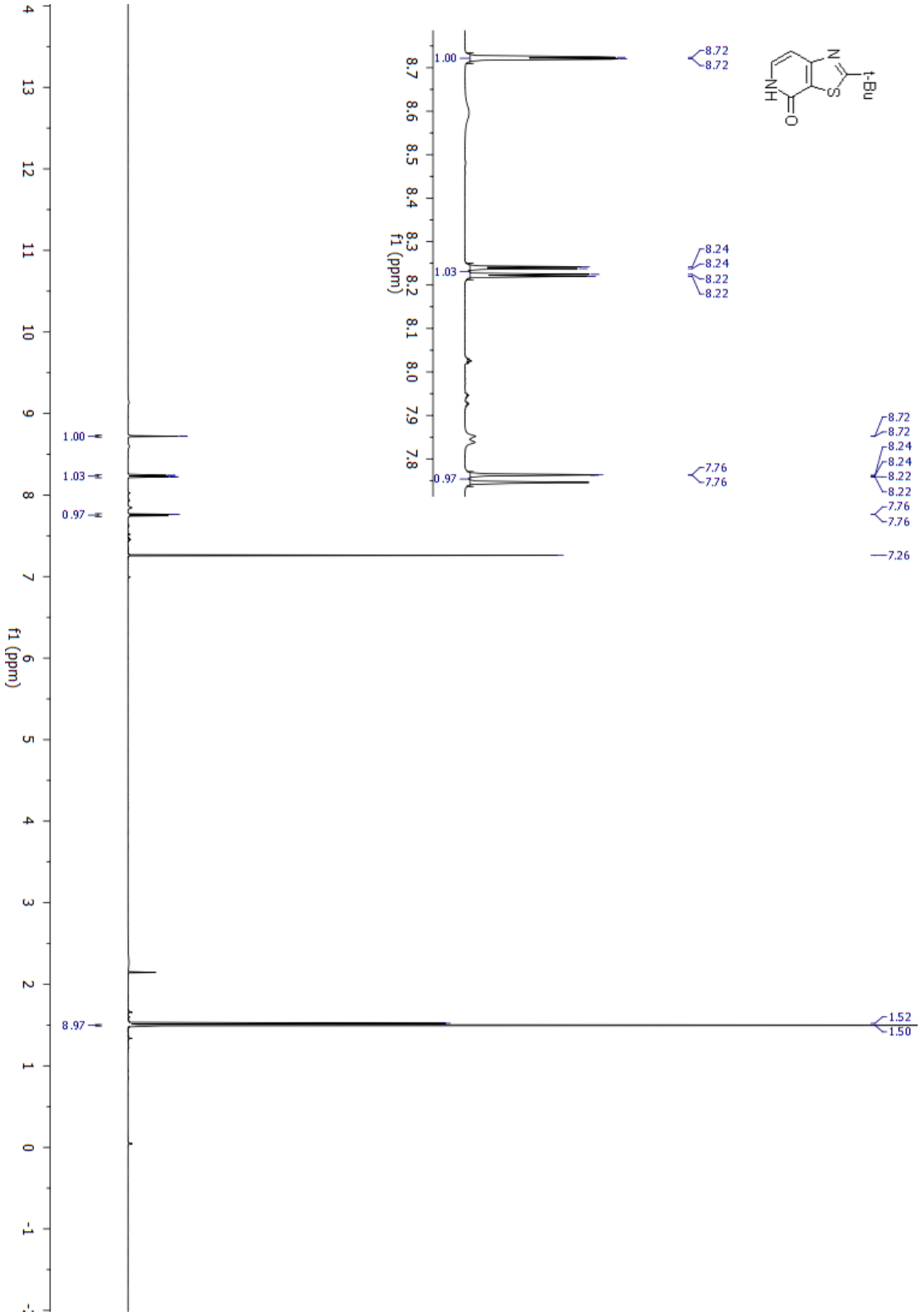

Figure 6.5.4 ^{1}H NMR of 2-(*tert*-butyl)thiazolo[5,4-*c*]pyridin-4(5*H*)-one

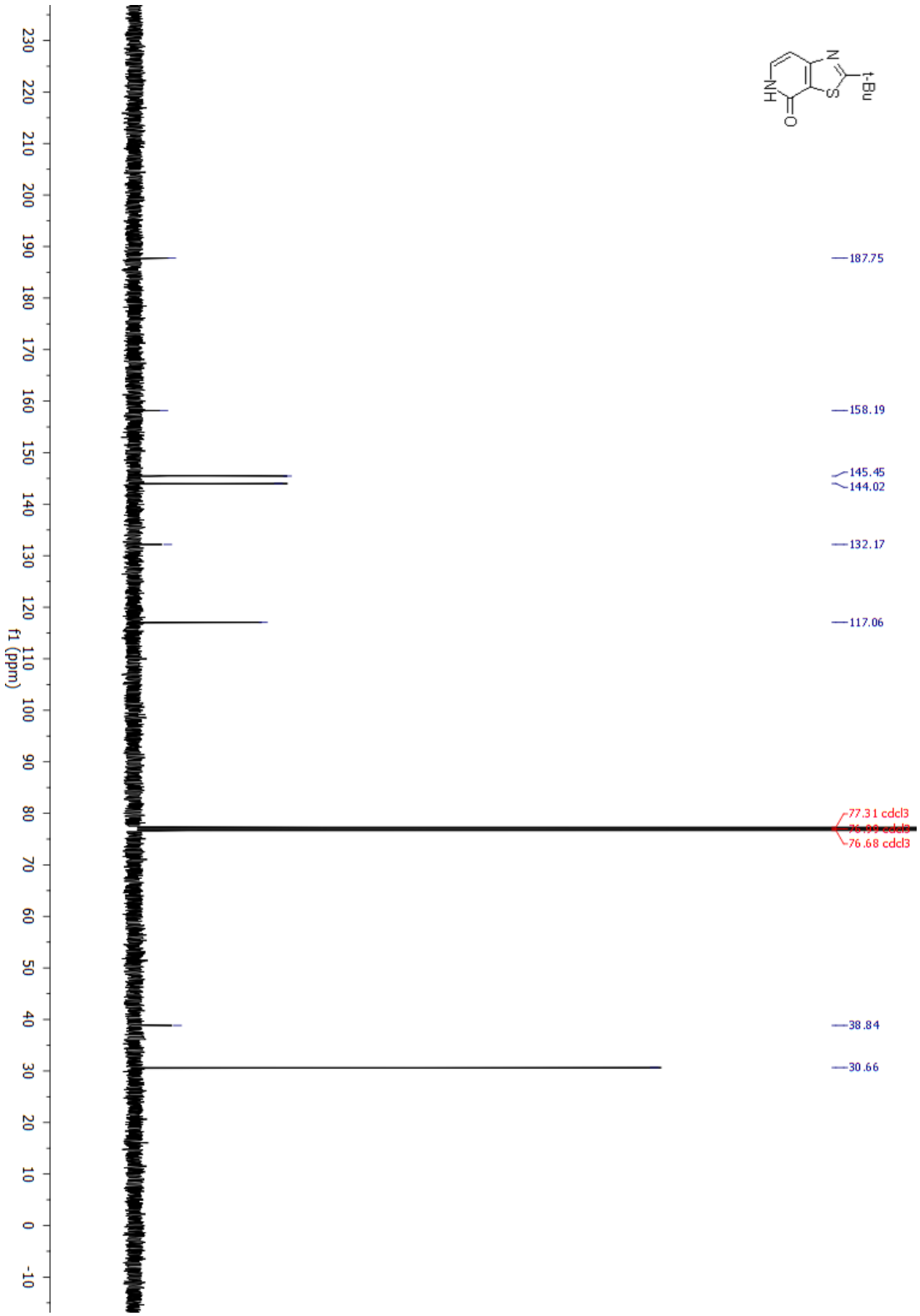

Figure 6.5.5 ^{13}C NMR of 2-(*tert*-butyl)thiazolo[5,4-*c*]pyridine

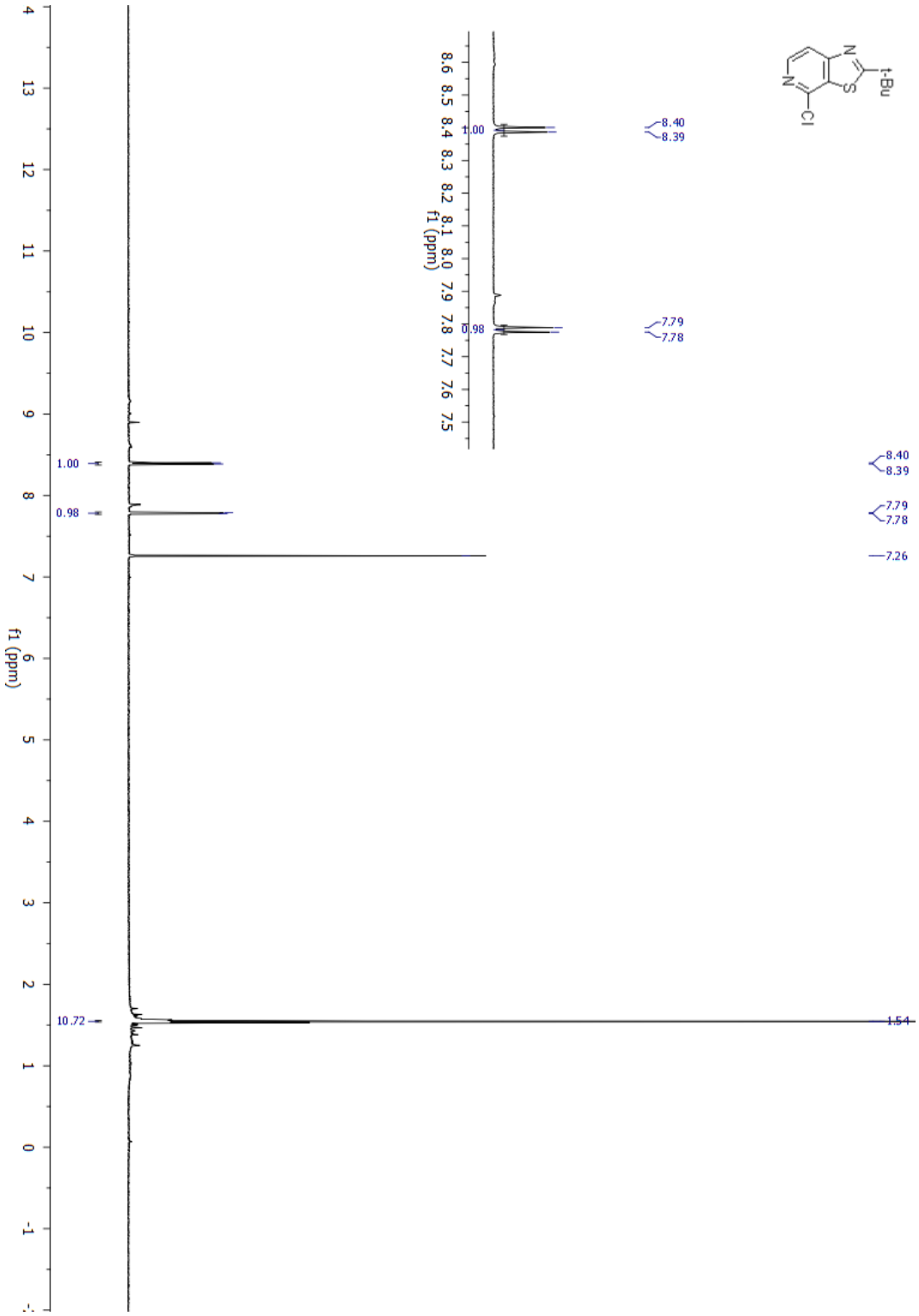

Figure 6.5.6 ^{1}H NMR of 2-(*tert*-butyl)-4-chlorothiazolo[5,4-*c*]pyridine

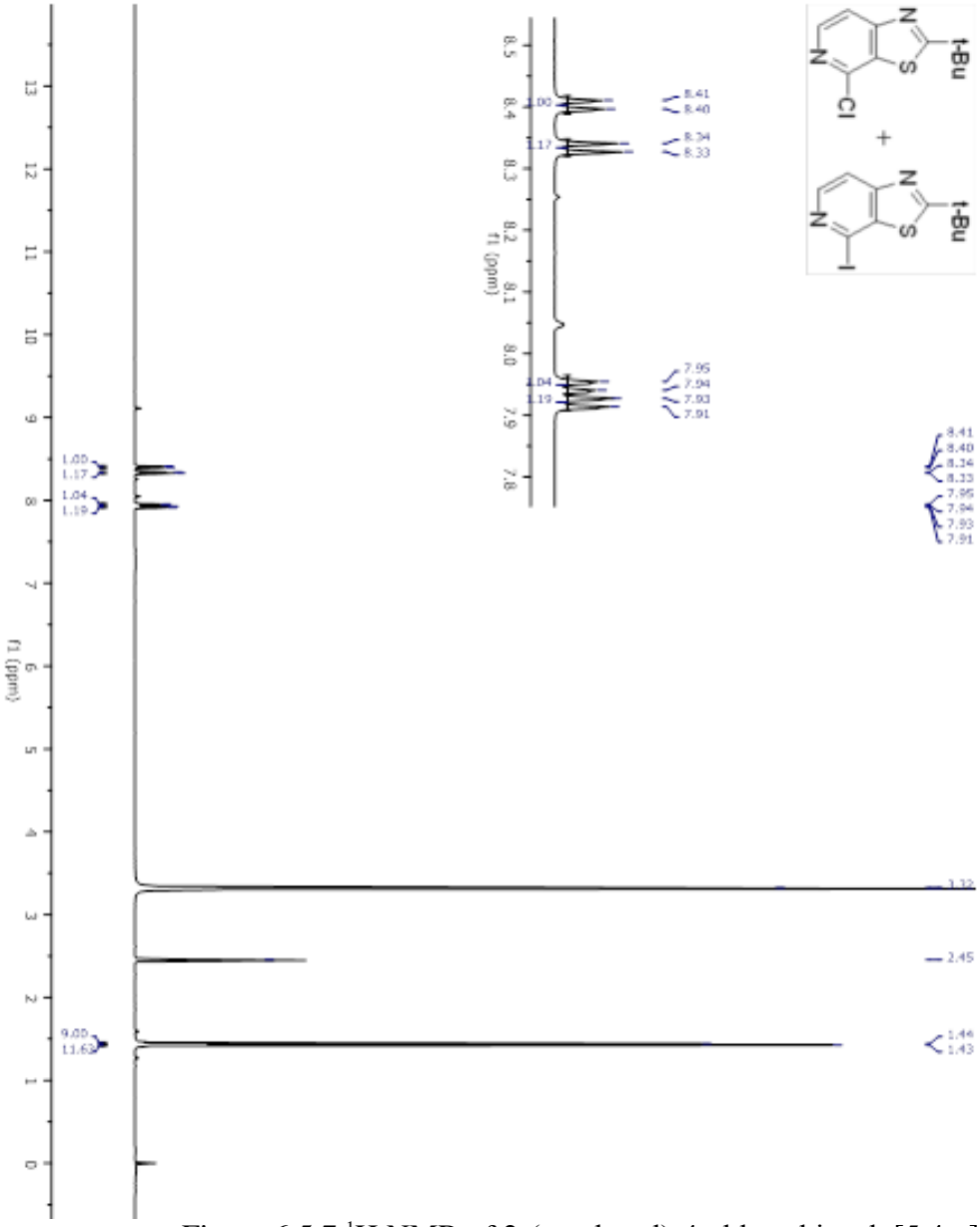

Figure 6.5.7 ^{1}H NMR of 2-(*tert*-butyl)-4-chlorothiazolo[5,4-*c*]pyridine and ^{1}H NMR of 2-(*tert*-butyl)-4-iodothiazolo[5,4-*c*]pyridine

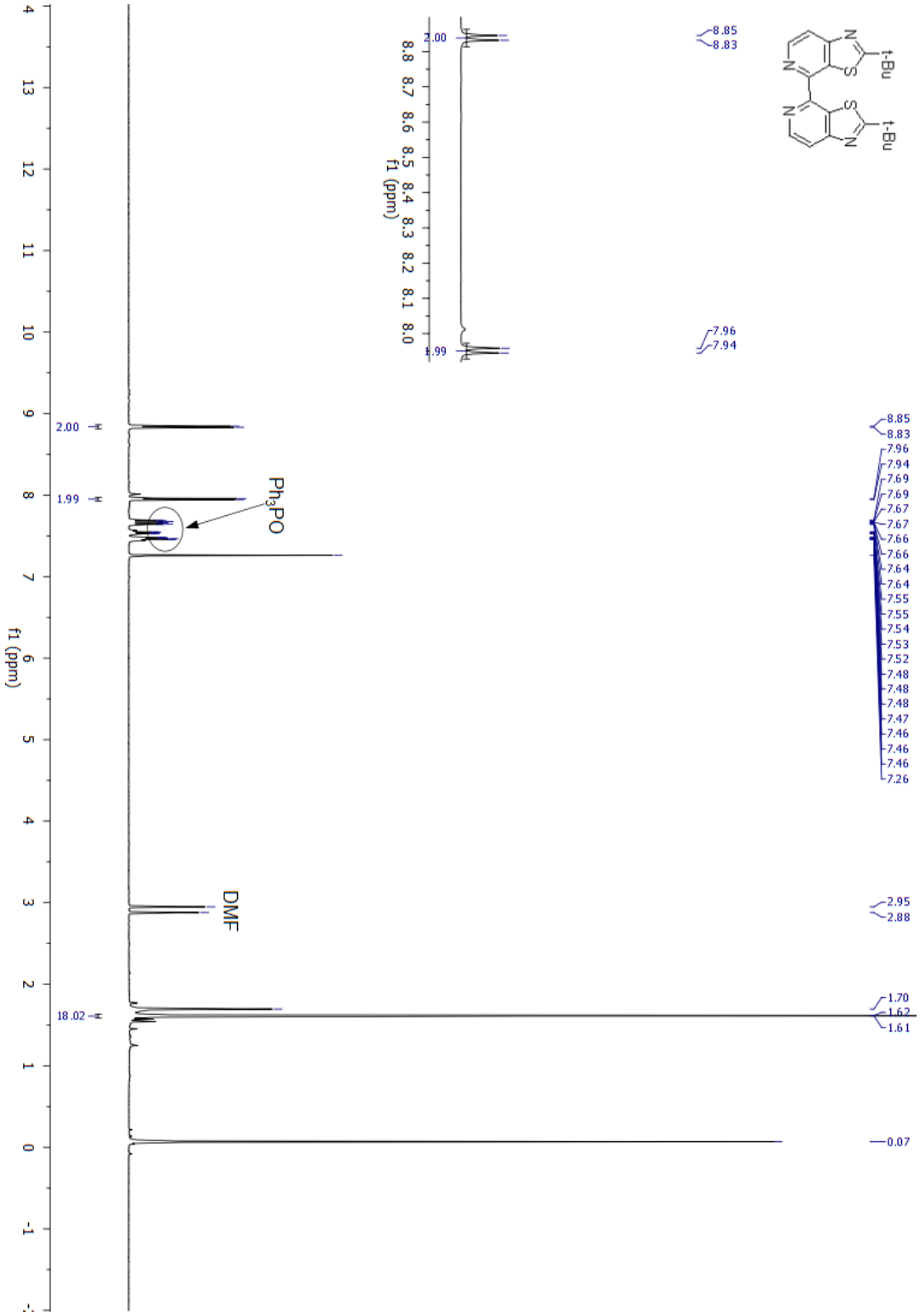

Figure 6.5.8 ^{1}H NMR of 2,2'-di-*tert*-butyl-4,4'-bithiazolo[5,4-*c*]pyridine (S2)

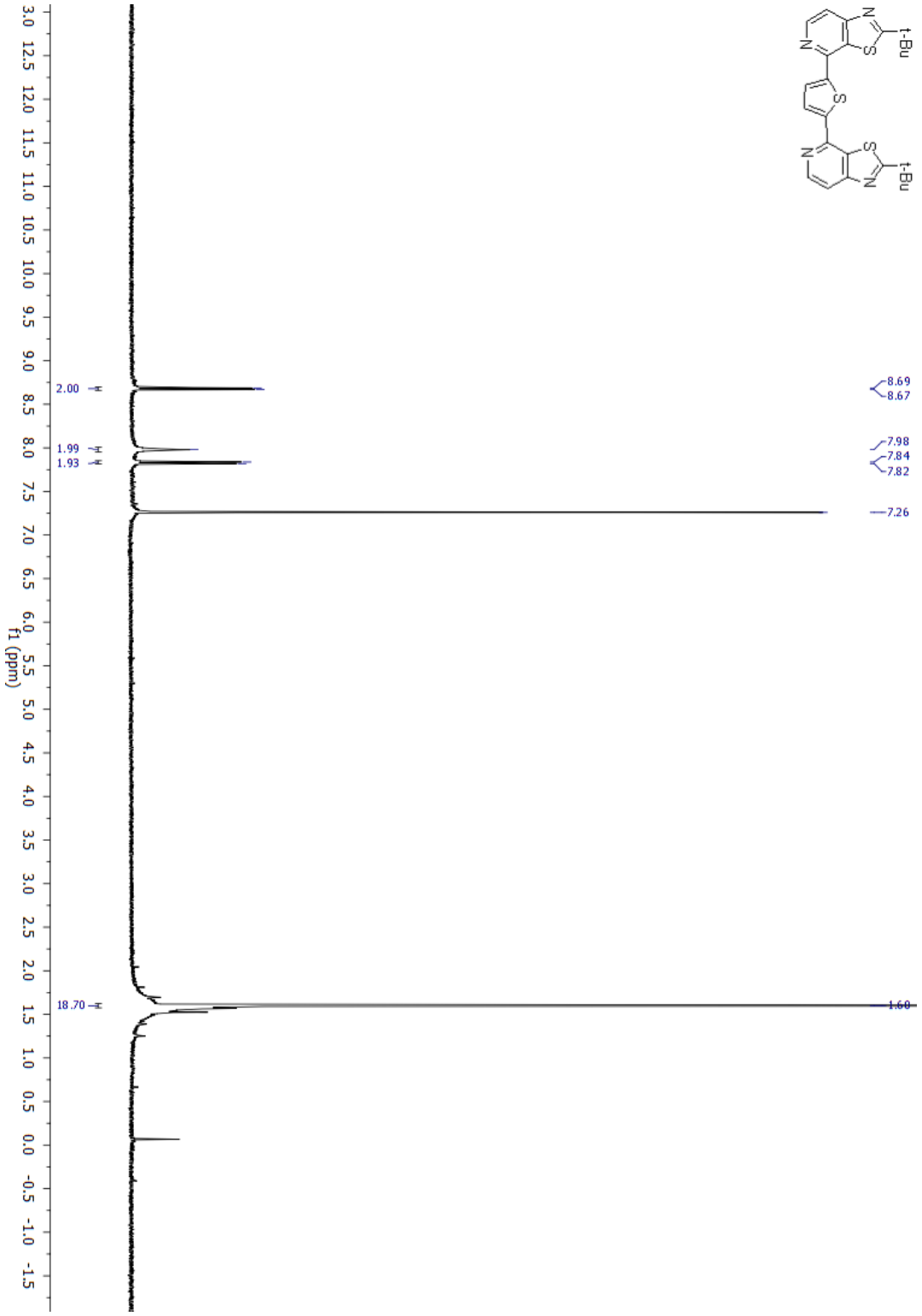

Figure 6.5.9 ^{1}H NMR of 2,5-bis(2-(*tert*-butyl)thiazolo[5,4-*c*]pyridin-4-yl)thiophene

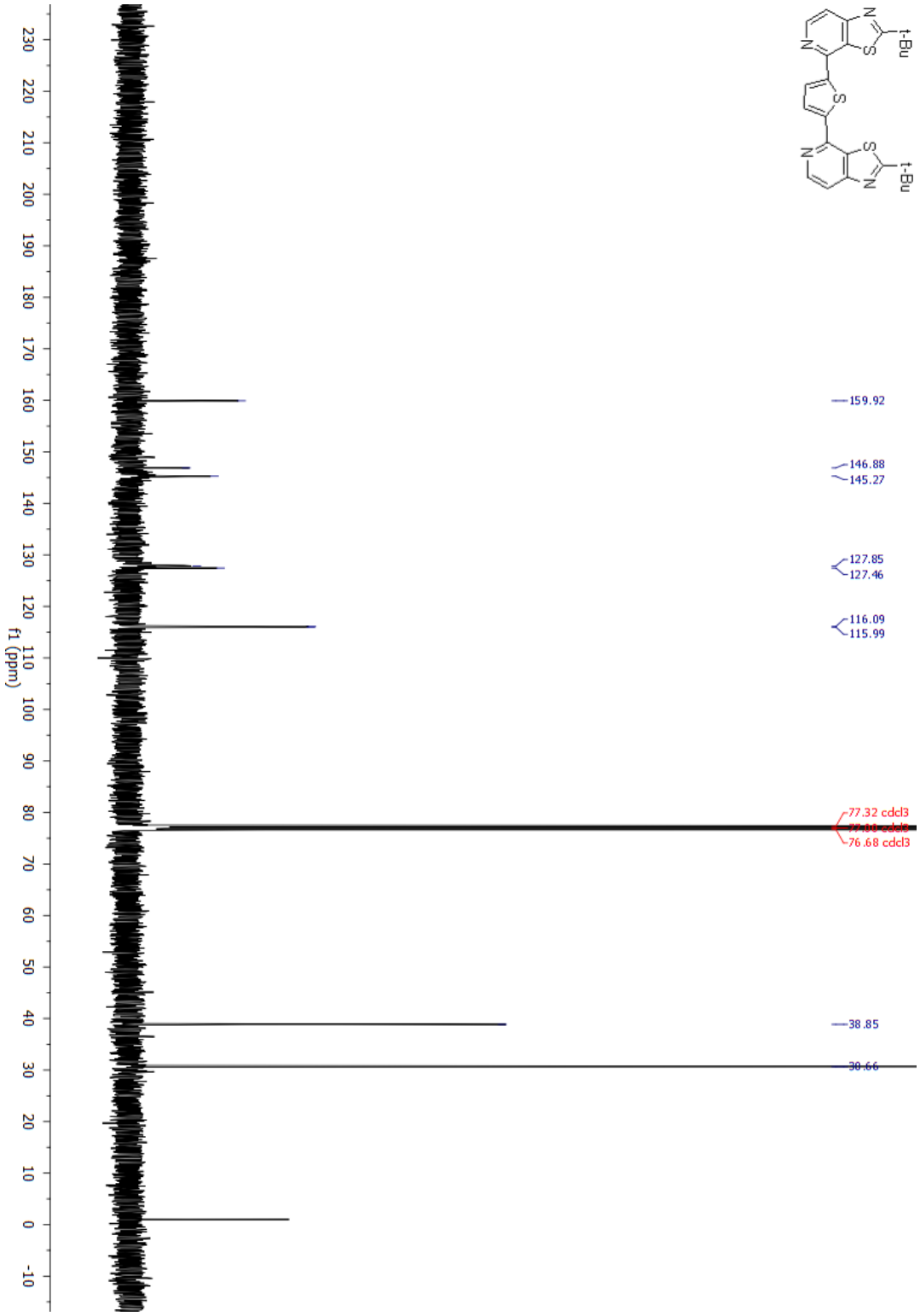

Figure 6.5.10 ^{13}C NMR of 2,5-bis(2-(*tert*-butyl)thiazolo[5,4-*c*]pyridin-4-yl)thiophene

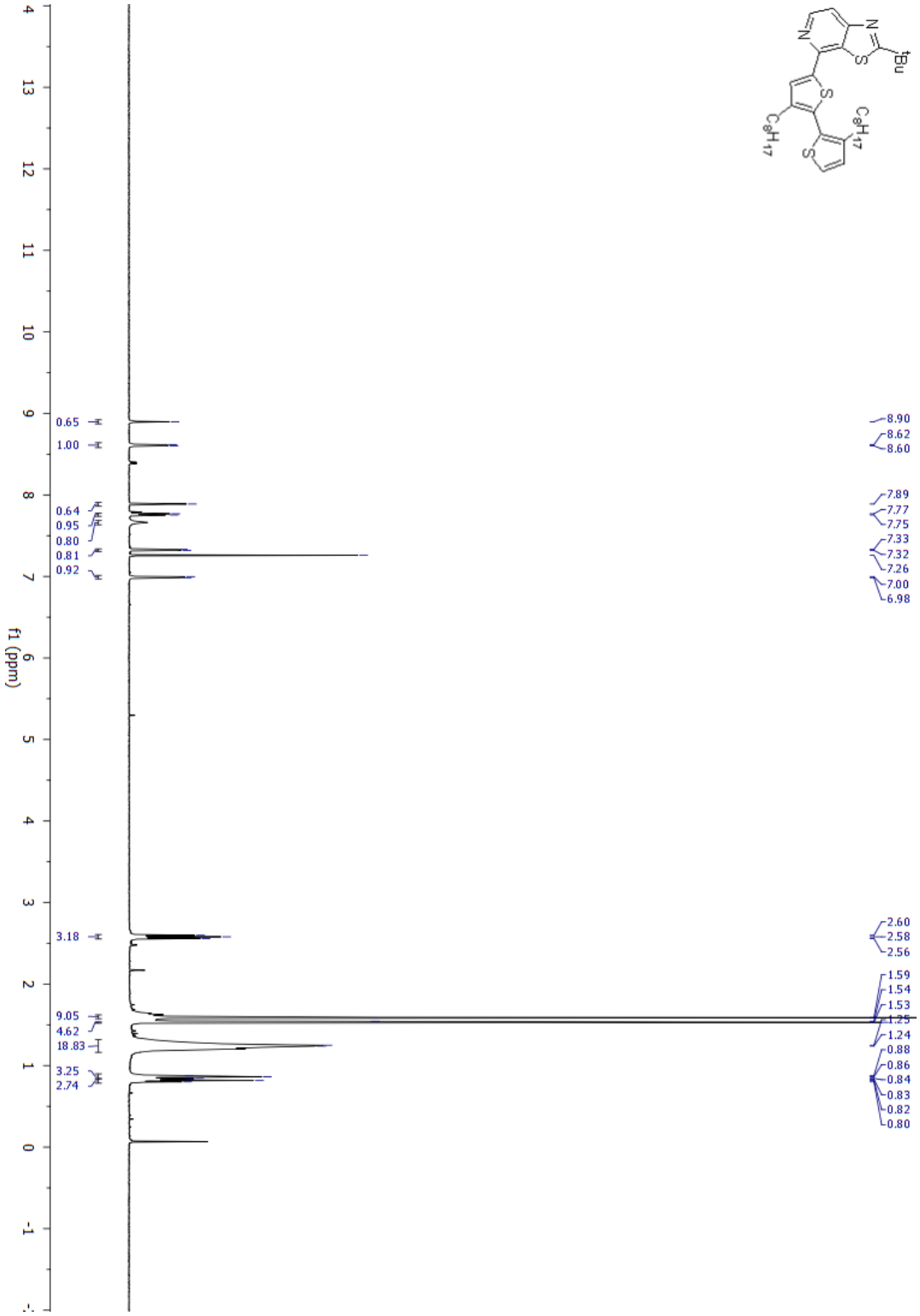

Figure 6.5.11 ^{1}H NMR of 2-(*tert*-butyl)-4-(3,3'-dioctyl-[2,2'-bithiophen]-5-yl)thiazolo[5,4-*c*]pyridine

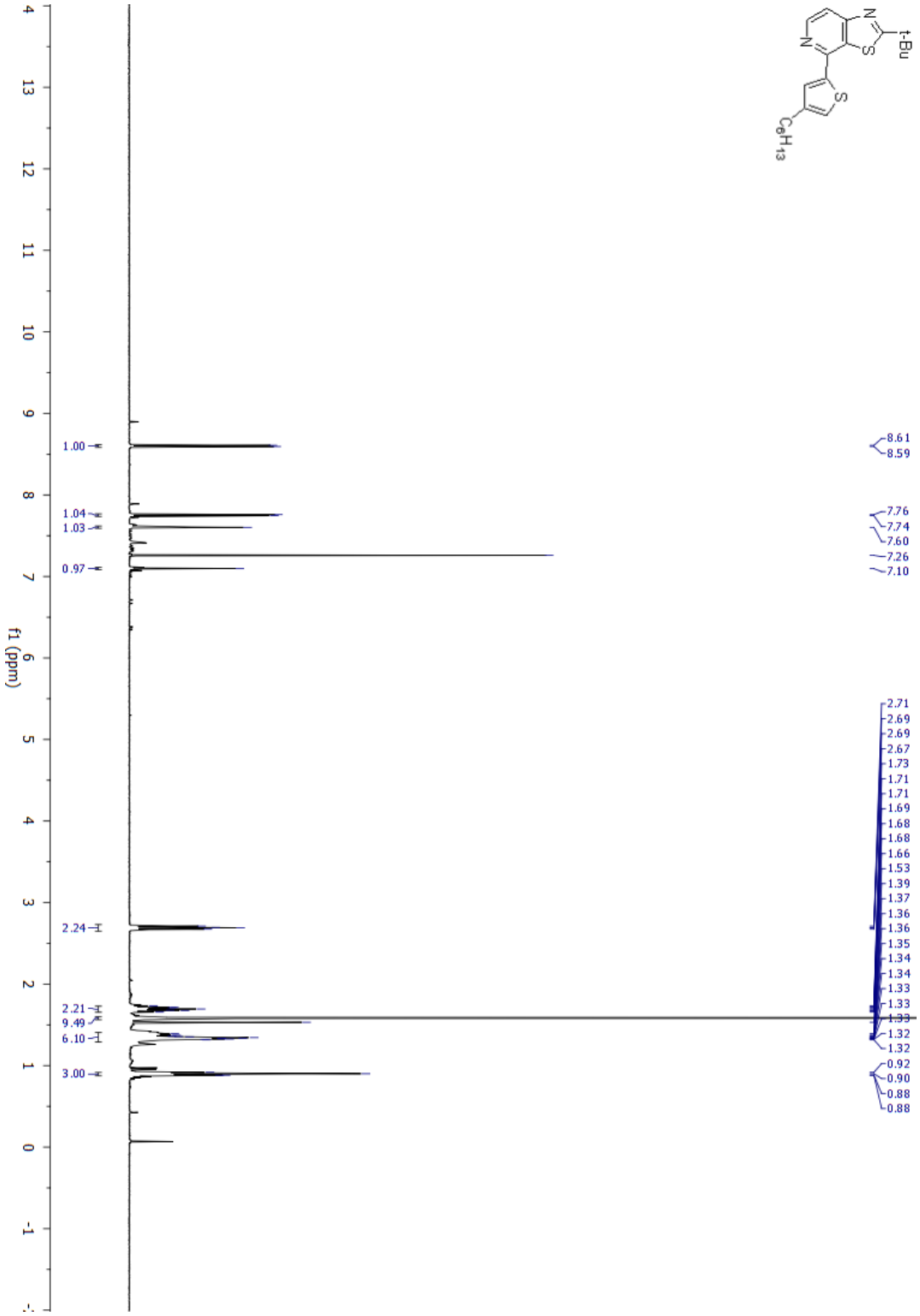

Figure 6.5.12 ^{1}H NMR of 2-(*tert*-butyl)-4-(4-hexylthiophen-2-yl)thiazolo[5,4-*c*]pyridine

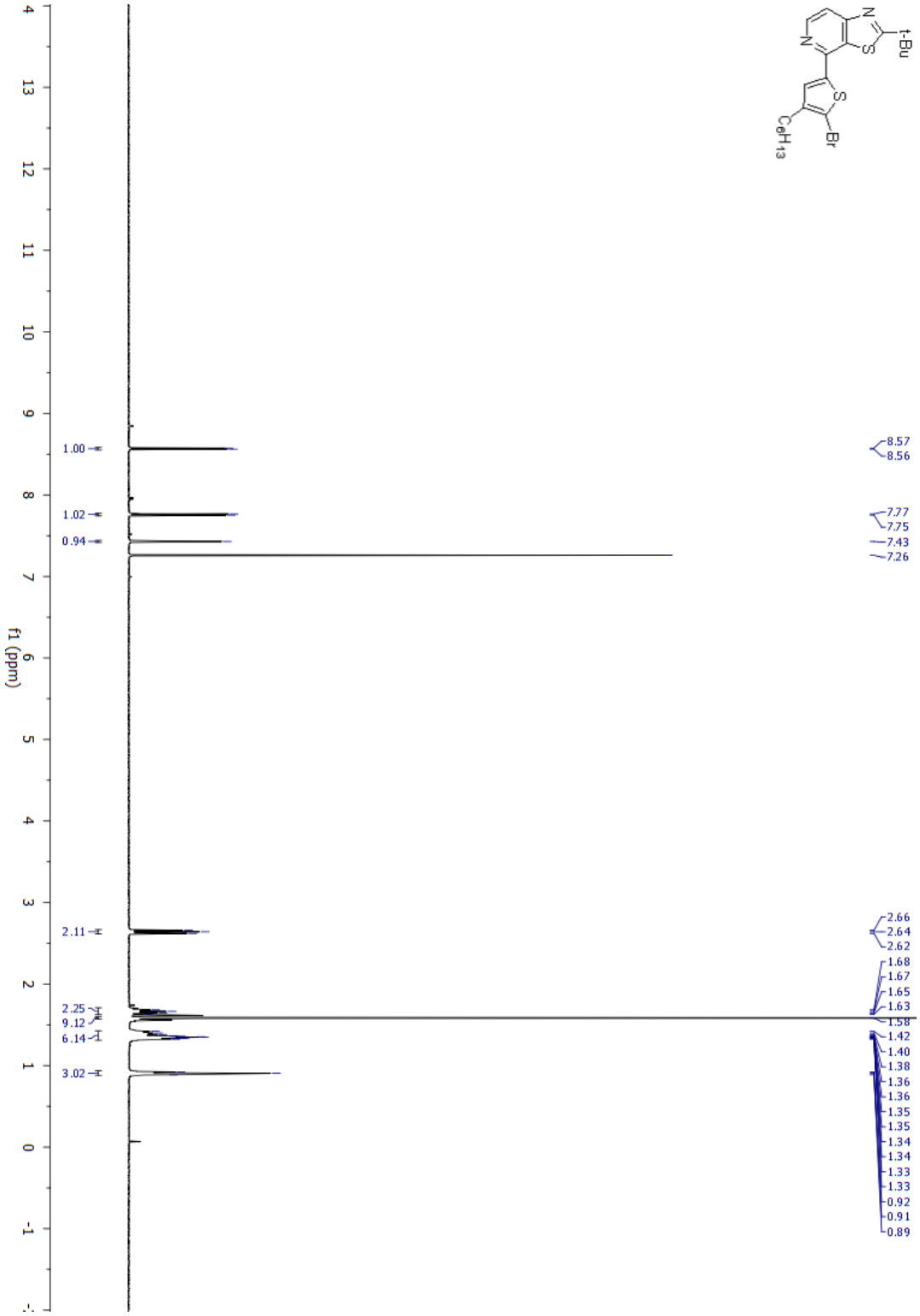

Figure 6.5.13 ^{1}H NMR of 4-(5-bromo-4-hexylthiophen-2-yl)-2-(*tert*-butyl)thiazolo[5,4-*c*]pyridine

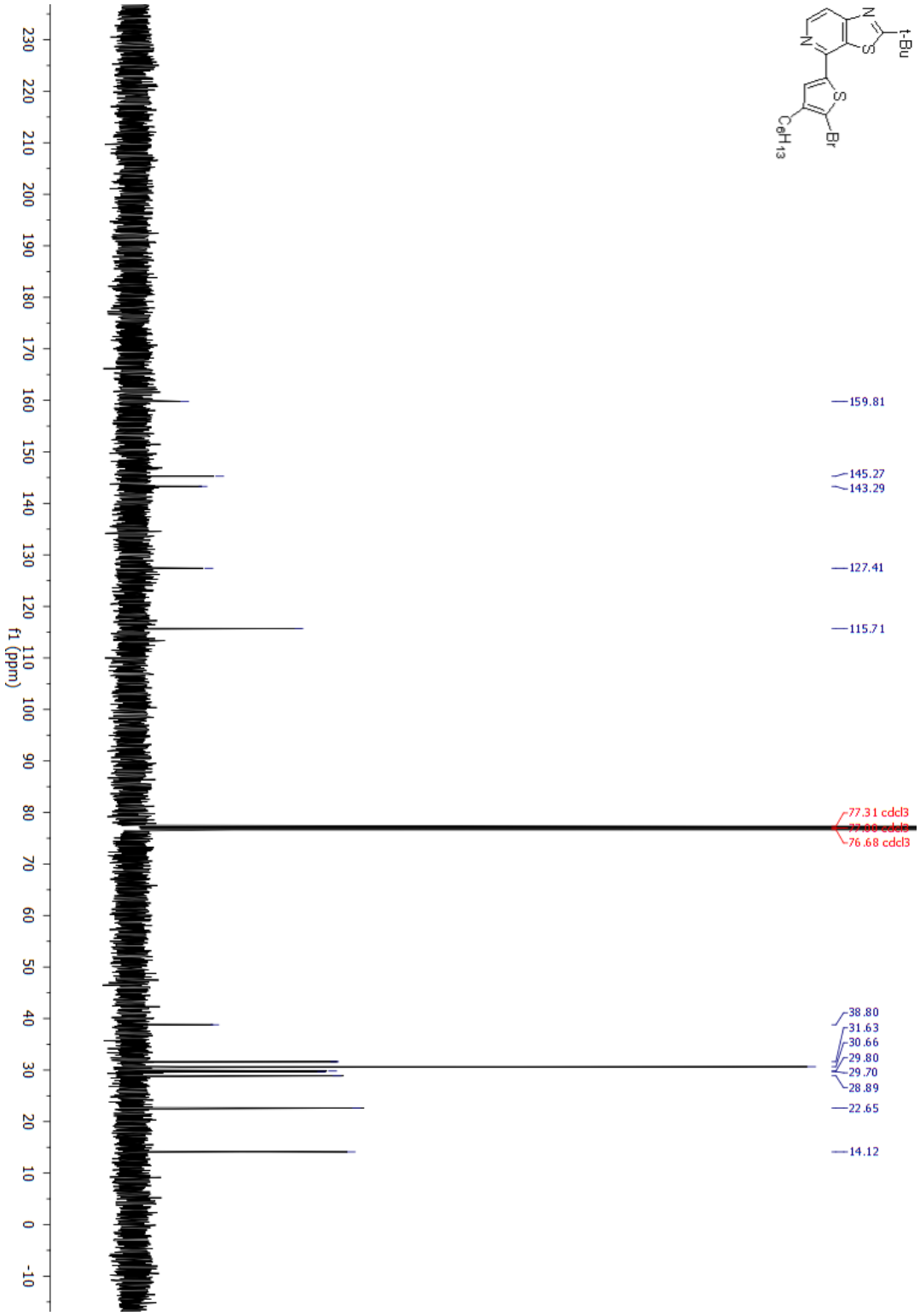

Figure 6.5.14 ^{13}C NMR of 4-(5-bromo-4-hexylthiophen-2-yl)-2-(*tert*-butyl)thiazolo[5,4-*c*]pyridine

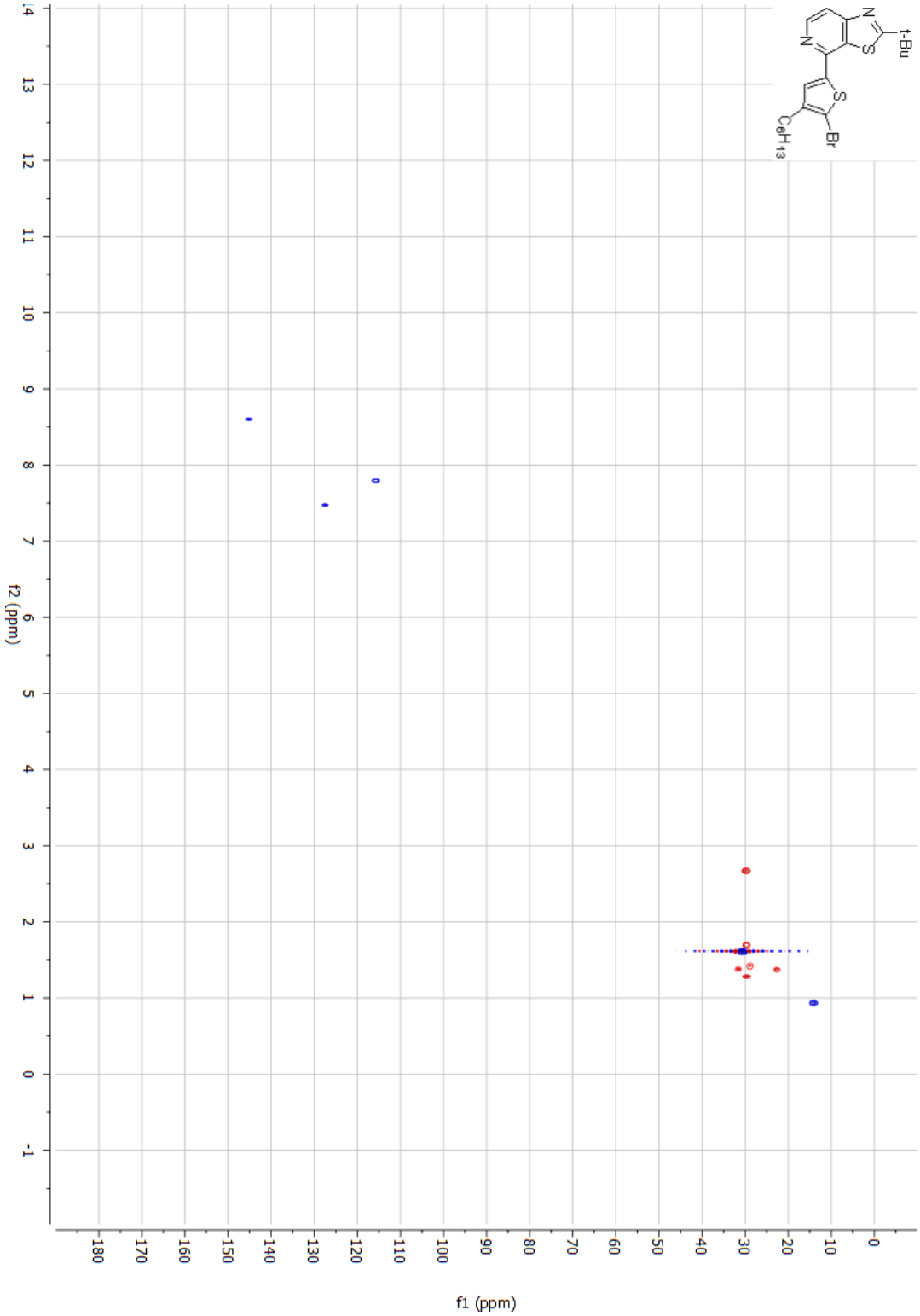

Figure 6.5.15 HSQC of 4-(5-bromo-4-hexylthiophen-2-yl)-2-(*tert*-butyl)thiazolo[5,4-*c*]pyridine

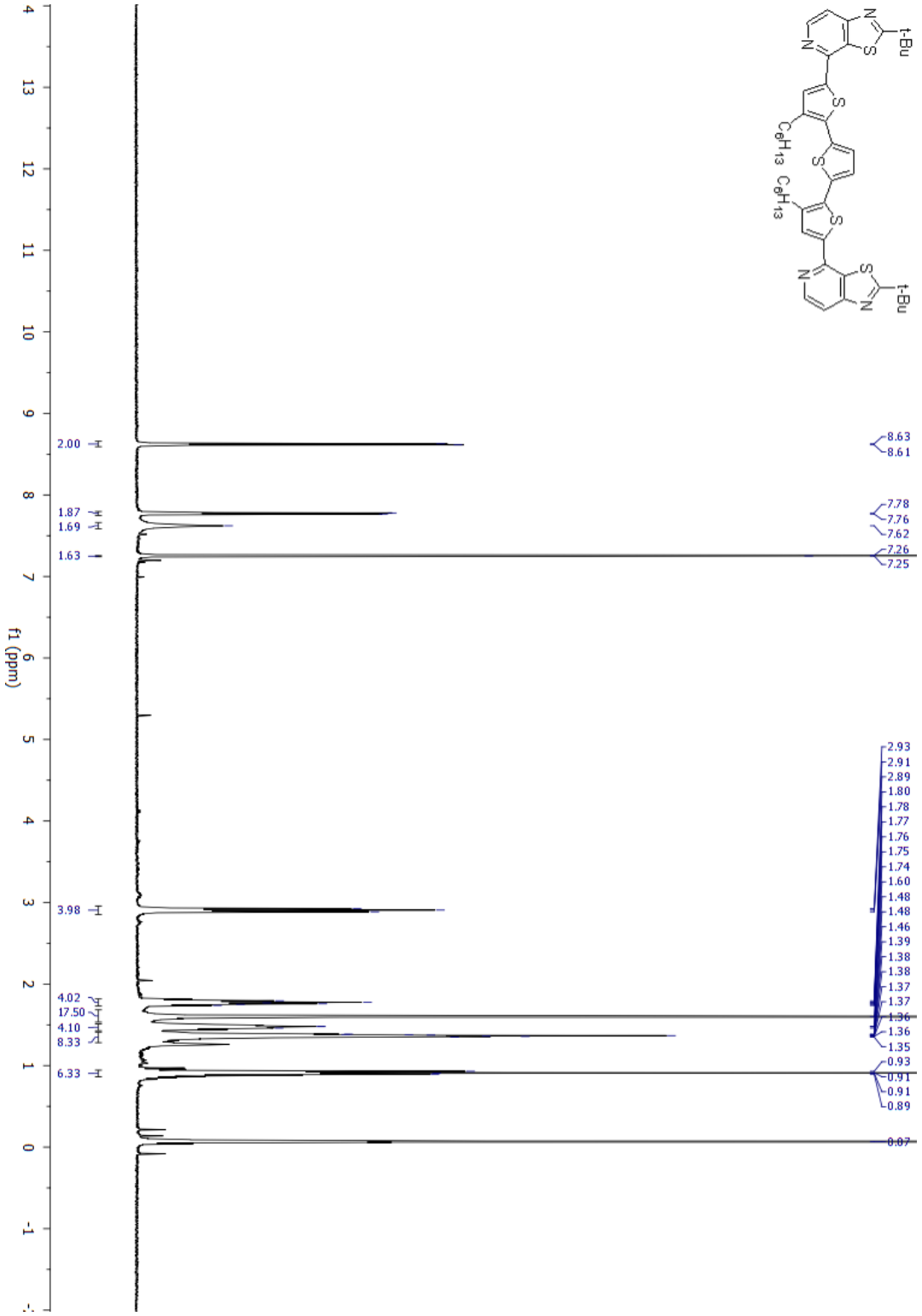

Figure 6.5.16 ^{1}H NMR of M2

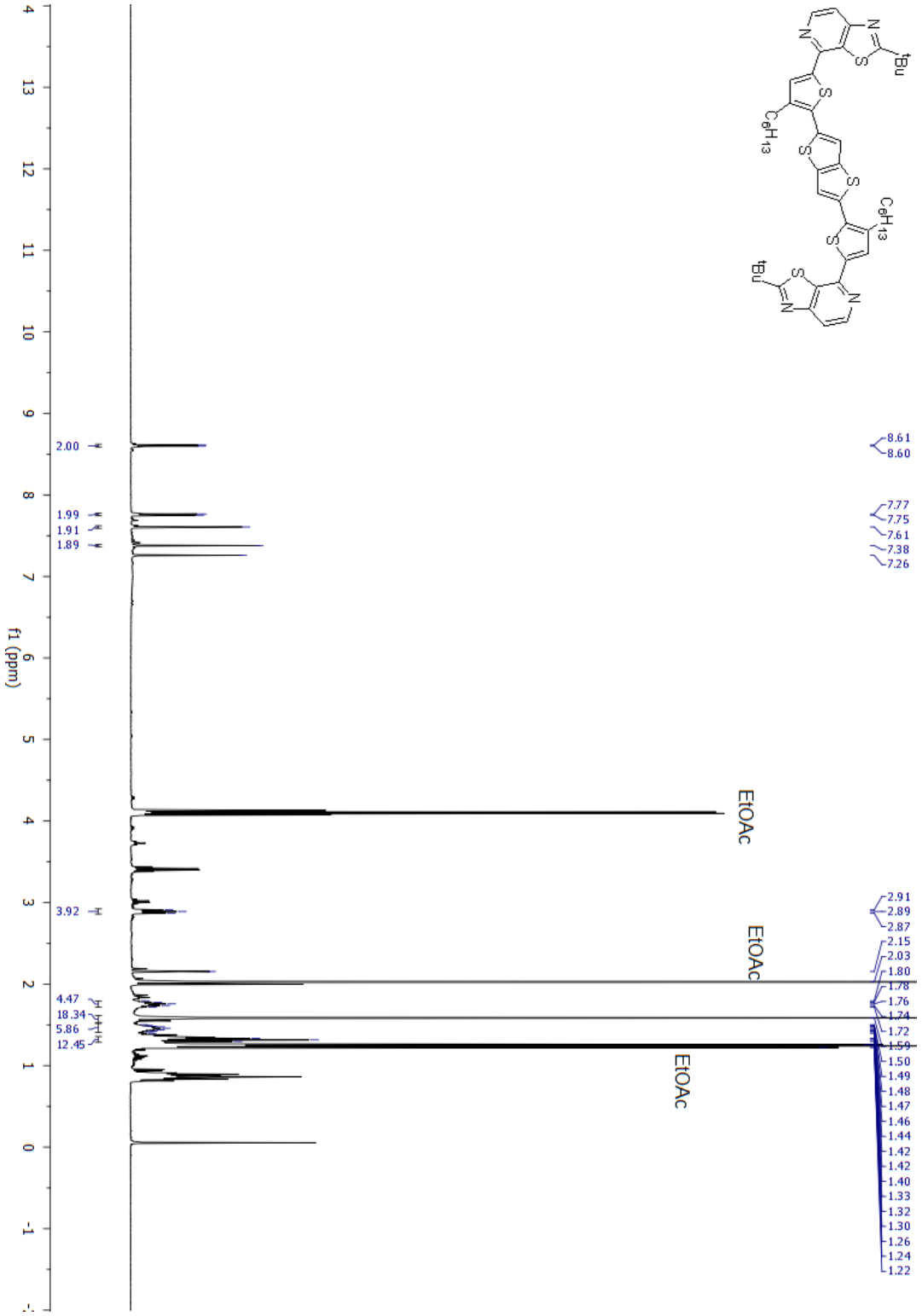

Figure 6.5.17 ^{1}H NMR of M3

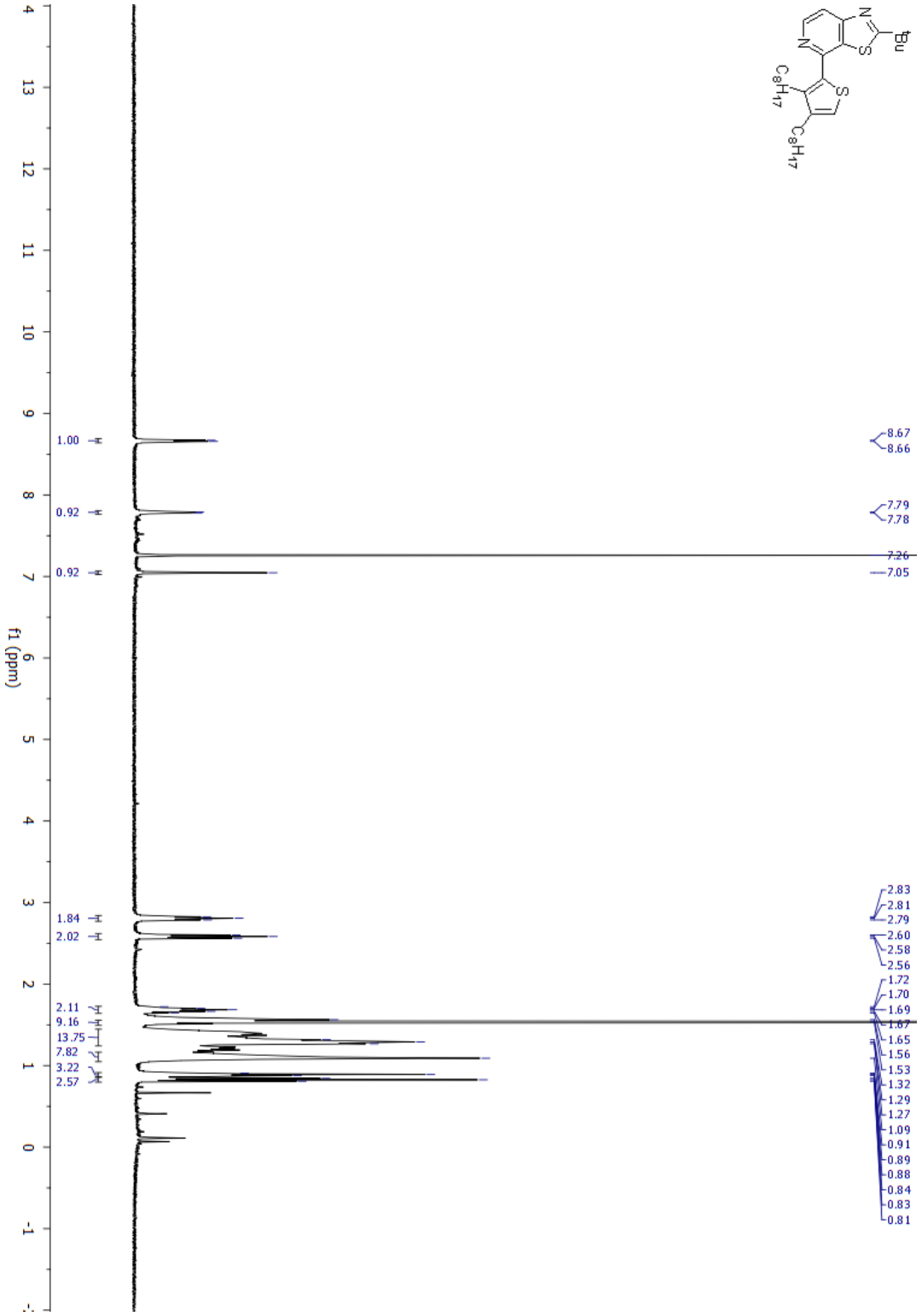

Figure 6.5.19 ^{1}H NMR of 2-(*tert*-butyl)-4-(3,4-dioctylthiophen-2-yl)thiazolo[5,4-*c*]pyridine.

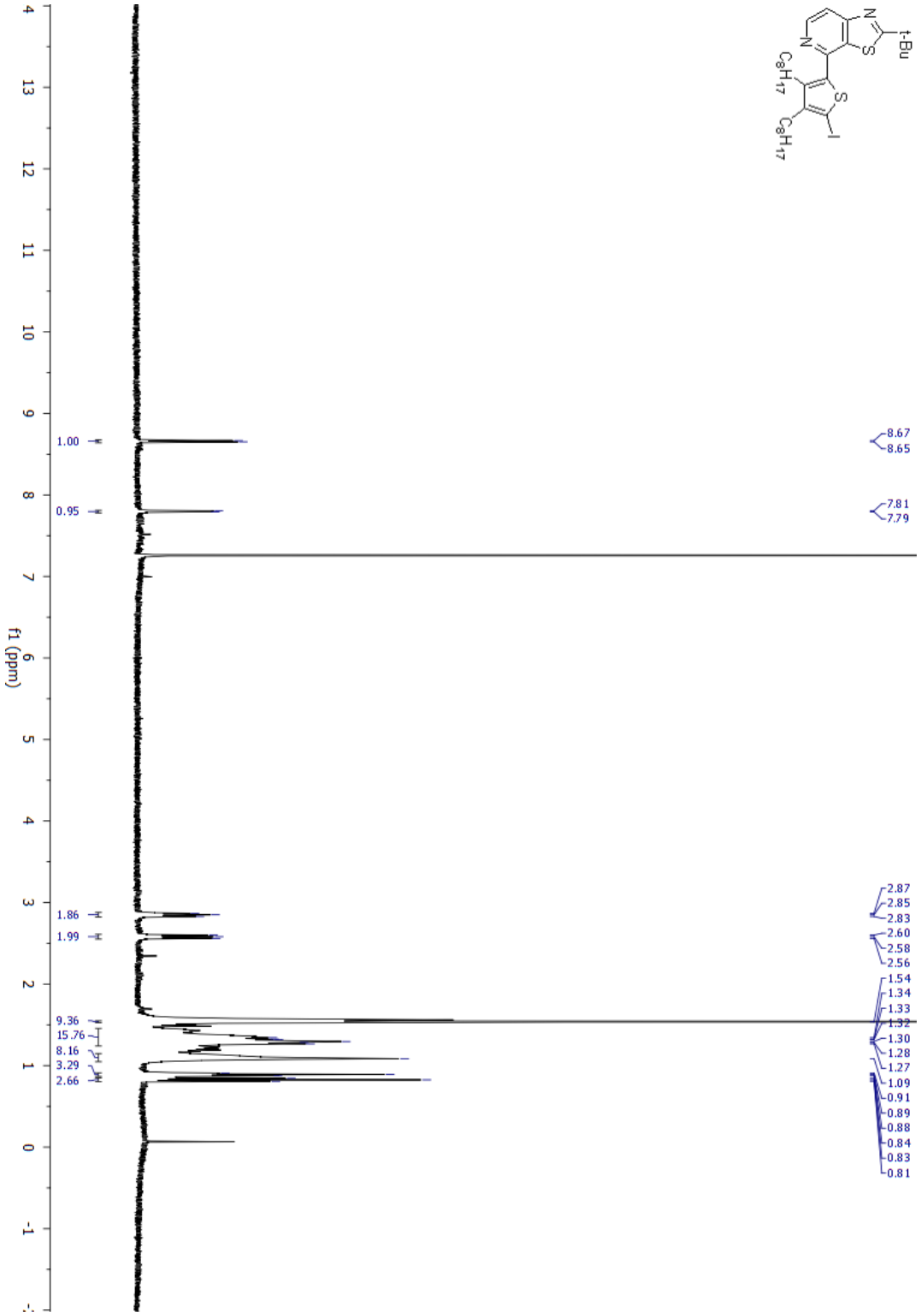

Figure 6.5.20 [1]H NMR of 2-(tert-butyl)-4-(5-iodo-3,4-dioctylthiophen-2-yl)thiazolo[5,4-c]pyridine

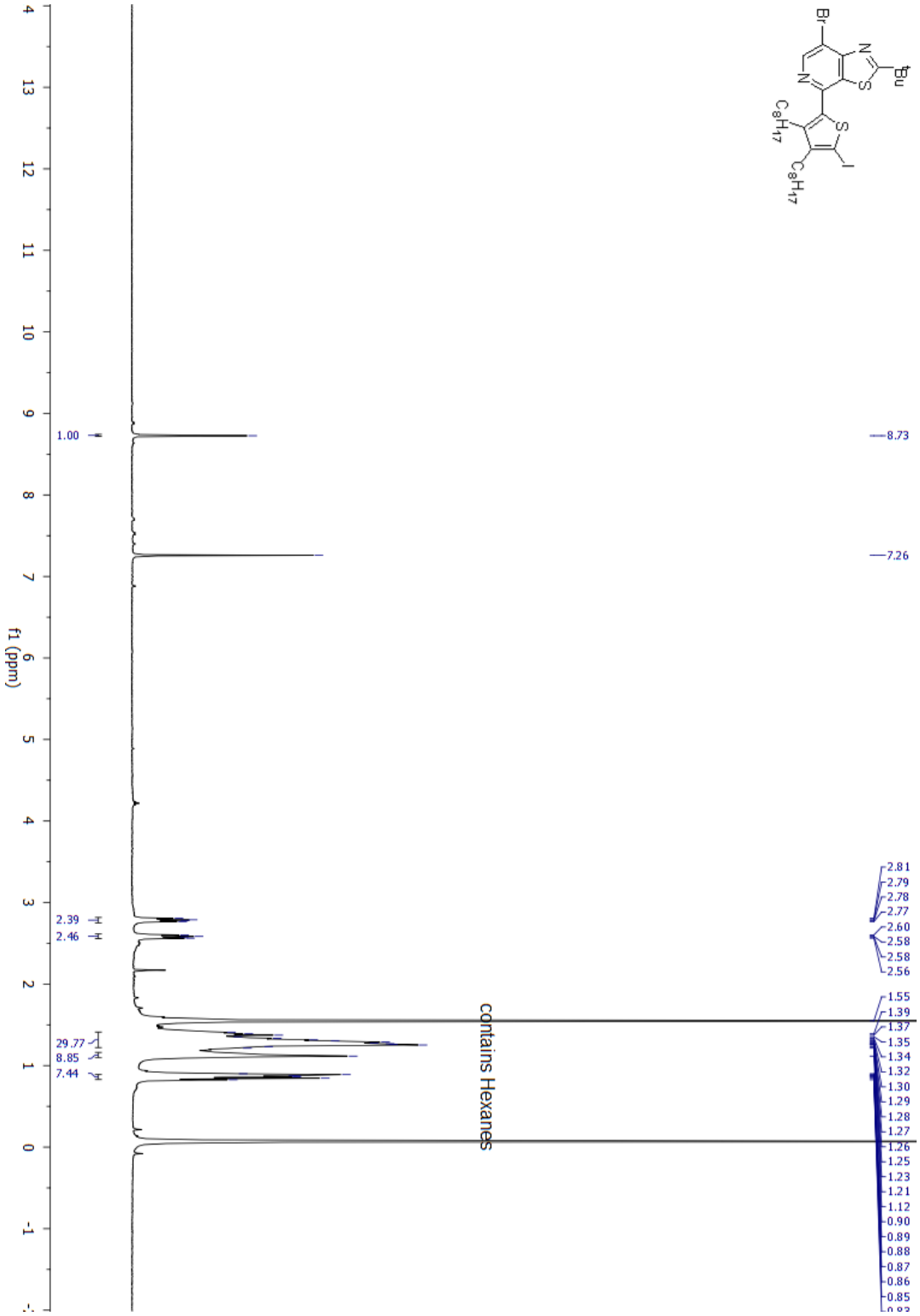

Figure 6.5.21 ^{1}H NMR of 7-bromo-2-(*tert*-butyl)-4-(5-iodo-3,4-dioctylthiophen-2-yl)thiazolo[*5,4-c*]pyridine.

6.6 REFERENCES

(1) Scharber, M.; Mühlbacher, D.; Koppe, M.; Denk, P.; Waldauf, C.; Heeger, A.; Brabec, C. *Advanced Materials* **2006**, *18*, 789.
(2) Bhuwalka, A.; Mike, J. F.; He, M.; Intemann, J. J.; Nelson, T.; Ewan, M. D.; Roggers, R. A.; Lin, Z.; Jeffries-El, M. *Macromolecules* **2011**, *44*, 9611.
(3) Liang, Y.; Xu, Z.; Xia, J.; Tsai, S.-T.; Wu, Y.; Li, G.; Ray, C.; Yu, L. *Advanced Materials* **2010**, *22*, E135.
(4) Tang, C. W.; VanSlyke, S. A. *Applied Physics Letters* **1987**, *51*, 913.
(5) Burroughes, J. H.; Bradley, D. D. C.; Brown, A. R.; Marks, R. N.; Mackay, K.; Friend, R. H.; Burns, P. L.; Holmes, A. B. *Nature* **1990**, *347*, 539.
(6) Duan, L.; Hou, L.; Lee, T.-W.; Qiao, J.; Zhang, D.; Dong, G.; Wang, L.; Qiu, Y. *Journal of Materials Chemistry* **2010**, *20*, 6392.
(7) Huang, H.; Zhou, N.; Ortiz, R. P.; Chen, Z.; Loser, S.; Zhang, S.; Guo, X.; Casado, J.; López Navarrete, J. T.; Yu, X.; Facchetti, A.; Marks, T. J. *Advanced Functional Materials* **2014**, *24*, 2782.
(8) Ahmed, E.; Subramaniyan, S.; Kim, F. S.; Xin, H.; Jenekhe, S. A. *Macromolecules* **2011**, *44*, 7207.
(9) Babel, A.; Jenekhe, S. A. *The Journal of Physical Chemistry B* **2002**, *106*, 6129.
(10) Brabec, C. J.; Cravino, A.; Meissner, D.; Sariciftci, N. S.; Fromherz, T.; Rispens, M. T.; Sanchez, L.; Hummelen, J. C. *Advanced Functional Materials* **2001**, *11*, 374.
(11) Brabec, C. J.; Gowrisanker, S.; Halls, J. J. M.; Laird, D.; Jia, S.; Williams, S. P. *Advanced Materials* **2010**, *22*, 3839.
(12) Coakley, K. M.; McGehee, M. D. *Chemistry of Materials* **2004**, *16*, 4533.
(13) Jo, J.; Pron, A.; Berrouard, P.; Leong, W. L.; Yuen, J. D.; Moon, J. S.; Leclerc, M.; Heeger, A. J. *Advanced Energy Materials* **2012**, *2*, 1397.
(14) Lu, L.; Yu, L. *Advanced Materials* **2014**, *26*, 4413.
(15) Chu, T.-Y.; Lu, J.; Beauprea, S.; Zhang, Y.; Pouliot, J.-R.; Wakim, S.; Zhou, J.; Leclerc, M.; Li, Z.; Ding, J.; Tao, Y. *Journal of the American Chemical Society* **2011**, *133*, 4250.
(16) Boudreault, P.-L. T.; Najari, A.; Leclerc, M. *Chemistry of Materials* **2010**, *23*, 456.
(17) Zou, Y.; Najari, A.; Berrouard, P.; Beaupré, S.; Réda Aïch, B.; Tao, Y.; Leclerc, M. *Journal of the American Chemical Society* **2010**, *132*, 5330.
(18) Dennler, G.; Scharber, M. C.; Brabec, C. J. *Advanced Materials* **2009**, *21*, 1323.
(19) Price, S. C.; Stuart, A. C.; Yang, L.; Zhou, H.; You, W. *Journal of the American Chemical Society* **2011**, *133*, 4625.
(20) Mi, D.; Kim, J. H.; Kim, H. U.; Xu, F.; Hwang, D. H. *Journal of nanoscience and nanotechnology* **2014**, *14*, 1064.
(21) He, Z.; Zhong, C.; Su, S.; Xu, M.; Wu, H.; Cao, Y. *Nat Photon* **2012**, *6*, 591.
(22) Sun, Y.; Welch, G. C.; Leong, W. L.; Takacs, C. J.; Bazan, G. C.; Heeger, A. J. *Nat Mater* **2012**, *11*, 44.
(23) Thompson, B. C.; Fréchet, J. M. J. *Angewandte Chemie International Edition* **2008**, *47*, 58.

(24) Zhou, J.; Zuo, Y.; Wan, X.; Long, G.; Zhang, Q.; Ni, W.; Liu, Y.; Li, Z.; He, G.; Li, C.; Kan, B.; Li, M.; Chen, Y. *Journal of the American Chemical Society* **2013**, *135*, 8484.
(25) Sharenko, A.; Proctor, C. M.; van der Poll, T. S.; Henson, Z. B.; Nguyen, T.-Q.; Bazan, G. C. *Advanced Materials* **2013**, *25*, 4403.
(26) Lin, Y.; Li, Y.; Zhan, X. *Chemical Society Reviews* **2012**, *41*, 4245.
(27) Liu, Y.; Yang, Y.; Chen, C.-C.; Chen, Q.; Dou, L.; Hong, Z.; Li, G.; Yang, Y. *Advanced Materials* **2013**, *25*, 4657.
(28) Zhou, J.; Wan, X.; Liu, Y.; Zuo, Y.; Li, Z.; He, G.; Long, G.; Ni, W.; Li, C.; Su, X.; Chen, Y. *Journal of the American Chemical Society* **2012**, *134*, 16345.
(29) Kyaw, A. K. K.; Wang, D. H.; Luo, C.; Cao, Y.; Nguyen, T.-Q.; Bazan, G. C.; Heeger, A. J. *Advanced Energy Materials* **2014**, *4*, n/a.
(30) Welch, G. C.; Perez, L. A.; Hoven, C. V.; Zhang, Y.; Dang, X.-D.; Sharenko, A.; Toney, M. F.; Kramer, E. J.; Nguyen, T.-Q.; Bazan, G. C. *Journal of Materials Chemistry* **2011**, *21*, 12700.
(31) Coughlin, J. E.; Henson, Z. B.; Welch, G. C.; Bazan, G. C. *Accounts of Chemical Research* **2013**, *47*, 257.
(32) Henson, Z. B.; Welch, G. C.; van der Poll, T.; Bazan, G. C. *Journal of the American Chemical Society* **2012**, *134*, 3766.
(33) Keith Smith, C. M. L., Ian K. Morris, Ian Matthews and Gareth J. Pritchard *Sulfur Letters* **1994**, *17*, 197
(34) Bissember, A. C.; Banwell, M. G. *The Journal of Organic Chemistry* **2009**, *74*, 4893.
(35) Corcoran, R. C.; Bang, S. H. *Tetrahedron Letters* **1990**, *31*, 6757.
(36) Chen, H.-Y.; Hou, J.; Hayden, A. E.; Yang, H.; Houk, K. N.; Yang, Y. *Advanced Materials* **2010**, *22*, 371.
(37) Kokubo, H.; Sato, T.; Yamamoto, T. *Macromolecules* **2006**, *39*, 3959.
(38) Brookings, D.; Davenport, R. J.; Davis, J.; Galvin, F. C. A.; Lloyd, S.; Mack, S. R.; Owens, R.; Sabin, V.; Wynn, J. *Bioorganic & Medicinal Chemistry Letters* **2007**, *17*, 562.

CHAPTER 7

DEVELOPING NEW ELECTRON RICH FURAN BASED SYSTEMS FOR ORGANIC PHOTOVOLTAIC CELLS.

7.1 Abstract:

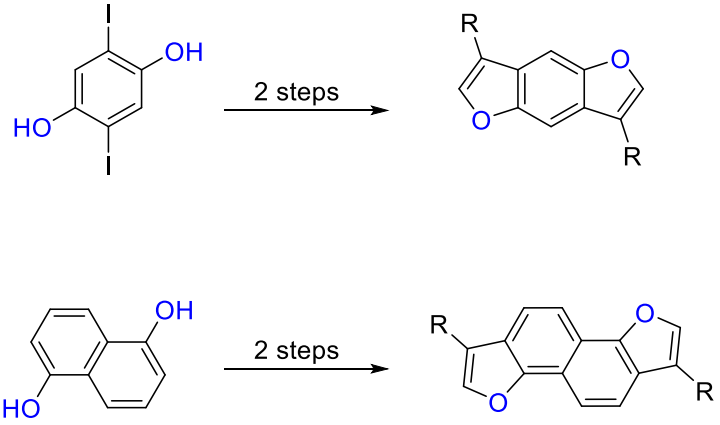

Electron rich 3,7-dialkylbenzo[1,2-*b*:4,5-*b*']difuran and 1,6-dialkylnaphtho[1,2-*b*:5,6-*b*']difuran have been developed for organic semiconducting polymers. A two-step synthetic route towards alkylated benzo[1,2-*b*:4,5-*b*']difurans starting from 1,5-dihydroxy-2,6-diiodobenzene has been established. To our knowledge, this is the first report for the synthesis of 3,7-dialkylbenzo[1,2-*b*:4,5-*b*']difurans. Similarly, 1,6-dialkylnaphtho[1,2-*b*:5,6-*b*']difurans with different alkyl chains have also been synthesized in two steps starting from 1,5-dihydroxynapthalene. Polymerization conditions for these materials are currently being optimized.

7.2 Introduction:

Organic semiconductors are lightweight, flexible, and solution processable.[1-3] They can be fabricated for large-area applications using relatively inexpensive techniques such as spin coating, inkjet printing or drop-casting.[4-6] Moreover, their optical and electronic properties can be altered by chemical synthesis.[7,8] Due to their synthetic flexibility and ease of fabrication, conjugated polymers are being thoroughly investigated for use in organic photovoltaic cells (OPV)s,[9-11] organic light emitting diodes (OLED)s,[12-14] and organic field effect transistors (OFET)s.[15-17] Remarkable progress in power conversion efficiencies (PCE)s has been made in OPVs employing conjugated polymers as donor materials and functionalized fullerenes as acceptors in a bulk heterojunction (BHJ) device architecture.[18-20] Through molecular engineering and optimization of device parameters, efficiencies over 9% have been achieved in conjugated polymers employing alternating donor and acceptor units in the polymer backbone.[21,22] The use of benzo[1,2-*b*:4,5-*b*′]dithiophene (BDT) as the donor unit has demonstrated particularly encouraging results, with PCEs over 8% being reported.[10,18] Polymers incorporating BDT donor and diketopyrollopyrrole (DPP) acceptor have shown PCEs between 8% - 9%.[23,24] The enhanced photovoltaic performance in such systems is attributed to the planar conjugated structure of BDT which facilitates π–π stacking and leads to high hole mobilities.[10]

Research based on conjugated polymers employing the analogous benzo[1,2-*b*:4,5-*b*′]difuran (BDF) has only recently taken off, with efficiencies of over 7% being

reported in early studies.[25] Furan based materials are promising for several reasons. Since furan is less aromatic than thiophene,[26] it should adopt the quinoid state more readily than thiophene leading to materials with narrower band gaps. At the same time, the smaller atomic radius of oxygen as compared to sulfur should reduce steric interaction between neighboring units reducing twisting in the polymer backbone.[27] Additionally, polymers incorporating furans have displayed better solubility than analogous polymers employing thiophene in their backbone. Due to these promising properties, the photovoltaic performance of BDF based polymers have been investigated and reported by our group.

Although several syntheses of BDFs has been reported in literature, in most of the syntheses the BDF units cannot be further functionalized due to the lack of synthetic handles.[28-30] In order to address this, a facile synthetic route to 3,7-diiodo-2,6-di(thiophen-2-yl)benzo[1,2-*b*:4,5-*b*′]difurans via an iodine-promoted double cyclization has been reported by our group (Scheme 7.1).[31] This route offers several advantages such as ease of synthesis of starting materials, high yields during synthesis as well as good solubility of intermediates imparted by the alkyl chains on the thiophene rings.[31] However, only 2,6-diarylbenzo[1,2-*b*:4,5-*b*′]difurans can be accessed by this synthetic route *i.e.* cyclization only occurs as long as the terminal groups are arenes. As a result, 'naked' BDFs cannot be synthesized by the above method.

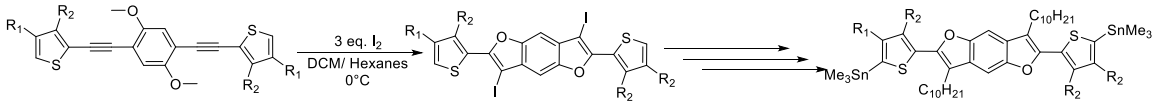

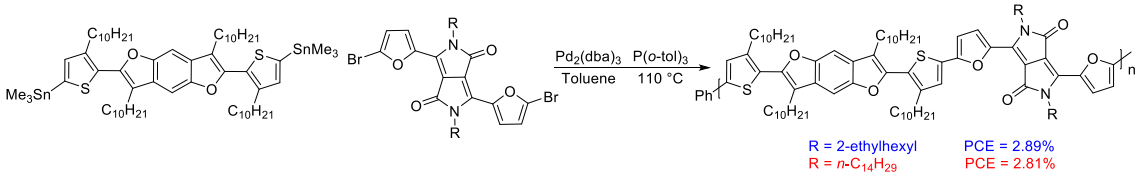

Scheme 7.1. Benzodifuran-diketopyrollopyrrole copolymers

In order to further develop the benzodifuran heterocycle for OPVs and improve on the initial PCEs of ~3%, a systematic study the structure-property relationship of polymers incorporating BDF is needed. In order to achieve this, a new synthetic route for 3,7-dialkylbenzo[1,2-*b*:4,5-*b'*]difurans has been developed and is reported in this article (Scheme 7.2). The steps leading to the monomer proceed in high yields and can be easily purified. As a result, the monomers can be accessed in multigram scales.

During our optimization of the BDF system, we also became interested in studying the NDF unit, which, due to its extended π delocalization and planar structure should result in materials with still narrower band gaps and higher charge carrier mobilities. In fact, NDF based materials used in OFETs have exhibited charge carrier mobilities of 3.6 $cm^2\ V^{-1}\ s^{-1}$ as opposed to 0.5 $cm^2\ V^{-1}s^{-1}$ exhibited by the isoelectronic NDT based materials.[32,33] OPVs employing NDF units in the polymer backbone have reported efficiencies nearing 5%.[34] In order to study the effects of replacing the diarylbenzodifuran with a fused π-extended heterocycle on the polymer properties, the NDF monomer was developed and studied. We expect that replacement of diarylBDF monomers with NDF should reduce twisting in the polymer backbone induced by steric interactions between the alkyl chains on the BDF and the thiophene spacer units, leading to greater effective conjugation length and narrow band gaps (Figure 7.1). The NDF

monomer was obtained via a three step synthesis starting from commercially available 1,5-dihydroxynapthalene.

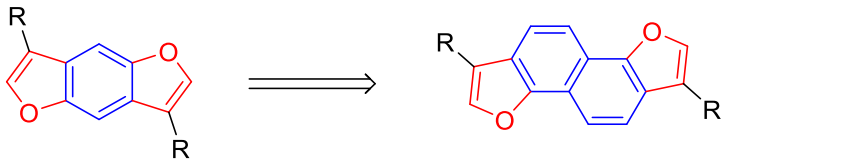

3,7-dialkylbenzo[1,2-*b*:4,5-*b*′]difuran 1,6-dialkylnaphtho[1,2-*b*:5,6-*b*′]difuran

Figure 7.1 Benzodifuran and Napthodifuran building blocks

7.3 SYNTHESIS AND CHARACTERIZATION

2,5-Diiodobenzene-1,4-diol was synthesized in two steps starting from commercially available 1,4-dimethoxybenzene. The α-bromoketone was synthesized by modified literature procedures.[35] The 3,7-dialkylbenzo[1,2-*b*:4,5-*b*′]difurans was then synthesized in 2 steps starting from 2,5-diiodobenzene-1,4-diol (Scheme 7.2). For example, the synthesis for 3,7-dihexylbenzo[1,2-*b*:4,5-*b*′]difurans started out with the reaction of diiodobenzene-1,4-diol **(1)** with 1-bromooctan-2-one to form 1,1'-((2,5-diiodo-1,4-phenylene)bis(oxy))bis(octan-2-one) **(2)**. This was cyclized by treatment with ^{n}BuLi, and then dehydrated in one pot to 3,7-dihexylbenzo[1,2-*b*:4,5-*b*′]difuran **(3)** with methanesulfonic acid (MSA). More recently, we found that quenching the cyclization reaction with trifluroacetic acid (TFA), heating it to a boil for 2-3 minutes and then cooling it to room temperature resulted in the formation of **3**. In fact, higher yield and lesser decomposition of the product was observed in this method as compared to dehydrating with MSA. Furthermore, it was found that cyclization only occurred if the starting material possessed two iodine groups. All attempts to cyclize 1,1'-((2,5-dibromo-1,4-phenylene)bis(oxy))bis(octan-2-one) led to only metal halogen exchange and no ring

closed product. Nonetheless, BDF derivatives with different alkyl chains can be accessed in this fashion.

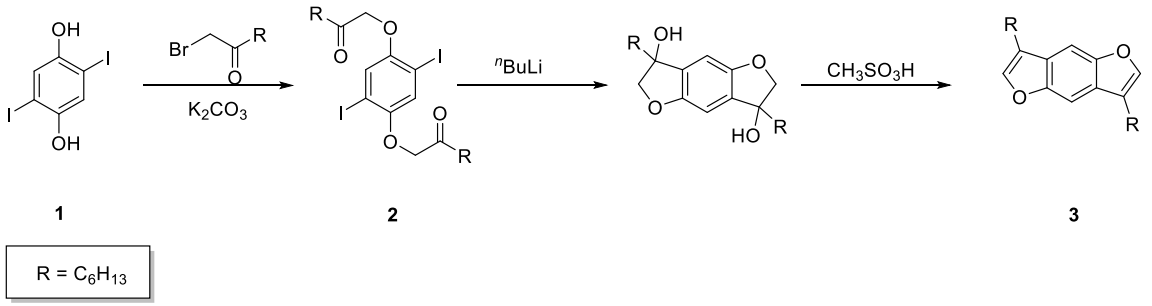

Scheme 7.2 Synthesis of 3,7-dihexylbenzo[1,2-*b*:4,5-*b*′]difuran.

Initially, attempts were made to synthesize NDF derivatives via iodo-cyclization, similar to the one reported for the synthesis of 3,7-diiodo-2,6-di(thiophen-2-yl)benzo[1,2-*b*:4,5-*b*′]difurans reported by our group (Scheme 7.3).[31,35] Since this method requires bisethynylarenes as the precursor for the iodine-mediated cyclization we set out to synthesize bisarylethynyldimethoxynapthalene. The synthesis started out with bromination of 1,5-dihydroxynapthalene **(4)** in the presence of bromine in acetic acid to yield 2,6-dibromo-1,5-dihydroxynapthalene. The phenolic hydroxyl groups were then transformed into methoxy groups in the presence of KOH and CH_3I using DMSO as the solvent. The next step in the synthesis involved a Sonogashira cross-coupling reaction between 2,6-dibromo-1,5-dimethoxynapthalene and 3-decyl-2-ethynylthiophene to form 2,2'-((1,5-dimethoxynaphthalene-2,6-diyl)bis(ethyne-2,1-diyl))bis(3-decylthiophene). However, after several attempts at optimizing the reaction conditions such as reaction time, temperature, catalyst, catalyst loading as well as reaction solvent, the reaction yielded a mixture of the monosubstituted (major product) and disubstituted (minor

product) products. These two products were inseparable and could not be isolated and purified.

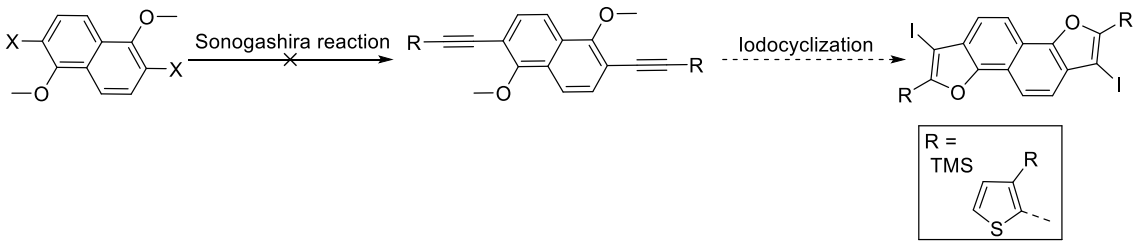

Scheme 7.3 Synthesis of NDF via iodine promoted iodocyclization method.

This was initially considered to be due to steric hindrance from the alkyl chains on the thiophene ring pointing towards the naphthalene core. Therefore, a Sonogashira cross coupling reaction, where the 3-decyl-2-ethynylthiophene was replaced with ethynyltrimethylsilane, was attempted. However, mainly monosubstituted product was obtained. This was thought to be due to the naphthalene ring not being very activated for transition – metal catalyzed cross-coupling reactions. This hypothesis was verified by the synthesis of (1,5-dimethoxynaphthalene-2,6-diyl)bis(ethyne-2,1-diyl))bis(trimethylsilane) via a Stille cross-coupling reaction which yielded mainly monosubstituted product. It seemed only logical that since iodine groups are more reactive in cross-coupling chemistry than bromine groups, that switching out the bromine groups for iodine groups should improve the reactivity of the ring towards transition – metal catalyzed cross-coupling reactions. Therefore 2,6-diiodo-1,5-dimethoxynaphthalene was synthesized in three steps starting from 2,6-dibromo-1,5-dimethoxynaphthalene. Once again, both the Stille cross-coupling reaction between trimethyl((trimethylstannyl)ethynyl)silane and 2,6-

diiodo-1,5-dimethoxynaphthalene as well as the Sonogashira reaction between ethynyltrimethylsilane and 2,6-diiodo-1,5-dimethoxynaphthalene afforded only monosubstituted products. In another attempt towards the synthesis for the precursor for iodocyclization, 2,6-dibromonaphthalene-1,5-diyl diacetate was synthesized and subjected to Sonogashira reaction conditions with 3-decyl-2-ethynylthiophene. The reaction yielded ~35 % of disubstitued product after isolation and purification. Although successful to synthesize the precursor, due to the lengthy syntheses and low yields, it was impractical to synthesize monomers via the above methodology. Therefore, all efforts to utilize iodo-cyclization to construct NDF building blocks were unsuccessful. Nonetheless, NDF derivatives were synthesized in a manner similar to the BDF derivatives illustrated in Scheme 7.2 via modified literature procedures.

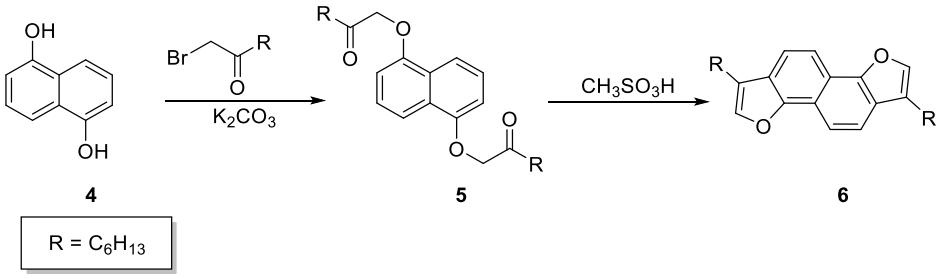

Scheme 7.4 Synthesis of 1,6-dialkylnaphtho[1,2-*b*:5,6-*b*′]difurans.

1,6-dialkylnaphtho[1,2-*b*:5,6-*b*′]difurans were synthesized starting from **4** via modified literature procedures (Scheme 7.4). For example, reaction of **4** with 1-bromododecan-2-one afforded 1,1'-(naphthalene-1,5-diylbis(oxy))bis(dodecan-2-one) **(5)** which was then cyclized in the presence of MSA to form 1,6-didecylnaphtho[1,2-*b*:5,6-

b′]difuran **(6)**. Derivatives with alkyl chains of different lengths were synthesized using the above synthetic methodology.

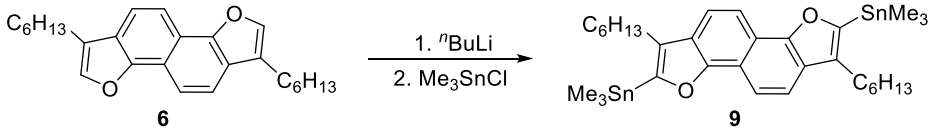

Scheme 7.5 Synthesis of (1,6-dihexylnaphtho[1,2-*b*:5,6-*b*′]difuran-2,7-diyl)bis(trimethylstannane)

6 was stannylated to yield **9** in high yields (Scheme 7.5), which was polymerized with DPP via a Stille reaction to form **P1** (Scheme 7.6). However, upon polymerization, only oligomers were formed. Optimization of polymerization conditions as well as synthesis of NDFs with longer alkyl chains for improved solubility is still under way.

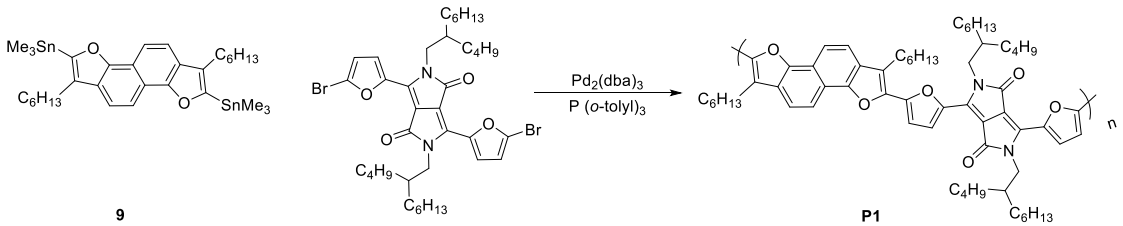

Scheme 7.6 Synthesis of **P1**

7.4 Experimental Data

7.4.1 Materials and General Experimental Details.

Tetrahydrofuran was dried using an Innovative Technologies solvent purification system. Starting materials including 1,5-dihydroxynapthalene and 1,-dimethoxybenzene were purchased from commercial sources and used without

further purification unless noted otherwise. All reactions were run under argon at ambient temperature unless otherwise noted. Chromatographic separation was performed using 35 – 70 μm silica gel, using the eluents indicated.

7.4.2 Instrumentation

Nuclear magnetic resonance spectra were obtained on a 400 MHz spectrometer (^{1}H at 400 MHz and ^{13}C at 100 MHz). ^{1}H NMR samples were referenced internally to residual protonated solvent ^{13}C NMR are referenced to the middle carbon peak of $CDCl_3$. In both instances chemical shifts are given in δ ppm relative to tetramethylsilane.

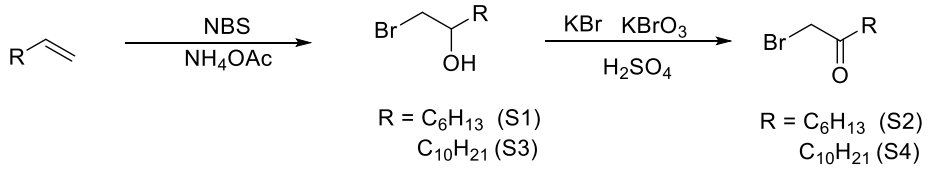

R = C_6H_{13} (S1)
$C_{10}H_{21}$ (S3)

R = C_6H_{13} (S2)
$C_{10}H_{21}$ (S4)

1-bromooctan-2-ol (S1). 1-octene (7.0 g, 62.4 mmol), NH_4OAc (0.29 g, 6.24 mmol), NBS (13.3 g, 72.0 mmol), water (60 mL) and acetone (60 mL) were added to a 2-neck round bottom flask equipped with a stir bar. The reaction changed colors from orange to yellow to colorless within 15 minutes. The reaction was allowed to stir overnight at room temperature after which it was poured into hexanes and the two layers were separated. The organic layers were washed with water followed by brine. The organic layer was dried over an. Na_2SO_4. It was then filtered into a pre-weighed round bottom flask and the solvent was removed under reduced pressure. The colorless oil obtained was purified by flash column chromatography using hexanes: ethyl acetate (95:5) as the eluent. 5.28 g (41%) of the product was obtained as colorless oil. ^{1}H NMR (400 MHz, Chloroform-*d*) δ

3.76 (m, 1H), 3.54 (dd, J = 10.3, 3.2 Hz, 1H), 3.38 (dd, J = 10.3, 7.1 Hz, 1H), 2.15 (s, 1H), 1.57 – 1.50 (m, 2H), 1.28 (s, 8H), 0.88 (d, J = 4.6 Hz, 3H).

1-bromooctan-2-one (S2). S1 (5.28 g, 25.3 mmol) and distilled water (100 mL) were added to a 3-neck 250 mL round bottom flask equipped with a stir bar and an addition funnel. KBr (2.10 g, 17.67 mmol) and $KBrO_3$ (1.48 g, 8.84 mmol) were added to the flask at room temperature. 10 % H_2SO_4 (13.0 mL) was then added via an addition funnel over a period of 6 h. The reaction was allowed to stir at room temperature overnight after which 10 drops of sat. $Na_2S_2O_3$ was added. The aqueous solution was extracted with DCM. The organic layer was washed with water and brine after which it was dried over an. Na_2SO_4. It was then filtered into a pre-weighed round bottom flask and the solvent was removed under reduced pressure. The crude product (4.42 g, 85%) was carried forward to the next step without further purification. ^{1}H NMR (400 MHz, Chloroform-*d*) δ 3.88 (s, 2H), 2.64 (t, J = 7.4 Hz, 2H), 1.61 (p, J = 7.3 Hz, 2H), 1.28 (s, 6H), 0.90 – 0.86 (m, 3H).

1-bromododecan-2-ol (S3). 1-dodecene (7.0 g, 41.6 mmol), NH_4OAc (0.32 g, 4.16 mmol), NBS (8.9 g, 49.9 mmol), water (40 mL) and acetone (40 mL) were added to a 2-neck round bottom flask equipped with a stir bar. The reaction changed colors from orange to yellow to colorless within 10 minutes. The reaction was allowed to stir overnight at room temperature after which it was poured into hexanes and the two layers were separated. The organic layers were washed with water followed by brine. The organic layer was dried over an. Na_2SO_4. It was then filtered into a pre-weighed round

bottom flask and the solvent was removed under reduced pressure. The colorless oil obtained was purified by flash column chromatography using hexanes: ethyl acetate (95:5) as the eluent. 9.14 g (83%) of the product was obtained as colorless oil.

1-bromododecan-2-one (S4). S3 (4.27 g, 16.10 mmol) and distilled water (65 mL) were added to a 3-neck 250 mL round bottom flask equipped with a stir bar and an addition funnel. KBr (1.35 g, 11.27 mmol) and $KBrO_3$ (0.94 g, 5.63 mmol) were added to the flask at room temperature. 10 % H_2SO_4 (8.2 mL) was then added via an addition funnel over a period of 6 h. The reaction was allowed to stir at room temperature overnight after which 10 drops of sat. $Na_2S_2O_3$ was added. The aqueous solution was extracted with DCM. The organic layer was washed with water and brine after which it was dried over an. Na_2SO_4. It was then filtered into a pre-weighed round bottom flask and the solvent was removed under reduced pressure. The crude product (4.10 g, 97%) was carried forward to the next step without further purification. ^{1}H NMR (300 MHz, Chloroform-*d*) δ 3.88 (s, 2H), 2.64 (t, J = 7.4 Hz, 2H), 1.60 (t, J = 7.3 Hz, 2H), 1.27 (s, 16H), 0.88 (t, J = 6 Hz, 3H).

1,1'-((2,5-diiodo-1,4-phenylene)bis(oxy))bis(octan-2-one) (2). 1 (5.0 g, 13.82 mmol), S2 (8.58 g, 41.45 mmol), K_2CO_3 (9.55 g, 69.08 mmol), and acetone (60 mL) were added to a 2-neck 100 mL round bottom flask equipped with a stir bar, reflux condenser and a gas inlet. The reaction was refluxed for 36 h after which it was cooled to room temperature. It was then poured into ice cold water. The solid obtained was filtered and recrystallized from isopropyl alcohol to yield 5.21 g (61%) of pure product as a white

solid. ^{1}H NMR (400 MHz, Chloroform-*d*) δ 7.10 (s, 2H), 4.50 (s, 4H), 2.70 (t, *J* = 8 Hz, 4H), 1.65 (m, 4H), 1.30 (s, 12H), 0.88 (t, *J* = 8 Hz, 6H). ^{13}C NMR (101 MHz, Chloroform-*d*) δ 206.81, 152.40, 122.92, 109.99, 85.87, 74.31, 39.52, 31.57, 28.89, 23.09, 22.49, 14.06.

3,7-dihexylbenzo[1,2-*b*:4,5-*b′*]difuran (3). 2 (1 g, 1.63 mmol) and 15 mL of anhydrous THF (15 mL) were added to a flame-dried round bottom flask equipped with a stir bar and gas inlet. The solution was cooled to -78 °C in a dry ice/ acetone bath. *n*-butyllithium (3.3 mL, 2.5 M in hexanes, 8.2 mmol) was added dropwise. After stirring for 1 h at -78 °C, the cooling bath was removed and the reaction mixture was allowed to warm slowly to room temperature. It was stirred at room temperature overnight. The reaction mixture was then cooled to 0 °C in an ice bath and quenched by the careful addition of sat. NH_4Cl followed by hexanes. The organic layer was separated and rinsed with brine. It was then dried over an. Na_2SO_4. The solution was filtered into a pre-weighed round bottom flask and the solvent was removed via rotary evaporation. Purification via column chromatography using hexanes: EtoAc (95:5) yielded 0.24 g (45%) product as a pale yellow solid. ^{1}H NMR (400 MHz, Chloroform-*d*) δ 7.52 (s, 1H), 7.41 (s, 1H), 2.68 (t, *J* = 8 Hz, 3H), 1.72 (m, 2H), 1.42 (m, 2H), 1.33 (m, 4H), 0.89 (t, *J* = 8 Hz, 3H). ^{13}C NMR (101 MHz, Chloroform-*d*) δ 152.17, 141.58, 126.35, 120.69, 100.64, 31.65, 29.18, 28.84, 23.70, 22.63, 14.10.

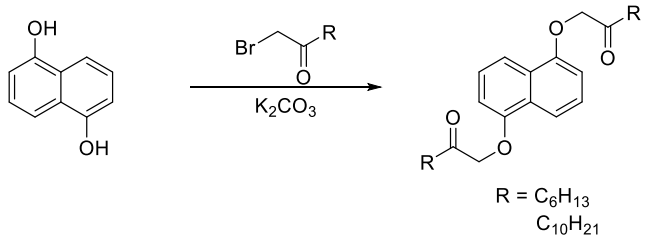

1,1'-(naphthalene-1,5-diylbis(oxy))bis(octan-2-one) (5). **4** (0.32 g, 2.0 mmol), S2 (1.24g, 5.99 mmol), K_2CO_3 (1.38 g, 10.0 mmol), and acetone (10 mL) were added to a 25 mL round bottom flask equipped with a stir bar, reflux condenser and a gas inlet. The reaction was refluxed for 36 h after which it was cooled to room temperature. It was then poured into ice cold water. The solid obtained was filtered and recrystallized from 95% EtOH to yield 0.6 g (73%) of pure product as a buff colored solid. ^{1}H NMR (400 MHz, Chloroform-*d*) δ 7.96 (d, *J* = 8.5 Hz, 2H), 7.40 (t, *J* = 8.1 Hz, 2H), 6.74 (d, *J* = 7.7 Hz, 2H),), 4.71 (s, 4H) 2.72 (t, *J* = 7.4 Hz, 4H), 1.66 (m, 4H), 1.29 (s, 12H), 0.87 (t, *J* = 8 Hz, 6H).

1,6-dihexylnaphtho[1,2-*b*:5,6-*b'*]difuran (6) Methanesulfonic acid (0.46 g, 4.85 mmol) was added to a round bottom flask containing **5** (0.20 g, 0.48 mmol) and DCM (10 mL) at 0 ˚C. The reaction was refluxed for 1 h after which it was cooled to room temperature. It was then poured into ice cold water. The organic layers were washed with water followed by brine. The organic layer was dried over an. Na_2SO_4. It was then filtered into a pre-weighed round bottom flask and the solvent was removed under reduced pressure. The crude product obtained was purified by flash column chromatography using hexanes as the eluent. 0.12 g (67%) of the product was obtained as yellow solid. ^{1}H NMR (400 MHz, Chloroform-*d*) δ 8.12 (d, *J* = 8.5 Hz, 2H), 7.72 (d, *J* = 8.5 Hz, 2H), 7.55 (s, 2H), 2.76 (t, *J*

= 7.6 Hz, 4H), 1.77 (m, 4H), 1.44 (m, 4H), 1.34 (s, 8H), 0.90 (t, *J* = 8Hz, 6H). ^{13}C NMR (101 MHz, Chloroform-*d*) δ 151.40, 140.07, 123.33, 122.00, 119.05, 118.69, 114.99, 31.70, 29.31, 29.23, 23.72, 22.67, 14.13, 1.06.

1,1'-(naphthalene-1,5-diylbis(oxy))bis(dodecan-2-one) (7). 4 (0.32 g, 2.0 mmol), S4 (1.58 g, 6.0 mmol), K_2CO_3 (1.38 g, 10.0 mmol), and acetone (20 mL) were added to a 50 mL round bottom flask equipped with a stir bar, reflux condenser and a gas inlet. The reaction was refluxed for 36 h after which it was cooled to room temperature. It was then poured into ice cold water. The solid obtained was filtered and was carried forward without further purification. 0.81 g (77%) of product was isolated as a buff colored solid. The crude NMR showed residual hexanes. ^{1}H NMR (400 MHz, Chloroform-*d*) δ 7.96 (d, *J* = 8.5 Hz, 2H), 7.39 (t, *J* = 8.1 Hz, 2H), 6.74 (d, *J* = 7.7 Hz, 2H), 4.70 (s, 4H), 2.70 (d, *J* = 7.3 Hz, 4H), 1.76 – 1.62 (m, 4H), 1.25 (s, 38H), 0.89 (t, *J* = 8 Hz, 8H).^{13}C NMR (101 MHz, Chloroform-*d*) δ 208.04, 153.37, 126.61, 125.37, 115.21, 105.82, 73.04, 39.22, 31.88, 29.54, 29.45, 29.40, 29.30, 29.22, 23.14, 22.67, 14.12.

1,6-didecylnaphtho[1,2-*b*:5,6-*b'*]difuran (8). Methanesulfonic acid (1.3 mL, 21.2 mmol) was added to a round bottom flask containing **5** (0.91 g, 1.73 mmol) and DCM (30 mL) at 0 ˚C. The reaction was refluxed for 1 h after which it was cooled to room temperature. It was then poured into ice cold water. The organic layers were washed with water followed by brine. The organic layer was dried over an. Na_2SO_4. It was then filtered into a pre-weighed round bottom flask and the solvent was removed under reduced pressure. The crude product obtained was purified by flash column

chromatography using hexanes as the eluent. 0.69 g (81%) of the product was obtained as yellow solid. ^{1}H NMR (300 MHz, Chloroform-*d*) δ 8.12 (d, *J* = 8.4 Hz, 2H), 7.72 (d, *J* = 8.5 Hz, 2H), 7.55 (s, 2H), 2.76 (t, *J* = 7.6 Hz, 4H), 1.76 (m, 4H), 1.26 (s, 28H), 0.86 (t, *J* = 6 Hz, 6H).^{13}C NMR (101 MHz, cdcl$_3$) δ 151.38, 140.08, 123.32, 121.99, 119.02, 118.71, 114.97, 31.90, 29.62, 29.52, 29.46, 29.34, 23.71, 22.68, 14.12, 1.02.

(1,6-dihexylnaphtho[1,2-*b*:5,6-*b′*]difuran-2,7-diyl)bis(trimethylstannane) (9). 6 (0.25 g, 0.66 mmol) was dissolved in 15 mL of anhydrous THF in a flame-dried round bottom flask. The solution was cooled to 0 °C in an ice bath. *n*-butyllithium (0.8 mL, 2.4 M in hexanes) was added dropwise. The resulting dianion was stirred at 0 °C for 1 h. Trimethyltin chloride (2.7 mL, 1 M in THF) was added. The reaction was slowly warmed to room temperature overnight. The reaction was quenched by addition of water. The product was extracted with DCM. The organic layer was washed with 1M KF followed by water and brine, and dried over Na_2SO_4. The solvent was removed under reduced pressure. Recrystallization from isopropanol afforded 0.36 g (78 %) of pure product as a yellow solid. ^{1}H NMR (300 MHz, Chloroform-*d*) δ 8.11 (d, *J* = 8.5 Hz, 2H), 7.67 (d, *J* = 8.4 Hz, 2H), 2.76 (t, *J* = 9 Hz, 4H), 1.27 (m, 22H), 0.88 (s, 10H), 0.47 (s, 9H).

2,2'-(1,6-didecylnaphtho[1,2-*b*:5,6-*b′*]difuran-2,7-diyl)bis(4,4,5,5-tetramethyl-1,3,2-dioxaborolane) (10). 6 (0.47 g, 1.25 mmol) was dissolved in 10 mL of anhydrous THF in a flame-dried round bottom flask. The solution was cooled to -78 °C in an acetone/ dry ice bath. *n*-butyllithium (1.3 mL, 2.5 M in hexanes) was added dropwise. The resulting dianion was stirred at -78 °C for 1 h. 2-isopropoxy-4,4,5,5-tetramethyl-1,3,2-

dioxaborolane (0.9 mL, 4.3 mmol) was added. The reaction was slowly warmed to room temperature overnight. The reaction was quenched by addition of water. The product was extracted with DCM. The organic layer was washed with water and brine, and dried over Na_2SO_4. The solvent was removed under reduced pressure. Cold crystallization from hexanes afforded 0.36 g (46 %) of pure product as a yellow solid. ^{1}H NMR (400 MHz, Chloroform-*d*) δ 8.30 (d, *J* = 8.6 Hz, 2H), 7.71 (d, *J* = 8.6 Hz, 2H), 3.04 (t, *J* = 7.5 Hz, 4H), 1.77 – 1.69 (m, 4H), 1.41 (s, 24H), 1.23-1.34 (s, 12H), 0.88 (t, *J* = 6.9 Hz, 6H). ^{13}C NMR (101 MHz, Chloroform-*d*) δ 154.05, 136.94, 124.26, 119.94, 118.71, 116.28, 83.95, 31.58, 30.61, 28.94, 24.84, 23.90, 22.63, 14.12, 1.02.

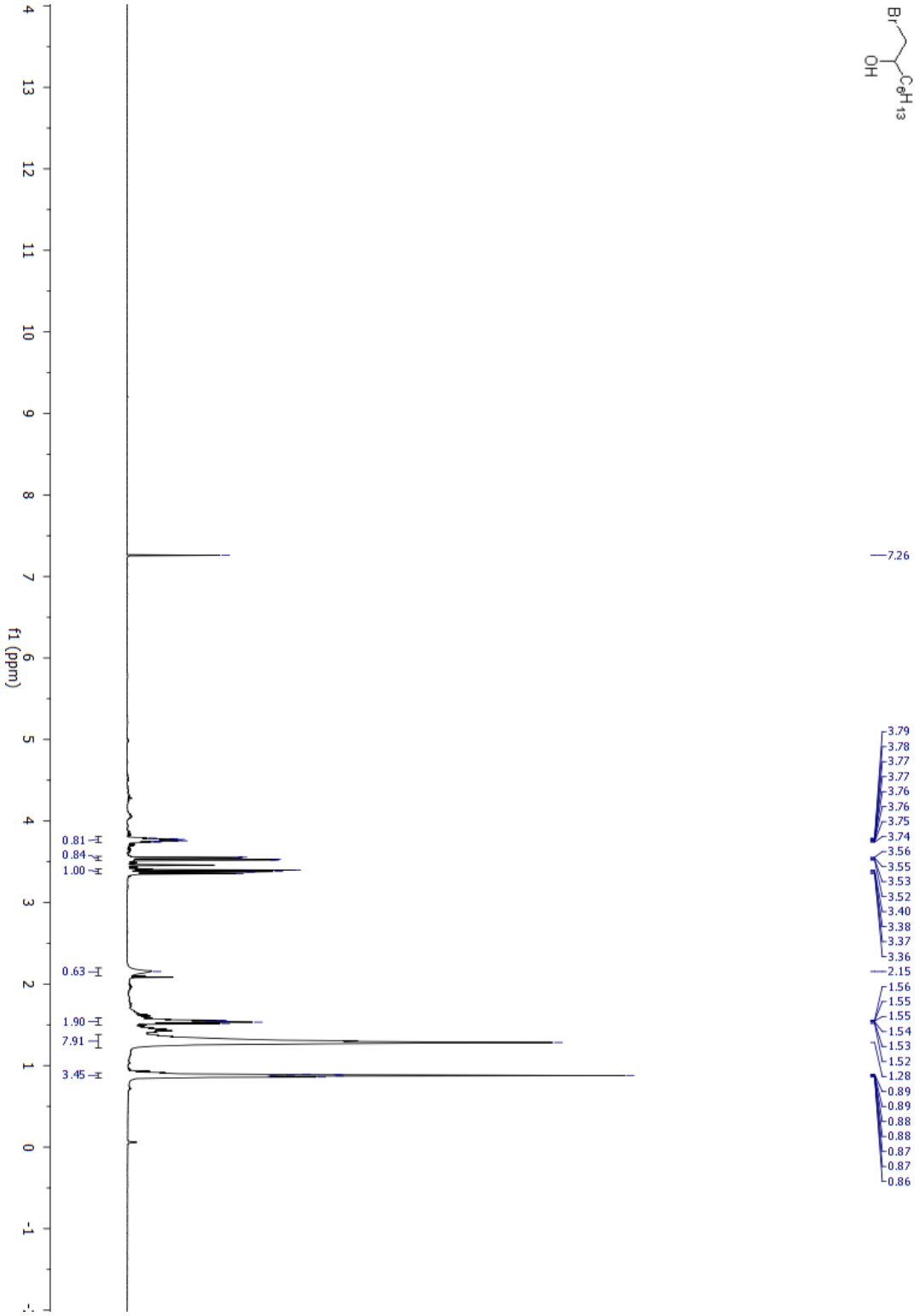

Figure 7.4.1 ^{1}H NMR of S1

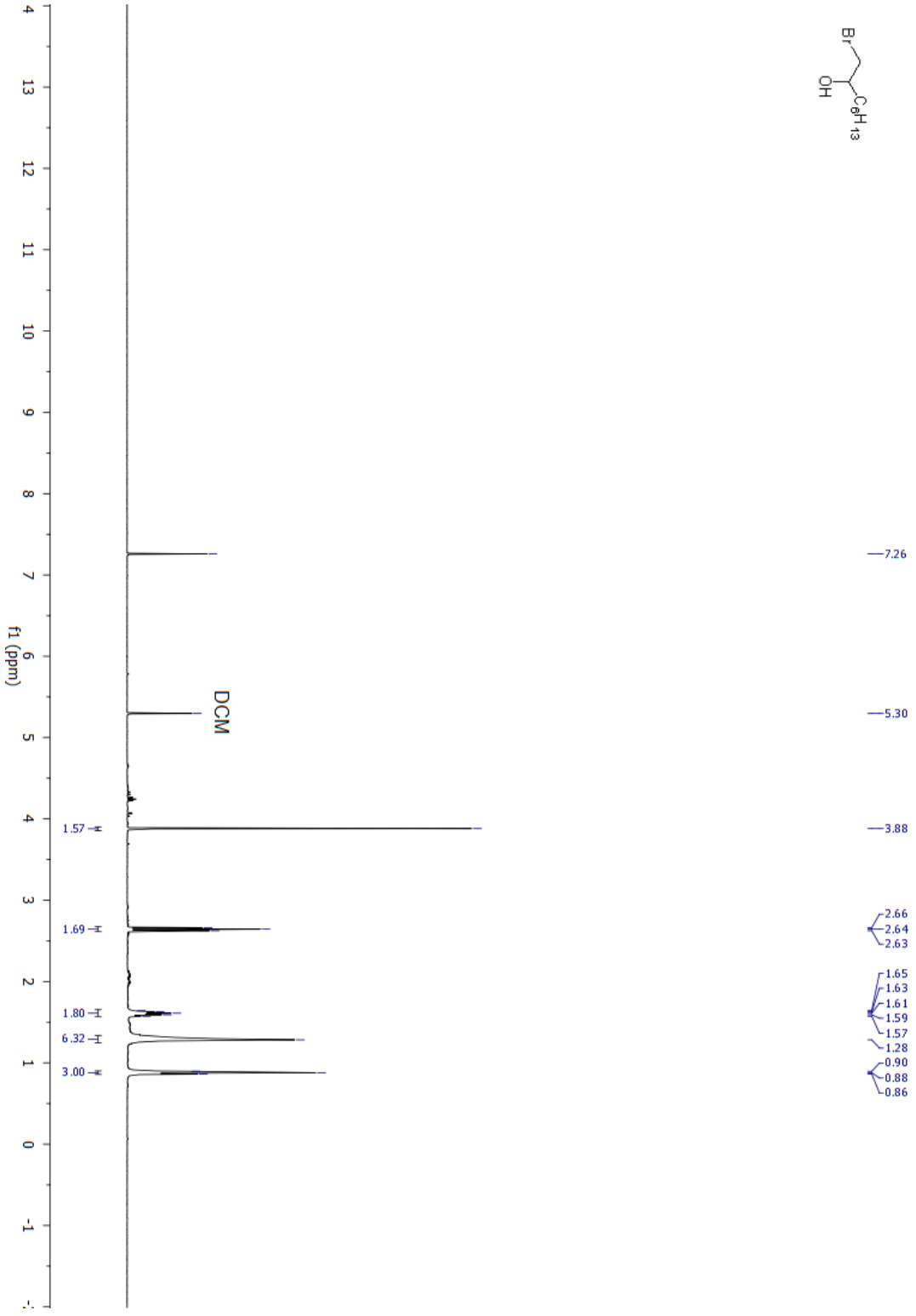

Figure 7.4.2 ^{1}H NMR of S2

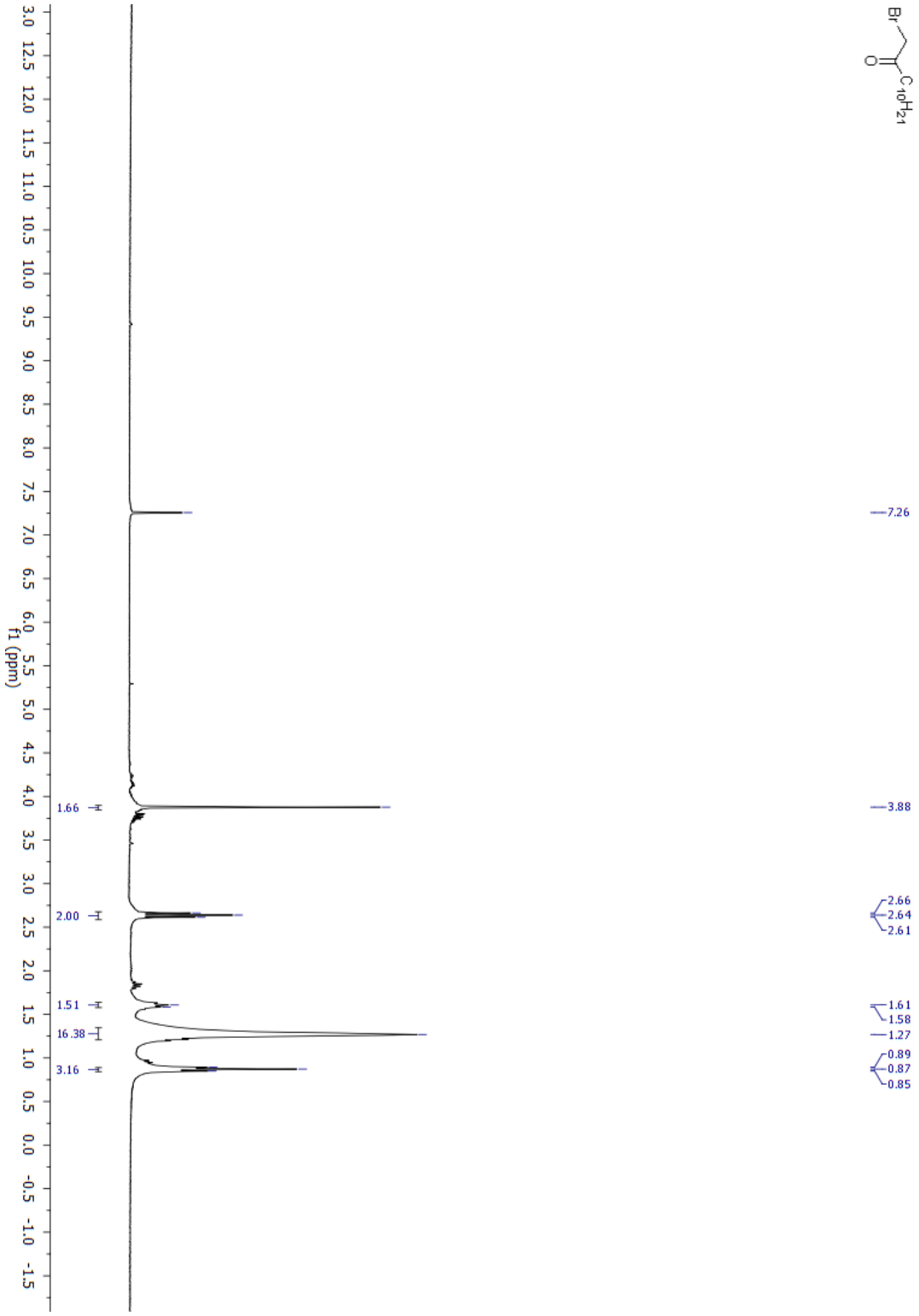

Figure 7.4.4 ^{1}H NMR of S4

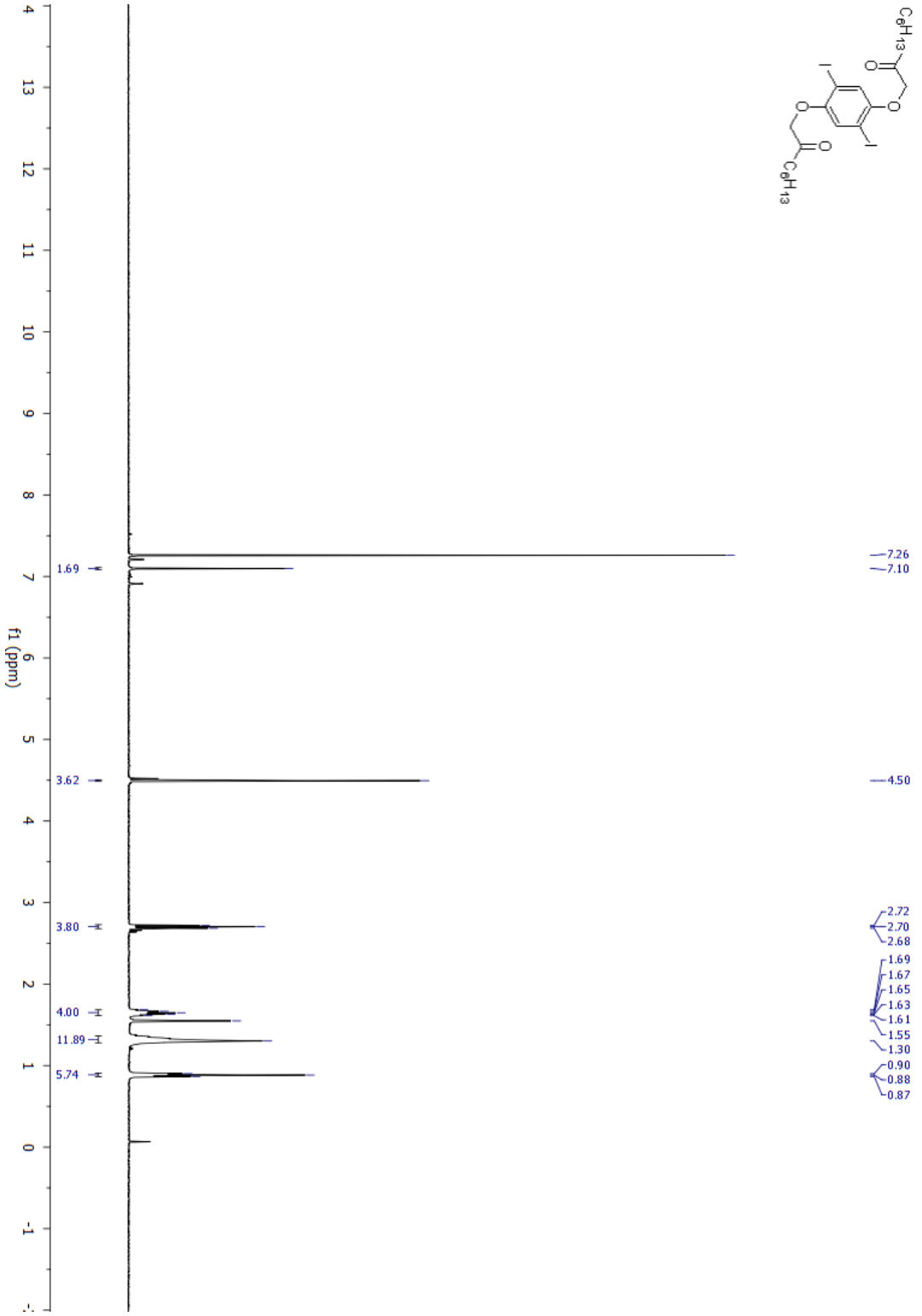

Figure 7.4.5 ^{1}H NMR of 2

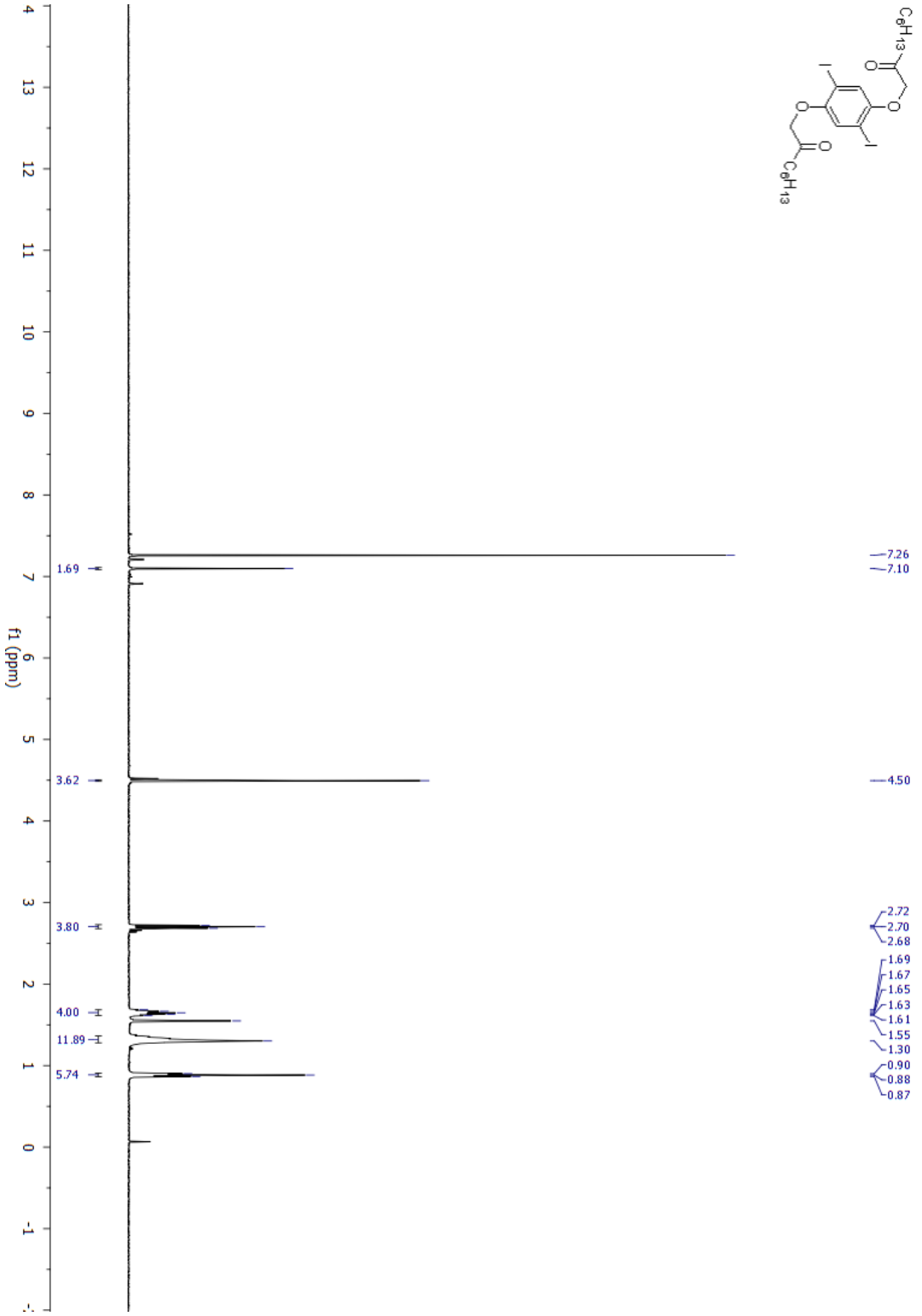

Figure 7.4.6 ^{13}C NMR of 2

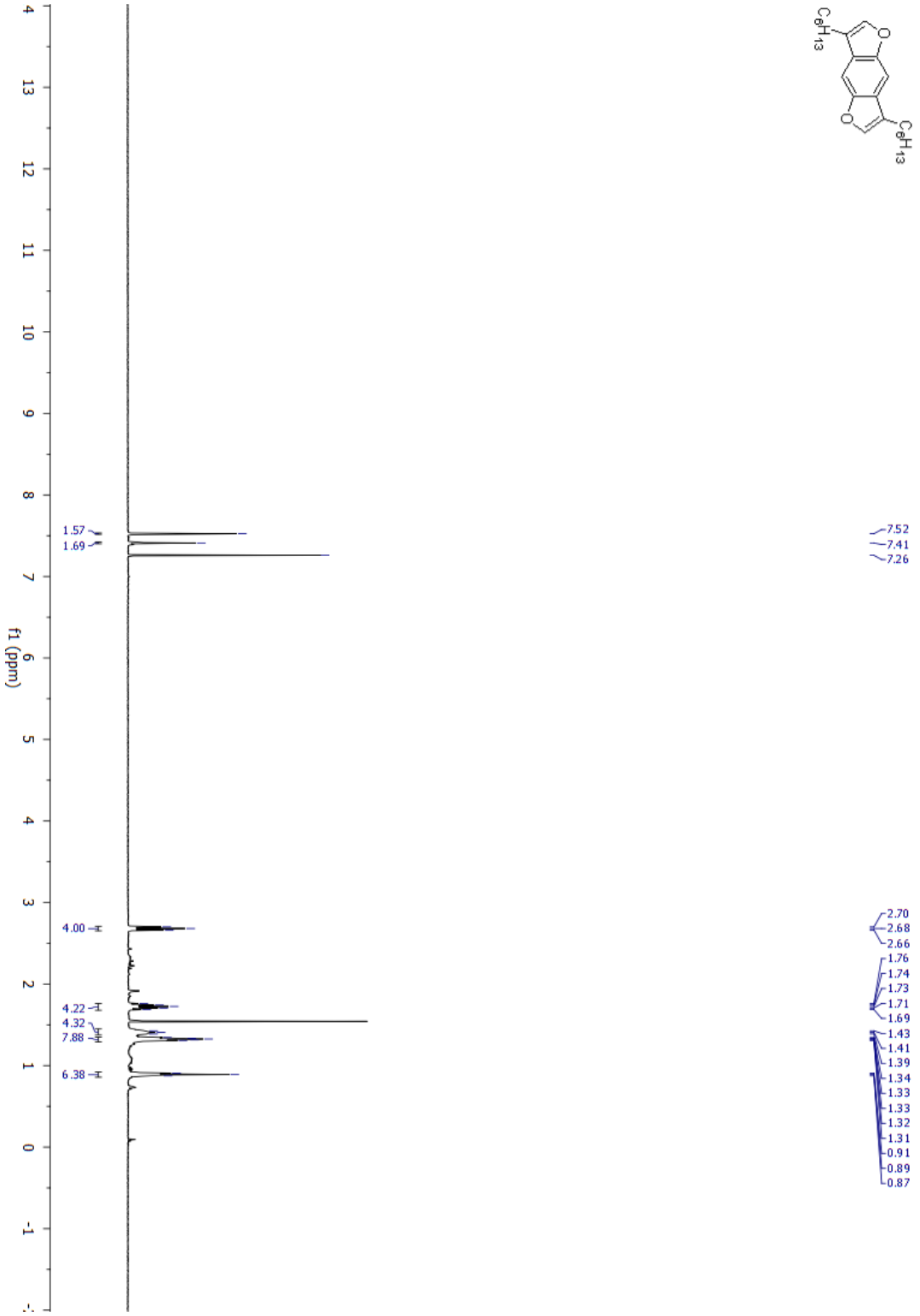

Figure 7.4.7 ^{1}H NMR of 3

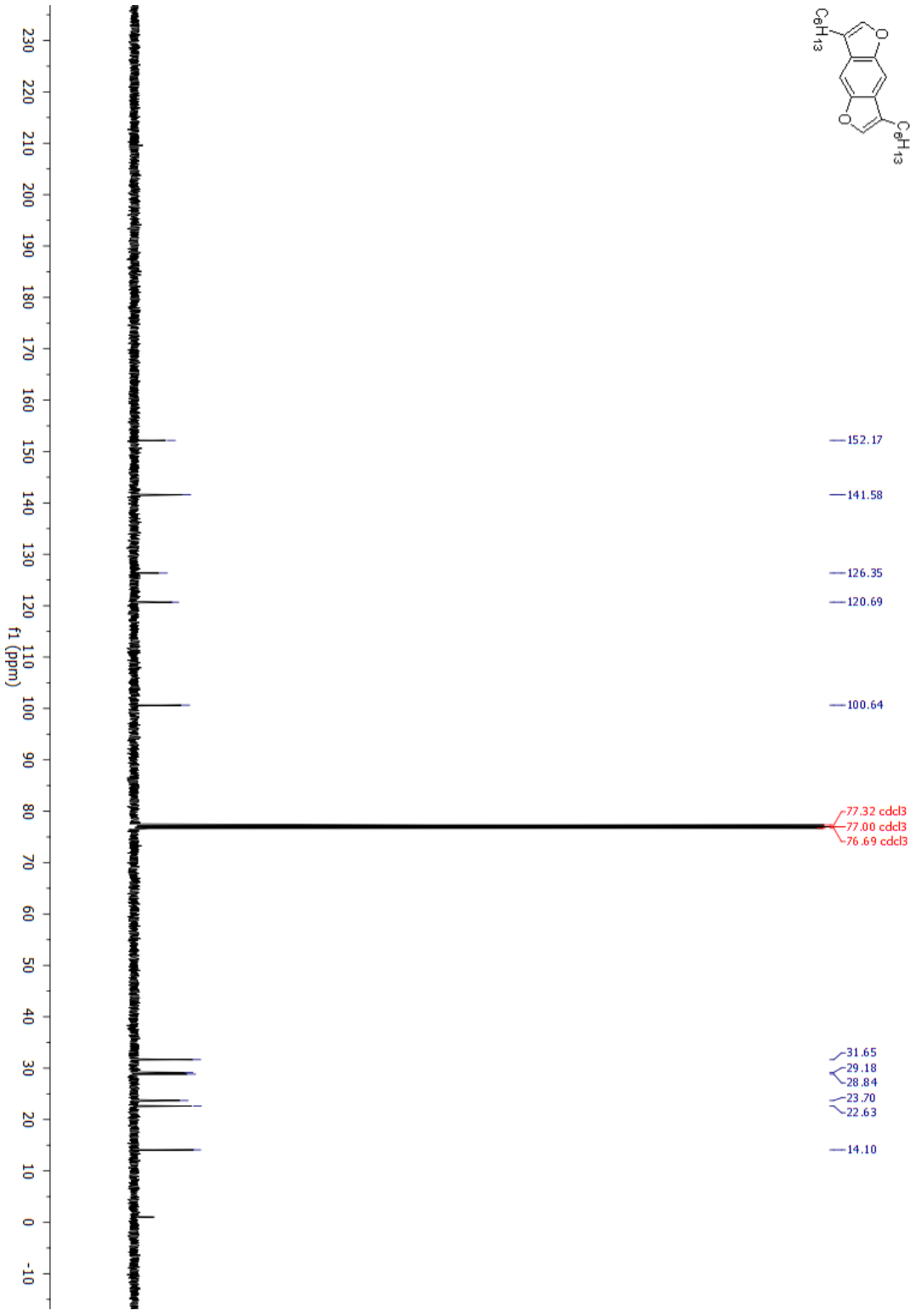

Figure 7.4.8 ^{13}C NMR of 3

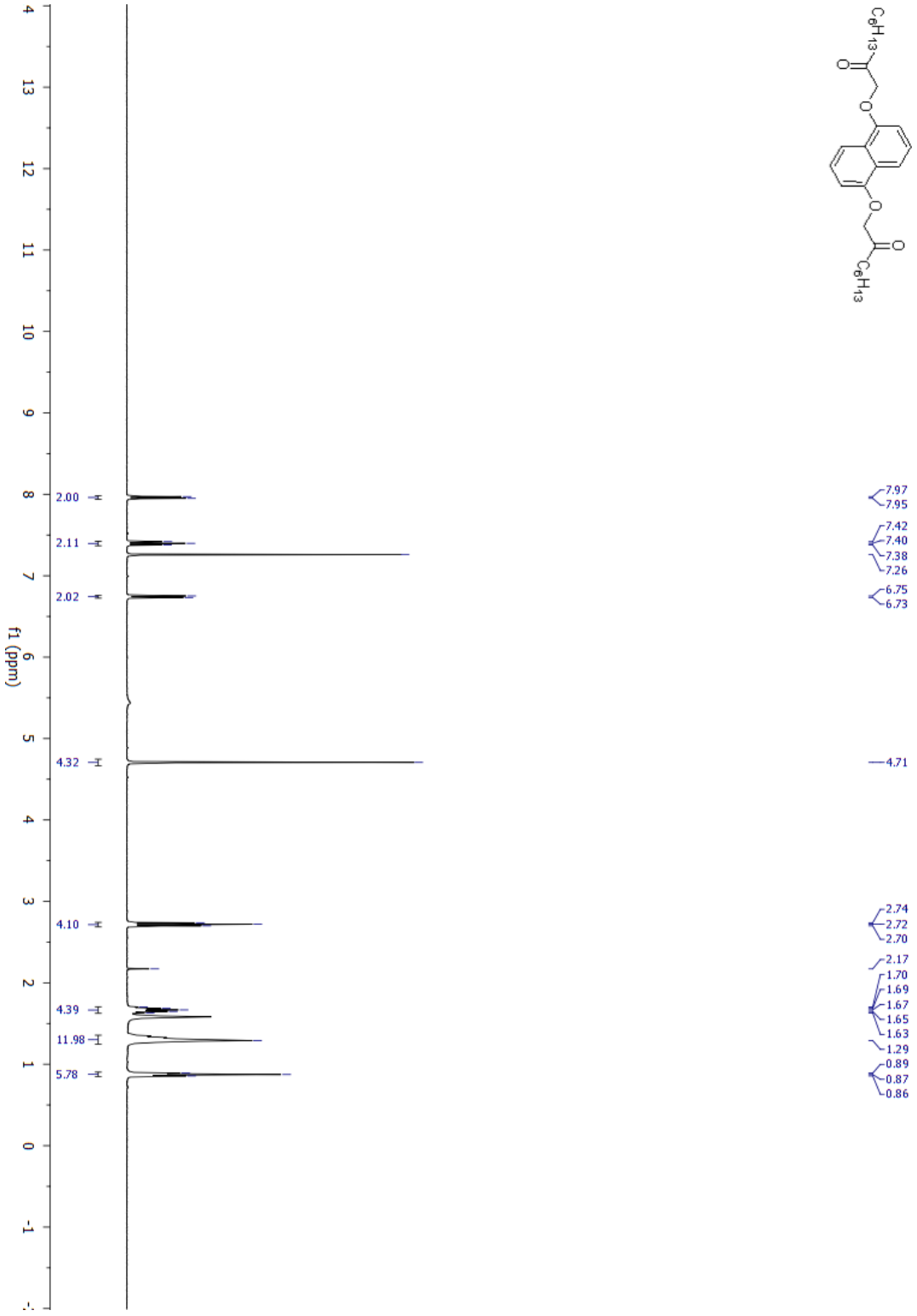

Figure 7.4.9 ^{1}H NMR of 5

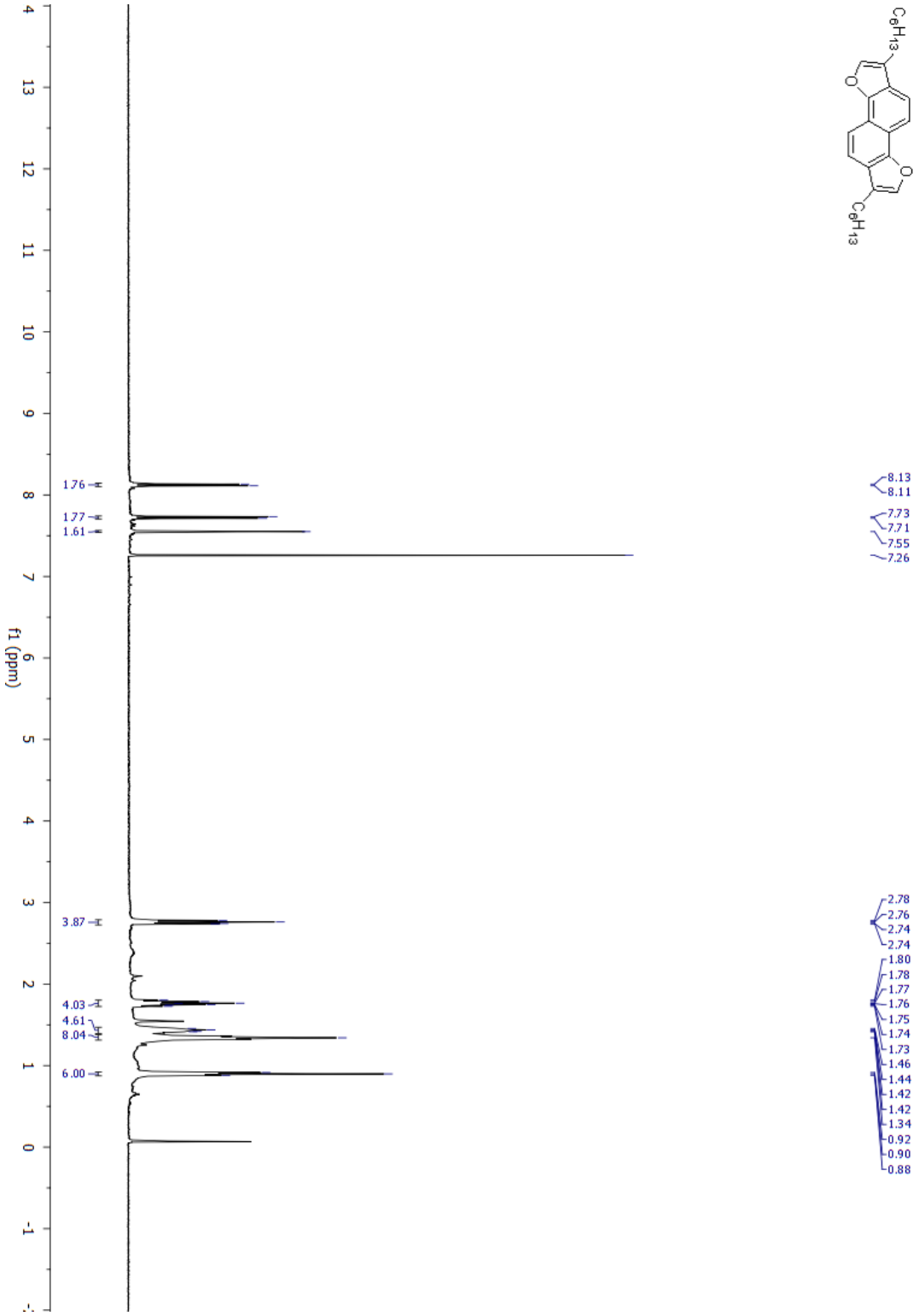

Figure 7.4.11 ^{1}H NMR of 6

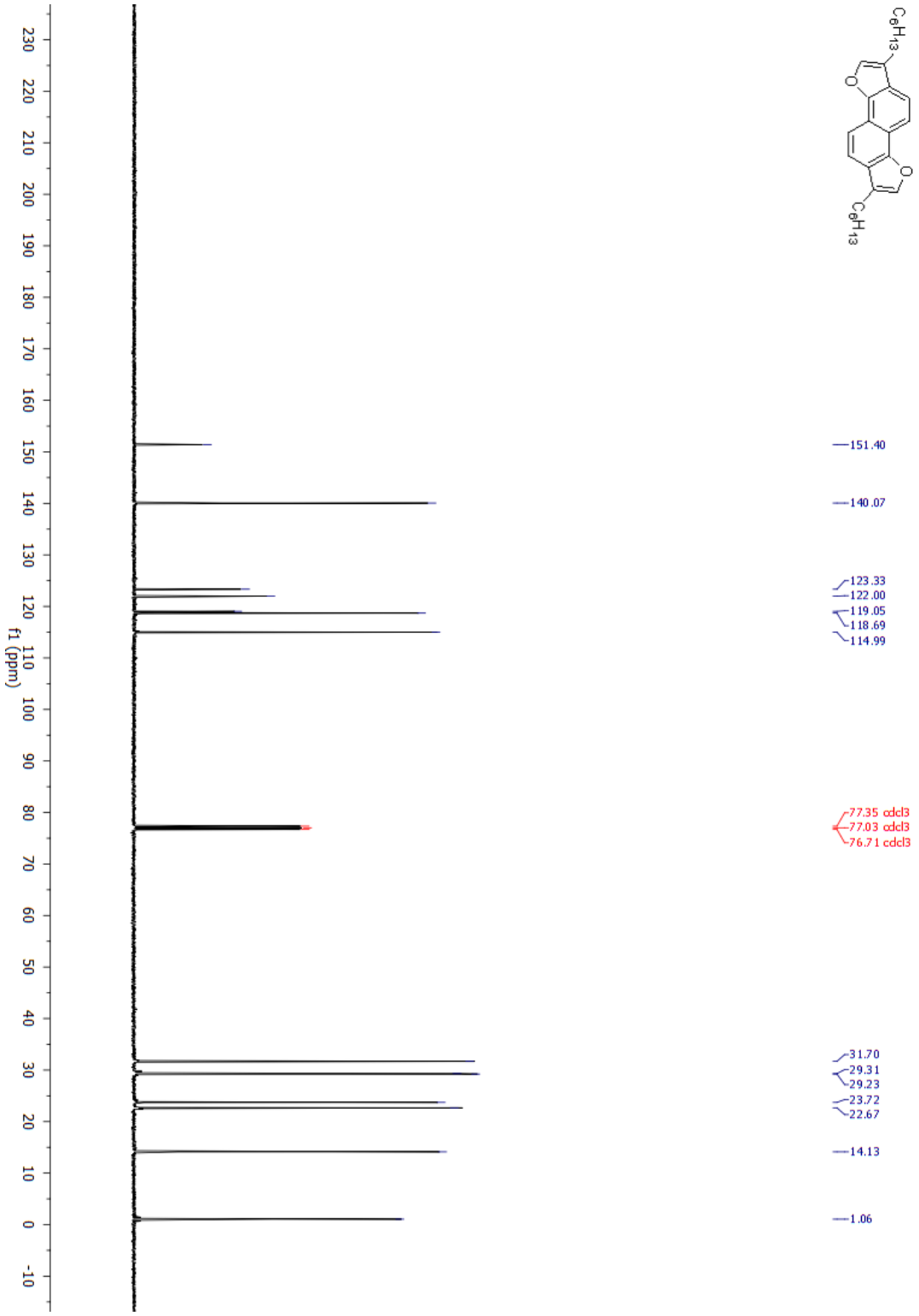

Figure 7.4.12 ^{13}C NMR of 6

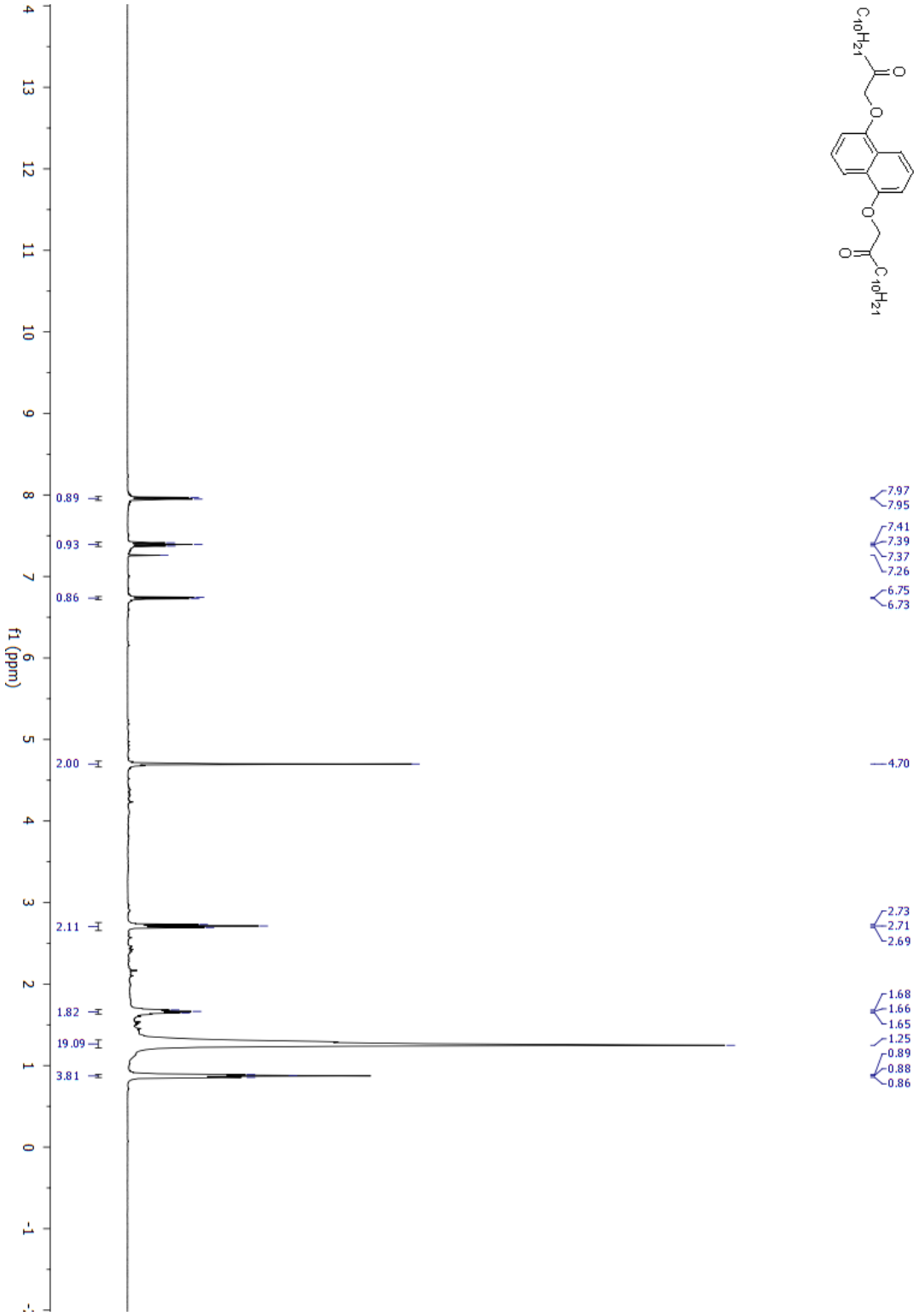

Figure 7.4.13 ^{1}H NMR of 7

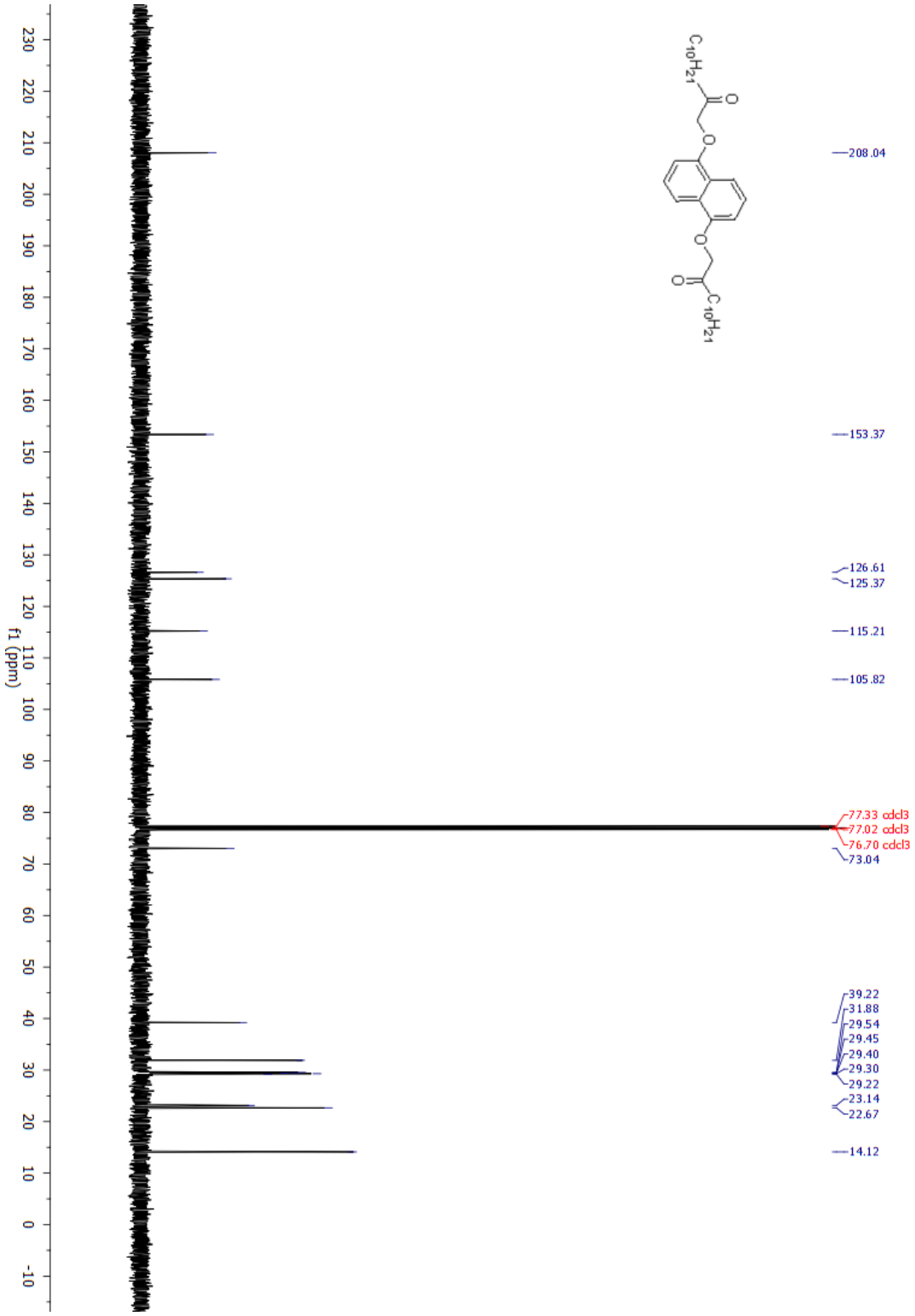

Figure 7.4.14 ^{13}C NMR of 7

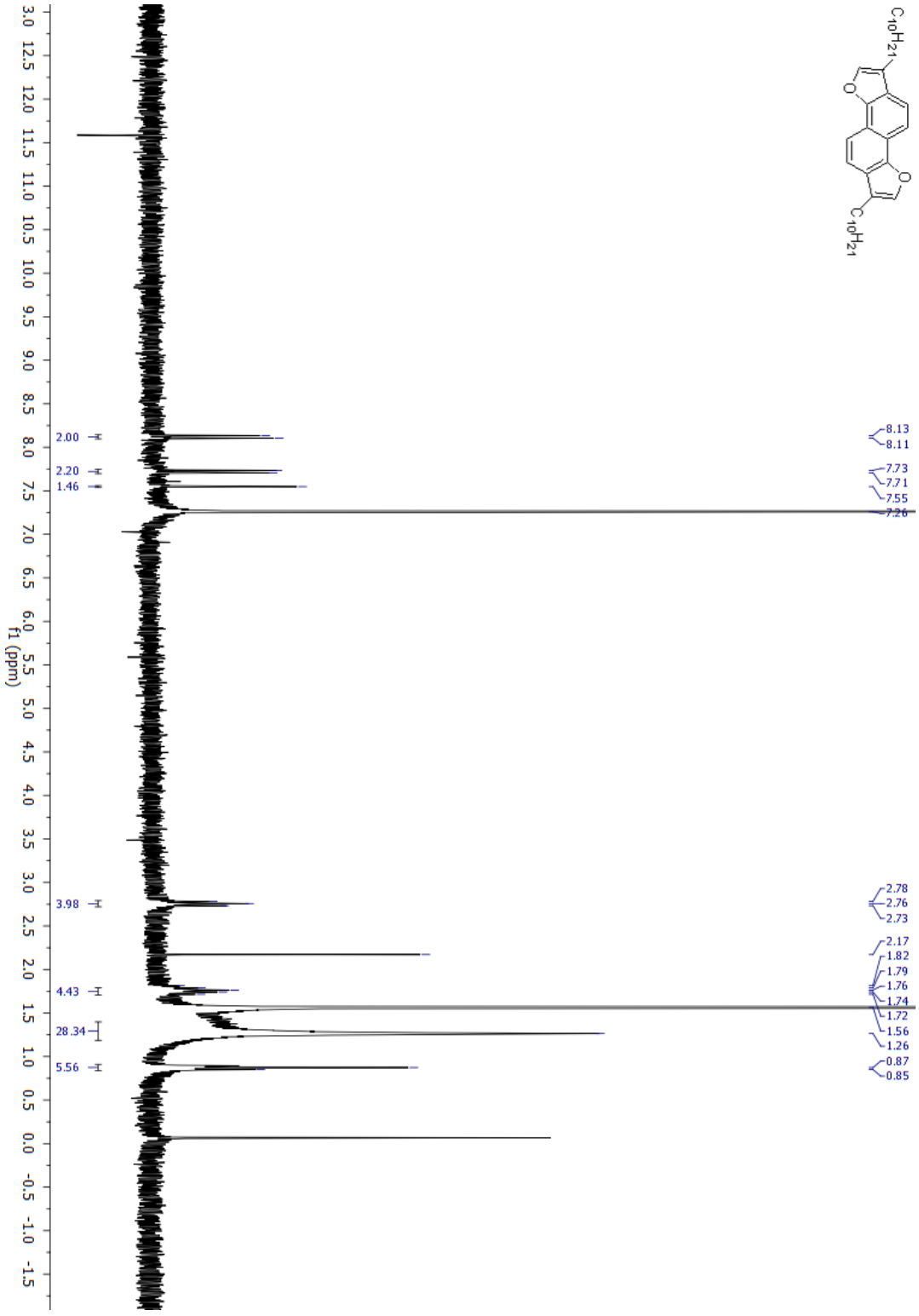

Figure 7.4.15 ^{1}H NMR of 8

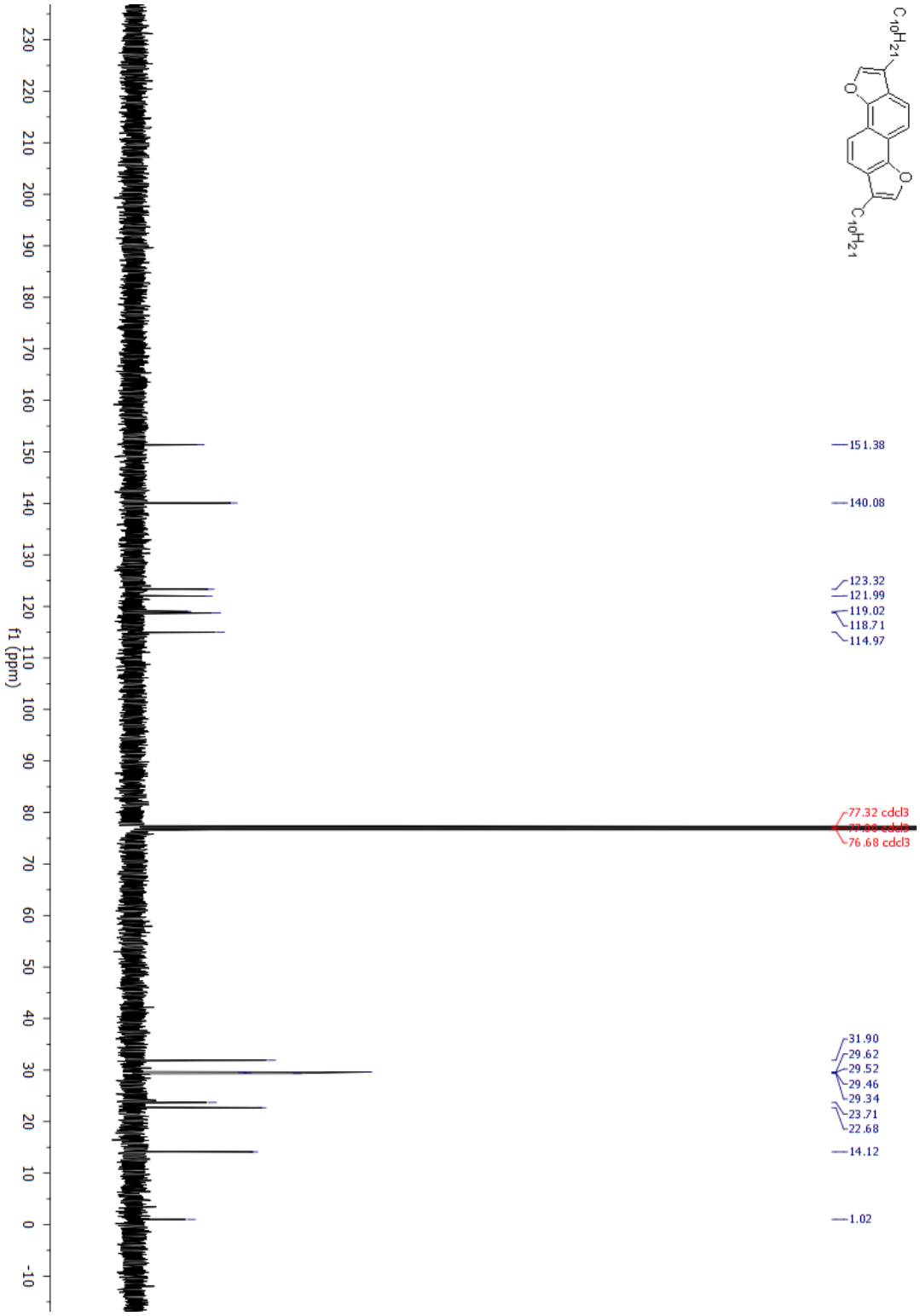

Figure 7.4.16 ^{13}C NMR of 8

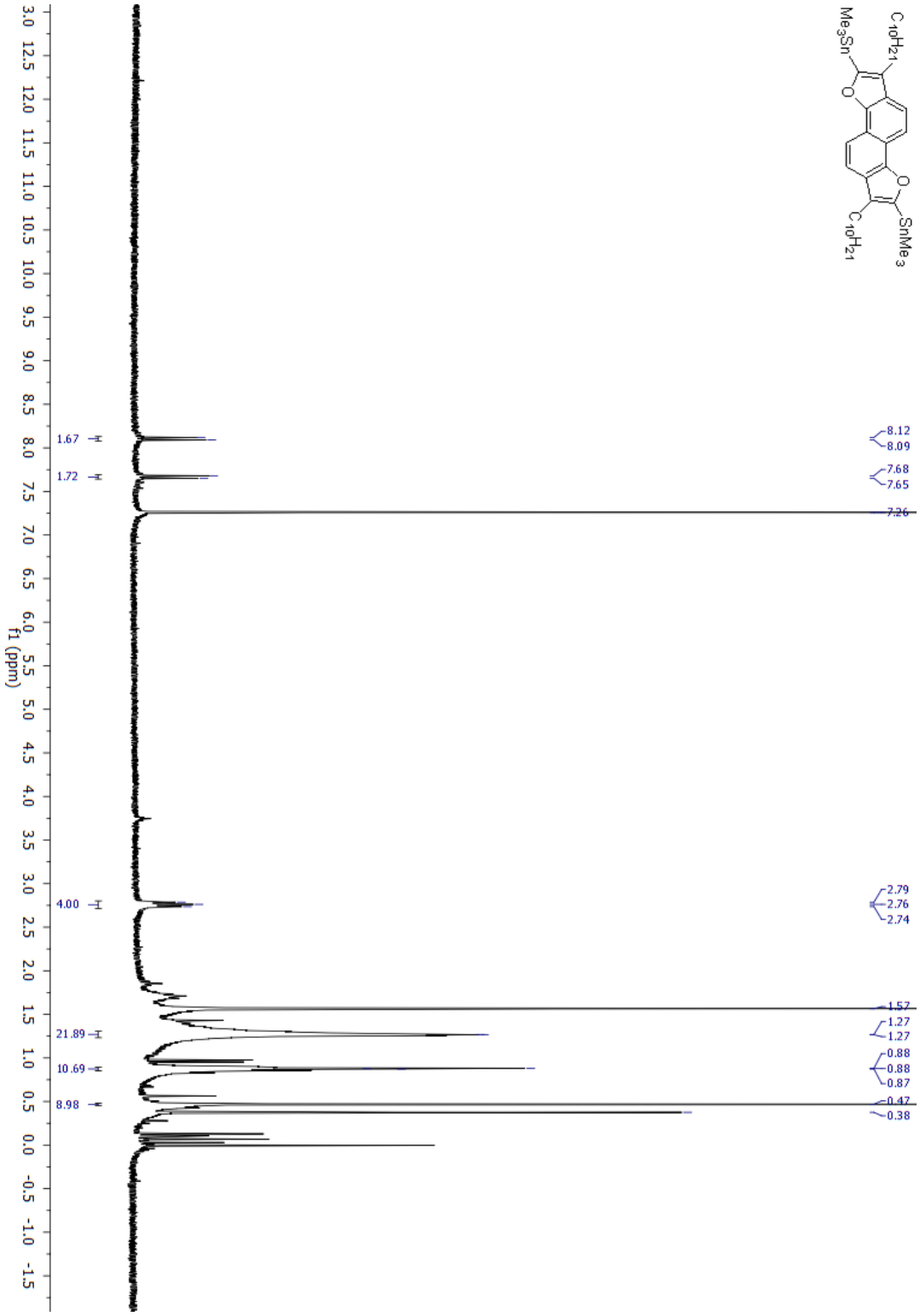

Figure 7.4.17 ^{1}H NMR of 9

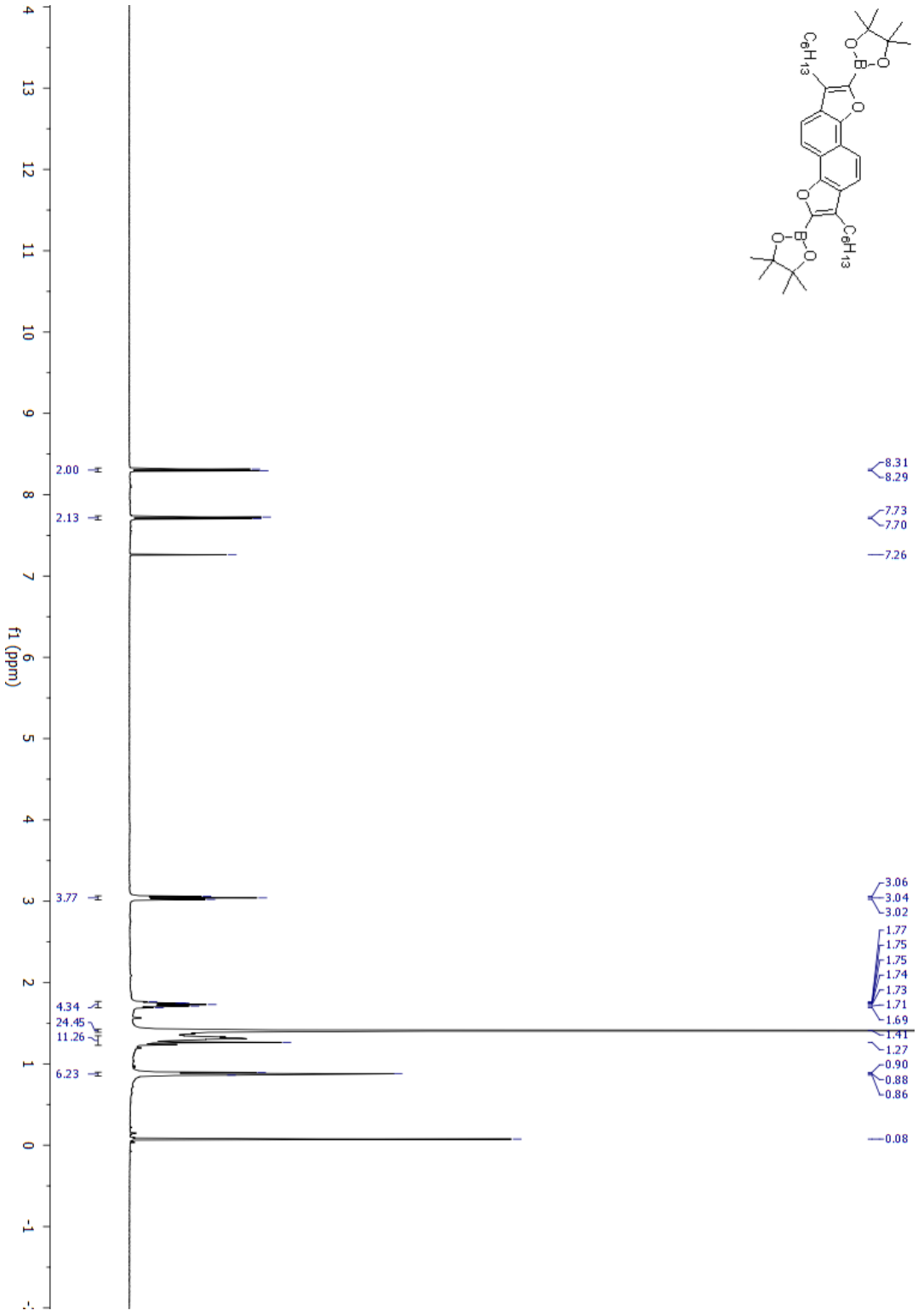

Figure 7.4.19 ^{1}H NMR of 10

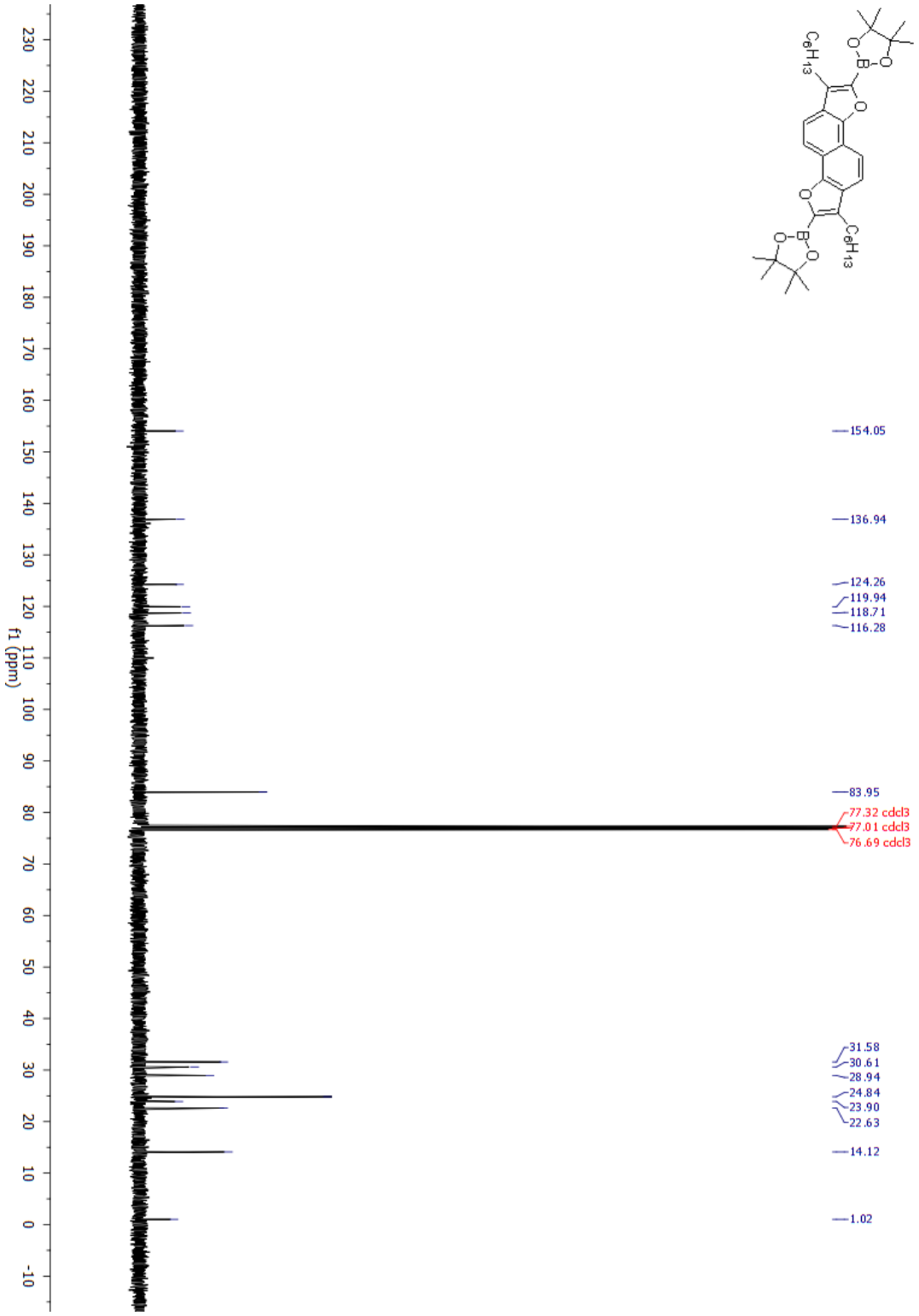

Figure 7.4.20 ^{13}C NMR of 10

7.5 References

(1) Allard, S.; Forster, M.; Souharce, B.; Thiem, H.; Scherf, U. *Angewandte Chemie International Edition* **2008**, *47*, 4070.

(2) Mike, J. F.; Nalwa, K.; Makowski, A. J.; Putnam, D.; Tomlinson, A. L.; Chaudhary, S.; Jeffries-El, M. *Physical Chemistry Chemical Physics* **2011**, *13*, 1338.

(3) Shaheen, S. E.; Ginley, D. S.; Jabbour, G. E. *MRS Bulletin* **2005**, *30*, 10.

(4) Hebner, T. R.; Wu, C. C.; Marcy, D.; Lu, M. H.; Sturm, J. C. *Applied Physics Letters* **1998**, *72*, 519.

(5) Hoth, C. N.; Schilinsky, P.; Choulis, S. A.; Brabec, C. J. *Nano Letters* **2008**, *8*, 2806.

(6) Yang, Y.; Wudl, F. *Advanced Materials* **2009**, *21*, 1401.

(7) Roncali, J. *Chemical Reviews* **1997**, *97*, 173.

(8) Günes, S.; Neugebauer, H.; Sariciftci, N. S. *Chemical Reviews* **2007**, *107*, 1324.

(9) Cheng, Y.-J.; Yang, S.-H.; Hsu, C.-S. *Chemical Reviews* **2009**, *109*, 5868.

(10) Lu, L.; Yu, L. *Advanced Materials* **2014**, *26*, 4413.

(11) Bhuwalka, A.; Mike, J. F.; He, M.; Intemann, J. J.; Nelson, T.; Ewan, M. D.; Roggers, R. A.; Lin, Z.; Jeffries-El, M. *Macromolecules* **2011**, *44*, 9611.

(12) Zhang, L.; Hu, S.; Chen, J.; Chen, Z.; Wu, H.; Peng, J.; Cao, Y. *Advanced Functional Materials* **2011**, *21*, 3760.

(13) Intemann, J. J.; Hellerich, E. S.; Tlach, B. C.; Ewan, M. D.; Barnes, C. A.; Bhuwalka, A.; Cai, M.; Shinar, J.; Shinar, R.; Jeffries-El, M. *Macromolecules* **2012**, *45*, 6888.

(14) Tang, C. W.; VanSlyke, S. A. *Applied Physics Letters* **1987**, *51*, 913.

(15) Bronstein, H.; Chen, Z.; Ashraf, R. S.; Zhang, W.; Du, J.; Durrant, J. R.; Shakya Tuladhar, P.; Song, K.; Watkins, S. E.; Geerts, Y.; Wienk, M. M.; Janssen, R. A. J.; Anthopoulos, T.; Sirringhaus, H.; Heeney, M.; McCulloch, I. *Journal of the American Chemical Society* **2011**, *133*, 3272.

(16) Jones, B. A.; Ahrens, M. J.; Yoon, M.-H.; Facchetti, A.; Marks, T. J.; Wasielewski, M. R. *Angewandte Chemie* **2004**, *116*, 6523.

(17) Zhan, X.; Tan, Z. a.; Domercq, B.; An, Z.; Zhang, X.; Barlow, S.; Li, Y.; Zhu, D.; Kippelen, B.; Marder, S. R. *Journal of the American Chemical Society* **2007**, *129*, 7246.

(18) Son, H. J.; Carsten, B.; Jung, I. H.; Yu, L. *Energy & Environmental Science* **2012**, *5*, 8158.

(19) Chu, T.-Y.; Lu, J.; Beaupré, S.; Zhang, Y.; Pouliot, J.-R.; Zhou, J.; Najari, A.; Leclerc, M.; Tao, Y. *Advanced Functional Materials* **2012**, *22*, 2345.

(20) Chu, T.-Y.; Lu, J.; Beauprea, S.; Zhang, Y.; Pouliot, J.-R.; Wakim, S.; Zhou, J.; Leclerc, M.; Li, Z.; Ding, J.; Tao, Y. *Journal of the American Chemical Society* **2011**, *133*, 4250.

(21) He, Z.; Zhong, C.; Su, S.; Xu, M.; Wu, H.; Cao, Y. *Nat Photon* **2012**, *6*, 591.

(22) http://www.heliatek.com/wp-content/uploads/2013/01/130116_PR_Heliatek_achieves_record_cell_effiency_for_OPV.pdf 2013.

(23) Dou, L.; You, J.; Yang, J.; Chen, C.-C.; He, Y.; Murase, S.; Moriarty, T.; Emery, K.; Li, G.; Yang, Y. *Nat Photon* **2012**, *6*, 180.
(24) Dou, L.; Gao, J.; Richard, E.; You, J.; Chen, C.-C.; Cha, K. C.; He, Y.; Li, G.; Yang, Y. *Journal of the American Chemical Society* **2012**, *134*, 10071.
(25) Warnan, J.; Cabanetos, C.; Labban, A. E.; Hansen, M. R.; Tassone, C.; Toney, M. F.; Beaujuge, P. M. *Advanced Materials* **2014**, *26*, 4357.
(26) Hosmane, R. S.; Liebman, J. F. *Tetrahedron Letters* **1992**, *33*, 2303.
(27) Bunz, U. H. F. *Angewandte Chemie International Edition* **2010**, *49*, 5037.
(28) Tsuji, H.; Mitsui, C.; Ilies, L.; Sato, Y.; Nakamura, E. *Journal of the American Chemical Society* **2007**, *129*, 11902.
(29) Nakano, M.; Shinamura, S.; Sugimoto, R.; Osaka, I.; Miyazaki, E.; Takimiya, K. *Organic Letters* **2012**, *14*, 5448.
(30) Hu, C.; Fu, Y.; Li, S.; Xie, Z.; Zhang, Q. *Polymer Chemistry* **2012**, *3*, 2949.
(31) Kobilka, B. M.; Dubrovskiy, A. V.; Ewan, M. D.; Tomlinson, A. L.; Larock, R. C.; Chaudhary, S.; Jeffries-El, M. *Chemical Communications* **2012**, *48*, 8919.
(32) Mitsui, C.; Soeda, J.; Miwa, K.; Tsuji, H.; Takeya, J.; Nakamura, E. *Journal of the American Chemical Society* **2012**, *134*, 5448.
(33) Osaka, I.; Abe, T.; Shimawaki, M.; Koganezawa, T.; Takimiya, K. *ACS Macro Letters* **2012**, *1*, 437.
(34) Li, S.; Yuan, Z.; Deng, P.; Sun, B.; Zhang, Q. *Polymer Chemistry* **2014**, *5*, 2561.
(35) Kobilka, B. M.; Hale, B. J.; Ewan, M. D.; Dubrovskiy, A. V.; Nelson, T. L.; Duzhko, V.; Jeffries-El, M. *Polymer Chemistry* **2013**, *4*, 5329.

CHAPTER 8

GENERAL CONCLUSIONS

8.1 Future Research

A new electron deficient system based on thiazolopyridines has been developed by the author of this dissertation. Initial studies have shown that incorporation of these materials as acceptors into alternating donor-acceptor conjugated backbones for organic semiconductors affords materials with medium band gaps, comparable to those of many conjugated polymers studied for organic photovoltaic cells (OPV)s. One strategy to reduce the band gaps and further shift the absorption towards longer wavelengths would involve extending the conjugated backbone. To this effect, the requisite starting material with two reactive handles has been synthesized.

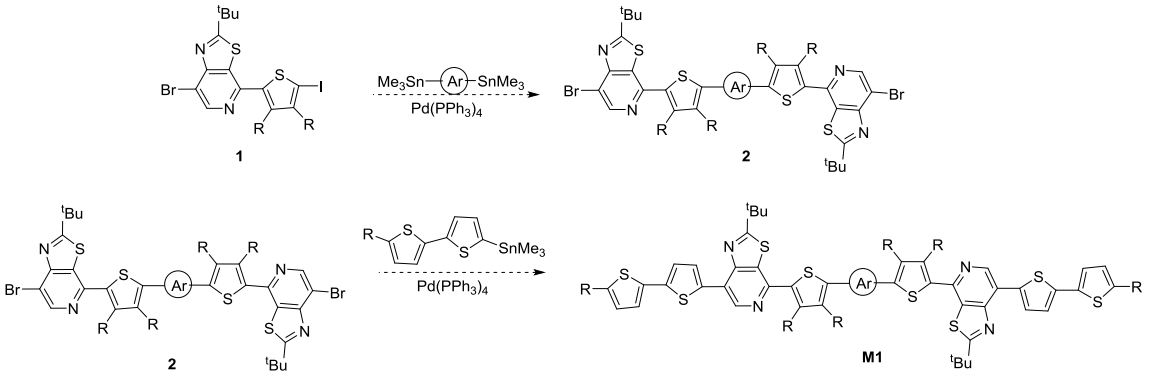

Scheme 8.1 Extending the conjugation of the small molecule.

The different reactive handles allow for selectively reacting one side of the small molecule over the other. As a result, different structures can be evaluated and the effect

of altering the structure on the material properties can be better investigated. The effect of heterocycle placement can also be studied.

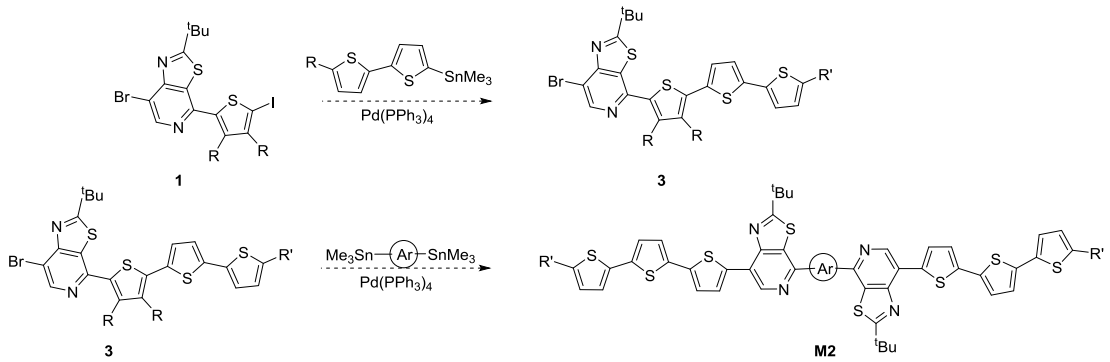

Scheme 8.2 Proposed synthesis of small molecules

As shown in Scheme 8.1, due to the increased reactivity of I as compared to Br in metal catalyzed cross coupling reactions, **1** can be reacted preferentially on the thiophene end with a donor bisstannane to form a dibromo substituted A-π-D-π-A system. A Stille coupling reaction between and the dibromo substituted A-π-D-π-A system and (5'-hexyl-[2,2'-bithiophen]-5-yl)trimethylstannane will afford the extended π system (**M1**) of D-π-A-π-D-π-A-π-D type. Conversely, as shown in Scheme 8.2, 1 can be reacted preferentially on the thiophene end to form 7-bromo-2-(*tert*-butyl)-4-(5''-hexyl-3,4-dioctyl-[2,2':5',2''-terthiophen]-5-yl)thiazolo[5,4-*c*]pyridine via palladium catalyzed Stille cross-coupling reaction. A second Stille reaction between a donor bisstannane and the bromo substituted pyridine will afford the extended π system (**M2**) of D-π-A-D-A-π-D type. Effect of heteroatom placement on material properties can therefore be studied. Based on data from initial studies, the band gap of the material can be further adjusted by varying donor strength as well as using weak electron acceptors as the arylbisstannanes.

Furthermore, the *tert*-butyl group on the pyridine ring can be substituted for a linear chain to improve π-stacking interactions in the solid state.

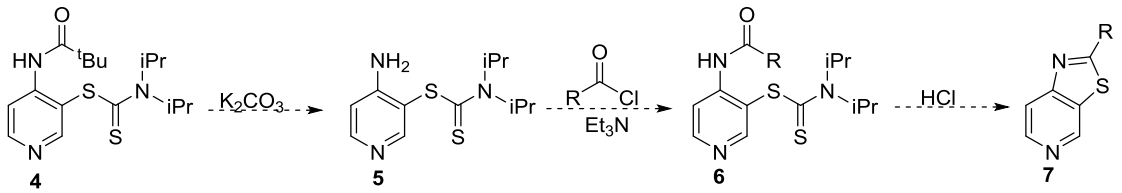

Scheme 8.3 Synthesis of 2-alkylthiazolo[5,4-*c*]pyridine

Additionally, the *tert*-butyl groups off the thiazole ring can be substituted for arenes such as thiophene or benzene and a new set of small molecules can be developed using the same donor molecules studied earlier. As a result, the difference in properties resulting from switching the conjugation axis can be studied. Based on the results from the structure- property studies further optimizations to the system can be made via either side chain modification, incorporating of different substituents on the small-molecule backbone or through the use of different conjugated π-systems.

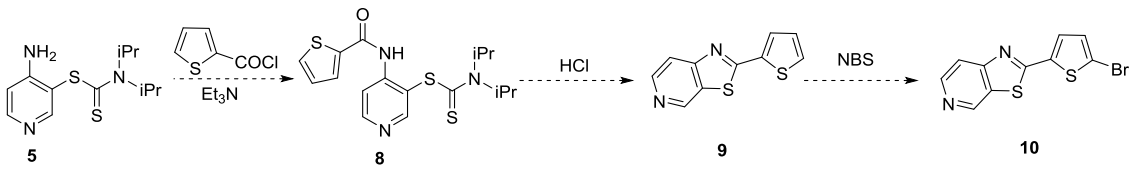

Scheme 8.4 Synthesis of 2-(5-bromothienyl)thiazolo[5,4-*c*]pyridine

8.2 Dissertation Conclusions

Over the course of graduate research in the Jeffries- EL group, the author of this dissertation has developed new electron-rich and electron-poor systems for organic semiconductors. A new and highly efficient synthetic route to a variety of bithiophene-based dicarboxaldehydes has been developed. This biggest advantage of this methodology is the ability to synthesize various donors for vinylene linked polymers from one common intermediate in high yields and purity. The donor molecules have been polymerized with benzobisazoles via Horner-Wordsworth-Emmons polycondensation reaction. The resulting polymers were found to have limited solubility in organic solvents at room temperature restricting their use as active layer materials in bulk heterojunction OPVs. This has been addressed by developing a new set of polymers utilizing alkylthienyl linkers instead of vinylene linkers. The additional alkyl groups on the thiophene ring were found to improve the solubility of these polymers in organic solvents. The effect of heteroatom placement and substitution as well as the effect of changing the donor on the properties of the resulting materials has been studied. The photovoltaic performance of solution processable polymers incorporating benzobisazoles has been evaluated and a nearly three-fold improvement in PCEs of benzobisoxale based OPVs has been reported. Moreover, new thiazolopyridine based materials have been developed from small-molecule OPVs. The A-π-D-π-A systems exhibited broad absorption in the shorter wavelength regions of the absorption spectrum and medium band gaps of 2.2 eV. Efforts to further narrow the band gap and improve absorption in the lower energy regions of the visible spectrum are currently underway. New synthetic route to electron rich benzodifurans has also been developed. The use of benzodifurans and

napthodifurans in donor-acceptor alternating copolymers is further being investigated in our research group.

8.3 Acknowledgements

I would like to thank my family for all their encouragement over the last few years without which this would have been impossible: in particular, my mother Renu for having immense faith in me and being my pillar of strength and support, in spite of being half way across the world. Mom, I love you. To my sister, Shwetankshi Bhuwalka, who has been a role model and has always encouraged me to work hard and remain focused, thank you. I would also like to thank my maternal grandparents for all their love and support, particularly my grandpa, Mr. Shivnath Kanoria, whose wisdom and teachings will always continue to guide me. My uncle, Mr. Arvind Lohia, for his constant faith and encouragement. I cannot forget to thank my dog Ray who has always been a ray of sunshine.

This journey would have been absolutely impossible without the constant support and encouragement provided by my advisor, Dr. Malika Jeffries-EL. She has patiently listened to my crazy ideas, encouraged creativity and yet kept me focused and motivated through the highs and lows of graduate school. Thank you for everything Malika, it has been an honor to work with you. I am also grateful to our collaborator, Dr. Sumit Chaudhary, for his helpful discussions and from whom I have learnt a great deal. I would also like to thank the National Science Foundation (NSF-DMR 0846607) for their generous financial support.

I would like to acknowledge past and present members of the Jeffries-EL group: Dr. Jared Mike, in particular, who has taught me a lot, entertained my crazy ideas and whose insanity has helped keep my sanity intact; Dr. Jeremy Intemann for teaching me a lot of the laboratory skills early on; Dr. Brandon Kobilka and for always encouraging me to ask questions and for being an awesome friend; Dr. Brian Tlach for always encouraging hard work; Ben Hale and Dana Drochner for helpful discussions and proof reading all the manuscripts and unpublished parts of this disserataion; Monique Ewan for being a really good friend and for all her love and support; Ramiro Chavez for always boosting my confidence and making me smile on the worst of days and Evan Muller for being my replacement in the Jeffries-EL group. I have also learnt a lot from Robyn Laskowski and Drew Makowski, and for them I am very grateful. I would like to acknowledge the assistance and helpful discussions provided by Dr Ellern Arkady and the ISU chemical instrumentation staff members: Dr. Kamel Harrata, Dr. Shu Xu, Dr. Dave Scott, and Dr. Sarah Cady. Much thanks to Dr. Anton Dubrovskiy and Dr. Nataliya Markina for their friendship, love and support over the past few years. The list is too long to name, but I am extremely fortunate for having met a lot of wonderful people and made some great friends (you know who you are) here. Thank you for always lifting my spirits and for always being there for me.

APPENDIX

List of Acronyms and Descriptions

Acronym	Description
2D	Two-Dimensional
AFM	Atomic Force Microscopy
BBO	Benzobisoxazole
BDF	Benzo[1,2-b:4,5-b']difuran
BDT	Benzo[1,2-b:4,5-b']dithiophene
BHJ	Bulk-Heterojunction
BLA	Bond Length Alternation
*c*BBO	benzo[1,2-d;5,4-d']bisoxazole
CN	1-Chloronapthalene
CP	Conjugated Polymer
CV	Cyclic Voltammerty
D-A	Donor-Acceptor
DIO	1,8-Diiodooctane
DP	Degree of Polymerization
DPP	Diketopyrrolepyrrole
DPV	Differential Pulse Voltammetry
DSC	Differential Scanning Calorimetry
DTS	Dithieno-[2,3-*b*:2',3'-*d*]silole
E_g	Band Gap

Acronym	Description
EA	Electron Affinity
EQE	External Quantum Efficiency
ESI	Electron-Spray Ionization
FF	Fill Factor
GPC	Gel Permeation Chromatography
HMW	High Molecular Weight
HOMO	Highest Occupied Molecular Orbital
HWE	Horner-Wadsworth-Emmons
HRMS	High Resolution Mass Spectrometry
ICT	Intramolecular charge transfer
ITO	Indium Tin Oxide
IP	Ionization Potential
J_{sc}	Short Circuit Current Density
LMW	Low Molecular Weight
LUMO	Lowest Unoccupied Molecular Orbital
MMW	Medium Molecular Weight
M_n	Number-Averaged Molecular Weight
MO	Molecular Orbital
M_w	Weight-Averaged Molecular Weight
NDT	Naphtho[1,2-*b*:5,6-*b'*]dithiophene
NDF	Naphtho[1,2-*b*:5,6-*b'*]difuran
NMR	Nuclear Magnetic Resonance

Acronym	Description
o-DCB	ortho-Dichlorobenzene
OFET	Organic Field-Effect Transistor
OLED	Organic Light-Emitting Diode
OPV	Organic Photovoltaic Cell
PA	Polyacetylene
PBO	Polybenzobisoxazole
P3AT	poly(3alkylthiophene)
P3HT	poly(3-hexylthiophene)
$PC_{61}BM$	[6,6]-Phenyl-C61-butyric acid methyl ester
$PC_{71}BM$	[6,6]-Phenyl-C71-butyric acid methyl ester
PCE	Power Conversion Efficiency
PDI	Poly Dispersity Index
PEDOT:PSS	Poly(3,4-ethylenedioxythiophene) poly(styrenesulfonate)
PITN	Polyisothianapthene
PPA	Polyphosphoric Acid
PPP	Poly(para-phenylenevinylene)
PPV	Poly(phenylenevinylene)
PT	Pyridalthiadiazole
PV	Photovoltaic
PVC	Photovoltaic Cell
SCLC	Space-Charge-Limited Current
SI	Supplemental Information

Acronym	Description
*t*BBO	benzo[1,2-*d*;4,5-*d'*]bisoxazole
*t*BBZT	benzo[1,2-*d*;4,5-*d'*]bisthiazole
T_d	Thermal Decomposition Temperature
Tg	Glass Transition Temperature
TDPP	3,6-di(2-thienyl)-1,4-diketopyrrolo[3,4-*c*]pyrrole
TFA	Trifluoroacetic acid
THF	Tetrahydrofuran
TGA	Thermal Gravimetric Analysis
TMS	Trimethylsilyl
TP	thiazolo[5,4-c]pyridine
TW	Terawatts
UPS	Ultraviolet Photoelectron Spectroscopy
V_{oc}	Open Circuit Voltage
Wt%	Weight Percent
XRD	X-Ray Diffraction